

Design, Synthesis and Biological Evaluation of Small Molecule Inhibitors for Treatment of Diseased States

Ph.D. Thesis

by

PREMANSH DUDHE



**DEPARTMENT OF CHEMISTRY
INDIAN INSTITUTE OF TECHNOLOGY INDORE
FEBRUARY 2021**

Design, Synthesis and Biological Evaluation of Small Molecule Inhibitors for Treatment of Diseased States

A THESIS

*Submitted in partial fulfillment of the
requirements for the award of the degree
of*

DOCTOR OF PHILOSOPHY

by

PREMANSH DUDHE



**DEPARTMENT OF CHEMISTRY
INDIAN INSTITUTE OF TECHNOLOGY INDORE
FEBRUARY 2021**



INDIAN INSTITUTE OF TECHNOLOGY INDORE

CANDIDATE'S DECLARATION

I hereby certify that the work which is being presented in the thesis entitled **Design, Synthesis and Biological Evaluation of Small Molecule Inhibitors for Treatment of Diseased States** in partial fulfillment of the requirements for the award of the degree of **DOCTOR OF PHILOSOPHY** and submitted in the **DEPARTMENT OF CHEMISTRY, INDIAN INSTITUTE OF TECHNOLOGY INDORE**, is an authentic record of my own work carried out during the time period from MAY 2015 to FEBRUARY 2021 under the supervision of **Dr. VENKATESH CHELVAM**, Associate Professor, Department of Chemistry, IIT Indore.

The matter presented in this thesis has not been submitted by me for the award of any other degree of this or any other institute.

February 02, 2021

**Signature of the student with date
(PREMANSH DUDHE)**

This is to certify that the above statement made by the candidate is correct to the best of my knowledge.

July 19, 2021

**Signature of Thesis Supervisor with date
(Dr. VENKATESH CHELVAM)**

PREMANSH DUDHE has successfully given his Ph.D. Oral Examination held on..... July 19, 2021

Signature of Chairperson (OEB)

Date: 19.7.2021

Dr. Amit Kumar
Associate Professor
Centre for Biosciences and
Biomedical Engineering (BSBE)
Indian Institute of Technology, Indore, India

Signature of External Examiner

Date: 19.7.2021

Signature(s) of Thesis Supervisor(s)

Date: 19.7.2021

Signature of PSPC Member #1

Date: 19.7.2021

Signature of PSPC Member #2

Date: 19.7.2021

Signature of Convener, DPGC

Date: 19.7.2021

Signature of Head of Department

Date: 19.7.2021

Acknowledgement

It is my great pleasure to acknowledge all the individuals who have helped and supported me over the last six years to complete this thesis work. I want to express my most profound sense of gratitude to my thesis supervisor, Dr. Venkatesh Chelvam, for giving me an excellent opportunity to work in his research group. His guidance, constant support, and encouragement have made this work possible.

I want to extend my gratitude to the PSPC committee members, Dr. Biswarup Pathak and Dr. Sudeshna Chattopadhyay, for their guidance and valuable suggestions during the research work.

I would like to express my profound sense of respect to Prof. Pratibha Sharma (DAVV, Indore), Dr. Paul Roach (Loughborough University, UK), and Prof. Ram Mohan (Illinois Wesleyan University, USA) for their kind guidance and support throughout this research work.

With great pleasure, I express my deep respect to the Director, IIT Indore, Dean of Academic Affairs (DOAA), and the Dean of Students Affairs (DOSA) for providing me with state-of-the-art research facilities, conferences, seminars, and workshops for an enriching research environment during my Ph.D. tenure. I would also like to acknowledge the Head, Department of Chemistry, the Department Post-Graduate Committee (DPGC) Convener, Department of Biosciences and Biomedical Engineering (BSBE), IIT Indore, along with other institute authorities for providing an excellent platform for conducting research. Further, I would like to thank faculty members in the Chemistry and BSBE departments for their guidance and support. I am grateful to the non-teaching staff in the departments of chemistry and BSBE for their help.

I am thankful to the Council of Scientific and Industrial Research (CSIR), New Delhi, for providing financial support in the form of research fellowship and contingencies during this work. I am honored to receive the Newton Bhabha Ph.D. placement award (2015-2016) jointly from the Department of Biotechnology (DBT), New Delhi, and the British Council (UK), and grateful for the opportunity to carry out

my research at Keele University and the Guy Hilton Research Centre, Staffordshire, UK.

I extend my most profound appreciation to all my colleagues in the chemistry and BSBE departments, for all the insightful discussions we had, over research problems and their kind suggestions.

I am thankful to the technical staff at SIC, IIT Indore, for providing me with the characterization data for the compounds reported herein. I also acknowledge the help of central library staff for providing all the latest literature references used in this work. I am grateful to my family members for their unconditional love and support.

PREMANSH DUDHE

*Dedicated to all the amazing
teachers, serving the society selflessly*

Abstract

Complex natural molecules often consist of small molecular entities in a systematic arrangement, and these architectural units usually make them useful as an overall bio-construct. Fused pyridine compounds belong to the largest family of aza-heteroaromatics. These are extensively distributed in nature in plants, marine organisms, insects, mammals, and human tissues body fluids. These heterocycles modulate a diverse set of biological activities by interacting with biomolecules like proteins in living systems. Hence, significant biological processes can be manipulated by cautious alteration of protein expressions using these external ligands (agonists and antagonists) as molecular tools. Often structural analogs of newly discovered molecules with the known ligands play a pivotal role in solving this riddle.

Azaindoles (pyrrolo-pyridines) are the closest bio-isosteres of indoles and purines and play an indispensable role in mimicking the natural ligand-target interactions. Recently, pyrrolo-pyridines have become an integral core unit in some critical drug candidates. However, their synthesis in the laboratory has always been a challenge for chemists. Due to the pyridine ring's electron-deficient nature, classical indole synthesis such as Fischer and Madelung cyclization are inefficient in azaindole synthesis. The recent advances in organometallic chemistry have enabled us to devise efficient methodologies for azaindole synthesis and functionalization. However, the developed protocols have not been realized sufficiently in the pharmaceutical industries. The use of the heavy metal catalyst in the synthetic strategy may lead to unwanted toxicity and inaccuracy in the biological studies.

Fused indolopyridines or carbolines are widely attributed to their DNA intercalation properties, inhibition of cyclin-dependent kinases (CDKs), topoisomerases, monoamine oxidase, interaction with benzodiazepine and 5-hydroxy serotonin receptors. This class of heterocycles has demonstrated a broad spectrum of pharmacological

properties, including sedative, anxiolytic, hypnotic, anti-convulsant, anti-viral, anti-parasitic, and anti-microbial activities. Although the synthesis of tailored carboline derivatives still remains a challenge to synthetic chemists, the overall assessment of existing protocols reveals low yield, limited substrate scope, use of specific substrates, and involvement of extreme thermal conditions, corrosive reagents, and toxic heavy metal catalysts.

Over the last two decades, the furopyridines have been extensively studied as bio-isosteres of indoles. Hence, these heterocycles have emerged as useful pharmacophores in therapeutic agents for treating cognitive or autoimmune disorders, migraine, irritable bowel syndrome, and asthma. Benzofuropyridine, another intriguing member of the fused pyridine class, has also found attention-grabbing applications in the pharmaceutical and OLED industry. The synthetic procedures for these important heterocyclic-cores have remained confined due to limited substrate scope and lack of innovative approaches. Azabenzofuran or pyridofuran has attracted more attention after the recent success of TAM16 against drug-susceptible and drug-resistant clinical isolates of *Mycobacterium tuberculosis*. The *in vitro* and *in vivo* studies of TAM16 have displayed comparable efficacy to the first-line TB drug isoniazid. In the process, polyketide synthase (Pks13) has emerged as a prime target for potential drug candidates in the field. It is essential for the synthesis of mycolic acids required for the cell wall of the pathogen.

The present thesis work describes the development of an unprecedented methodology for the synthesis of fused-pyridine heterocycles such as substituted 5-azaindoles, γ -carbolines, furo[3,2-*c*]pyridines, and benzofuro[3,2-*c*]pyridines. Subsequently, these nitrogen-heterocycles have been transformed into potential bio-constructs for therapeutic applications. The thesis work comprises of following chapters:

1. Serendipitous base-catalyzed condensation-heteroannulation of iminoesters: A regioselective route to the synthesis of 4,6-disubstituted 5-azaindoles

2. Synthesis of 1-indolyl-3,5,8-substituted γ -carbolines: One-pot metal-solvent free protocol and biological evaluation
3. One-pot synthesis of furo[3,2-*c*]pyridines and benzofuro[3,2-*c*]pyridines: Development of isatin molecular hybrids for treatment of tuberculosis

1. Serendipitous base-catalyzed condensation-heteroannulation of iminoesters: A regioselective route to the synthesis of 4,6-disubstituted 5-azaindoles

In this chapter, we discuss a serendipitous discovery of a one-pot approach to prepare 4,6-disubstituted 5-azaindoles from simple precursors such as pyrrole-2-carboxaldehyde and glycine alkyl esters using common non-nucleophilic base diisopropylethylamine (DIPEA). This novel methodology is a metal-free, solvent-free protocol with an easy operational method to access the above-mentioned heterocyclic framework in moderate to good yields. The unprecedented approach discloses an interesting condensation-heterocyclization reaction mechanistically. The *in situ* formed iminoester of pyrrole-2-aldehydes, and glycine ester goes into a condensation reaction with excess pyrrole-2-aldehyde to give the title compound 4,6-disubstituted 5-azaindole. The heterocyclic core structure is unequivocally characterized by various spectroscopic techniques (^1H , ^{13}C , DEPT, HRMS, IR), including single-crystal XRD for a representative 5-azaindole derivative **3aa**. Several other 6-substituted derivatives of 5-azaindoles with functional groups such as carboxylic acid, cyanide, primary alcohol, carbaldehyde are synthesized, which are otherwise difficult to prepare by conventional methods. Theoretical (DFT) studies also support the proposed mechanism for the formation of 5-azaindole regioisomer. A structural analog of selective CB2 agonist GSK554418A has been synthesized with potential anticancer activity.

2. Synthesis of 1-indolyl-3,5,8-substituted γ -carbolines: One-pot metal-solvent free protocol and biological evaluation

This chapter comprises the development of a novel metal-free, solvent-free protocol synthetic protocol for 1-indolyl-3,5,8-substituted γ -carbolines. The substrates utilized are not expensive and readily available. The developed protocol is operationally simple with easy work-up procedures, single-step purification, and high product yield. The synthesized γ -carboline core offers a broad range of tunable optical activity. The novel compounds have also been examined for their innate cytotoxicity against a panel of cancer cell lines. Delightfully, the above-mentioned fluorescent compounds are cytotoxic in the micromolar range of concentrations. We have also performed the cell uptake studies on the title compounds, and a decent cytosolic uptake has been observed, even in sub-micromolar concentrations.

3. One-pot synthesis of furo[3,2-*c*]pyridines and benzofuro[3,2-*c*]pyridines: Development of isatin molecular hybrids for treatment of tuberculosis

This chapter describes the development of a novel protocol for the synthesis of substituted furo[3,2-*c*]pyridines and benzofuro[3,2-*c*]pyridines. With reference to the recent success of benzofuran core molecule TAM16 and newly developed isatin hybrids against multidrug-resistant clinical isolates of *Mycobacterium tuberculosis*, the synthesized novel molecules herein are transformed into corresponding isatin hybrids to develop an unprecedented series of anti-mycobacterial compounds. The new molecular hybrids were tested against non-virulent and virulent species of *mycobacterium* to check their efficacy as anti-mycobacterial. The bacterial growth was examined by calculating CFU (colony forming unit) with known concentrations of compounds for fixed time intervals such as 6, 12, 24, and 48 h. According to these *in vitro* studies, the newly developed hybrid **15ba** is active against *M. Smegmatis* and *M. bovis* BCG with IC₅₀ values 50–100 μ M.

List of Patent and Publications

1. Chelvam V., **Dudhe P.**, Krishnan M.A., Sonawane A. (2019), Method and System for Metal-free Solvent-free Synthesis of Fused-pyrido Heterocycles, Indian Patent, 366986, (Granted)
2. Chelvam V., **Dudhe P.**, Krishnan M.A., Sonawane A. (2020), Method and System for Metal-free Solvent-free Synthesis of Fused-pyrido Heterocycles, China Patent, 202010697100.X, (Provisional)
3. Chelvam V., **Dudhe P.**, Krishnan M.A., Sonawane A. (2021), Metal-free Solvent-free Synthesis of Fused-pyrido Heterocycles and Biomedical Applications, USA Patent, US 2021/0070765 A1, (Published)
4. **Dudhe P.**, Venkatasubbaiah K., Pathak B., Chelvam V. (2020), Serendipitous base-catalyzed condensation-heteroannulation of iminoesters: A novel highly regioselective synthesis of 4,6 substituted 5-azaindoles, *Org Biomol Chem*, 18, 1582–1587 (DOI: 10.1039/c9ob02657f) (Impact Factor: 3.550)
5. **Dudhe P.**, Krishnan M.A., Yadav K., Roy D., Venkatasubbaiah K., Pathak B., Chelvam V. (2021), Synthesis of 1-indolyl-3,5,8-substituted γ -carboline: One-pot solvent-free protocol and biological evaluation, *Beilstein J Org Chem*, 17, 1453–1463 (DOI: 10.3762/bjoc.17.101) (Impact Factor: 2.622)
6. **Dudhe P.**, Krishnan M.A., Behera A., Sonawane A., Chelvam V. (2021), One-pot synthesis of furo[3,2-*c*]pyridines and benzofuro[3,2-*c*]pyridines: Development of isatin molecular hybrids for treatment of tuberculosis, (Under preparation)
7. Krishna Rao A.V.R., **Dudhe P.**, Chelvam V. (2021), Role of oxygen defects in the basicity of Se doped ZnO nanocatalyst for enhanced triglyceride transesterification in biodiesel production, *Catal Commun*, 149, 106258 (DOI: 10.1016/j.catcom.2020.106258) (Impact Factor: 3.800)
8. Reddy R.B., **Dudhe P.**, Chelvam V. (2019), Synthesis of the deacetoxytubuvaline fragment of pretubulysin and its lipophilic

analogues for enhanced permeability in cancer cell lines, *Synlett*, 30, 77–81 (DOI: 10.1055/s-0037-1611359) (Impact Factor: 2.420)

9. Sengupta S., Krishnan M.A., Pandit A., **Dudhe P.**, Sharma R., Chelvam V. (2019), Tyrosine-based asymmetric urea ligand for prostate carcinoma: Tuning biological efficacy through *in silico* studies, *Bioorg Chem*, 91, 103154 (DOI: 10.1016/j.bioorg.2019.103154) (Impact Factor: 3.940)
10. Sengupta S., Krishnan M.A., **Dudhe P.**, Reddy R.B., Giri B., Chattopadhyay S., Chelvam V. (2018), Novel solid-phase strategy for the synthesis of ligand-targeted fluorescent-labelled chelating peptide conjugates as a theranostic tool for cancer, *Beilstein J Org Chem*, 14, 2665–2679 (DOI: 10.3762/bjoc.14.244) (Impact Factor: 2.540)
11. Reddy R.B., **Dudhe P.**, Chouhan P., Sengupta S., Chelvam V. (2018), Synthesis of tubuphenylalanine and epi-tubuphenylalanine via regioselective hydroboration-oxidation of 1,1-substituted amino alkenes, *Tetrahedron*, 74, 6946–6953 (DOI: 10.1016/j.tet.2018.10.024) (Impact Factor: 2.460)

TABLE OF CONTENTS

1	List of Figures	XIV
2	List of Tables	XXX
3	List of Schemes	XXXI
4	Acronyms	XXXV
5	Symbols/Units	XXXVI
Chapter 1	Introduction	1–26
1.1	Fused-pyrido heterocycles	1
1.2	Review of recent literature for the synthesis of fused-pyrido heterocycles	4
1.2.1	Synthesis of 5-azaindoles	4
1.2.2	Synthesis of γ -carboline	7
1.2.3	Synthesis of furo[3,2-c]pyridines	11
1.2.4	Synthesis of benzofuro[3,2-c]pyridines	13
1.3	The role of 5-azaindoles in cancer therapy	14
1.4	Biological applications of γ -carboline	16
1.5	Tuberculosis: Current status and the emerging role of small molecules in the management of disease	18
1.6	Benzofuropyridine core and its biological application	20
1.7	Organization of the thesis	20
1.8	References	21
Chapter 2	Serendipitous base-catalyzed condensation-heteroannulation of iminoesters: A regioselective route to the synthesis of 4,6-disubstituted 5-azaindoles	27–106
2.1	Introduction	27
2.2	Results and discussion	28
2.3	Conclusion	40
2.4	Experimental section	40
2.4.1	General information	40
2.4.2	Experimental details and	41

	characterization data	
2.4.2.1	Synthesis of starting materials 1a–i and 2b	41
2.4.2.2	General procedure for synthesis of <i>Alkyl 4-(1H-pyrrol-2-yl)-1H-pyrrolo[3,2-c]pyridine-6-carboxylate</i> derivatives 3aa–fa	48
2.4.2.3	Synthesis of 5-azaindole derivatives 10–16	58
2.4.2.4	Density Functional Theory Calculations	64
2.4.3	Copies of ¹ H, ¹³ C NMR spectra for synthesized compounds	65
2.5	References	102
Chapter 3	Synthesis of 1-indolyl-3,5,8-substituted γ-carbolines: One-pot solvent-free protocol and biological evaluation	107–192
3.1	Introduction	107
3.2	Results and discussion	109
3.3	Conclusion	123
3.4	Experimental section	124
3.4.1	General information	124
3.4.2	Experimental details and characterization data	125
3.4.2.1	Synthesis of precursors or indole substrates 1a–h	125
3.4.2.2	General procedure for the synthesis of 1-indolyl-3,5,8-substituted γ -carbolines 3aa–ac , 3ba–ea and 1-indolyl-1,2-dihydro-3,5-substituted γ -carbolines 3ga derivatives	141
3.4.2.3	UV calibration of γ -carboline 3ac in organic solvents	152
3.4.2.4	<i>In vitro</i> cytotoxicity studies	152
3.4.2.4.1	Cytotoxicity analysis in cancer and	152

	macrophage cells	
	3.4.2.4.2 HeLa cell uptake study of γ -carboline 3ac	153
	3.4.2.5 Density Functional Theory Calculations	153
	3.4.3 Copies of ^1H , ^{13}C NMR spectra for synthesized compounds	154
3.5	References	185
Chapter 4	One-pot synthesis of furo[3,2-<i>c</i>]pyridines and benzofuro[3,2-<i>c</i>]pyridines: Development of isatin molecular hybrids for treatment of tuberculosis	193–236
4.1	Introduction	193
4.2	Results and discussion	195
4.3	Conclusion	207
4.4	Experimental section	208
	4.4.1 General information	208
	4.4.2 Experimental section and characterization data	209
	4.4.2.1 General procedure for the synthesis of furo[3,2- <i>c</i>]pyridines 3aa–ba and benzofuro[3,2- <i>c</i>]pyridines 3da–dc	209
	4.4.2.2 Synthesis of furo[3,2- <i>c</i>]pyridine-isatin hybrid 15ba	214
	4.4.2.3 Density Functional Theory Calculations	218
	4.4.3 Copies of ^1H , ^{13}C NMR spectra for synthesized compounds	219
4.5	References	234
Chapter 5	Conclusions and scope for future work	237–240
5.1	Conclusion	237
5.2	Scope for future work	238

List of Figures

Chapter 1	Introduction	1–26
Figure 1.1	Pyridine subunit highlighted in biomolecules 1–3	1
Figure 1.2	US-FDA approved aza-heterocyclic small molecules 4–11 for oncology in 2019	2
Figure 1.3	Pyrido-fused bicyclic (5-6) and tricyclic (6-5-6) systems with two heteroatoms (1:1)	3
Figure 1.4	Natural azaindole derivatives found in antartic sponges: Variolins	14
Figure 1.5	Biologically active 5-azaindole derivatives	15
Figure 1.6	Biologically active γ -carboline derivatives	17
Figure 1.7	Polyketide synthetase 13 (Pks13) inhibitors	19
Figure 1.8	Antidepressant benzofuro[3,2-c]pyridine based molecule	20
Chapter 2	Serendipitous base-catalyzed condensation-heteroannulation of iminoesters: A regioselective route to the synthesis of 4,6-disubstituted 5-azaindoles	27–106
Figure 2.1	Pharmacologically active molecules containing the 5-azaindole core	28
Figure 2.2	Molecular structure of 3aa (CCDC 1836867)	31
Figure 2.3	¹ H NMR spectrum of <i>1-benzyl-1H-pyrrole-2-carbaldehyde (1a)</i>	65
Figure 2.4	¹³ C NMR spectrum of <i>1-benzyl-1H-pyrrole-2-carbaldehyde (1a)</i>	65
Figure 2.5	¹ H NMR spectrum of <i>1-(4-methoxybenzyl)-1H-pyrrole-2-carbaldehyde (1b)</i>	66
Figure 2.6	¹³ C NMR spectrum of <i>1-(4-methoxybenzyl)-1H-pyrrole-2-</i>	66

	<i>carbaldehyde (1b)</i>	
Figure 2.7	¹ H NMR spectrum of <i>1-methyl-1H-pyrrole-2-carbaldehyde (1c)</i>	67
Figure 2.8	¹³ C NMR spectrum of <i>1-methyl-1H-pyrrole-2-carbaldehyde (1c)</i>	67
Figure 2.9	¹ H NMR spectrum of <i>1-tosyl-1H-pyrrole-2-carbaldehyde (1d)</i>	68
Figure 2.10	¹³ C NMR spectrum of <i>1-tosyl-1H-pyrrole-2-carbaldehyde (1d)</i>	68
Figure 2.11	¹ H NMR spectrum of <i>N5,N5,N10,N10-tetramethyl-5,10-dihydrodipyrrolo[1,2-a:1',2'-d]pyrazine-5,10-diamine</i>	69
Figure 2.12	¹ H NMR spectrum of <i>1-benzyl-5-methyl-1H-pyrrole-2-carbaldehyde (1f)</i>	69
Figure 2.13	¹³ C NMR spectrum of <i>1-benzyl-5-methyl-1H-pyrrole-2-carbaldehyde (1f)</i>	70
Figure 2.14	¹ H NMR spectrum of <i>1-(2-bromobenzyl)-1H-pyrrole-2-carbaldehyde (1g)</i>	70
Figure 2.15	¹³ C NMR spectrum of <i>1-(2-bromobenzyl)-1H-pyrrole-2-carbaldehyde (1g)</i>	71
Figure 2.16	¹ H NMR spectrum of <i>tert-butyl 2-formyl-1H-pyrrole-1-carboxylate (1h)</i>	71
Figure 2.17	¹³ C NMR spectrum of <i>tert-butyl 2-formyl-1H-pyrrole-1-carboxylate (1h)</i>	72
Figure 2.18	¹ H NMR spectrum of <i>5H-pyrrolo[2,1-a]isoindole-3-carbaldehyde (1i)</i>	72
Figure 2.19	¹³ C NMR spectrum of <i>5H-pyrrolo[2,1-a]isoindole-3-carbaldehyde (1i)</i>	73
Figure 2.20	¹ H NMR spectrum of <i>glycine ethyl ester HCl salt (2b)</i>	73
Figure 2.21	¹³ C NMR spectrum of <i>glycine ethyl ester HCl salt (2b)</i>	74
Figure 2.22	¹ H NMR spectrum (500 MHz) of <i>methyl 1-</i>	74

benzyl-4-(1-benzyl-1H-pyrrol-2-yl)-1H-pyrrolo[3,2-c]pyridine-6-carboxylate
(**3aa**)

Figure 2.23 ^{13}C NMR spectrum of *methyl 1-benzyl-4-* 75

(1-benzyl-1H-pyrrol-2-yl)-1H-pyrrolo[3,2-c]pyridine-6-carboxylate (**3aa**)

Figure 2.24 DEPT-135° spectrum of *methyl 1-benzyl-* 75

4-(1-benzyl-1H-pyrrol-2-yl)-1H-pyrrolo[3,2-c]pyridine-6-carboxylate
(**3aa**)

Figure 2.25 HRMS data of *methyl 1-benzyl-4-(1-* 76

benzyl-1H-pyrrol-2-yl)-1H-pyrrolo[3,2-c]pyridine-6-carboxylate (**3aa**)

Figure 2.26 ^1H NMR spectrum of *methyl 1-(4-* 76

methoxybenzyl)-4-(1-(4-methoxybenzyl)-1H-pyrrol-2-yl)-1H-pyrrolo[3,2-c]pyridine-6-carboxylate (**3ba**)

Figure 2.27 ^{13}C NMR spectrum of *methyl 1-(4-* 77

methoxybenzyl)-4-(1-(4-methoxybenzyl)-1H-pyrrol-2-yl)-1H-pyrrolo[3,2-c]pyridine-6-carboxylate (**3ba**)

Figure 2.28 HRMS data of *methyl 1-(4-* 77

methoxybenzyl)-4-(1-(4-methoxybenzyl)-1H-pyrrol-2-yl)-1H-pyrrolo[3,2-c]pyridine-6-carboxylate (**3ba**)

Figure 2.29 ^1H NMR spectrum of *methyl 1-methyl-4-* 78

(1-methyl-1H-pyrrol-2-yl)-1H-pyrrolo[3,2-c]pyridine-6-carboxylate (**3ca**)

Figure 2.30 ^{13}C NMR spectrum of *methyl 1-methyl-4-* 78

(1-methyl-1H-pyrrol-2-yl)-1H-pyrrolo[3,2-c]pyridine-6-carboxylate (**3ca**)

Figure 2.31 HRMS data of *methyl 1-methyl-4-(1-* 79

methyl-1H-pyrrol-2-yl)-1H-pyrrolo[3,2-

	<i>c</i>]pyridine-6-carboxylate (3ca)	
Figure 2.32	¹ H NMR spectrum of <i>tert</i> -butyl 1-benzyl-4-(1-benzyl-1 <i>H</i> -pyrrol-2-yl)-1 <i>H</i> -pyrrolo[3,2- <i>c</i>]pyridine-6-carboxylate (3ac)	79
Figure 2.33	¹³ C NMR spectrum of <i>tert</i> -butyl 1-benzyl-4-(1-benzyl-1 <i>H</i> -pyrrol-2-yl)-1 <i>H</i> -pyrrolo[3,2- <i>c</i>]pyridine-6-carboxylate (3ac)	80
Figure 2.34	HRMS data of <i>tert</i> -butyl 1-benzyl-4-(1-benzyl-1 <i>H</i> -pyrrol-2-yl)-1 <i>H</i> -pyrrolo[3,2- <i>c</i>]pyridine-6-carboxylate (3ac)	80
Figure 2.35	¹ H NMR spectrum of ethyl 1-methyl-4-(1-methyl-1 <i>H</i> -pyrrol-2-yl)-1 <i>H</i> -pyrrolo[3,2- <i>c</i>]pyridine-6-carboxylate (3cb)	81
Figure 2.36	¹³ C NMR spectrum of ethyl 1-methyl-4-(1-methyl-1 <i>H</i> -pyrrol-2-yl)-1 <i>H</i> -pyrrolo[3,2- <i>c</i>]pyridine-6-carboxylate (3cb)	81
Figure 2.37	HRMS data of ethyl 1-methyl-4-(1-methyl-1 <i>H</i> -pyrrol-2-yl)-1 <i>H</i> -pyrrolo[3,2- <i>c</i>]pyridine-6-carboxylate (3cb)	82
Figure 2.38	¹ H NMR spectrum of ethyl 1-benzyl-4-(1-benzyl-1 <i>H</i> -pyrrol-2-yl)-1 <i>H</i> -pyrrolo[3,2- <i>c</i>]pyridine-6-carboxylate (3ab)	82
Figure 2.39	¹³ C NMR spectrum of ethyl 1-benzyl-4-(1-benzyl-1 <i>H</i> -pyrrol-2-yl)-1 <i>H</i> -pyrrolo[3,2- <i>c</i>]pyridine-6-carboxylate (3ab)	83
Figure 2.40	HRMS data of ethyl 1-benzyl-4-(1-benzyl-1 <i>H</i> -pyrrol-2-yl)-1 <i>H</i> -pyrrolo[3,2- <i>c</i>]pyridine-6-carboxylate (3ab)	83
Figure 2.41	¹ H NMR spectrum of ethyl 1-(4-methoxybenzyl)-4-(1-(4-methoxybenzyl)-1 <i>H</i> -pyrrol-2-yl)-1 <i>H</i> -pyrrolo[3,2- <i>c</i>]pyridine-6-carboxylate (3bb)	84
Figure 2.42	¹³ C NMR spectrum of ethyl 1-(4-methoxybenzyl)-4-(1-(4-methoxybenzyl)-1 <i>H</i> -pyrrol-2-yl)-1 <i>H</i> -pyrrolo[3,2- <i>c</i>]pyridine-6-carboxylate (3bb)	84

methoxybenzyl)-4-(1-(4-methoxybenzyl)-1H-pyrrol-2-yl)-1H-pyrrolo[3,2-c]pyridine-6-carboxylate (3bb)

Figure 2.43 HRMS data of *ethyl 1-(4-methoxybenzyl)-4-(1-(4-methoxybenzyl)-1H-pyrrol-2-yl)-1H-pyrrolo[3,2-c]pyridine-6-carboxylate (3bb)* 85

Figure 2.44 ¹H NMR spectrum of *tert-butyl 1-(4-methoxybenzyl)-4-(1-(4-methoxybenzyl)-1H-pyrrol-2-yl)-1H-pyrrolo[3,2-c]pyridine-6-carboxylate (3bc)* 85

Figure 2.45 ¹³C NMR spectrum of *tert-butyl 1-(4-methoxybenzyl)-4-(1-(4-methoxybenzyl)-1H-pyrrol-2-yl)-1H-pyrrolo[3,2-c]pyridine-6-carboxylate (3bc)* 86

Figure 2.46 HRMS data of *tert-butyl 1-(4-methoxybenzyl)-4-(1-(4-methoxybenzyl)-1H-pyrrol-2-yl)-1H-pyrrolo[3,2-c]pyridine-6-carboxylate (3bc)* 86

Figure 2.47 ¹H NMR spectrum of *methyl 1-tosyl-4-(1-tosyl-1H-pyrrol-2-yl)-1H-pyrrolo[3,2-c]pyridine-6-carboxylate (3da)* 87

Figure 2.48 ¹³C NMR spectrum of *methyl 1-tosyl-4-(1-tosyl-1H-pyrrol-2-yl)-1H-pyrrolo[3,2-c]pyridine-6-carboxylate (3da)* 87

Figure 2.49 HRMS data of *methyl 1-tosyl-4-(1-tosyl-1H-pyrrol-2-yl)-1H-pyrrolo[3,2-c]pyridine-6-carboxylate (3da)* 88

Figure 2.50 ¹H NMR spectrum of *methyl 1-(phenylsulfonyl)-4-(1-(phenylsulfonyl)-1H-pyrrol-2-yl)-1H-pyrrolo[3,2-c]pyridine-6-carboxylate (3ea)* 88

Figure 2.51 ¹³C NMR spectrum of *methyl 1-* 89

	<i>(phenylsulfonyl)-4-(1-(phenylsulfonyl)-1H-pyrrol-2-yl)-1H-pyrrolo[3,2-c]pyridine-6-carboxylate (3ea)</i>	
Figure 2.52	HRMS data of <i>methyl 1-(phenylsulfonyl)-4-(1-(phenylsulfonyl)-1H-pyrrol-2-yl)-1H-pyrrolo[3,2-c]pyridine-6-carboxylate (3ea)</i>	89
Figure 2.53	¹ H NMR spectrum of <i>methyl 1-benzyl-4-(1-benzyl-5-methyl-1H-pyrrol-2-yl)-2-methyl-1H-pyrrolo[3,2-c]pyridine-6-carboxylate (3fa)</i>	90
Figure 2.54	¹³ C NMR spectrum of <i>methyl 1-benzyl-4-(1-benzyl-5-methyl-1H-pyrrol-2-yl)-2-methyl-1H-pyrrolo[3,2-c]pyridine-6-carboxylate (3fa)</i>	90
Figure 2.55	HRMS data of <i>methyl 1-benzyl-4-(1-benzyl-5-methyl-1H-pyrrol-2-yl)-2-methyl-1H-pyrrolo[3,2-c]pyridine-6-carboxylate (3fa)</i>	91
Figure 2.56	¹ H NMR spectrum of <i>1-benzyl-4-(1-benzyl-1H-pyrrol-2-yl)-1H-pyrrolo[3,2-c]pyridine-6-carboxamide (10)</i>	91
Figure 2.57	¹³ C NMR spectrum of <i>1-benzyl-4-(1-benzyl-1H-pyrrol-2-yl)-1H-pyrrolo[3,2-c]pyridine-6-carboxamide (10)</i>	92
Figure 2.58	Mass data of <i>1-benzyl-4-(1-benzyl-1H-pyrrol-2-yl)-1H-pyrrolo[3,2-c]pyridine-6-carboxamide (10)</i>	92
Figure 2.59	¹ H NMR spectrum of <i>1-benzyl-4-(1-benzyl-1H-pyrrol-2-yl)-1H-pyrrolo[3,2-c]pyridine-6-carbonitrile (11)</i>	93
Figure 2.60	¹³ C NMR spectrum of <i>1-benzyl-4-(1-benzyl-1H-pyrrol-2-yl)-1H-pyrrolo[3,2-c]pyridine-6-carbonitrile (11)</i>	93

- Figure 2.61 HRMS data of *1-benzyl-4-(1-benzyl-1H-pyrrol-2-yl)-1H-pyrrolo[3,2-c]pyridine-6-carbonitrile (11)* 94
- Figure 2.62 ¹H NMR spectrum of *1-benzyl-4-(1-benzyl-1H-pyrrol-2-yl)-1H-pyrrolo[3,2-c]pyridin-6-yl)methanol (12)* 94
- Figure 2.63 ¹³C NMR spectrum of *1-benzyl-4-(1-benzyl-1H-pyrrol-2-yl)-1H-pyrrolo[3,2-c]pyridin-6-yl)methanol (12)* 95
- Figure 2.64 HRMS data of *1-benzyl-4-(1-benzyl-1H-pyrrol-2-yl)-1H-pyrrolo[3,2-c]pyridin-6-yl)methanol (12)* 95
- Figure 2.65 ¹H NMR spectrum of *1-benzyl-4-(1-benzyl-1H-pyrrol-2-yl)-1H-pyrrolo[3,2-c]pyridine-6-carbaldehyde (13)* 96
- Figure 2.66 ¹³C NMR spectrum of *1-benzyl-4-(1-benzyl-1H-pyrrol-2-yl)-1H-pyrrolo[3,2-c]pyridine-6-carbaldehyde (13)* 96
- Figure 2.67 HRMS data of *1-benzyl-4-(1-benzyl-1H-pyrrol-2-yl)-1H-pyrrolo[3,2-c]pyridine-6-carbaldehyde (13)* 97
- Figure 2.68 Crude ¹H NMR spectrum of *1-methyl-4-(1-methyl-1H-pyrrol-2-yl)-1H-pyrrolo[3,2-c]pyridine-6-carboxylic acid (14)* 97
- Figure 2.69 Crude ¹³C NMR spectrum of *1-methyl-4-(1-methyl-1H-pyrrol-2-yl)-1H-pyrrolo[3,2-c]pyridine-6-carboxylic acid (14)* 98
- Figure 2.70 HRMS data of *1-methyl-4-(1-methyl-1H-pyrrol-2-yl)-1H-pyrrolo[3,2-c]pyridine-6-carboxylic acid (14)* 98
- Figure 2.71 ¹H NMR spectrum of *1-methyl-4-(1-methyl-1H-pyrrol-2-yl)-1H-pyrrolo[3,2-c]pyridin-6-yl)(morpholino)methanone* 99

	(15)	
Figure 2.72	¹³ C NMR spectrum of <i>1-methyl-4-(1-methyl-1H-pyrrol-2-yl)-1H-pyrrolo[3,2-c]pyridin-6-yl(morpholino)methanone</i> (15)	99
Figure 2.73	HRMS data of <i>1-methyl-4-(1-methyl-1H-pyrrol-2-yl)-1H-pyrrolo[3,2-c]pyridin-6-yl(morpholino)methanone</i> (15)	100
Figure 2.74	¹ H NMR spectrum of <i>methyl 1-benzyl-4-(1-tosyl-1H-pyrrol-2-yl)-1H-pyrrolo[3,2-c]pyridine-6-carboxylate</i> (16)	100
Figure 2.75	¹³ C NMR spectrum of <i>methyl 1-benzyl-4-(1-tosyl-1H-pyrrol-2-yl)-1H-pyrrolo[3,2-c]pyridine-6-carboxylate</i> (16)	101
Figure 2.76	HRMS data of <i>methyl 1-benzyl-4-(1-tosyl-1H-pyrrol-2-yl)-1H-pyrrolo[3,2-c]pyridine-6-carboxylate</i> (16)	101
Chapter 3	Synthesis of 1-indolyl-3,5,8-substituted γ-carboline: One-pot solvent-free protocol and biological evaluation	107–192
Figure 3.1	Selected examples of compounds containing γ -carboline core	108
Figure 3.2	Single-crystal XRD structure of 3ac (CCDC: 1897787)	114
Figure 3.3	DFT relative energy calculation for the formation of γ -carboline 9a over β -carboline 9c regioisomer using B3LYP/6-311++G** level of theory	117
Figure 3.4	UV-vis absorption (left side) and emission (right side) spectra of 3ac measured in different solvents	119
Figure 3.5	Fluorescence decay profile of 3ac in DMSO (left side; λ_{exc} 360 nm) and 10 ⁻⁵ M	119

	solutions of compound 3ac in four different solvents under UV chamber (right side)	
Figure 3.6	Dose vs response or IC ₅₀ curves for the representative γ -carbolines, 3ac , 3bc , 3ca , and 3ga and doxorubicin against cancer cell lines	121–122
Figure 3.7	Dose vs response curve of γ -carbolines 3ac , 3bc , 3ca , 3ga in the macrophage cell line, RAW 264.7	123
Figure 3.8	Laser scanning confocal microscopy studies ($\lambda_{\text{ex}} = 405$ nm; collection range= 420–470 nm) for uptake of 3ac in HeLa cells	124
Figure 3.9	UV calibration curve for γ -carboline 3ac in different solvents	153
Figure 3.10	¹ H NMR spectrum of <i>1-methyl-1H-indole-2-carbaldehyde</i> (1a)	155
Figure 3.11	¹³ C NMR spectrum of <i>1-methyl-1H-indole-2-carbaldehyde</i> (1a)	155
Figure 3.12	¹ H NMR spectrum of <i>1-benzyl-1H-indole-2-carbaldehyde</i> (1b)	156
Figure 3.13	¹³ C NMR spectrum of <i>1-benzyl-1H-indole-2-carbaldehyde</i> (1b)	156
Figure 3.14	¹ H NMR spectrum of <i>1-(4-methoxybenzyl)-1H-indole-2-carbaldehyde</i> (1c)	157
Figure 3.15	¹³ C NMR spectrum of <i>1-(4-methoxybenzyl)-1H-indole-2-carbaldehyde</i> (1c)	157
Figure 3.16	¹ H NMR spectrum of <i>1-butyl-1H-indole-2-carbaldehyde</i> (1d)	158
Figure 3.17	¹³ C NMR spectrum of <i>1-butyl-1H-indole-2-carbaldehyde</i> (1d)	158

Figure 3.18	¹ H NMR spectrum of 5-methoxy-1-methyl-1 <i>H</i> -indole-2-carbaldehyde (1e)	159
Figure 3.19	¹³ C NMR spectrum of 5-methoxy-1-methyl-1 <i>H</i> -indole-2-carbaldehyde (1e)	159
Figure 3.20	¹ H NMR spectrum of 1-methyl-5-phenyl-1 <i>H</i> -indole-2-carbaldehyde (1f)	160
Figure 3.21	¹³ C NMR spectrum of 1-methyl-5-phenyl-1 <i>H</i> -indole-2-carbaldehyde (1f)	160
Figure 3.22	¹ H NMR spectrum of 1-tosyl-1 <i>H</i> -indole-2-carboxylate (1g)	161
Figure 3.23	¹³ C NMR spectrum of 1-tosyl-1 <i>H</i> -indole-2-carboxylate (1g)	161
Figure 3.24	¹ H NMR spectrum of <i>tert</i> -butyl 2-formyl-1 <i>H</i> -indole-1-carboxylate (1h)	162
Figure 3.25	¹³ C NMR spectrum of <i>tert</i> -butyl 2-formyl-1 <i>H</i> -indole-1-carboxylate (1h)	162
Figure 3.26	¹ H NMR spectrum of methyl 5-methyl-1-(1-methyl-1 <i>H</i> -indol-2-yl)-5 <i>H</i> -pyrido[4,3- <i>b</i>]indole-3-carboxylate (3aa)	163
Figure 3.27	¹³ C NMR spectrum of methyl 5-methyl-1-(1-methyl-1 <i>H</i> -indol-2-yl)-5 <i>H</i> -pyrido[4,3- <i>b</i>]indole-3-carboxylate (3aa)	163
Figure 3.28	HRMS of methyl 5-methyl-1-(1-methyl-1 <i>H</i> -indol-2-yl)-5 <i>H</i> -pyrido[4,3- <i>b</i>]indole-3-carboxylate (3aa)	164
Figure 3.29	¹ H NMR spectrum of ethyl 5-methyl-1-(1-methyl-1 <i>H</i> -indol-2-yl)-5 <i>H</i> -pyrido[4,3- <i>b</i>]indole-3-carboxylate (3ab)	164
Figure 3.30	¹³ C NMR spectrum of ethyl 5-methyl-1-(1-methyl-1 <i>H</i> -indol-2-yl)-5 <i>H</i> -pyrido[4,3- <i>b</i>]indole-3-carboxylate (3ab)	165
Figure 3.31	HRMS of ethyl 5-methyl-1-(1-methyl-1 <i>H</i> -indol-2-yl)-5 <i>H</i> -pyrido[4,3- <i>b</i>]indole-3-	165

	<i>carboxylate (3ab)</i>	
Figure 3.32	¹ H NMR spectrum of <i>tert-butyl 5-methyl-1-(1-methyl-1H-indol-2-yl)-5H-pyrido[4,3-b]indole-3-carboxylate (3ac)</i>	166
Figure 3.33	¹³ C NMR spectrum of <i>tert-butyl 5-methyl-1-(1-methyl-1H-indol-2-yl)-5H-pyrido[4,3-b]indole-3-carboxylate (3ac)</i>	166
Figure 3.34	HRMS of <i>tert-butyl 5-methyl-1-(1-methyl-1H-indol-2-yl)-5H-pyrido[4,3-b]indole-3-carboxylate (3ac)</i>	167
Figure 3.35	¹ H NMR spectrum of <i>methyl 5-benzyl-1-(1-benzyl-1H-indol-2-yl)-5H-pyrido[4,3-b]indole-3-carboxylate (3ba)</i>	167
Figure 3.36	¹³ C NMR spectrum of <i>methyl 5-benzyl-1-(1-benzyl-1H-indol-2-yl)-5H-pyrido[4,3-b]indole-3-carboxylate (3ba)</i>	168
Figure 3.37	HRMS of <i>methyl 5-benzyl-1-(1-benzyl-1H-indol-2-yl)-5H-pyrido[4,3-b]indole-3-carboxylate (3ba)</i>	168
Figure 3.38	¹ H NMR spectrum of <i>ethyl 5-benzyl-1-(1-benzyl-1H-indol-2-yl)-5H-pyrido[4,3-b]indole-3-carboxylate (3bb)</i>	169
Figure 3.39	¹³ C NMR spectrum of <i>ethyl 5-benzyl-1-(1-benzyl-1H-indol-2-yl)-5H-pyrido[4,3-b]indole-3-carboxylate (3bb)</i>	169
Figure 3.40	HRMS of <i>ethyl 5-benzyl-1-(1-benzyl-1H-indol-2-yl)-5H-pyrido[4,3-b]indole-3-carboxylate (3bb)</i>	170
Figure 3.41	¹ H NMR spectrum of <i>tert-butyl 5-benzyl-1-(1-benzyl-1H-indol-2-yl)-5H-pyrido[4,3-b]indole-3-carboxylate (3bc)</i>	170
Figure 3.42	¹³ C NMR spectrum of <i>tert-butyl 5-benzyl-1-(1-benzyl-1H-indol-2-yl)-5H-pyrido[4,3-</i>	171

	<i>b</i>]indole-3-carboxylate (3bc)	
Figure 3.43	HRMS of <i>tert</i> -butyl 5-benzyl-1-(1-benzyl-1 <i>H</i> -indol-2-yl)-5 <i>H</i> -pyrido[4,3- <i>b</i>]indole-3-carboxylate (3bc)	171
Figure 3.44	¹ H NMR spectrum of methyl 5-(4-methoxybenzyl)-1-(1-(4-methoxybenzyl)-1 <i>H</i> -indol-2-yl)-5 <i>H</i> -pyrido[4,3- <i>b</i>]indole-3-carboxylate (3ca)	172
Figure 3.45	¹³ C NMR spectrum of methyl 5-(4-methoxybenzyl)-1-(1-(4-methoxybenzyl)-1 <i>H</i> -indol-2-yl)-5 <i>H</i> -pyrido[4,3- <i>b</i>]indole-3-carboxylate (3ca)	172
Figure 3.46	HRMS of methyl 5-(4-methoxybenzyl)-1-(1-(4-methoxybenzyl)-1 <i>H</i> -indol-2-yl)-5 <i>H</i> -pyrido[4,3- <i>b</i>]indole-3-carboxylate (3ca)	173
Figure 3.47	¹ H NMR spectrum of methyl 5-butyl-1-(1-butyl-1 <i>H</i> -indol-2-yl)-5 <i>H</i> -pyrido[4,3- <i>b</i>]indole-3-carboxylate (3da)	173
Figure 3.48	¹³ C NMR spectrum of methyl 5-butyl-1-(1-butyl-1 <i>H</i> -indol-2-yl)-5 <i>H</i> -pyrido[4,3- <i>b</i>]indole-3-carboxylate (3da)	174
Figure 3.49	HRMS of methyl 5-butyl-1-(1-butyl-1 <i>H</i> -indol-2-yl)-5 <i>H</i> -pyrido[4,3- <i>b</i>]indole-3-carboxylate (3da)	174
Figure 3.50	¹ H NMR spectrum of methyl 8-methoxy-1-(5-methoxy-1-methyl-1 <i>H</i> -indol-2-yl)-5-methyl-5 <i>H</i> -pyrido[4,3- <i>b</i>]indole-3-carboxylate (3ea)	175
Figure 3.51	¹³ C NMR spectrum of methyl 8-methoxy-1-(5-methoxy-1-methyl-1 <i>H</i> -indol-2-yl)-5-methyl-5 <i>H</i> -pyrido[4,3- <i>b</i>]indole-3-carboxylate (3ea)	175
Figure 3.52	HRMS of methyl 8-methoxy-1-(5-methoxy-	176

	<i>1-methyl-1H-indol-2-yl)-5-methyl-5H-pyrido[4,3-b]indole-3-carboxylate (3ea)</i>	
Figure 3.53	¹ H NMR spectrum of methyl 5-tosyl-1-(1-tosyl-1H-indol-2-yl)-2,5-dihydro-1H-pyrido[4,3-b]indole-3-carboxylate (3ga)	176
Figure 3.54	¹³ C NMR spectrum of methyl 5-tosyl-1-(1-tosyl-1H-indol-2-yl)-2,5-dihydro-1H-pyrido[4,3-b]indole-3-carboxylate (3ga)	177
Figure 3.55	HRMS of methyl 5-tosyl-1-(1-tosyl-1H-indol-2-yl)-2,5-dihydro-1H-pyrido[4,3-b]indole-3-carboxylate (3ga)	177
Figure 3.56	¹ H NMR spectrum of 1-methyl-1H-indole (12a)	178
Figure 3.57	¹³ C NMR spectrum of 1-methyl-1H-indole (12a)	178
Figure 3.58	¹ H NMR spectrum of 1-benzyl-1H-indole (12b)	179
Figure 3.59	¹³ C NMR spectrum of 1-benzyl-1H-indole (12b)	179
Figure 3.60	¹ H NMR spectrum of 5-methoxy-1-methyl-1H-indole (12e)	180
Figure 3.61	¹³ C NMR spectrum of 5-methoxy-1-methyl-1H-indole (12e)	180
Figure 3.62	¹ H NMR spectrum of 1-methyl-5-phenyl-1H-indole (12f)	181
Figure 3.63	¹³ C NMR spectrum of 1-methyl-5-phenyl-1H-indole (12f)	181
Figure 3.64	¹ H NMR spectrum of 5-bromo-1-methyl-1H-indole (12i)	182
Figure 3.65	¹³ C NMR spectrum of 5-bromo-1-methyl-1H-indole (12i)	182
Figure 3.66	¹ H NMR spectrum of ethyl 1-butyl-1H-indole-2-carboxylate (14d)	183

Figure 3.67	^{13}C NMR spectrum of <i>ethyl 1-butyl-1H-indole-2-carboxylate</i> (14d)	183
Figure 3.68	^1H NMR spectrum of <i>ethyl 1-tosyl-1H-indole-2-carboxylate</i> (14g)	184
Figure 3.69	^{13}C NMR spectrum of <i>ethyl 1-tosyl-1H-indole-2-carboxylate</i> (14g)	184
Figure 3.70	^1H NMR spectrum of <i>1H-indole-2-carbaldehyde</i> (15)	185
Figure 3.71	^{13}C NMR spectrum of <i>1H-indole-2-carbaldehyde</i> (15)	185
Chapter 4	One-pot synthesis of furo[3,2-<i>c</i>]pyridines and benzofuro[3,2-<i>c</i>]pyridines: Development of isatin molecular hybrids for treatment of tuberculosis	193–236
Figure 4.1	Potent anti-mycobacterial compounds targeting Pks13; (A) The structure of TAM16, (B) The furopyridine derivative active against MDR-TB	195
Figure 4.2	DFT relative energy calculation for the formation of furo or benzofuro[3,2- <i>c</i>]pyridines 9a over furo or benzofuro[3,2- <i>d</i>]pyridines 9c regioisomer using B3LYP/6-311++G** level of theory	203
Figure 4.3	Anti-tuberculosis studies of furopyridine-isatin hybrid 15ba on non-virulent strain <i>Mycobacterium smegmatis</i>	206
Figure 4.4	Anti-tuberculosis studies of furopyridine-isatin hybrid 15ba on virulent strain <i>Mycobacterium bovis</i> BCG	207
Figure 4.5	^1H NMR spectrum of <i>methyl 4-(furan-2-yl)furo[3,2-<i>c</i>]pyridine-6-carboxylate</i> (3aa)	219

Figure 4.6	¹³ C NMR spectrum of <i>methyl 4-(furan-2-yl)furo[3,2-c]pyridine-6-carboxylate (3aa)</i>	220
Figure 4.7	HRMS of <i>methyl 4-(furan-2-yl)furo[3,2-c]pyridine-6-carboxylate (3aa)</i>	220
Figure 4.8	¹ H NMR spectrum of <i>ethyl 4-(furan-2-yl)furo[3,2-c]pyridine-6-carboxylate (3ab)</i>	221
Figure 4.9	¹³ C NMR spectrum of <i>ethyl 4-(furan-2-yl)furo[3,2-c]pyridine-6-carboxylate (3ab)</i>	221
Figure 4.10	HRMS of <i>ethyl 4-(furan-2-yl)furo[3,2-c]pyridine-6-carboxylate (3ab)</i>	222
Figure 4.11	¹ H NMR spectrum of <i>tert-butyl 4-(furan-2-yl)furo[3,2-c]pyridine-6-carboxylate (3ac)</i>	222
Figure 4.12	¹³ C NMR spectrum of <i>tert-butyl 4-(furan-2-yl)furo[3,2-c]pyridine-6-carboxylate (3ac)</i>	223
Figure 4.13	HRMS of <i>tert-butyl 4-(furan-2-yl)furo[3,2-c]pyridine-6-carboxylate (3ac)</i>	223
Figure 4.14	¹ H NMR spectrum of <i>methyl 2-methyl-4-(5-methylfuran-2-yl)furo[3,2-c]pyridine-6-carboxylate (3ba)</i>	224
Figure 4.15	¹³ C NMR spectrum of <i>methyl 2-methyl-4-(5-methylfuran-2-yl)furo[3,2-c]pyridine-6-carboxylate (3ba)</i>	224
Figure 4.16	¹ H NMR spectrum of <i>methyl 1-(benzofuran-2-yl)benzofuro[3,2-c]pyridine-3-carboxylate (3da)</i>	225
Figure 4.17	¹³ C NMR spectrum of <i>methyl 1-(benzofuran-2-yl)benzofuro[3,2-c]pyridine-3-carboxylate (3da)</i>	225
Figure 4.18	HRMS of <i>methyl 1-(benzofuran-2-yl)benzofuro[3,2-c]pyridine-3-carboxylate (3da)</i>	226
Figure 4.19	¹ H NMR spectrum of <i>ethyl 1-(benzofuran-</i>	226

	<i>2-yl)benzofuro[3,2-c]pyridine-3-carboxylate (3db)</i>	
Figure 4.20	¹³ C NMR spectrum of <i>ethyl 1-(benzofuran-2-yl)benzofuro[3,2-c]pyridine-3-carboxylate (3db)</i>	227
Figure 4.21	HRMS of <i>ethyl 1-(benzofuran-2-yl)benzofuro[3,2-c]pyridine-3-carboxylate (3db)</i>	227
Figure 4.22	¹ H NMR spectrum of <i>tert-butyl 1-(benzofuran-2-yl)benzofuro[3,2-c]pyridine-3-carboxylate (3dc)</i>	228
Figure 4.23	¹³ C NMR spectrum of <i>tert-butyl 1-(benzofuran-2-yl)benzofuro[3,2-c]pyridine-3-carboxylate (3dc)</i>	228
Figure 4.24	Mass data of <i>tert-butyl 1-(benzofuran-2-yl)benzofuro[3,2-c]pyridine-3-carboxylate (3dc)</i>	229
Figure 4.25	¹ H NMR spectrum of <i>(2-methyl-4-(5-methylfuran-2-yl)furo[3,2-c]pyridin-6-yl)methanol (10ba)</i>	229
Figure 4.26	¹³ C NMR spectrum of <i>(2-methyl-4-(5-methylfuran-2-yl)furo[3,2-c]pyridin-6-yl)methanol (10ba)</i>	230
Figure 4.27	HRMS of <i>(2-methyl-4-(5-methylfuran-2-yl)furo[3,2-c]pyridin-6-yl)methanol (10ba)</i>	230
Figure 4.28	Mass data of <i>2-methyl-4-(5-methylfuran-2-yl)-6-((prop-2-yn-1-yloxy)methyl)furo[3,2-c]pyridine (11ba)</i>	230
Figure 4.29	¹ H NMR spectrum of <i>1-(2-bromoethyl)indoline-2,3-dione (13)</i>	231
Figure 4.30	¹³ C NMR spectrum of <i>1-(2-bromoethyl)indoline-2,3-dione (13)</i>	231
Figure 4.31	¹ H NMR spectrum of <i>1-(2-</i>	232

	<i>azidoethyl</i>)indoline-2,3-dione (14)	
Figure 4.32	¹³ C NMR spectrum of <i>1</i> -(2- <i>azidoethyl</i>)indoline-2,3-dione (14)	232
Figure 4.33	¹ H NMR of <i>1</i> -(2-(4-(((2-methyl-4-(5- <i>methylfuran</i> -2-yl)furo[3,2- <i>c</i>]pyridin-6- yl)methoxy)methyl)-1 <i>H</i> -1,2,3-triazol-1- yl)ethyl)indoline-2,3-dione (15ba)	233
Figure 4.34	HRMS of <i>1</i> -(2-(4-(((2-methyl-4-(5- <i>methylfuran</i> -2-yl)furo[3,2- <i>c</i>]pyridin-6- yl)methoxy)methyl)-1 <i>H</i> -1,2,3-triazol-1- yl)ethyl)indoline-2,3-dione (15ba)	233
Chapter 5	Conclusions and scope for future work	237–240

List of Tables

Chapter 1	Introduction	1–26
Chapter 2	Serendipitous base-catalyzed condensation-heteroannulation of iminoesters: A regioselective route to the synthesis of 4,6-disubstituted 5- azaindoles	27–106
Table 2.1	Optimization of reaction conditions for formation of 3aa	30
Chapter 3	Synthesis of 1-indolyl-3,5,8-substituted γ-carbolines: One-pot solvent-free protocol and biological evaluation	107–192
Table 3.1	Optimization of reaction conditions	111–112
Table 3.2	Optical data for γ-carboline 3ac	120
Table 3.3	IC ₅₀ values of γ-carbolines 3ac , 3bc , 3ca , 3ga and doxorubicin in various cancer cell lines	123

Chapter 4	One-pot synthesis of furo[3,2-<i>c</i>]pyridines and benzofuro[3,2-<i>c</i>]pyridines: Development of isatin molecular hybrids for treatment of tuberculosis	193–236
Table 4.1	Optimization of reaction conditions	197
Chapter 5	Conclusions and Scope for Future Work	237–240

List of Schemes

Chapter 1	Introduction	1–26
Scheme 1.1	Palladium-catalyzed one-pot synthesis of 4-, 5-, 6-, and 7-azaindoles	5
Scheme 1.2	Palladium-catalyzed cascade C–N cross-coupling/Heck reaction	5
Scheme 1.3	Selenium catalyzed intramolecular amination of substituted <i>o</i> -vinyl aminopyridines 16 for the synthesis of 1,2,3-trisubstituted azaindoles 17	6
Scheme 1.4	Palladium-catalyzed hetero-annulation reaction of 2- or 6-chloro-4-acetamido-3-iodopyridines 18 with <i>p</i> -substituted diaryl alkynes	7
Scheme 1.5	[3+2] Dipolar cycloaddition for the synthesis of 2,3-disubstituted-5-azaindoles	7
Scheme 1.6	Cu/Ir mediated stereoselective synthesis of tetrahydro- γ -carboline	8
Scheme 1.7	Heterocyclization of α -indol-2-	8

	ylmethyl TosMIC derivative in the presence of an electrophile to 1,3-disubstituted γ -carbolines	
Scheme 1.8	Synthesis of ingenine B derivative	9
	32	
Scheme 1.9	Palladium-catalyzed C-H activation/nitrile addition/heterocyclization for the synthesis of β - and γ -carbolines	10
Scheme 1.10	Iodine catalyzed formal [3+3] cycloaddition to synthesize spirodihydro carbolines	11
Scheme 1.11	Synthesis of 2-aryl-2,3- dihydrofuropyridines	11
Scheme 1.12	Silver catalyzed anion relay enabled [3+3] annulations	12
Scheme 1.13	DDQ catalyzed synthesis of dihydrofuro[3,2-c]pyridine-2,3- dicarbonitriles	12
Scheme 1.14	Synthesis of 2,6-disubstituted furo[3,2-c]pyridine	13
Scheme 1.15	Synthesis of substituted benzofuro[3,2-c]pyridine	13
Chapter 2	Serendipitous base-catalyzed condensation-heteroannulation of iminoesters: A regioselective route to the synthesis of 4,6- disubstituted 5-azaindoles	27–106
Scheme 2.1	Imination of pyrrole-2- carboxaldehydes: A comparison between previous and present studies	29
Scheme 2.2	Synthesis of 5-azaindole derivatives	33
	3aa–fa	

Scheme 2.3	Plausible mechanism for the formation of the 5-azaindole core	35
Scheme 2.4	Relative energy between the formation of 5-azaindole (9a) and 6-azaindole (9c) regioisomers calculated using the B3LYP/6-311++G** level of theory	36
Scheme 2.5	Synthesis of novel 5-azaindole derivatives	37
Scheme 2.6	Effects of C-4 and C-5 substituents on the heterocyclization	38
Scheme 2.7	Synthesis of a possible CB2 agonist molecule	39
Scheme 2.8	Crossover experiment to form 5-azaindole 16	40
Chapter 3	Synthesis of 1-indolyl-3,5,8-substituted γ-carbolines: One-pot solvent-free protocol and biological evaluation	107–192
Scheme 3.1	The synthetic strategy of present work in comparison with previous reports	109
Scheme 3.2	Series of 1-indolyl-3,5,8-substituted γ -carboline 3aa–ac , 3ba–ea and 1-indolyl-1,2-dihydro-3,5-substituted γ -carboline 3ga derivatives	113
Scheme 3.3	Plausible mechanism for the formation of 1,2-dihydro- γ -carboline derivative 3ga and 1-indolyl-3,5,8-substituted γ -carbolines 3aa–ac and 3ba–ea	116

Scheme 3.4	Synthesis of <i>N</i> -substituted indole-2-carboxaldehyde derivatives 1a , 1b , 1e , and 1f	126
Scheme 3.5	Preparation of 12f by Suzuki (sp^2C - sp^2C) reaction	127
Scheme 3.6	Synthesis of <i>N</i> -substituted indole-2-carboxaldehyde derivatives 1d and 1g	127
Scheme 3.7	Synthesis of <i>N</i> -substituted indole-2-carboxaldehydes 1c and 1h	128
Chapter 4	One-pot synthesis of furo[3,2-<i>c</i>]pyridines and benzofuro[3,2-<i>c</i>]pyridines: Development of isatin molecular hybrids for treatment of tuberculosis	193–236
Scheme 4.1	Synthesis of furo[3,2- <i>c</i>]pyridine derivatives 3aa–ba and benzofuro[3,2- <i>c</i>]pyridine derivatives 3da–dc	198
Scheme 4.2	Plausible mechanism for the formation of 4-(furo-2-yl) furo[3,2- <i>c</i>]pyridine-6-carboxylate 3aa–ba and 1-(benzofuro-2-yl) benzofuran[3,2- <i>c</i>]pyridine-3-carboxylate 3da–3dc derivatives	201
Scheme 4.3	Synthesis of terminal alkyne derivative 11ba	204
Scheme 4.4	Synthesis of azido isatin derivative 14	205
Scheme 4.5	Synthesis of triazole-tethered furopyridine-isatin hybrid 15ba	205
Chapter 5	Conclusions and scope for future work	237–240

Acronyms

Abbreviations used for solvents, techniques, substituents, reagents, etc., are largely in accordance with the recommendations of the IUPAC-IUB commission on Biochemical Nomenclature, 1974, Pure and Applied Chemistry. Few additional abbreviations used in this thesis are listed below.

ACN	Acetonitrile
Bn	Benzyl
Boc	<i>tert</i> -butoxycarbonyl
CDCl ₃	Chloroform-d
DCM	Dichloromethane
DIPEA	Diisopropylethyl amine
DMAP	4-Dimethylaminopyridine
DMF	Dimethyl formamide
DMSO	Dimethyl sulfoxide
ESI-MS	Electrospray Ionization Mass Spectrum
Et	Ethyl
EtOAc	Ethyl acetate
HCl	Hydrochloric acid
HRMS	High Resolution Mass Spectrum
MeOH	Methanol
Na ₂ SO ₄	Sodium sulphate
NaCl	Sodium chloride
NaHCO ₃	Sodium hydrogen carbonate
<i>n</i> -Bu	<i>n</i> -Butyl
NMR	Nuclear Magnetic Resonance
PhSO ₂	Phenyl Sulfonyl
PMB	<i>para</i> -Methoxy Benzyl

^t Bu	Tertiary butyl
THF	Tetrahydrofuran
Ts	Tosyl

Symbols/Units

α	Alfa
Å	Angstrom
a. u.	Arbitrary Unit
β	Beta
cm	Centimetre
°	Degree
°C	Degree Centigrade
δ	Delta
ϵ	Extinction coefficient
γ	Gamma
μm	Micrometre
μM	Micromolar
mmol	Millimole
mL	Millilitre
μL	Microlitre
nm	Nanometre
nM	Nanomolar
π	Pi
λ	Wavelength

Chapter 1

Introduction

1.1 Fused-pyrido heterocycles

Nitrogen-containing heterocyclic compounds are the most privileged class of organic compounds. These are present in the core of a wide range of bio-molecules such as nucleic acids, amino acids, vitamins, and carbohydrates, and alkaloids (Figure 1.1).

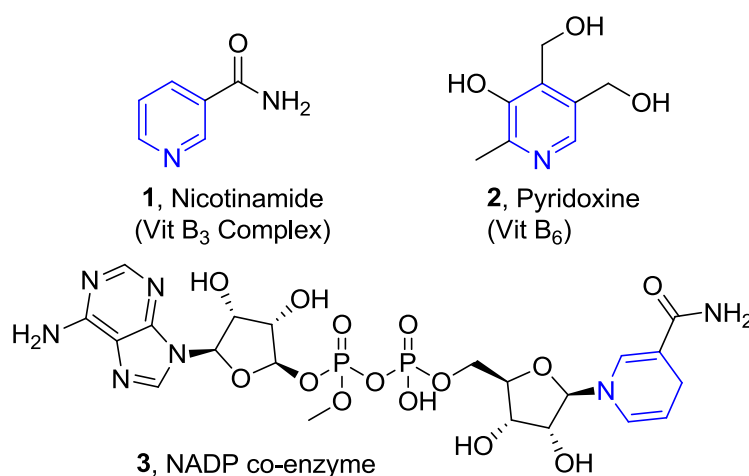


Figure 1.1 Pyridine subunit highlighted in the biomolecules 1–3

The aza-heterocycles are prevalent in the number of drug molecules, and new entries are added in the list every year. The structural analysis of FDA approved small-molecule drugs in the year 2019 confirm that around 85% of drugs (27 out of 32) belong to the category of nitrogen-heterocycles [1]. Moreover, most of the approved small molecules are anticancer drugs (Figure 1.2). Six-membered nitrogen atom containing heterocyclic unit, i.e., a pyridine ring, is present in many natural products such as vitamins, co-enzymes, and alkaloids. Nature has preferred pyridine moiety in these bio-molecules to improve water solubility using its innate weak basicity.

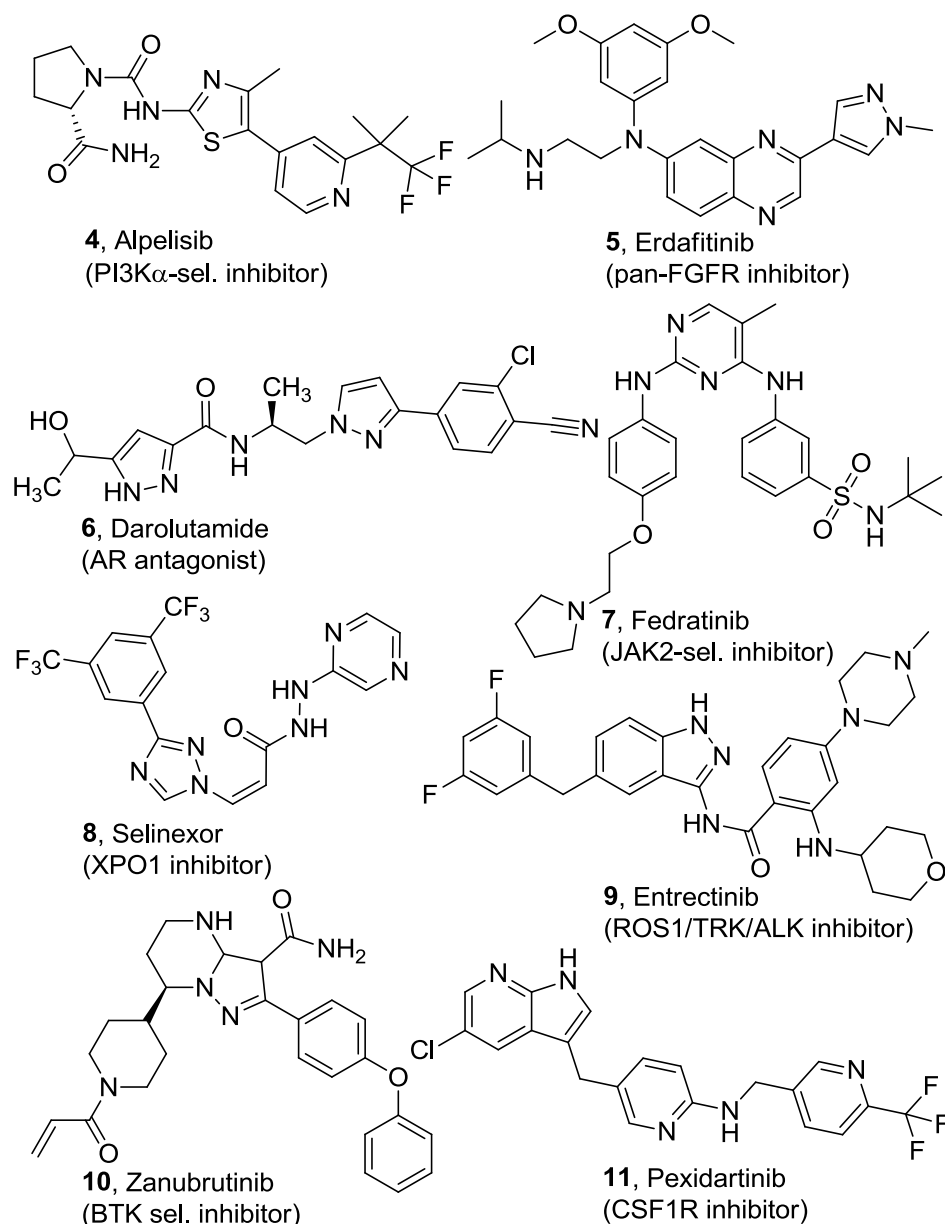


Figure 1.2 US-FDA approved aza-heterocyclic small molecules **4–11** for oncology in 2019

The fused-pyrido heterocycles mainly constitute pyrrollopyridines (azaindoles), furopyridines, and thienopyridines in 5:6 (bicyclic) systems. Indolopyridines (carbolines), benzofuropyridines, and benzothienopyridines are the members of 6:5:6 (tricyclic) systems.

According to the position of the heteroatom in the pyrrollopyridine or azaindole, the heterocyclic system is designated as 4-, 5-, 6- or 7-

azaindole in a 5:6 bicyclic system (both rings have a nitrogen heteroatom) or in the case of benzo-fused azaindole, the heterocyclic system is called as α -, β -, γ -, or δ -carboline or indolopyridine in a 6:5:6 tricyclic system. The respective position of the oxygen and nitrogen atoms in furopyridines constitute four isomers of this class (Figure 1.3).

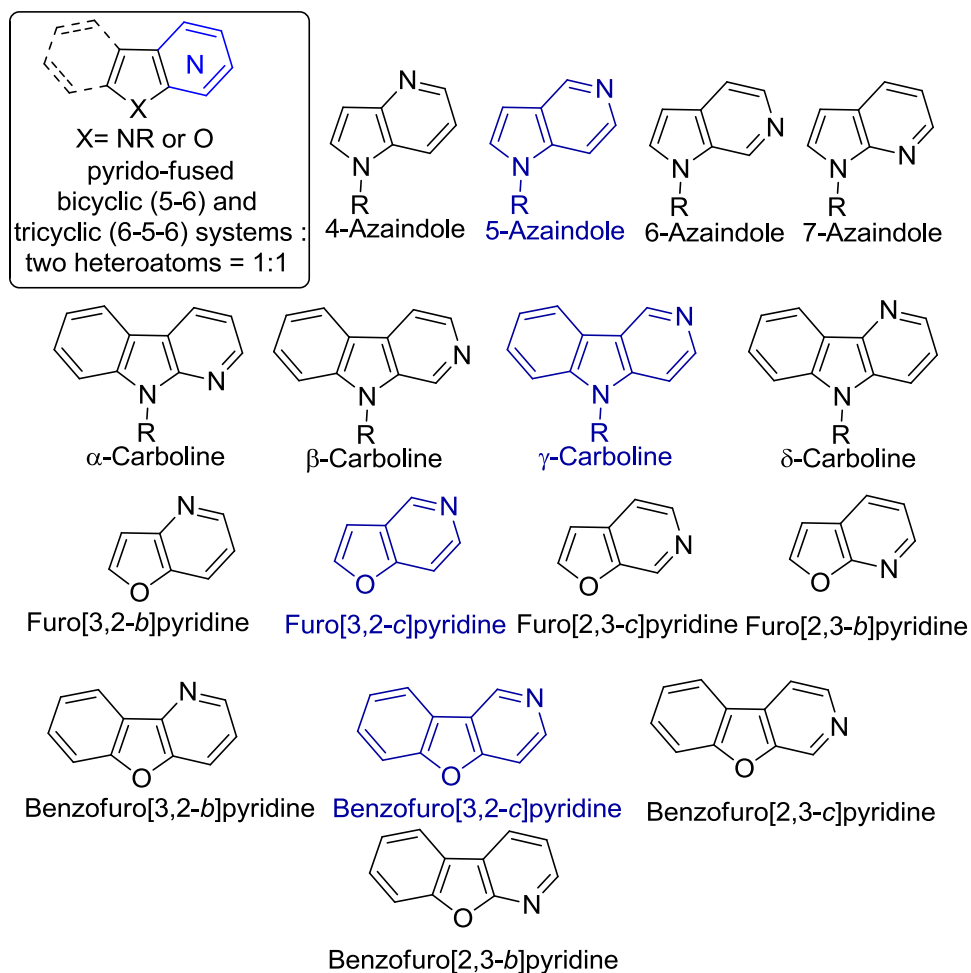


Figure 1.3 Pyrido-fused bicyclic (5-6) and tricyclic (6-5-6) systems with two heteroatoms (1:1)

Azaindoles are rare in nature; few examples like variolins are present in marine alkaloids. However, many synthetic azaindoles are an integral part of various drug-like molecules, including several kinase inhibitors [2]. β -carboline sub-unit is often present in indole alkaloids [3]. Other carboline isomers viz., α -carboline, γ -carboline, and δ -carboline are

mostly synthetic and extensively used in drug-like molecular architectures [4].

In the past two decades, furopyridines have emerged as crucial structural subunits in drug-like molecules due to their structural analogy with indoles and azaindoles [5]. The recent applications of benzofuran [6] and pyridofuran [7] derivatives as Pks13 inhibitors to control mycolic acid synthesis in *Mycobacterium tuberculosis* have attracted a tremendous amount of attention from the scientific community. Inhibitors of Pks13, including the most potent TAM16 (MIC 0.09 μ M), belong to the benzofuran-5-ol framework and is structurally very close to furo[3,2-*c*]pyridine. Benzofuro[3,2-*c*]pyridine is another member of the class with critical biological applications [8].

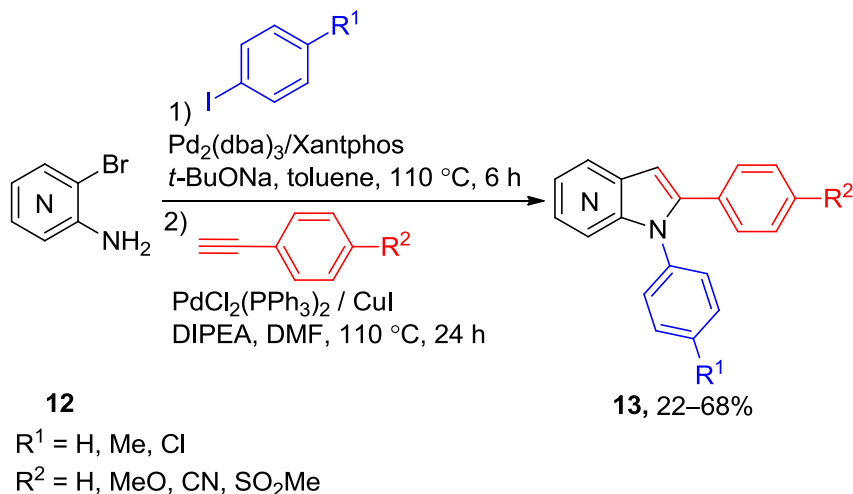
The research work described in this thesis revolves around the design and development of synthetic protocols for the synthesis of fused-pyrido heterocycles such as 5-azaindoles, γ -carbolines, furo[3,2-*c*]pyridine, and benzofuro[3,2-*c*]pyridines (highlighted chemical structures in figure 1.3) and their biological applications. Therefore, in this chapter, we provide a review of the synthesis and applications of the above-mentioned heterocyclic frameworks.

1.2 Review of recent literature for the synthesis of fused-pyrido heterocycles

1.2.1 Synthesis of azaindoles and carbolines

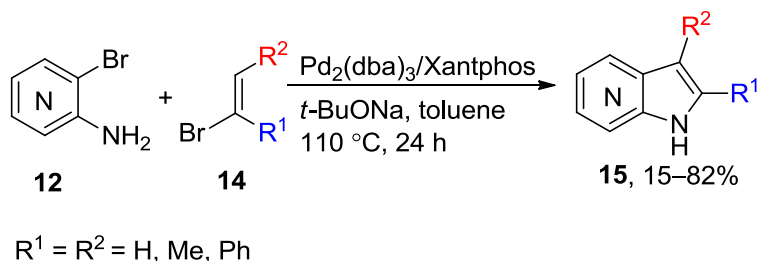
Purificação *et al.* have recently introduced a palladium-catalyzed versatile approach to synthesize 4-, 5-, 6-, and 7-azaindoles [9]. The developed one-pot synthesis has a broad substrate scope compatibility with electron-withdrawing and electron-donating groups. In this method, *o*-aminobromopyridines **12** undergoes *N*-arylation, followed by the Sonogashira coupling reaction with substituted terminal aryl alkynes, and subsequent cyclization in one-pot to furnish *N*-substituted-2-aryl-4- or 5-

or 6- or 7-azaindoles **13** in 22-68% yields. The straightforward procedure developed herein avoids multiple purification steps and gives an excellent yield of the product (Scheme 1.1).



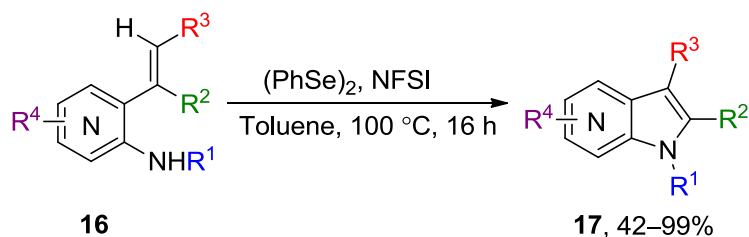
Scheme 1.1 Palladium-catalyzed one-pot synthesis of 4-, 5-, 6-, and 7-azaindoles

Pires *et al.* have developed a one-pot palladium-catalyzed cascade C–N cross-coupling/Heck reaction of alkenyl bromides **14** with *o*-aminobromopyridines **12** as a practical approach for the synthesis of 2,3-disubstituted azaindoles **15** via one-step methodology [10]. The substrate scope is broad, and several substituted 2,3-disubstituted azaindoles **15** have been prepared by this procedure (Scheme 1.2).



Scheme 1.2 Palladium-catalyzed cascade C–N cross-coupling/Heck reaction

Ortgies *et al.* synthesized various 1,2,3-trisubstituted substituted azaindoles **17** by selenium catalyzed intramolecular amination of substituted *o*-vinyl aminopyridines **16** using *N*-fluorobenzenesulfonimide as an oxidant [11]. In this methodology, selenium catalyst activates alkene side-chain for the formation of C(sp²)-N bond leading to intramolecular amination. The developed protocol shows excellent functional group tolerance resulting in the synthesis of a library of azaindole heterocycles (Scheme 1.3).



R¹ = Ts, Ns, Ms, Ac

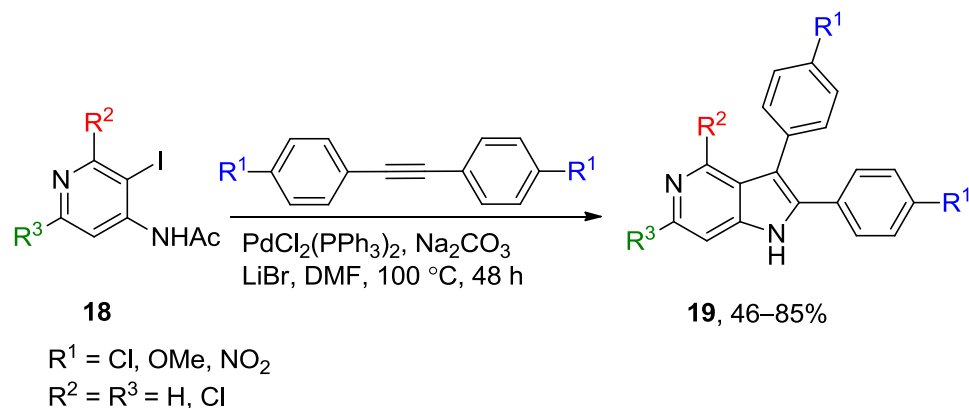
R² = H, alkyl, aryl

R³ = Alkyl, aryl

R⁴ = H, Me, CF₃, F, Cl, Br

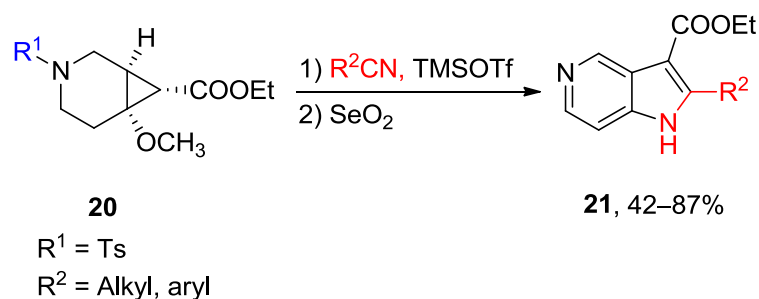
Scheme 1.3 Selenium catalyzed intramolecular amination of substituted *o*-vinyl aminopyridines **16** for the synthesis of 1,2,3-trisubstituted azaindoles **17**.

Calvet *et al.* demonstrated that 2- or 6-chloro-4-acetamido-3-iodopyridines **18** could readily undergo hetero-annulation reaction with *p*-substituted diaryl alkynes in the presence of palladium catalyst [12]. The optimized reaction herein provides 2,3,4,6-tetrasubstituted 5-azaindoles **19** in excellent yields (Scheme 1.4).



Scheme 1.4 Palladium-catalyzed hetero-annulation reaction of 2- or 6-chloro-4-acetamido-3-iodopyridines **18** with p -substituted diaryl alkynes

Moustafa *et al.* reported [3+2] dipolar cycloaddition between substituted 3,4-cyclopropano-*N*-tosylpiperidines **20** and alkyl or aryl nitriles [13] followed by oxidation using SeO_2 , detosylation, and aromatization to furnish 2,3-disubstituted 5-azaindoles **21** in excellent yields. The substrates are easy to prepare, and the authors have reported a gram-scale synthesis of the same (Scheme 1.5).

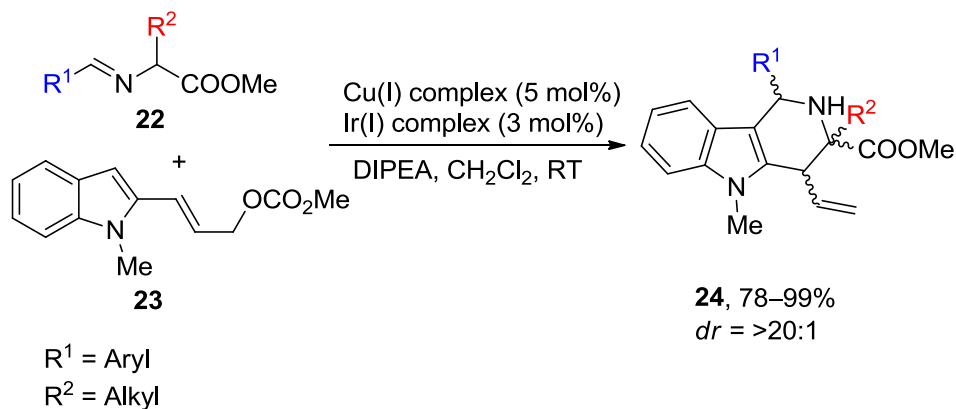


Scheme 1.5 [3+2] Dipolar cycloaddition for the synthesis of 2,3-disubstituted-5-azaindoles

1.2.2 Synthesis of γ -carboline

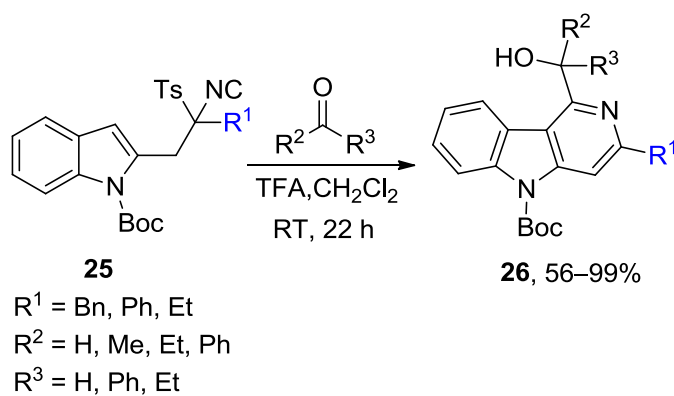
Xu *et al.* have recently reported a synergistic copper/iridium catalyzed asymmetric cascade allylation reaction of aldimine esters **22** and

indolyl allylic carbonates **23** [14] for the synthesis of several tetrahydro- γ -carboline **24** with multiple chiral centers in high stereo-selectivity and optical purity (Scheme 1.6).



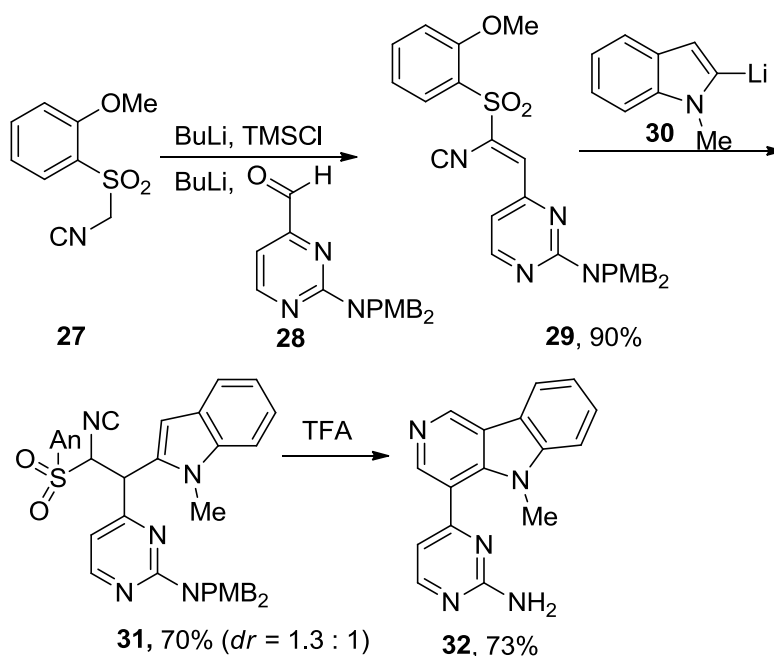
Scheme 1.6 Cu/Ir mediated stereoselective synthesis of tetrahydro- γ -carboline

In TosMIC (tosylmethyl isocyanide) chemistry, isocyanide derivatives are important building blocks due to the amphiphilic nature of the isocyanide moiety. The cyclization of a TosMIC derivative by aromatic electrophilic substitution and isocyanide attack on electrophile often occurs in a tandem process. Gutierrez *et al.* have recently reported (Scheme 1.7) preparation of a series of 1,3-disubstituted γ -carboline **26** by heterocyclization of α -indol-2-yl-methyl TosMIC **25** in the presence of trifluoroacetic acid or aluminum chloride and an electrophile [15].



Scheme 1.7 Heterocyclization of α -indol-2-ylmethyl TosMIC derivative in the presence of an electrophile to 1,3-disubstituted γ -carbolines

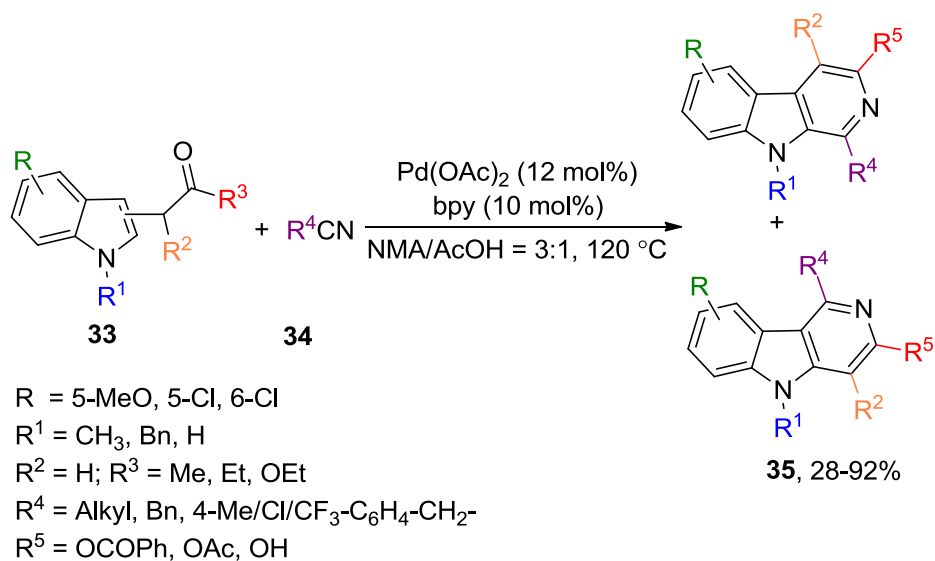
Chepyshev *et al.* have synthesized *N*-methyl ingenine B, a natural product using isocyanide chemistry (Scheme 1.8). The natural product, ingenine B (γ -carboline alkaloid, **58** shown in figure 1.6) was first isolated from the Indonesian sponge *Acanthostrongylophora ingens* and was found to have prominent cytotoxicity against murine lymphoma cells L5178Y. *o*-Methoxyaryl-2-sulfonylmethylisocyanide **27** undergoes *in situ* silylation/olefination with aldehyde **28** to provide alkenyl isocyanide **29**. The conjugate addition of **29** with lithiated *N*-methyl indole **30** provides sulfonylisocyanide derivative **31**, which on exposure to trifluoroacetic acid was converted to *N*-methyl ingenine B **32** [16].



Scheme 1.8 Synthesis of ingenine B derivative **32**

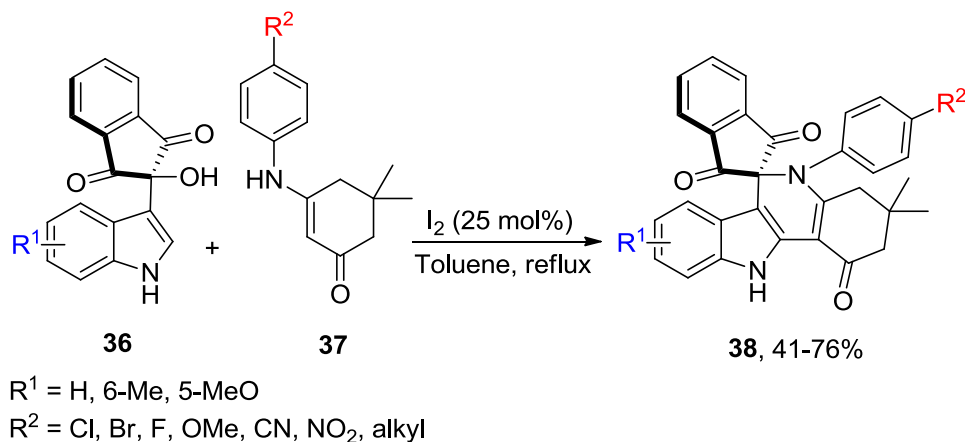
Wang *et al.* have developed a novel protocol for synthesis of substituted β - and γ -carbolines through redox-free palladium-catalyzed heterocyclization of C(3) or C(2)-substituted indoles and nitriles [17]. 1-(1-Methyl or benzyl-1*H*-indol-3/2-yl)propan-2-one or acetate **33** undergoes Pd catalyzed C-H activation to make a palladium complex. The

co-ordination of nitrile compound **34** to Pd-center gives a ketimine intermediate, which leads to the formation of β - or γ -carboline framework **35**.



Scheme 1.9 Palladium-catalyzed C-H activation/nitrile addition/heterocyclization for the synthesis of β - and γ -carboline

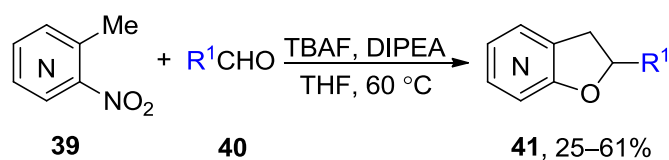
Hao *et al.* developed a simple but efficient method for the synthesis of spirodihydro carboline [18]. A catalytic amount of iodine promotes dehydration of indolyl alcohol derivative **36**, leading to an indolyl carbocation formation. The attack of enaminone **37** on this carbocation induces a cascade [3+3] cycloaddition to furnish γ -carboline core **38** in moderate to good yields (Scheme 1.10).



Scheme 1.10 Iodine catalyzed formal [3+3] cycloaddition to synthesize spirodihydro carbolines

1.2.3 Synthesis of furo[3,2-*c*]pyridines

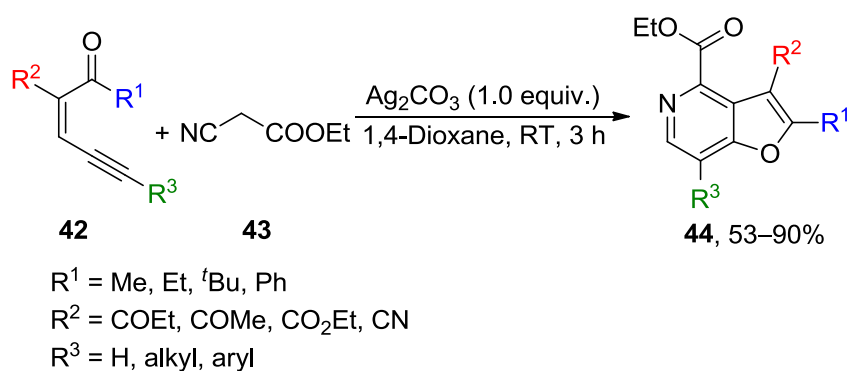
Kueth developed a rapid strategy to access 2-aryl-2,3-dihydrofuro[3,2-*b*], [3,2-*c*], and [2,3-*b*]pyridines **41** from *o*-nitropicolines **39** and aryl aldehydes in the presence of tetrabutylammonium fluoride and Hunig's base (DIPEA) [19]. In the presence of a base, *o*-nitropicoline **39** and aryl aldehydes **40** condense to form an aldol product (Scheme 1.11). The aldol intermediate is activated by tetrabutylammonium fluoride in the presence of a polar aprotic solvent at high temperature for aromatic nucleophilic substitution leading to the replacement of nitro group on the pyridine ring and furnish the 2-aryl-2,3-dihydrofuro[3,2-*b*]pyridines **41**.



Scheme 1.11 Synthesis of 2-aryl-2,3-dihydrofuro[3,2-*b*]pyridines

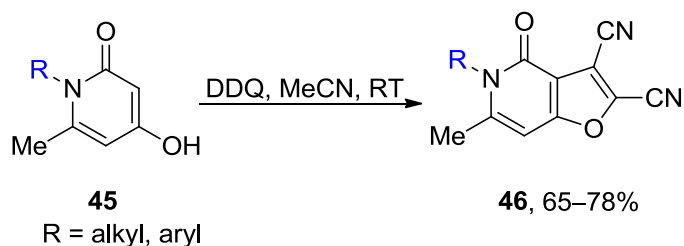
Anion relay enabled [3+3] annulation of conjugated ene-yne-ketones **42** and active methylene isocyanides **43** was developed by Dong

et al. for efficient synthesis of biologically valuable furo[3,2-*c*]pyridine derivatives [20]. Silver carbonate abstracts a proton from the active methylene center of isocyanide **43** to form a carbanion, which undergoes intermolecular Michael addition on α,β -unsaturated ketone **42** to form an intermediate. Next, a silver catalyzed anion relay-based cycloaddition enables the formation of densely substituted furo[3,2-*c*]pyridines **44** (Scheme 1.12).



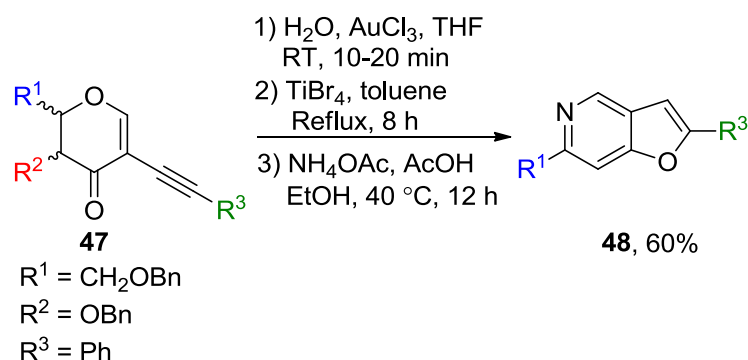
Scheme 1.12 Silver catalyzed anion relay enabled [3+3] annulation

Li *et al.* developed a new methodology for synthesis of N-substituted-6-methyl-4-oxo-4,5-dihydrofuro[3,2-*c*]pyridine-2,3-dicarbonitriles **46** using 2,3-dichloro-5,6-dicyanobenzoquinone (DDQ) as building block and oxidant [21]. The methodology resulted in the formation of furan-based heterocycles from simple synthetic precursors such as N-substituted 4-hydroxyl-5-methylpyridinones **45**.



Scheme 1.13 DDQ catalyzed synthesis of dihydrofuro[3,2-*c*]pyridine-2,3-dicarbonitriles

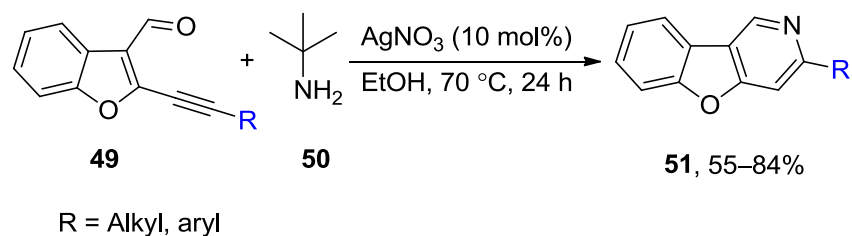
Mal *et al.* described a gold (III) catalyzed route for synthesis of chiral 3-formyl furans from suitably protected (1-alkynyl)-2,3-dihydropyran-4-one **47** [22]. The furan derivative was transformed into a corresponding 1,5-dicarbonyl compound through a titanium tetrabromide catalyzed reaction, which on further treatment with ammonium acetate under mildly acidic conditions form furo[3,2-*c*]pyridine derivative **48** (Scheme 1.14).



Scheme 1.14 Synthesis of 2,6-disubstituted furo[3,2-*c*]pyridine

1.2.4 Synthesis of benzofuro[3,2-*c*]pyridines

Kumar *et al.* devised a silver catalyzed tandem approach to synthesize benzofuopyridines by the reaction of *o*-alkynyl aldehyde with *tert*-butylamine under mild conditions [23]. A series of deuterium labeling experiments determined the role of solvent ethanol in the protocol (Scheme 1.15).



Scheme 1.15 Synthesis of substituted benzofuro[3,2-*c*]pyridines

1.3 The role of 5-azaindoles in cancer therapy

Cancer is a common name for a large group of malignant diseases. The disease cancer may begin from a single abnormal cell, and it is characterized by excessive and uncontrolled cell growth leading to the formation of tumors. The abnormal cells slowly spread throughout the body (metastasis) and result in several other health complications [24].

Kinases are enzymes to regulate the activation (by phosphorylation) of biomolecules by using ATP. The human kinome comprises more than 500 protein kinases, which play a vital role in cell cycle management. These protein kinases are excellent targets in oncology, and protein kinases inhibition has been widely explored in cancer research [2].

Azaindoles (pyrrollopyridines) are the closest bio-isostere of indoles and purines. They are rare in nature except for few marine alkaloids like variolins (Figure 1.4). Variolin B was first isolated from rare antarctic sponge *Kirkpatrickia variolosa* in 1994. It was later found to be a potent cyclin-dependent kinases (CDKs) inhibitor regulating the cell cycle by taking control of cell division, cell differentiation, and apoptosis [25].

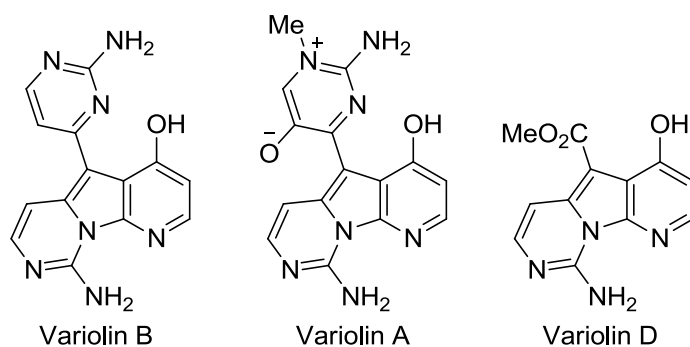
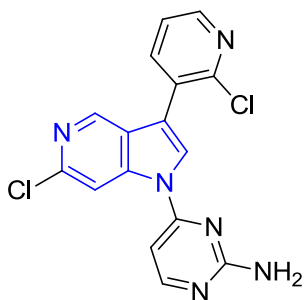


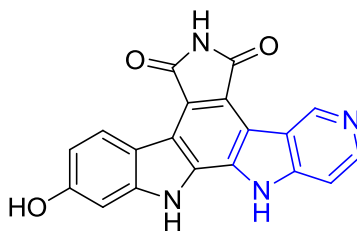
Figure 1.4 Natural azaindole derivatives found in antarctic sponges: Variolins

Cell division cycle 7 kinase (cdc7 kinase) is a protein kinase, responsible for cell cycle regulation with the help of DNA helicase enzyme that unwinds DNA double-strand. The function of cdc7 kinase is essential in the initiation of DNA replication. A very high concentration of cdc7 kinase has been noticed in several types of cancers, including leukemia, breast, lung, and colon cancers. Bryan and co-workers have developed 5-azaindole core-based potent and selective cdc7 kinase inhibitor **52** (Figure 1.5) with improved metabolic stability [26].

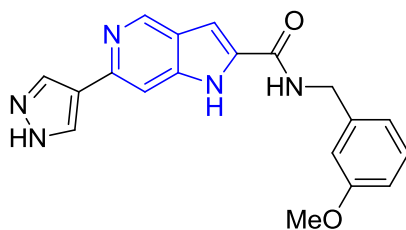
Chk1 or checkpoint kinase 1 regulates DNA damage response in the cell cycle. It helps in maintaining sustainable growth in healthy cells by keeping the damaged cells out of the system. Lefoix *et al.* have discovered a series of symmetrical and unsymmetrical 5-azaindolocarbazole **53** (Figure 1.5) and proved their potent chk1 inhibition activity experimentally. These compounds have significant applications in multi-drug anticancer therapy [27].



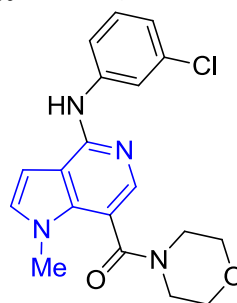
52, Cdc7 Kinase inhibitor
(IC₅₀ = 30 nM)



53, Chk1 inhibitor
(IC₅₀ = 14 nM)



54, Rho Kinase inhibitor
ROCK-I; IC₅₀ = 0.87 μ M
ROCK-II; IC₅₀ = 0.19 μ M



55, CB2 agonist (GSK554418A)
CB2 EC₅₀ = 5 nM
CB1 EC₅₀ = 6300 nM

Figure 1.5 Biologically active 5-azaindole derivatives

Rho-kinase (ROCK) plays a fundamental role in cell-signaling pathways responsible for cell adhesion-migration and cellular contractions. Rho-kinase inhibition has been profoundly studied in cancer metastasis. Moreover, ROCK inhibition has also been studied in the management and therapy of hypertension, glaucoma, asthma, stroke, and erectile dysfunction. Chowdhury *et al.* synthesized a series of azaindole-based potent and highly selective ROCK inhibitors **54** (Figure 1.5) to treat cancer and other ailments [28].

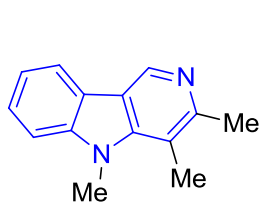
Cannabinoid receptors are transmembrane proteins belonging to G-protein coupled receptor superfamily. These receptors are of two types, namely CB1 and CB2. The cannabinoid-cannabinoid receptor interaction is well studied for its anti-palliative effects. The selective targeting of the CB2 receptor by the agonist **55** (Figure 1.5) is well-established to treat neuropathic pain [29]. Contemporary literature shows that CB2 protein may become a vital target for developing new anticancer molecules as CB2 agonists regulate key cell signaling pathways, including cell survival, angiogenesis, and metastasis [30].

1.4 Biological applications of γ -carbolines

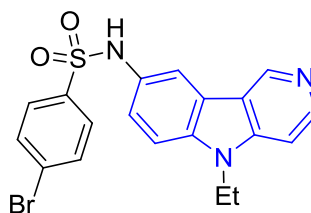
Bovine viral diarrhea (BVD) is a fatal disease of cattle caused by a virus and is a significant reason for cattle-loss worldwide. Sako *et al.* have developed a novel series of γ -carbolines **56** with anti-BVDV activity (Figure 1.6). These compounds have EC₅₀ values in the nanomolar range with high selectivity index and minimal off-site activity [31].

Chen *et al.* have synthesized γ -carboline based tubulin polymerization inhibitor **57** (Figure 1.6). The novel N- γ -carboline aryl sulfonamide bind to the colchicines binding site of tubulin, arresting the cell cycle in the G₂/M phase. The anticancer property of **57** was examined against a panel of cancer cell lines such as lung (A549 cells) and breast

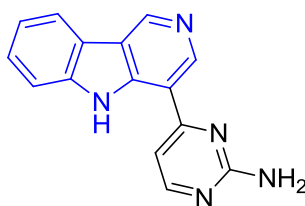
(MCF-7 cells) cancers, and the compounds were found to be active in the micromolar range of concentrations [32].



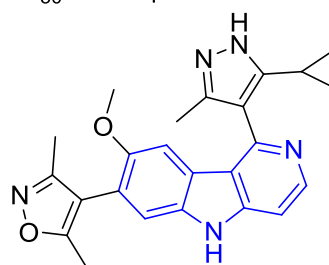
56, SK3M4M5M
EC₅₀ = 3.5 nM
against BVDV



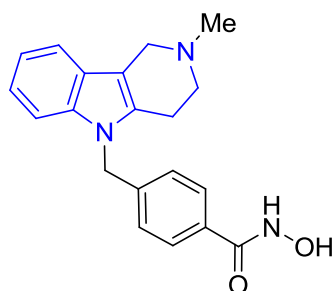
57, Tubulin polymerization inhibitor
IC₅₀ = 1.88 μM in A549 cells
IC₅₀ = 3.79 μM in MCF-7 cells



58, Ingenine B
(ED₅₀ = 9.1 μg/mL)



59, BET inhibitor
BRD4BD1; IC₅₀ = 75 nM
BRD4BD2; IC₅₀ = 36 nM



60, Tubastatin A
HDAC6 inhibitor
(IC₅₀ = 15 nM)

Figure 1.6 Biologically active γ -carboline derivatives

Bromodomain and extra terminal (BET) proteins have recently emerged as a novel class of therapeutic targets for treating cancer. There are 46 bromodomain-containing proteins encoded in the human genome, and broadly these are classified into eight subfamilies. The literature survey suggests that careful regulation of gene transcription by selective targeting of bromodomains may bring innovative changes in treating cancer. BET inhibitors, IBET-762 and OTX015, are rapidly advancing into clinical trials for various human cancers. Ran *et al.* have synthesized a

new γ -carboline derivative **59** (Figure 1.6) with promising bromodomain inhibitor activity at low nanomolar concentrations and very high selectivity [33].

Tubastatin A is a potent ($IC_{50} = 15$ nM) and selective HDAC6 inhibitor promoting neuron re-growth in neurodegenerative diseases and brain injury. In 2010, Butler *et al.* demonstrated that tubastatin-A **60** (Figure 1.6) induces elevated levels of acetylated α -tubulin in primary neuron cultures leading to neuron regeneration [34].

1.5 Tuberculosis: Current status and the emerging role of small molecules in the management of disease

Tuberculosis (TB) caused by *Mycobacterium tuberculosis* (Mtb) is one of the leading causes of death worldwide, surpassing HIV/AIDS. Millions of people are affected by tuberculosis every year. The statistics in the last two decades show the rapid emergence of multidrug-resistant (MDR) and extremely drug-resistant (XDR) Mtb strains. *Mycobacterium tuberculosis* strains resistant to the anti-TB drugs, isoniazid, and rifampicin, are termed multidrug-resistant TB (MDR-TB) strains. Extensively drug-resistant TB (XDR-TB) is a severe case of multidrug resistance in which pathogens are resistant to all second-line drugs. Both MDR-TB and XDR-TB do not respond to the standard anti-TB drugs and are emerging threats to the success of anti-TB programs. According to the latest WHO report, an estimated 480,000 new MDR-TB and an additional 100,000 rifampicin-resistant TB (RR-TB) cases have been reported, with 50% of these cases are from China and India. The current anti-TB regime involves six to nine months long administration of a cocktail of antibiotics. In the case of MDR-TB and XDR-TB, the treatment duration may vary from several months to years. The use of second-line antibiotics has made the problem even more complicated. The partial elimination of these drug-resistant bacteria strains often results in a relapse of the disease with higher mortality rates [35]. Furthermore, Mtb forms well-structured

extracellular matrix called “biofilms” responsible for increased drug tolerance and chronic illness [36]. Therefore, with available over-the-counter drugs, we are unable to keep a check on this fatal disease. This leads to an urgent need for new antibiotics with alternative working principles.

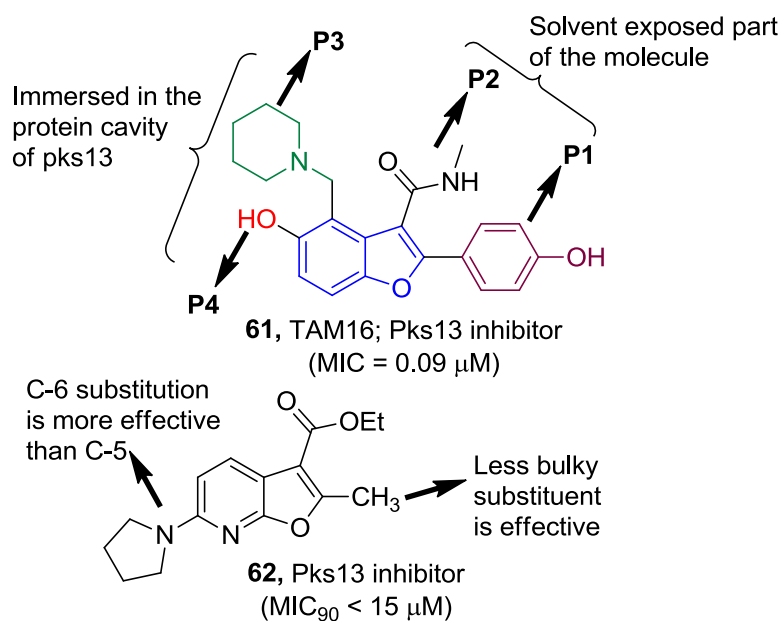


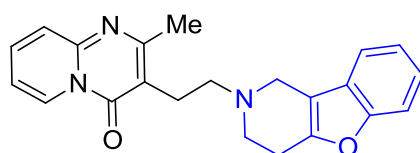
Figure 1.7 Polyketide synthetase 13 (Pks13) inhibitors [6,7]

Polyketide synthase is a class of enzymes in bacteria, which catalyze condensation reaction to produce α -alkyl β -ketoacids, the direct precursors of mycolic acids. The majority of mycolic acid derivatives form the mycolate-containing lipids, which play a decisive role in pathologies caused by the mycobacteria, act either as pro-inflammatory agents or as T cell activators. More recently, benzofuran inhibitors of polyketide synthetase 13 (pks13) have shown encouraging results in the *in vitro* and *in vivo* studies. One such derivative **61**, TAM16, was found to be potent against acute and chronic mouse TB models when administered orally as a single dose. The simplified dosing regimen, increasing patient compliance, and zero pre-existing resistance in clinical strains of TB have increased the chances of its clinical success [6].

The success of benzofuran based molecules has inspired the development of several new pyridofuran derivatives **62** as a treatment for drug-resistant tuberculosis due to structural similarity [7]. These molecules are further transformed into molecular hybrids to fine-tune their biological activities.

1.6 Benzofuopyridine core and its biological application

Kennis *et al.* developed a series of compounds with high affinity to α_2 -adrenoreceptor. *In vitro* and *in vivo* evaluation of the most potent derivative **63** show great potential for a new class of antidepressants [8].



63, Adrenoreceptor antagonist
 pIC_{50} for α_1 = 6.46, α_{2A} = 9.26,
 α_{2B} = 8.59, α_{2C} = 8.77

Figure 1.8 Antidepressant benzofuro[3,2-c]pyridine based molecule

1.7 Organization of the thesis

The present thesis has been summarized into five chapters to gain deep insight into the complete research work.

Chapter 1 describes the introduction to the topic and the scope of the thesis. A review of the recently developed synthetic protocols for fused-pyrido heterocycles and their biological applications is included herein.

Chapter 2 describes the serendipitous discovery of a novel protocol for the synthesis of substituted 5-azaindoles. The application of this methodology is described in this chapter.

Chapter 3 describes the design and development of an unprecedented one-pot protocol for the synthesis of γ -carboline derivatives. These newly

synthesized carbolines possess interesting biological and optical properties.

Chapter 4 deals with the development of a one-pot synthesis for substituted furo[3,2-*c*]pyridines and substituted benzofuro[3,2-*c*]pyridines. This chapter contains the design, synthesis, and biological evaluation of novel furopyridine-isatin hybrids to treat tuberculosis.

Chapter 5 deals with the conclusion of the thesis work and its future scope.

1.8 References

- [1] de la Torre B.G., Albericio F. (2020), The pharmaceutical industry in 2019 an analysis of FDA drug approvals from the perspective of molecules, *Molecules*, 25, 745–757 (DOI: 10.3390/molecules25030745)
- [2] Mérour J.Y., Buron F., Plé K., Bonnet P., Routier, S. (2014), The azaindole framework in the design of kinase inhibitors, *Molecules*, 19, 19935–19979 (DOI: 10.3390/molecules191219935)
- [3] Cao R., Peng W., Wang Z., Xu A. (2007), β -Carboline alkaloids: Biochemical and pharmacological functions, *Curr Med Chem*, 14, 479–500 (DOI: 10.2174/092986707779940998)
- [4] Dai J., Dan W., Zhang Y. and Wang J. (2018), Recent developments on synthesis and biological activities of γ -carboline, *Eur J Med Chem*, 157, 447–461 (DOI: 10.1016/j.ejmech.2018.08.015)
- [5] Jasselin-Hinschberger A., Comoy C., Chartoire A., Fort Y. (2015), Elaboration of furopyridine scaffolds, *Eur J Med Chem*, 11, 2321–2331 (DOI: 10.1002/ejoc.201403412)
- [6] Aggarwal A., Parai M.K., Shetty N., Wallis D., Woolhiser L., Hastings C., Dutta N.K., Galaviz S., Dhakal R.C., Shrestha R., Wakabayashi S. (2017), Development of a novel lead that targets M. tuberculosis polyketide synthase 13, *Cell*, 170, 249–259 (DOI: 10.1016/j.cell.2017.06.025)

- [7] Fumagalli F., de Melo S.M.G., Ribeiro C.M., Solcia M.C., Pavan F.R., Silva Emery F. (2019), Exploiting the furo[2,3-*b*]pyridine core against multidrug-resistant *Mycobacterium tuberculosis*, *Bioorg Med Chem Lett*, 29, 974–977 (DOI: 10.1016/j.bmcl.2019.02.019)
- [8] Kennis L.E., Bischoff F.P., Mertens C.J., Love C.J., Van den Keybus F.A., Pieters S., Braeken M., Megens A.A., Leysen J.E. (2000), New 2-substituted 1,2,3,4-tetrahydrobenzofuro[3,2-*c*] pyridine having highly active and potent central α_2 -antagonistic activity as potential antidepressants, *Bioorg Med Chem Lett*, 10, 71–74 (DOI: 10.1016/S0960-894X(99)00591-0)
- [9] Purificação S.I., Pires M.J., Rippel R., Santos A.S., Marques M.M.B. (2017), One-pot synthesis of 1, 2-disubstituted 4-, 5-, 6-, and 7-azaindoles from amino-*o*-halopyridines via N-arylation/Sonogashira/cyclization reaction. *Org Lett*, 19, 5118–5121 (DOI: 10.1021/acs.orglett.7b02403)
- [10] Pires M.J., Poeira D.L., Purificacao S.I., Marques M.M.B. (2016), Synthesis of substituted 4-, 5-, 6-, and 7-azaindoles from aminopyridines via a cascade C–N cross-coupling/heck reaction, *Org Lett*, 18, 3250–3253 (DOI: 10.1021/acs.orglett.6b01500)
- [11] Ortgies S., Breder A. (2015), Selenium-catalyzed oxidative C (sp²)–H amination of alkenes exemplified in the expedient synthesis of (aza-) indoles, *Org Lett*, 17, 2748–2751 (DOI: 10.1021/acs.orglett.5b01156)
- [12] Calvet G., Livecchi M., Schmidt F. (2011), Synthesis of polysubstituted 5-azaindoles via palladium-catalyzed heteroannulation of diarylalkynes, *J Org Chem*, 76, 4734–4740 (DOI: 10.1021/jo200480h)
- [13] Moustafa, M.M.A.R., Pagenkopf, B.L. (2010), Synthesis of 5-azaindoles via a cycloaddition reaction between nitriles and donor-acceptor cyclopropanes. *Org Lett*, 12, 3168–3171 (DOI: 10.1021/ol101078z)

- [14] Xu S.M., Wei L., Shen C., Xiao L., Tao H.Y. Wang C.J. (2019), Stereodivergent assembly of tetrahydro- γ -carbolines via synergistic catalytic asymmetric cascade reaction, *Nat Commun*, 10, 1–11 (DOI: 10.1038/s41467-019-13529-z)
- [15] Gutiérrez S., Sucunza D., Vaquero J.J. (2018), γ -Carboline synthesis by heterocyclization of TosMIC derivatives, *J Org Chem*, 83, 6623–6632 (DOI: 10.1021/acs.joc.8b00906)
- [16] Chepyshev S.V., Lujan-Montelongo J.A., Chao A. Fleming F.F. (2017), Alkenyl isocyanide conjugate additions: A rapid route to γ -carbolines. *Angew Chem Int Ed*, 129, 4374–4377 (DOI: 10.1002/anie.201612574)
- [17] Wang T.T., Zhang D., Liao W.W. (2018), Versatile synthesis of functionalized β -and γ -carbolines via Pd-catalyzed C–H addition to nitriles/cyclization sequences, *Chem Comm*, 54, 2048–2051 (DOI: 10.1039/c8cc00040a)
- [18] Hao W.J., Wang S.Y., Ji S.J. (2013), Iodine-catalyzed cascade formal [3+3] cycloaddition reaction of indolyl alcohol derivatives with enamines: Constructions of functionalized spirodihydrocarbolines, *ACS Catal*, 3, 2501–2504 (DOI: 10.1021/cs400703u)
- [19] Kuethe J.T. (2019). A concise synthesis of functionalized 2,3-dihydrofuro[3,2-*b*],[3,2-*c*], and [2,3-*b*] pyridines, *Tetrahedron*, 75, 130446 (DOI: 10.1016/j.tet.2019.07.004)
- [20] Dong J., Bao L., Hu Z., Ma S., Zhou X., Hao M., Li N., Xu X. (2018), Anion relay enabled [3+3]-annulation of active methylene isocyanides and ene-yne-ketones, *Org Lett*, 20, 1244–1247 (DOI: 10.1021/acs.orglett.8b00186)
- [21] Li J.S., Yang Q., Chen G.Q., Li Z.W., Huang P.M. (2018), Facile reagent-free synthesis of furo[3,2-*c*]pyridinones and their polynuclear analogues with DDQ as precursor, *ChemistrySelect*, 3, 10621–10623 (DOI: 10.1002/slct.201802686)

- [22] Mal K., Sharma A., Das I. (2014), Gold (III) chloride catalyzed synthesis of chiral substituted 3-formyl furans from carbohydrates: Application in the synthesis of 1,5-dicarbonyl derivatives and furo[3,2-*c*]pyridine, *Chem Eur J*, 20, 11932–11945 (DOI: 10.1002/chem.201402286)
- [23] Kumar S., Cruz-Hernández C., Pal S., Saunthwal R.K., Patel M., Tiwari R.K., Juaristi E., Verma A.K. (2015), Tandem approach to benzothieno-and benzofuopyridines from *o*-alkynyl aldehydes via silver-catalyzed 6-endo-dig ring closure, *J Org Chem*, 80, 10548–10560 (DOI: 10.1021/acs.joc.5b01647)
- [24] Lun Z.R., Lai D.H., Wen Y.Z., Zheng L.L., Shen J.L., Yang T.B., Zhou W.L., Qu L.H., Hide G., Ayala F.J. (2015), Cancer in the parasitic protozoans *Trypanosoma brucei* and *Toxoplasma gondii*, *Proc Natl Acad Sci USA*, 112, 8835–8842 (DOI: 10.1073/pnas.1502599112)
- [25] Walker S.R., Carter E.J., Huff B.C., Morris J.C. (2009), Variolins and related alkaloids, *Chem Rev*, 109, 3080–3098 (DOI: 10.1021/cr900032s)
- [26] Bryan M.C., Falsey J.R., Frohn M., Reichelt A., Yao G., Bartberger M.D., Bailis J.M., Zalameda L., San Miguel T., Doherty E.M., Allen J.G. (2013), N-substituted azaindoles as potent inhibitors of Cdc7 kinase, *Bioorg Med Chem Lett*, 23, 2056–2060 (DOI: 10.1016/j.bmcl.2013.02.007)
- [27] Lefoix M., Coudert G., Routier S., Pfeiffer B., Caignard D.H., Hickman J., Pierré A., Golsteyn R.M., Léonce S., Bossard C., Mérour J.Y. (2008), Novel 5-azaindolocarbazoles as cytotoxic agents and Chk1 inhibitors, *Bioorg Med Chem*, 16, 5303–5321 (DOI: 10.1016/j.bmc.2008.02.086)
- [28] Chowdhury S., Sessions E.H., Pocas J.R., Grant W., Schröter T., Lin L., Ruiz C., Cameron M.D., Schürer S., LoGrasso P., Bannister T.D. (2011), Discovery and optimization of indoles and 7-azaindoles as Rho

- kinase (ROCK) inhibitors (part-I), *Bioorg Med Chem Lett*, 21, 7107–7112 (DOI: 10.1016/j.bmcl.2011.09.083)
- [29] Giblin G.M.P., Billinton A., Briggs M., Brown A.J., Chessell I.P., Clayton N.M., Eatherton A.J., Goldsmith P., Haslam C., Johnson M. R., Mitchell W.L., Naylor A., Perboni A., Slingsby B.P., Wilson A.W. (2009), Discovery of 1-[4-(3-chlorophenylamino)-1-methyl-1*H*-pyrrolo[3,2-*c*]pyridin-7-yl]-1-morpholin-4-ylmethanone (GSK554418A), a brain penetrant 5-azaindole CB2 agonist for the treatment of chronic pain, *J Med Chem*, 52, 5785–5788 (DOI: 10.1021/jm9009857)
- [30] Laezza C., Pagano C., Navarra G., Pastorino O., Proto M.C., Fiore D., Piscopo C., Gazzero P., Bifulco, M. (2020), The endocannabinoid system: a target for cancer treatment, *Int J Mol Sci*, 21, 747–767 (DOI: 10.3390/ijms21030747)
- [31] Sako K., Aoyama H., Sato S., Hashimoto Y., Baba M. (2008), γ -Carboline derivatives with anti-bovine viral diarrhea virus (BVDV) activity, *Bioorg Med Chem*, 16, 3780–3790 (DOI: 10.1016/j.bmc.2008.01.052)
- [32] Chen J., Liu T., Wu R., Lou J., Cao J., Dong X., Yang B., He Q., Hu Y. (2010), Design, synthesis, and biological evaluation of novel *N*- γ -carboline arylsulfonamides as anticancer agents, *Bioorg Med Chem*, 18, 8478–8484 (DOI: 10.1016/j.bmc.2010.10.047)
- [33] Ran X., Zhao Y., Liu L., Bai L., Yang C.Y., Zhou B., Meagher J.L., Chinnaswamy K., Stuckey J.A., Wang S. (2015) Structure-based design of γ -carboline analogues as potent and specific BET bromodomain inhibitors, *J Med Chem*, 58, 4927–4939 (DOI: 10.1021/acs.jmedchem.5b00613)
- [34] Butler K.V., Kalin J., Brochier C., Vistoli G., Langley B., Kozikowski A.P. (2010), Rational design and simple chemistry yield a superior, neuroprotective HDAC6 inhibitor, tubastatin A, *J Am Chem Soc*, 132, 10842–10846 (DOI: 10.1021/ja102758v)

- [35] Shah I., Poojari V., Meshram H. (2020), Multi-drug resistant and extensively-drug resistant tuberculosis, *Indian J Pediatr*, 87, 833–839 (DOI: 10.1007/s12098-020-03230-1)
- [36] Chakraborty P., Kumar A. (2019), The extracellular matrix of mycobacterial biofilms: Could we shorten the treatment of mycobacterial infections, *Microb Cell*, 6, 105–122 (DOI: 10.15698/mic2019.02.667)

Chapter 2

Serendipitous base catalysed condensation-heteroannulation of iminoesters: A regioselective route to synthesis of 4,6-disubstituted 5-azaindoles

2.1 Introduction

Azaindoles are privileged heterocycles as they are the closest bioisosteres of indoles and purines. They are rare, except in few marine alkaloids such as variolins [1] and martinellie acid [2] along with their derivatives. In particular, the 5-azaindole core moiety is well exploited in drug design due to its strong homology with 5-hydroxy indole, a main metabolite of indole moiety present in several biomolecules like melatonin, serotonin, and 5-hydroxy indole acetic acid [3]. Many important drug candidates [4–7] have been discovered recently which contain the 5-azaindole core (Figure 2.1) and research is being carried out to exploit the full potential of this heterocyclic motif.

A review of the literature reveals that several methods [8] are available for the synthesis of azaindole moiety. The classical Fischer indolization and Bartoli indole synthesis are not very efficient at synthesizing azaindole core due to the electron deficient nature of the pyridine ring which does not favour an essential step involving a [3,3] sigmatropic rearrangement during the synthesis [9]. In contrast, the standard indole synthetic protocols including methodologies developed by Leimgruber-Batcho [10], Larock [11], and Hemetsberger–Knittel [12] have been successfully extended to synthesize 5-azaindole core by careful selection of specific substrates. Moreover, Heck [13] and Sonogashira [14] C–C cross coupling reactions have been proved to be instrumental in developing new methodologies for a vast range of heterocycles of this category. In addition, zirconocene mediated cross-coupling reaction [15]

of silanes with organonitriles and TiCl_3 catalysed [16] cyclisation of isonicotinoyl derivatives of aminopyridines are noteworthy contributions of transition metal mediated synthesis of 5-azaindoles.

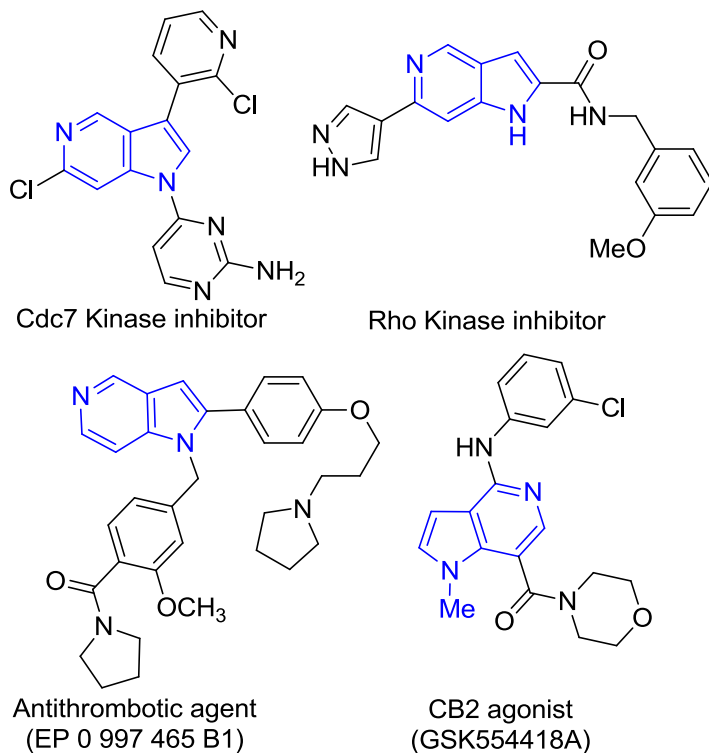


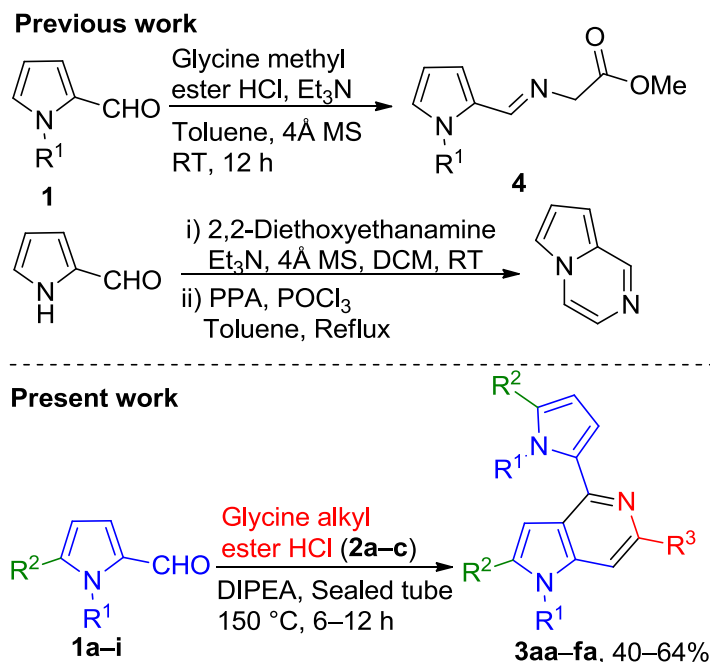
Figure 2.1 Pharmacologically active molecules containing the 5-azaindole core [4–7]

Most of these strategies involve multistep reactions including harsh conditions in one or more steps during their synthesis. Additionally, these methods rely on highly functionalized nitro or amino-pyridine derivatives, which are expensive and not available easily. The limited substrate scope results in the formation of highly substituted products with very less flexibility for further modifications.

2.2 Results and discussion

During our ongoing exploration of pyrrole iminoester **4** as versatile building block for heterocycle synthesis, we have serendipitously

encountered a novel and highly regioselective route to synthesize the 5-azaindole core through one-pot condensation-heteroannulation of iminoester **4** derived from pyrrole-2-aldehyde **1a** and glycine ester **2a**. The results of these studies are presented in this chapter.



Scheme 2.1 Imination of pyrrole-2-carboxaldehydes: A comparison between previous [17, 18] and present studies

The condensation of amino methylene compounds with pyrrole-2-aldehydes **1** is well reported in the literature [17, 18]. These studies have motivated us to prepare pyrrole iminoester **4** that can be used for synthesizing new biologically active heterocycles (Scheme 2.1). However, reported procedure [17] for the synthesis of **4** was not reproducible, and only traces of **4** were observed in our experiments (Table 2.1).

In order to optimize the reaction, various reaction conditions were screened including the usage of an organic base such as diisopropylethylamine ($pK_a = 10.75$) under reflux in toluene in presence of 4 Å molecular sieves to sequester the eliminated water molecules during

condensation reaction between pyrrole-2-aldehyde and glycine ester hydrochloride (Entry 1, Table 2.1).

S. No	No. of equiv. of 1a used	No. of equiv. of 2a used	Base (equiv.)	Solvent	Additive	Temp.	Reaction Time	Yield*
1	1.0	1.0	DIPEA (3.5)	Toluene	4Å MS	Reflux	48 h	38% (3aa)
2	1.0	1.0	Et ₃ N (3.5)	Toluene	4Å MS	Reflux	48 h	No product
3	2.0	1.0	NaH (3.5)	THF	-	RT to reflux	24 h	No product
4	2.0	1.0	K ₂ CO ₃ (6.5)	Et ₂ O	-	RT to reflux	24 h	No product
5	2.0	1.0	Cs ₂ CO ₃ (2.0)	DMF	-	RT to reflux	24 h	No product
6	2.0	1.0	DIPEA (3.5)	-	-	150°C/ Sealed tube	6 h	58% (3aa)
7	1.0	5.0	DIPEA (15.0)	-	-	100°C/ Sealed tube	48 h	34% (3aa)
8	2.0	1.0	DBU (3.5)	-	-	150°C/ Sealed tube	6 h	31% (3aa)
9	2.0	1.0	DIPEA (3.5)	-	-	150°C/ 200 mbar (micro wave)	10 min	Trace (3aa)
10	2.0	1.0	DIPEA (3.5)	-	DDQ (1.0)	150°C/ Sealed tube	16 h	No product

11	2.0	1.0	DIPEA (3.5)	-	-	50°C/ Sealed tube	24 h	No product
equiv. = no. of equivalents; *isolated yield								

Table 2.1 Optimization of reaction conditions for formation of **3aa**

To our surprise, the product was not the expected iminoester **4** but was characterized and confirmed by X-ray diffraction study (Figure 2.2) as methyl 1-benzyl-4-(1-benzyl-1*H*-pyrrol-2-yl)-1*H*-pyrrolo[3,2-*c*]pyridine-6-carboxylate **3aa** or 5-azaindole in 38% yield.

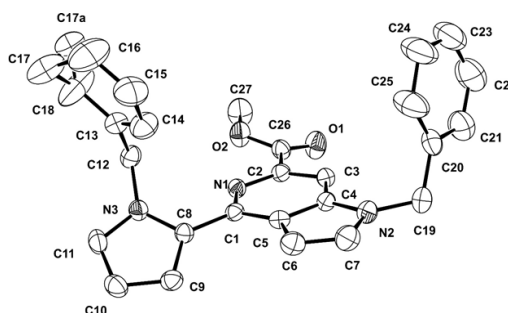


Figure 2.2 Molecular structure of **3aa** (CCDC 1836867)

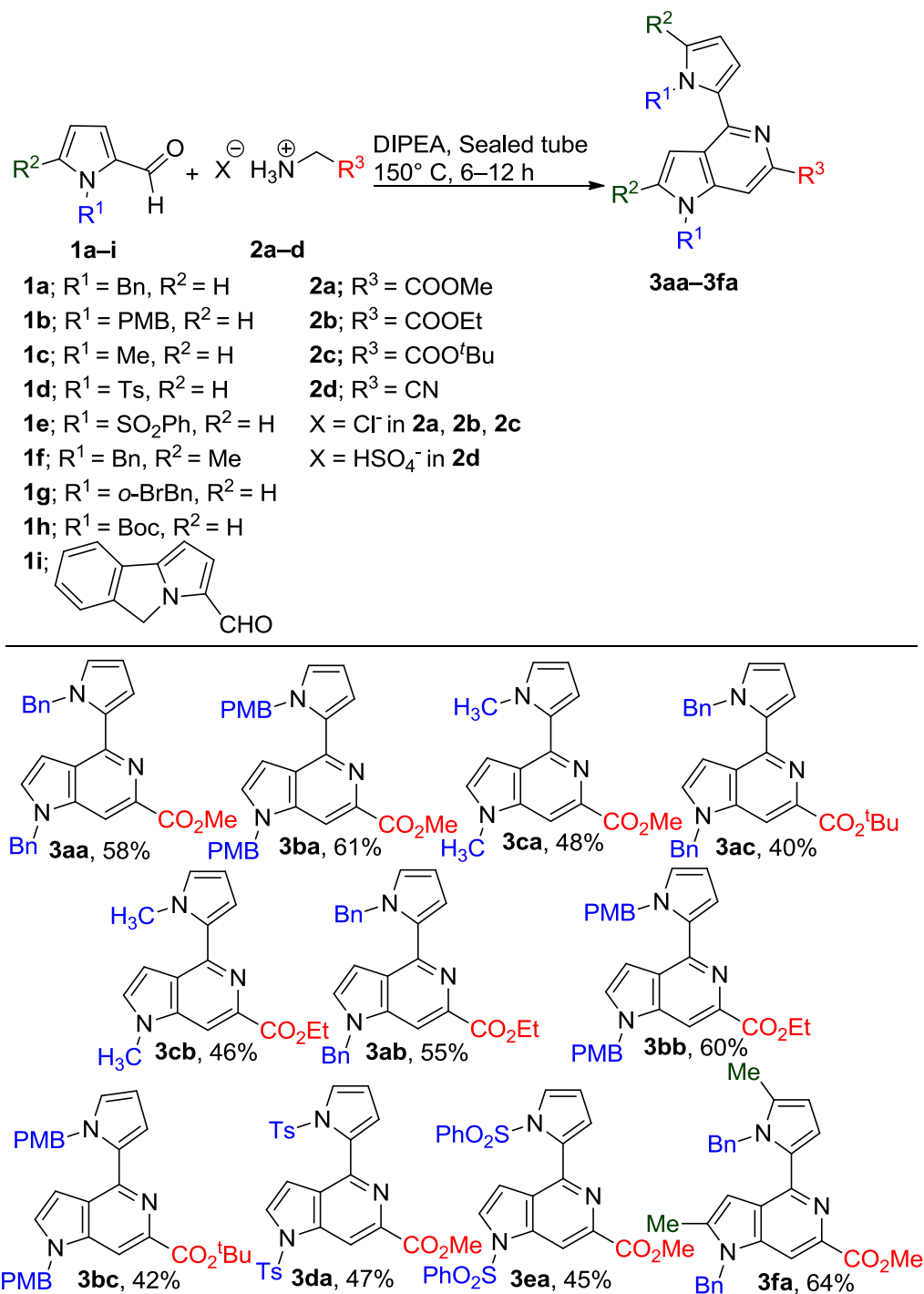
With the above findings, next we carried out the optimization of the reaction conditions to synthesize **3aa** from **1a** and **2a** using various organic or inorganic bases in different solvents at different reaction temperatures (Entries 2–5, Table 2.1). However, neither **3aa** nor the iminoester **4** was obtained when mild organic base (Et₃N, Entry 2), strong (NaH, Entry 3) or weak inorganic bases such as K₂CO₃ (Entry 4) or Cs₂CO₃ (Entry 5) were utilized. Subsequently, it was found that under solvent-free conditions, when *N*-benzyl pyrrole-2-carboxaldehyde **1a** (2.0 equiv.) was reacted with glycine methyl ester HCl salt **2a** (1.0 equiv.) in the presence of DIPEA (3.5 equiv.) at 150 °C in a sealed tube for 6 h, the reaction proceeded smoothly to provide **3aa** in an improved yield of 58% (Entry 6, Table 2.1). Increasing the equivalents of glycine ester **2a** to 5.0 equiv. and DIPEA to 15 equiv. resulted only in the degradation of **3aa** to

34% yield (Entry 7, Table 2.1). Use of stronger base such as DBU (Entry 8) resulted in further decrease of yield of **3aa** to 31%. Microwave irradiation (Entry 9) or use of additives such as DDQ at 150 °C didn't facilitate the formation of **3aa** due to the decomposition of DDQ by water molecules generated during the formation of intermediates **4** and **7** (Entry 10). Moreover, decreasing the reaction temperature to 50 °C under solvent free condition was completely detrimental and prevented the formation of **3aa** (Entry 11).

The methodology was further extended to other *N*-substituted pyrrole-2-carboxaldehydes **1b–h** and **1i** along with a range of aminomethylene compounds **2b–d** to examine the scope of the reaction for a general 5-azaindole synthesis, and the results are summarized in Scheme 2.2. In general, electron rich pyrrole-2-aldehydes **1a–c** having higher nucleophilicity in the pyrrole ring resulted in the formation of corresponding 4,6-disubstituted 5-azaindoles **3ab–bc** and **3fa** in good yields, whereas electron deficient pyrrole-2-aldehydes **1d** and **1e** yielded 4,6-disubstituted 5-azaindoles **3da–ea** in moderate yields.

Interestingly, *N*-(4-methoxybenzyl) and 5-methyl substituents increase the nucleophilicity of the pyrrole ring to afford **3ba** and **3fa** in 61% and 64% yields, respectively, under optimized reaction conditions. Pyrrole-2-carboxaldehyde derivatives with moderate electron withdrawing groups (**1d** and **1e**) including tosyl and benzene sulfonyl were also successfully transformed into their corresponding 5-azaindole products (**3da** and **3ea**), but comparatively with lower yields and a longer reaction time (12 h). In general, glycine methyl ester HCl salt **2a** was found to be more effective in terms of higher yields in a given transformation in comparison to ethyl ester and *tert*-butyl esters of glycine. However, reaction of 2-aminoacetonitrile **2d** with **1a** did not result in the formation of cyano derivative of 5-azaindole, **3ad**.

Overall, the observed results show that nucleophilicity of the pyrrole ring plays a decisive role in the formation of 5-azaindole product under the newly developed protocol. The pyrrole unit with higher electron density may exhibit slower rate of imine formation. However, as soon as the iminoester intermediate **4** is formed, it readily generates a carbon nucleophile **5** to facilitate condensation reaction of **5** with another molecule of pyrrole-2-aldehyde to give the corresponding 4,6-disubstituted 5-azaindoles.



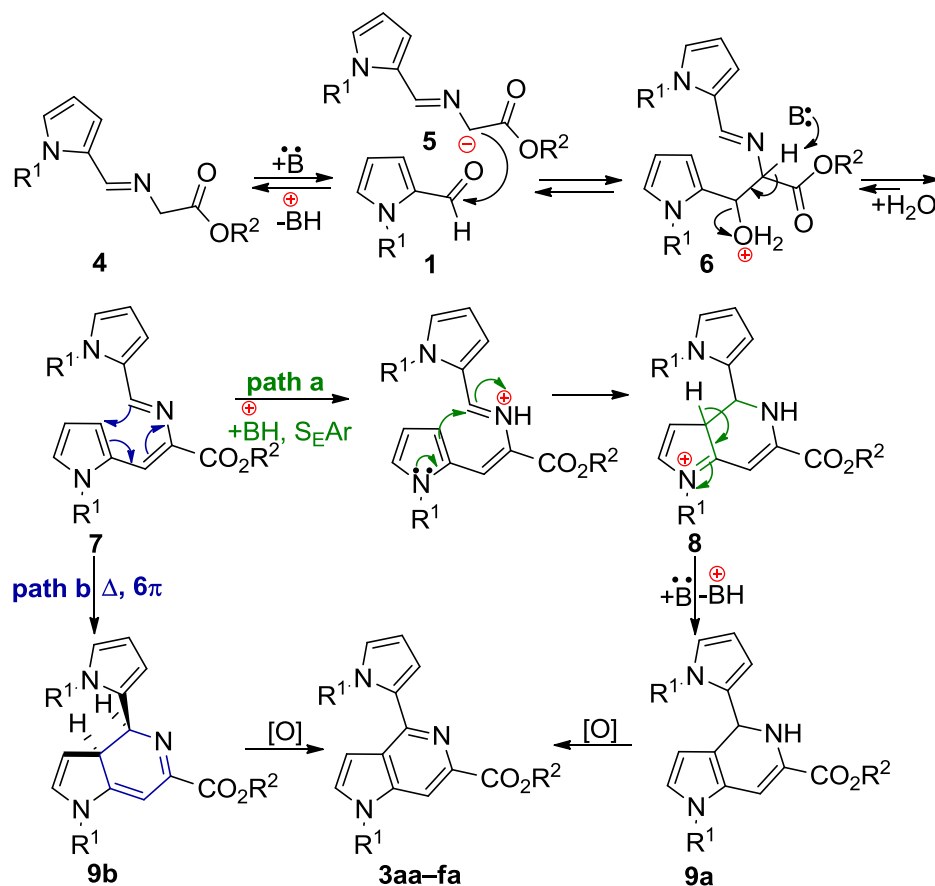
Scheme 2.2 Synthesis of 5-azaindole derivatives **3aa-fa**

Pyrrole-2-aldehydes **1g** and **1h** and fused pyrrole-2-aldehyde **1i** failed to form the corresponding 5-azaindoles **3ga**, **3ha** and **3ia**. The

presence of electron withdrawing halogen group in the *N*-benzyl substituent, as in the case of **1g** (2'-bromo-*N*-benzyl), inhibits the formation of iminoester intermediate **4g**, which is necessary for further condensation with another molecule of **1g** to form 5-azaindole **3ga**. Even though the presence of EWG on the nitrogen atom of the pyrrole ring was tolerated well as in the case of aldehydes **1d** and **1e**, *N*-Boc-pyrrole-2-aldehyde **1h** does not result in the formation of the desired 5-azaindole product, **3ha**. Probably this is due to the labile nature of *N*-Boc group at higher temperature leading to severe decomposition of the aldehyde **1h**. Benzocyclopenta fused pyrrole-2-aldehyde **1i** did not result in the formation of 5-azaindole because of severe steric crowding.

The probable mechanism (Scheme 2.3) for the conversion of pyrrole-2-aldehydes (**1a–e**) to 5-azaindoles (**3aa–fa**) involves initial formation of *trans* iminoester **4** from *N*-protected pyrrole-2-aldehyde **1** and glycine alkyl esters (**2a–c**). In the presence of Hunig's base, carbon nucleophile **5** is generated by abstraction of active methylene proton from *trans* iminoester **4** which further undergoes nucleophilic addition with another molecule of *N*-protected pyrrole-2-aldehyde **1** to give an intermediate imino alcohol **6**. Iminoalcohol **6** eliminates a molecule of water under the reaction conditions to give an iminoenamine intermediate **7** which can undergo ring closure reaction *via* path a or path b.

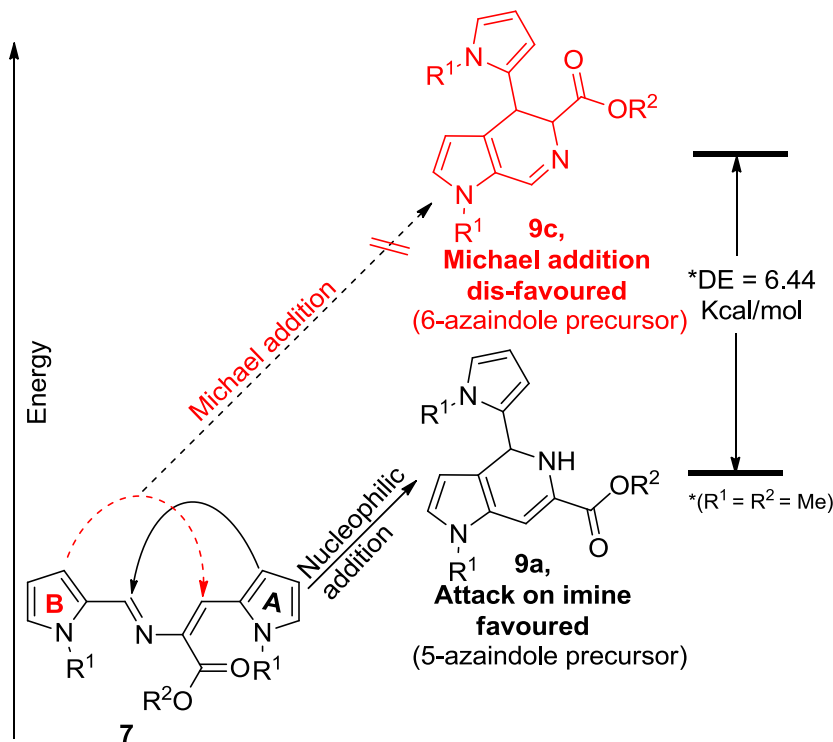
In path a, imine nitrogen of intermediate **7** is protonated by the conjugate acid (+BH) to form the iminium intermediate which undergoes electrophilic aromatic substitution at the 3-position of the pyrrole unit to form the second C–C bond in **8**. Intermediate **8** aromatises by the loss of proton to give 4,6-disubstituted 4,5-dihydroazaindole **9a**. In path b, **7** would undergo thermal 6- π electrocyclic reaction of a conjugated triene system to form 4,6-disubstituted 4,8-dihydroazaindole **9b**. *In situ* dehydrogenation of **9a** or **9b** by aerial oxidation leads to the formation of 4,6-disubstituted-5-azaindoles **3aa–fa**.



Scheme 2.3 Plausible mechanism for the formation of the 5-azaindole core

During the formation of azaindoles, all the substrates, **1a–f**, were exclusively transformed to 5-azaindoles and no traces of 6-azaindole regioisomers were observed which proves that the heterocyclization reaction is highly regioselective (Scheme 2.4). The exclusive formation of the 5-azaindole regioisomer is explained by proposing an intermediate **7** before heteroannulation takes place. Pyrrole ring A predominantly prefers to participate in nucleophilic addition on intermediate **7** compared to the standard Michael type addition of pyrrole ring B. Density functional theoretical (details in the experimental section) calculations also show that nucleophilic addition is favoured (by 6.44 kcal/mol) over Michael addition, between the formation of 5- and 6-dihydroazaindoles **9a** and **9c**.

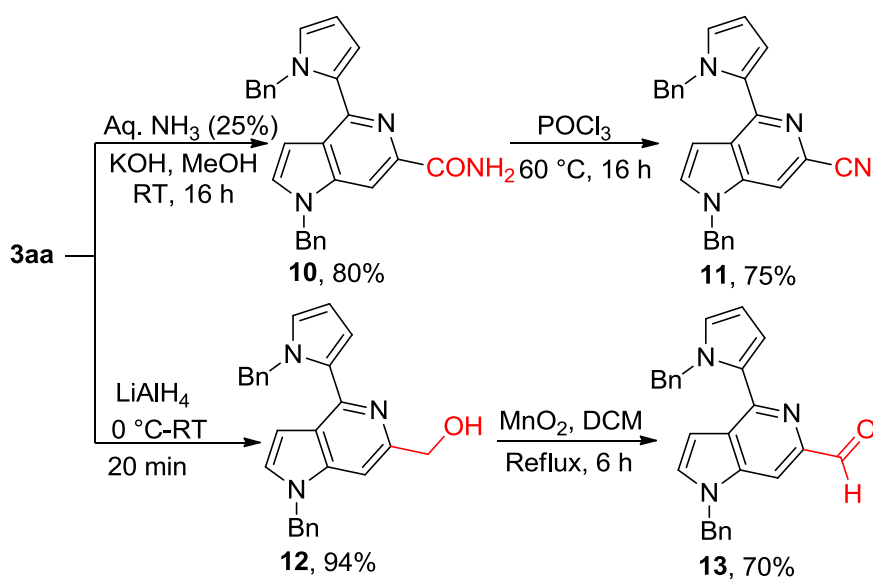
This indicates that **9a** is thermodynamically stable over **9c**. This may be the reason for the selective formation of 5-azaindole regioisomer in the developed protocol (Scheme 2.4).



Scheme 2.4 Relative energy between the formation of 5-azaindole (**9a**) and 6-azaindole (**9c**) regioisomers calculated using the B3LYP/6-311++G** level of theory

The carboxylic ester functionality in **3aa** can be easily transformed into variety of 6-substituted 5-azaindole derivatives **10–13**. Ester **3aa** was reacted with aqueous ammonia in alkaline methanolic solution to yield the corresponding 6-carboxamide 5-azaindole derivative **10**. Mild dehydration of **10** using phosphoryl chloride provided 6-cyano 5-azaindole **11**. The carboxylic ester in **3aa** was smoothly transformed into primary alcohol **12** in good yield using lithium aluminium hydride as the reducing agent. The introduction of a formyl group into the pyridine ring of 5-azaindole without affecting the highly nucleophilic C-2 and C-3 positions of the

pyrrole ring was also achieved by controlling the oxidation of primary alcohol **12** to 6-carbaldehyde 5-azaindole **13** using manganese dioxide as a mild oxidizing agent (Scheme 2.5). It is imperative to note that the introduction of electron withdrawing functional groups in the pyridine ring of 5-azaindole is difficult and rare.

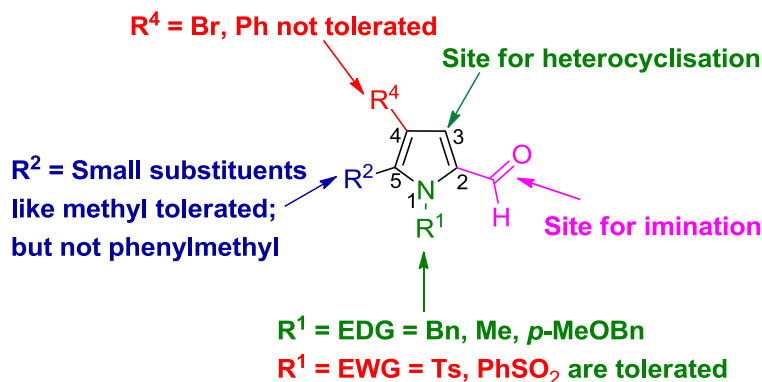


Scheme 2.5 Synthesis of novel 5-azaindole derivatives

The effects of substituents at C-4 and C-5 positions of pyrrole-2-carboxaldehyde were thoroughly investigated for understanding the synthetic scope of the reaction and summarized in Scheme 2.6.

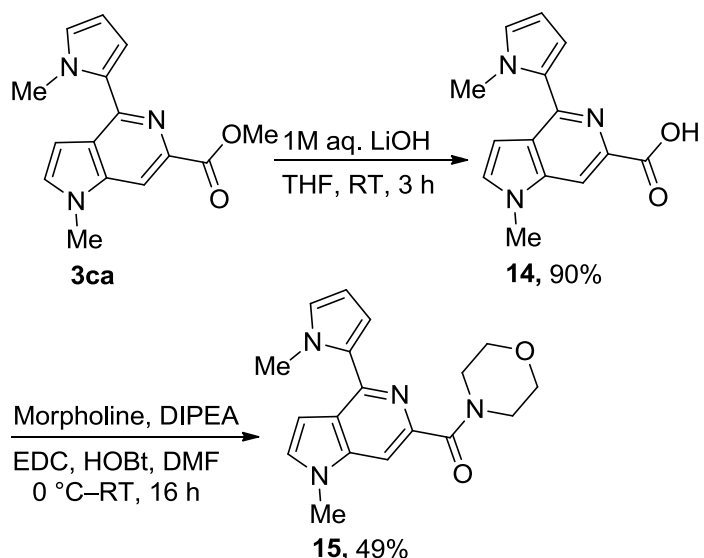
A range of C-4 and C-5 substituted pyrrole-2-carboxaldehyde derivatives were synthesized via reported procedures [19] and were subjected to heterocyclization reactions. It was found out that any substitution (Br or Ph) at the C-4 position of pyrrole-2-carboxaldehyde is not conducive to heterocyclization. Small substituents such as the methyl group are well tolerated at the C-5 position of pyrrole-2-carboxaldehyde; however, bulkier substituents such as the benzyl group are not tolerated in the new protocol for conversion into the corresponding 2-substituted 5-azaindole derivatives. Electron donating (Bn, Me, 4-MeO-benzyl) or

withdrawing substituents (tosyl, PhSO_2) at the 1-position of pyrrole are also well tolerated (Scheme 2.6).



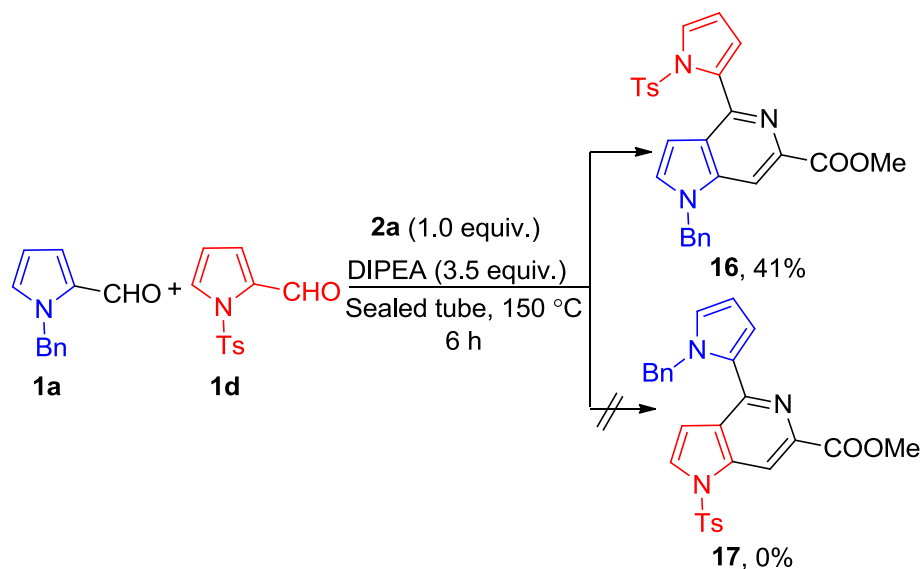
Scheme 2.6 Effects of C-4 and C-5 substituents on the heterocyclization reaction

We also envisaged that the 5-azaindole derivative **15** has remarkable structural similarity to the selective CB2 agonist GSK554418A (Figure 2.1) and is expected to have a similar biological profile. Subsequently, the methyl ester in **3ca** was hydrolysed to 6-carboxylic acid 5-azaindole, **14**, which was coupled with morpholine to give 6-morpholino amide derivative **15** in moderate yield (Scheme 2.7). *In vitro* analysis of **15** to confirm the CB2 agonistic activity in cancer cell lines was carried out in our laboratory, and unfortunately no significant cell death was observed in these experiments.



Scheme 2.7 Synthesis of a possible CB2 agonist molecule

A crossover experiment with two different pyrrole-2-aldehydes **1a** and **1d** produced a single crossover product **16**, which indicates that this reaction solely goes through an intermolecular and chemoselective fashion (Scheme 2.8). Electron deficient *N*-tosylpyrrole-2-aldehyde **1d** reacts with glycine methyl ester initially to form an iminoester intermediate **4**, which undergoes nucleophilic addition with electron rich *N*-benzylpyrrole-2-aldehyde **1a** followed by sequence of transformations as described in Scheme 2.3 to give 4,6-disubstituted-5-azaindole **16** as the product and not the other isomer **17**. This is because glycine methyl ester reacts faster with **1d** to form iminoester intermediate **4** due to the increased electrophilicity of the 2-aldehyde functionality in **1d**. This experiment opens a new avenue to prepare various 5-azaindole derivatives with different *N*-protecting groups in the side chain pyrrole and fused pyridopyrrole moieties.



Scheme 2.8 Crossover experiment to form 5-azaindole **16**

2.3 Conclusion

In summary, we have discovered an unprecedented one-pot protocol for the synthesis of 4,6-disubstituted 5-azaindole derivatives. The approach discloses mechanistically an interesting heterocyclization reaction through imination of pyrrole-2-aldehydes with glycine esters and *in situ* condensation of the imino ester to another molecule of pyrrole-2-aldehyde to afford 4,6-disubstituted 5-azaindoles in moderate to good yields.

2.4 Experimental section

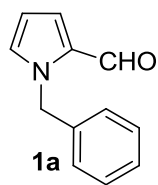
2.4.1 General information

All reactions were carried out in oven dried glass wares with magnetic stirring. **1e**, **2a**, **2c**, **2d** along with other reagents were obtained from commercial supplier and used without further purification. NMR spectra were recorded on AvanceIII400 Ascend Bruker. CDCl₃ and D₂O were used as NMR solvents. Chemical shifts (δ) reported as part per million (ppm) and TMS was used as internal reference. High resolution mass

spectra were obtained through Bruker Daltonik High Performance LC MS (Electrospray Ionization Quadrupole time-of-flight) spectrometer. X-ray structure analysis was carried out at Single crystal X-ray diffractometer Bruker KAPPA APEXII. Melting points (m.p.) are uncorrected and were measured on Veego melting point apparatus (Capillary method). Analytical thin layer chromatography (TLC) was carried out on silica gel plates (silica gel 60 F254 aluminium supported plates); the spots were visualized with an UV lamp (254 nm and 365 nm) or using chemical staining with Brady's reagent, KMnO_4 , ninhydrin, iodine, and bromocresol. Column chromatography was performed using silica gel (100–200 mesh or 230–400 mesh) and neutral alumina (175 mesh). DMF, DCM, DMA, toluene, and acetonitrile were dried using CaH_2 and distilled over flame-dried 4Å molecular sieves. THF and Et_2O were dried over Na/benzophenone and stored over flame-dried 4Å molecular sieves under inert atmosphere prior to use. Organic bases including DIPEA, Et_3N , and DBU were stored over anhydrous KOH pellets.

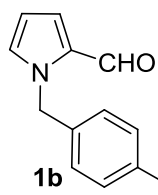
2.4.2 Experimental details and characterization data

2.4.2.1 Synthesis of starting materials **1a–i** and **2b**



1-Benzyl-1H-pyrrole-2-carbaldehyde (1a). Crushed potassium hydroxide (1.175 gm, 21 mmol) was dissolved in dimethyl sulfoxide (5 mL) in a round-bottom flask (100 mL) by stirring for 5 min at room temperature. Solid pyrrole-2-carboxaldehyde (500 mg, 5.25 mmol) was added to the reaction mixture in one portion and stirred for 45 min at the same temperature. Subsequently, the reaction mixture was cooled to 0 °C and benzyl bromide (1.25 mL, 10.5 mmol) was added through a glass syringe drop-wise over a period of 5 min. The reaction mixture was warmed to room temperature, monitored by TLC and stirred for another

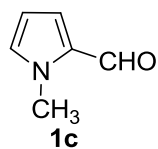
45 min. After the completion of reaction, the reaction mixture was quenched with milli-Q water (MQ, 10 mL) and extracted with diethyl ether (3×10 mL). The combined organic layers was dried over anhydrous Na₂SO₄, filtered, and concentrated under reduced pressure. The crude residue was purified over silica gel (100–200 mesh) column chromatography using hexane:EtOAc (99.5:0.5) as eluent to afford **1a**. Yield 85% (824 mg); Yellow oily liquid; *R_f* 0.50 (9:1 hexane-EtOAc); ¹H NMR (400 MHz, CDCl₃) δ 9.47 (s, 1H), 7.27–7.13 (m, 3H), 7.12–7.00 (m, 2H), 6.93–6.80 (m, 2H), 6.18 (dd, *J* = 3.2, 2.7 Hz, 1H), 5.47 (s, 2H); ¹³C NMR (100 MHz, CDCl₃) δ 179.5, 137.6, 131.6, 131.4, 128.7, 127.7, 127.3, 124.8, 110.2, 52.0.



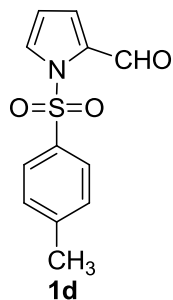
1-(4-Methoxybenzyl)-1H-pyrrole-2-carbaldehyde (**1b**).

Under inert atmosphere, in a two-neck round-bottom flask (50 mL), sodium hydride (55–60% suspension in oil, 100 mg, 2.52 mmol) was suspended in dry dimethyl formamide (3 mL) at room temperature. Pyrrole-2-carboxaldehyde (200 mg, 2.10 mmol) was added to the reaction mixture in one portion and stirred for 30 min at the same temperature. Subsequently, the reaction mixture was cooled to 0 °C and 4-methoxy benzyl chloride (0.34 mL, 2.52 mmol) was added through a glass syringe drop-wise over a period of 5 min under inert atmosphere. The reaction mixture was allowed to warm to room temperature, stirred for another 2 h and monitored by TLC. After the completion of the reaction, the reaction mixture was quenched with milli-Q water (MQ, 10 mL) and extracted with CH₂Cl₂ (3 × 5 mL). The combined organic layers was dried over anhydrous Na₂SO₄, filtered, and concentrated under reduced pressure. The crude residue was purified over silica gel (230–400 mesh) column chromatography using hexane:EtOAc (98.0:2.0) as eluent to afford **1b**.

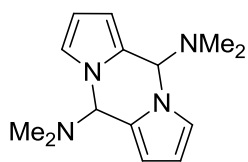
Yield 95% (430 mg); Dark yellow oily liquid; R_f 0.45 (4:1 hexane-EtOAc); ^1H NMR (400 MHz, CDCl_3) δ 9.55 (s, 1H), 7.13 (d, J = 8.3 Hz, 2H), 6.98–6.91 (m, 2H), 6.83 (d, J = 8.3 Hz, 2H), 6.24 (dd, J = 2.8, 2.4 Hz, 1H), 5.48 (s, 2H), 3.76 (s, 3H); ^{13}C NMR (100 MHz, CDCl_3) δ 179.5, 159.2, 131.5, 131.2, 129.6, 128.9, 124.9, 114.1, 110.1, 55.3, 51.5.



1-Methyl-1H-pyrrole-2-carbaldehyde (1c). Potassium tertiary butoxide (1.188 gm, 10.50 mmol) and 18-crown-6 ether (0.16 mL, 0.72 mmol) were suspended in diethyl ether (10 mL) in a two-neck round-bottom flask (50 mL) at room temperature. Pyrrole-2-carboxaldehyde (1.0 gm, 10.50 mmol) was added to the reaction mixture in one portion and stirred for 15 min at the same temperature. Subsequently, the reaction mixture was cooled to 0 °C and methyl iodide (0.32 mL, 5.25 mmol) was added through a glass syringe drop-wise over a period of 5 min. Reaction mixture was allowed to warm to room temperature, stirred for another 24 h and monitored by TLC. After the completion of reaction, the reaction mixture was quenched with milli-Q water (MQ, 10 mL) and extracted with EtOAc (3 × 5 mL). The combined organic layers were dried over anhydrous Na_2SO_4 , filtered, and concentrated under reduced pressure. The crude residue was purified over silica gel (230–400 mesh) column chromatography using hexane:EtOAc (99:1) as eluent to afford **1c**. Yield 83% (950 mg); Light yellow liquid; R_f 0.25 (4:1 hexane-EtOAc); ^1H NMR (400 MHz, CDCl_3) δ 9.54 (s, 1H), 6.98–6.88 (m, 1H), 6.88–6.83 (m, 1H), 6.25–6.17 (m, 1H), 3.95 (s, 3H); ^{13}C NMR (100 MHz, CDCl_3) δ 179.6, 132.1, 132.0, 124.1, 109.5, 36.5.

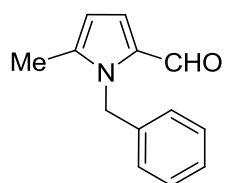


1-Tosyl-1H-pyrrole-2-carbaldehyde (1d). Sodium hydride (55–60% suspension in oil, 50 mg, 1.31 mmol) was suspended in dry dimethyl formamide (3 mL) in a two-neck round-bottom flask (50 mL) at room temperature under an inert atmosphere. Pyrrole-2-carboxaldehyde (100 mg, 1.05 mmol) was added to the reaction mixture in one portion at 0°C and stirred for 20 min. Subsequently, tosyl chloride (200 mg, 1.05 mmol) was added in one portion and reaction mixture was stirred at room temperature overnight (monitored by TLC). After the completion of reaction, the reaction mixture was quenched with milli-Q water (MQ, 10 mL) and extracted with EtOAc (3 × 10 mL). The combined organic layers were dried over anhydrous Na₂SO₄, filtered, and concentrated under reduced pressure. The crude residue was purified over silica gel (230–400 mesh) column chromatography using hexane:EtOAc (95:5) as eluent to afford **1d**. Yield 80% (210 mg); Yellow liquid; *R_f* 0.25 (9:1 hexane-EtOAc); ¹H NMR (400 MHz, CDCl₃) δ 9.96 (s, 1H), 7.78 (d, *J* = 8.3 Hz, 2H), 7.64–7.55 (m, 1H), 7.30 (d, *J* = 8.3 Hz, 2H), 7.14 (dd, *J* = 3.3, 1.2 Hz, 1H), 6.39 (dd, *J* = 3.3, 3.0 Hz, 1H), 2.40 (s, 3H); ¹³C NMR (100 MHz, CDCl₃) δ 179.0, 146.0, 130.2, 129.6, 129.5, 127.8, 127.5, 124.5, 112.4, 38.0.



*N⁵,N⁵,N¹⁰,N¹⁰-tetramethyl-5,10-dihydrodipyrrolo[1,2-*a*:1',2'-*d*]pyrazine-5,10-diamine.* A solution of pyrrole-2-carboxaldehyde (500 mg, 5.25 mmol) in dimethylamine (1.05 mL, 40% in H₂O) was stirred at room temperature for 3 h. The precipitated solid was collected by

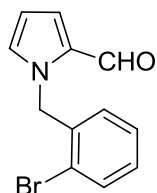
filtration and dried under reduced pressure. The crude solid was recrystallized from hot EtOAc (10 mL) and hexane (5 mL) to afford the dimer. Yield 67% (430 mg); Pink solid; R_f 0.30 (8:2 hexane-EtOAc); ^1H NMR (400 MHz, CDCl_3) δ 6.99–6.91 (m, 2H), 6.29–6.23 (m, 2H), 6.20–6.13 (m, 2H), 5.87 (s, 2H), 2.22 (s, 12H).

**1f**

1-Benzyl-5-methyl-1H-pyrrole-2-carbaldehyde (**1f**).

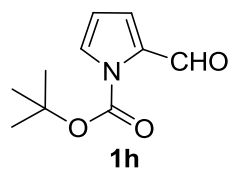
Freshly prepared N^5, N^5, N^{10}, N^{10} -tetramethyl-5,10-dihydrodipyrrolo[1,2-a:1',2'-d]pyrazine-5,10-diamine (1.0 gm, 4.09 mmol) was dissolved in dry THF (15 mL) in a round bottom flask (100 mL) under an inert atmosphere at 0 °C. *n*-BuLi (1.6 M in hexane, 5.62 mL, 9.00 mmol) was added to the reaction mixture slowly, through a glass syringe over a period of 10 min at the same temperature. The reaction mixture warmed to 5 °C and continued for stirring for another 2 h. The reaction mixture was once again cooled to 0 °C and methyl iodide (1.02 mL, 16.36 mmol) was added through a glass syringe over a period of 10 min. The reaction mixture was warmed to room temperature and stirred for 5 h. Saturated NaHCO_3 (25 mL) and MQ water (25 mL) were added and the mixture was heated at 80 °C for 16 h. The reaction mixture was extracted with DCM (3×20 mL). The combined organic layers were dried over anhydrous Na_2SO_4 , filtered, and concentrated under reduced pressure. The crude residue with crushed KOH (1.234 gm, 22.00 mmol) were dissolved in DMSO (6 mL) in a round bottom flask (100 mL) at room temperature with stirring. Benzyl bromide (0.98 mL, 8.25 mmol) was added using a glass syringe drop-wise over a period of 10 min and further stirred for overnight at room temperature. The reaction mixture was quenched with milli-Q water (15 mL) and extracted with EtOAc (5×10 mL). The combined organic layers were dried over anhydrous Na_2SO_4 , filtered, and concentrated under reduced

pressure. The crude residue was purified over silica gel (230–400 mesh) column chromatography using hexane:acetone (96:4) as eluent to afford **1f**. Yield 55% (600 mg); Dark yellow oily liquid; R_f 0.45 (9:1 hexane-acetone); ^1H NMR (400 MHz, CDCl_3) δ 9.45 (s, 1H), 7.37–7.17 (m, 3H), 6.97 (m, 2H), 6.91 (d, J = 3.8 Hz, 1H), 6.08 (d, J = 3.8 Hz, 1H), 5.63 (s, 2H), 2.19 (s, 3H); ^{13}C NMR (100 MHz, CDCl_3) δ 178.6, 140.9, 137.6, 131.8, 128.7, 127.2, 126.2, 125.2, 110.4, 48.3, 12.2.

**1g**

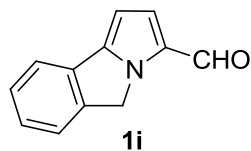
1-(2-Bromobenzyl)-1H-pyrrole-2-carbaldehyde (1g). Sodium hydride (55–60% suspension in oil, 100 mg, 2.52 mmol) was suspended in dry dimethyl formamide (2 mL) in a two-neck round-bottom flask (50 mL) at room temperature under an inert atmosphere. Pyrrole-2-carboxaldehyde (200 mg, 2.10 mmol) was added to the reaction mixture in one portion and stirred for 20 min at the same temperature. Subsequently, the reaction mixture was cooled to 0 °C and 2-bromobenzyl chloride (0.31 mL, 2.52 mmol) was added using a glass syringe drop-wise over a period of 5 min. The reaction mixture was warmed to room temperature and stirred for further 2 h (monitored by TLC). After the completion of reaction, the reaction mixture was quenched with milli-Q water (10 mL) and extracted with EtOAc (3 × 5 mL). The combined organic layers was dried over anhydrous Na_2SO_4 , filtered, and concentrated under reduced pressure. The crude residue was purified over silica gel (230–400 mesh) column chromatography using hexane:EtOAc (99.0:1.0) as eluent to afford **1g**. Yield 78% (430 mg); White solid; R_f 0.60 (8:2hexane-EtOAc); ^1H NMR (400 MHz, CDCl_3) δ 9.57 (s, 1H), 7.56 (d, J = 7.8 Hz, 1H), 7.19 (dd, J = 7.5, 7.5 Hz, 1H), 7.12 (dd, J = 7.8, 7.3 Hz, 1H), 7.00 (d, J = 3.0 Hz, 1H), 6.98–6.93 (m, 1H), 6.67 (d, J = 7.5 Hz, 1H), 6.30 (dd, J = 3.0, 2.6

Hz, 1H), 5.65 (s, 2H); ^{13}C NMR (100 MHz, CDCl_3) δ 179.5, 137.1, 132.8, 131.7, 131.5, 129.2, 128.3, 127.9, 124.7, 122.7, 110.4, 52.1.



Tert-butyl 2-formyl-1H-pyrrole-1-carboxylate (1h).

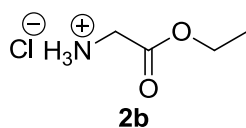
Pyrrole-2-carboxaldehyde (500 mg, 5.25 mmol) and *N,N*-dimethylamino pyridine (65 mg, 0.52 mmol) were dissolved in acetonitrile (5 mL) in a two-neck round-bottom flask (50 mL) at room temperature. Boc anhydride (1.44 mL, 6.30 mmol) was added to the reaction mixture through a glass syringe over a period of 5 min at room temperature under inert atmosphere and stirred for further 2 h (monitored by TLC). After the completion of reaction, the reaction mixture was quenched with milli-Q water (10 mL) and extracted with EtOAc (3×5 mL). The combined organic layers were dried over anhydrous Na_2SO_4 , filtered, and concentrated under reduced pressure. The crude residue was purified over silica gel (230–400 mesh) column chromatography using hexane:EtOAc (99:1) as eluent to afford **1h**. Yield 92% (950 mg); Pale yellow oily liquid; R_f 0.35 (9:1 hexane-EtOAc); ^1H NMR (400 MHz, CDCl_3) δ 10.30 (s, 1H), 7.44–7.39 (m, 1H), 7.16 (d, $J = 2.5$ Hz, 1H), 6.26 (dd, $J = 3.3, 2.5$ Hz, 1H), 1.62 (s, 9H); ^{13}C NMR (100 MHz, CDCl_3) δ 182.3, 148.4, 134.8, 127.4, 121.2, 111.7, 85.8, 28.0.



5H-Pyrrolo[2,1-a]isoindole-3-carbaldehyde (1i).

1-(2-Bromobenzyl)-1H-pyrrole-2-carbaldehyde (1g, 300 mg, 1.14 mmol) was dissolved in dry *N,N*-Dimethyl acetamide (DMA, 2 mL) in a three-neck round-bottom flask (50 mL) and the solution was degassed (through N_2 bubbling). KOAc (112 mg, 1.14 mmol) and $\text{Pd}(\text{PPh}_3)_4$ (70 mg, 0.06 mmol) were added to the reaction mixture at room temperature in one portion.

The reaction mixture was heated at 140 °C using oil bath under inert atmosphere, monitored by TLC for another 7 h. After the completion of reaction, the reaction mixture was quenched with brine (5 mL) and extracted with EtOAc (3 × 5 mL). The combined organic layers were dried over anhydrous Na₂SO₄, filtered, and concentrated under reduced pressure. The crude residue was purified over silica gel (230–400 mesh) column chromatography using hexane:EtOAc (98:2) as eluent to afford **1i**. Yield 76% (160 mg); Yellow crystalline solid; m.p. = 128–130 °C; *R_f* 0.70 (2:1 hexane-EtOAc); ¹H NMR (400 MHz, CDCl₃) δ 9.58 (s, 1H), 7.69–7.59 (m, 1H), 7.53–7.46 (m, 1H), 7.45–7.29 (m, 2H), 7.12–7.03 (m, 1H), 6.52–6.41 (m, 1H), 5.20 (s, 2H); ¹³C NMR (100 MHz, CDCl₃) δ 178.3, 146.1, 141.9, 131.4, 129.8, 128.2, 127.4, 125.7, 123.5, 120.5, 101.3, 52.4.

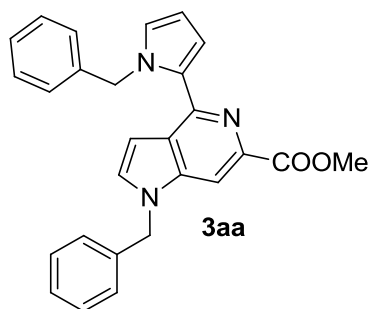


Glycine ethyl ester HCl salt (**2b**). Glycine (5.0gm, 66.60 mmol) was suspended in dry ethanol (30 mL) in around-bottom flask (250 mL). The suspension was cooled to 0 °C and thionyl chloride (7.3 mL, 100 mmol) was added drop-wise through a glass syringe over a period of 10 min. The reaction mixture was refluxed overnight and monitored using TLC. The excess solvent was evaporated under reduced pressure and the residue was further washed with diethyl ether (3 × 10 mL) to afford **2b**. Crude yield 97% (8.980 gm); Off white solid; ¹H NMR (400 MHz, D₂O) δ 4.29 (q, *J* = 7.3 Hz, 2H), 3.90 (s, 2H), 1.28 (t, *J* = 7.3 Hz, 3H); ¹³C NMR (100 MHz, D₂O) δ 168.2, 63.4, 40.3, 13.2.

2.4.2.2 General procedure for synthesis of Alkyl 4-(1*H*-pyrrol-2-yl)-1*H*-pyrrolo[3,2-*c*]pyridine-6-carboxylate derivatives **3aa–fa**

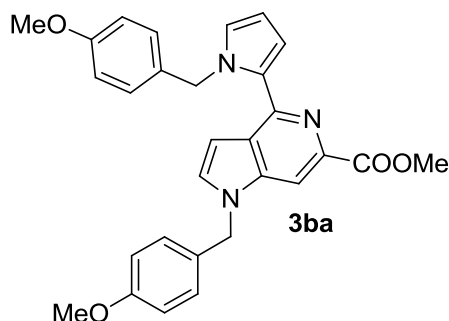
A mixture of glycine alkyl ester hydrochloride (**2a–c**, 1 mmol), aldehyde (**1a–i**, 2 mmol) and *N,N*-Diisopropylethylamine (DIPEA, 3.5 mmol) was heated at 150 °C for 6–12 h in a sealed tube (25 mL, Borosilicate) with

constant stirring (monitored by TLC). The reaction mixture was cooled to room temperature, diluted with CH₂Cl₂ (1 × 10 mL) and washed with brine (1 × 10 mL). The reaction mixture was further extracted with CH₂Cl₂ (3 × 10 mL). The combined organic layer was dried over anhydrous Na₂SO₄, filtered, concentrated, and purified over neutral alumina (175 mesh) column chromatography using hexane-EtOAc solvent mixture as eluent.

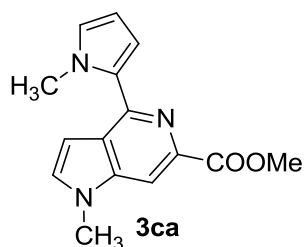


Methyl 1-benzyl-4-(1-benzyl-1H-pyrrol-2-yl)-

1H-pyrrolo[3,2-c]pyridine-6-carboxylate (3aa). According to the general procedure mentioned above, **1a** (100 mg, 0.54 mmol), **2a** (34 mg, 0.27 mmol) and DIPEA (0.165 mL, 0.95 mmol) were heated in a sealed tube at 150 °C for 6 h. After workup, the crude residue was purified through alumina (neutral, 175 mesh) column chromatography using hexane-EtOAc (94:6) as eluent; Yield 58% (66 mg); Yellow crystalline solid; m.p. = 134–136 °C; R_f 0.65 (2:1 hexane-EtOAc); IR (KBr) 3028 (=C–H), 2922–2850 (C–H), 1722 (C=O), 1712–1554 (C=C), 1357 (C–H bend), 779 (=C–H bend) cm⁻¹; ¹H NMR (500 MHz, CDCl₃) δ 8.01 (s, 1H), 7.35–7.27 (m, 3H), 7.24 (d, *J* = 3.2 Hz, 1H), 7.18–7.13 (m, 2H), 7.12–7.08 (m, 3H), 7.07–7.02 (m, 2H), 6.91 (d, *J* = 3.2 Hz, 1H), 6.90–6.87 (m, 1H), 6.82 (dd, *J* = 3.7, 1.7 Hz, 1H), 6.29 (dd, *J* = 2.9, 2.3 Hz, 1H), 5.88 (s, 2H), 5.34 (s, 2H), 3.95 (s, 3H); ¹³C NMR (100 MHz, CDCl₃) δ 167.4, 145.8, 140.5, 139.6, 138.7, 136.2, 131.2, 130.4, 129.0, 128.2, 128.2, 127.1, 127.0, 126.8, 125.7, 125.0, 113.2, 108.2, 105.7, 103.7, 52.5, 51.7, 50.2; HRMS (ESI) calcd for [C₂₇H₂₃N₃O₂+H⁺] 422.1863, found 422.1859.

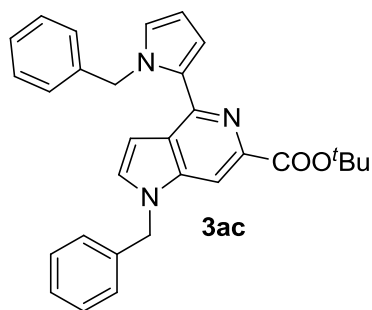


Methyl 1-(4-methoxybenzyl)-4-(1-(4-methoxybenzyl)-1H-pyrrol-2-yl)-1H-pyrrolo[3,2-c]pyridine-6-carboxylate (3ba). According to the general procedure mentioned above, **1b** (100 mg, 0.46 mmol), **2a** (29 mg, 0.23 mmol) and DIPEA (0.140 mL, 0.81 mmol) were heated in a sealed tube at 150 °C for 6 h. After workup, the crude residue was purified through alumina (neutral, 175 mesh) column chromatography using hexane-EtOAc (88:12) as eluent; Yield 61% (68 mg); Yellow liquid; R_f 0.60 (1:1 hexane-EtOAc); IR (KBr) 3073 (=C–H), 2958–2851 (C–H), 1743 (C=O), 1109–1029 (C–O) cm^{-1} ; ^1H NMR (400 MHz, CDCl_3) δ 8.04 (s, 1H), 7.22 (d, J = 3.2 Hz, 1H), 7.08 (d, J = 8.5 Hz, 2H), 7.02 (d, J = 8.5 Hz, 2H), 6.90–6.81 (m, 4H), 6.78 (dd, J = 3.5, 1.5 Hz, 1H), 6.69 (d, J = 8.8 Hz, 2H), 6.25 (dd, J = 3.3, 2.6 Hz, 1H), 5.77 (s, 2H), 5.28 (s, 2H), 3.97 (s, 3H), 3.78 (s, 3H), 3.69 (s, 3H); ^{13}C NMR (100 MHz, CDCl_3) δ 166.7, 158.8, 157.8, 145.1, 139.6, 137.9, 130.9, 130.3, 129.6, 127.9, 127.8, 127.4, 124.7, 124.4, 113.7, 112.9, 112.5, 107.3, 105.0, 102.8, 54.6, 54.4, 51.7, 50.4, 49.0; HRMS (ESI) calcd for $[\text{C}_{29}\text{H}_{27}\text{N}_4\text{O}_3+\text{H}^+]$ 482.2074, found 482.2074.



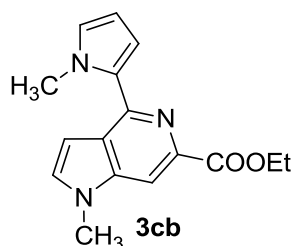
Methyl 1-methyl-4-(1-methyl-1H-pyrrol-2-yl)-1H-pyrrolo[3,2-c]pyridine-6-carboxylate (3ca). According to the general procedure mentioned above, **1c** (100 mg, 0.92 mmol), **2a** (29 mg, 0.46 mmol) and DIPEA (0.281 mL, 1.61 mmol) were heated in a sealed tube at

150 °C for 6 h. After workup, the crude residue was purified through alumina (neutral, 175 mesh) column chromatography using hexane-EtOAc (92:8) as eluent; Yield 48% (59 mg); Yellowish-brown liquid; R_f 0.60 (1:1 hexane-EtOAc); IR (KBr) 3126–3084 (=C–H), 2926–2852 (C–H), 1732 (C=O), 1714–1556 (C=C), 1350 (C–H bend), 721 (=C–H bend) cm^{-1} ; ^1H NMR (400 MHz, CDCl_3) δ 8.04 (s, 1H), 7.24–7.17 (m, 1H), 6.89–6.81 (m, 1H), 6.80–6.74 (m, 1H), 6.73–6.68 (m, 1H), 6.25–6.13 (m, 1H), 4.03 (s, 3H), 3.97 (s, 3H), 3.85 (s, 3H); ^{13}C NMR (100 MHz, CDCl_3) δ 167.5, 145.7, 140.7, 138.5, 132.0, 130.7, 126.2, 124.9, 112.6, 107.5, 105.5, 103.1, 52.5, 36.4, 33.1; HRMS (ESI) calcd for $[\text{C}_{15}\text{H}_{15}\text{N}_3\text{O}_2+\text{H}^+]$ 270.1237, found 270.1233.



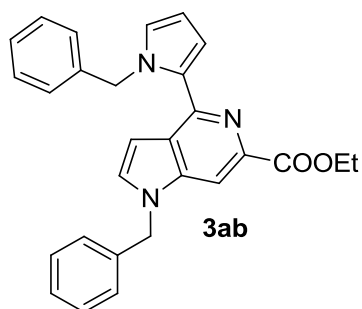
Tert-butyl-1-benzyl-4-(1-benzyl-1H-pyrrol-2-yl)-1H-pyrrolo[3,2-c]pyridine-6-carboxylate (3ac). According to the general procedure mentioned above, **1a** (100 mg, 0.54 mmol), **2c** (45 mg, 0.27 mmol) and DIPEA (0.165 mL, 1.61 mmol) were heated in a sealed tube at 150 °C for 8 h. After workup, the crude residue was purified through alumina (neutral, 175 mesh) column chromatography using hexane-EtOAc (95:5) as eluent; Yield 40% (50 mg); Yellow liquid; R_f 0.50 (4:1 hexane-EtOAc); IR (KBr) 3063 (=C–H), 2976–2849 (C–H), 1732 (C=O), 1701–1564 (C=C), 1363 (C–H bend), 723 (=C–H bend) cm^{-1} ; ^1H NMR (400 MHz, CDCl_3) δ 7.93 (s, 1H), 7.37–7.26 (m, 3H), 7.22 (d, $J = 3.2$ Hz, 1H), 7.19–7.04 (m, 7H), 6.91 (d, $J = 3.2$ Hz, 1H), 6.89–6.82 (m, 2H), 6.26 (dd, $J = 3.2, 3.0$ Hz, 1H), 6.03 (s, 2H), 5.33 (s, 2H), 1.59 (s, 9H); ^{13}C NMR (100 MHz, CDCl_3) δ 166.0, 145.4, 140.7, 140.2, 139.8, 136.3, 130.9, 130.5, 129.0, 128.3, 128.1, 127.2, 127.0, 126.8, 125.8, 124.3,

113.3, 108.1, 105.0, 103.5, 81.1, 51.8, 50.1, 28.3; HRMS (ESI) calcd for $[C_{30}H_{29}N_3O_2+H^+]$ 464.2333, found 464.2334.



Ethyl 1-methyl-4-(1-methyl-1H-pyrrol-2-yl)-1H-

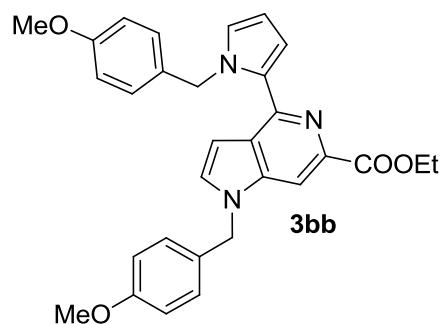
pyrrolo[3,2-c]pyridine-6-carboxylate (3cb). According to the general procedure mentioned above, **1c** (100 mg, 0.92 mmol), **2b** (64 mg, 0.46 mmol) and DIPEA (0.281 mL, 1.61 mmol) were heated in a sealed tube at 150 °C for 7 h. After workup, the crude residue was purified through alumina (neutral, 175 mesh) column chromatography using hexane-EtOAc (92:8) as eluent Yield 46% (60 mg); Light yellow liquid; R_f 0.50 (2:1 hexane-EtOAc); IR (KBr) 3077 (=C–H), 2957–2850 (C–H), 1731 (C=O), 1714–1558 (C=C), 1374 (C–H bend), 725 (=C–H bend) cm^{-1} ; 1H NMR (400 MHz, $CDCl_3$) δ 8.04 (s, 1H), 7.24–7.19 (m, 1H), 6.92–6.85 (m, 1H), 6.83–6.78 (m, 1H), 6.78–6.72 (m, 1H), 6.27–6.19 (m, 1H), 4.46 (q, J = 6.8 Hz, 2H), 4.10 (s, 3H), 3.88 (s, 3H), 1.45 (t, J = 6.8 Hz, 3H); ^{13}C NMR (100 MHz, $CDCl_3$) δ 166.9, 145.5, 140.7, 138.7, 131.9, 130.7, 126.3, 124.6, 112.7, 107.5, 105.2, 103.0, 61.3, 36.6, 33.1, 14.4; HRMS (ESI) calcd for $[C_{16}H_{17}N_3O_2+H^+]$ 284.1394, found 284.1389.



Ethyl 1-benzyl-4-(1-benzyl-1H-pyrrol-2-yl)-

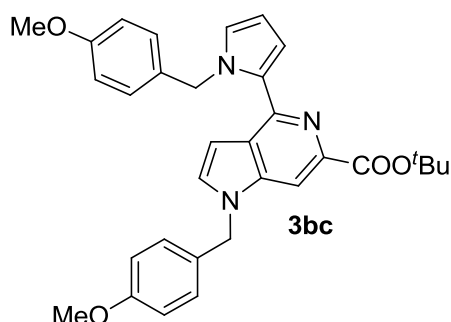
1H-pyrrolo[3,2-c]pyridine-6-carboxylate (3ab). According to the general procedure mentioned above, **1a** (100 mg, 0.54 mmol), **2b** (38 mg, 0.27 mmol) and DIPEA (0.165 mL, 0.95 mmol) were heated in a sealed tube at

150 °C for 6 h. After workup, the crude residue was purified through alumina (neutral, 175 mesh) column chromatography using hexane-EtOAc (94:6) as eluent; Yield 55% (65 mg); Yellow liquid; R_f 0.60 (4:1 hexane-EtOAc); IR (KBr) 3056 (=C-H), 2977–2851 (C-H), 1729 (C=O), 1712–1554 (C=C), 1367 (C-H bend), 726 (=C-H bend) cm^{-1} ; ^1H NMR (400 MHz, CDCl_3) δ 7.99 (s, 1H), 7.38–7.26 (m, 3H), 7.26–7.21 (m, 1H), 7.19–7.13 (m, 2H), 7.13–7.02 (m, 5H), 6.95–6.90 (m, 1H), 6.90–6.86 (m, 1H), 6.85–6.80 (m, 1H), 6.33–6.24 (m, 1H), 5.94 (s, 2H), 5.35 (s, 2H), 4.41 (q, J = 6.8 Hz, 2H), 1.38 (t, J = 6.8 Hz, 3H); ^{13}C NMR (100 MHz, CDCl_3) δ 166.9, 145.7, 140.6, 139.7, 139.0, 136.3, 131.1, 130.4, 129.0, 128.3, 128.2, 127.2, 127.0, 126.8, 125.8, 124.8, 113.3, 108.2, 105.5, 103.6, 61.3, 51.7, 50.2, 14.4; HRMS (ESI) calcd for $[\text{C}_{28}\text{H}_{25}\text{N}_3\text{O}_2+\text{H}^+]$ 436.2020, found 436.2024.



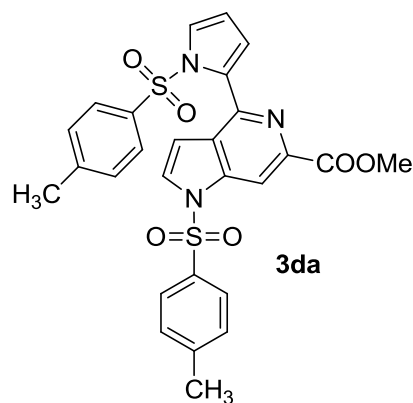
Ethyl 1-(4-methoxybenzyl)-4-(1-(4-methoxybenzyl)-1H-pyrrol-2-yl)-1H-pyrrolo[3,2-c]pyridine-6-carboxylate (3bb). According to the general procedure mentioned above, **1b** (100 mg, 0.46 mmol), **2b** (32 mg, 0.23 mmol) and DIPEA (0.140 mL, 0.81 mmol); Yield 60% (68 mg) were heated in a sealed tube at 150 °C for 8 h. After workup, the crude residue was purified through alumina (neutral, 175 mesh) column chromatography using hexane-EtOAc (90:10) as eluent; Yellow liquid; R_f 0.55 (2:1 hexane-EtOAc); IR (KBr) 3067 (=C-H), 2955–2852 (C-H), 1738 (C=O), 1713–1515 (C=C), 1369 (C-H bend), 1106–1028 (C-O), 727 (=C-H bend) cm^{-1} ; ^1H NMR (400 MHz, CDCl_3) δ 8.03 (s, 1H), 7.21 (d, J = 3 Hz, 1H), 7.08 (d, J = 8.5 Hz, 2H), 7.05 (d, J =

8.8 Hz, 2H), 6.88 (d, $J = 3.0$ Hz, 1H), 6.87–6.82 (m, 3H), 6.80 (dd, $J = 3.3, 1.2$ Hz, 1H), 6.69 (d, $J = 8.8$ Hz, 2H), 6.26 (dd, $J = 3.0, 2.5$ Hz, 1H), 5.83 (s, 2H), 5.28 (s, 2H), 4.43 (q, $J = 7.0$ Hz, 2H), 3.78 (s, 3H), 3.70 (s, 3H), 1.40 (t, $J = 7.0$ Hz, 3H); ^{13}C NMR (100 MHz, CDCl_3) δ 167.0, 159.5, 158.5, 145.7, 140.4, 138.9, 131.7, 130.9, 130.3, 128.6, 128.6, 128.2, 125.4, 124.8, 114.4, 113.7, 113.2, 108.0, 105.5, 103.5, 61.3, 55.3, 55.2, 51.1, 49.7, 14.4; HRMS (ESI) calcd for $[\text{C}_{30}\text{H}_{29}\text{N}_3\text{O}_4+\text{H}^+]$ 496.2231, found 496.2230.

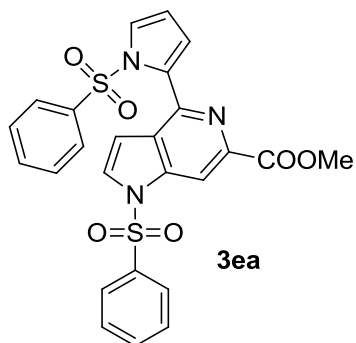


Tert-butyl 1-(4-methoxybenzyl)-4-(1-(4-methoxybenzyl)-1H-pyrrol-2-yl)-1H-pyrrolo[3,2-c]pyridine-6-carboxylate (3bc). According to the general procedure mentioned above, **1b** (100 mg, 0.46 mmol), **2c** (39 mg, 0.23 mmol) and DIPEA (0.140 mL, 0.81 mmol) were heated in a sealed tube at 150 °C for 7 h. After workup, the crude residue was purified through alumina (neutral, 175 mesh) column chromatography using hexane-EtOAc (9:1) as eluent; Yield 42% (50 mg); Yellow-orange oily liquid; R_f 0.55 (2:1 hexane-EtOAc); IR (KBr) 3066 (=C-H), 2995–2833 (C-H), 1730 (C=O), 1715–1554 (C=C), 1366 (C–H bend), 1113–1033 (C–O), 727 (=C–H bend) cm^{-1} ; ^1H NMR (400 MHz, CDCl_3) δ 7.96 (s, 1H), 7.19 (d, $J = 3.3$ Hz, 1H), 7.08 (d, $J = 8.6$ Hz, 2H), 7.04 (d, $J = 8.5$ Hz, 2H), 6.88 (d, $J = 3.3$ Hz, 1H), 6.87–6.79 (m, 4H), 6.69 (d, $J = 8.5$ Hz, 2H), 6.25 (dd, $J = 3.5, 2.4$ Hz, 1H), 5.93 (s, 2H), 5.26 (s, 2H), 3.78 (s, 3H), 3.69 (s, 3H), 1.61 (s, 9H); ^{13}C NMR (100 MHz, CDCl_3) δ 166.1, 159.5, 158.5, 145.4, 140.6, 140.1, 131.8, 130.7, 130.4, 128.7, 128.6, 128.3, 125.5, 124.3, 114.4, 113.7, 113.3, 108.0, 105.0,

103.4, 81.1, 55.3, 55.2, 51.3, 49.7, 28.3; HRMS (ESI) calcd for $[C_{32}H_{33}N_3O_4+H^+]$ 524.2544, found 524.2551.



Methyl 1-tosyl-4-(1-tosyl-1H-pyrrol-2-yl)-1H-pyrrolo[3,2-c]pyridine-6-carboxylate (3da). According to the general procedure mentioned above, **1d** (100 mg, 0.40 mmol), **2a** (25 mg, 0.20 mmol) and DIPEA (0.122 mL, 0.70 mmol) were heated in a sealed tube at 150 °C for 12 h. After workup, the crude residue was purified through alumina (neutral, 175 mesh) column chromatography using hexane-EtOAc (85:15) as eluent; Yield 47% (52 mg); Off white solid; m.p. = 120–122 °C; R_f 0.50 (1:1 hexane-EtOAc); IR (KBr) 3132–3064 (=C–H), 2955–2850 (C–H), 1728 (C=O), 1710–1512 (C=C), 1371 (C–H bend), 1309 (N–S=O), 1145 (S=O), 725 (=C–H bend) cm^{-1} ; 1H NMR (400 MHz, $CDCl_3$) δ 8.72 (s, 1H), 7.93 (d, J = 8.0 Hz, 2H), 7.86 (d, J = 8.3 Hz, 2H), 7.70 (d, J = 3.8 Hz, 1H), 7.41–7.36 (m, 1H), 7.32 (d, J = 8.0 Hz, 2H), 7.29–7.25 (m, 2H), 6.66 (d, J = 3.8 Hz, 1H), 6.41–6.36 (m, 1H), 6.33 (dd, J = 3.3, 2.6 Hz, 1H), 4.03 (s, 3H), 2.40 (s, 3H), 2.38 (s, 3H); ^{13}C NMR (100 MHz, $CDCl_3$) δ 166.1, 146.2, 145.5, 145.0, 142.0, 139.3, 136.0, 134.8, 131.0, 130.5, 130.2, 129.8, 129.3, 128.3, 127.2, 124.3, 117.3, 112.2, 110.2, 108.1, 53.0, 29.8, 21.7; HRMS (ESI) calcd for $[C_{27}H_{23}N_3O_6S_2+H^+]$ 550.1101, found 550.1096.

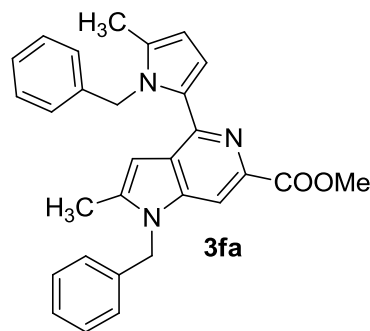


Methyl

1-(phenylsulfonyl)-4-(1-

(phenylsulfonyl)-1H-pyrrol-2-yl)-1H-pyrrolo[3,2-c]pyridine-6-

carboxylate (**3ea**). According to the general procedure mentioned above, **1e** (100 mg, 0.43 mmol), **2a** (27 mg, 0.21 mmol) and DIPEA (0.128 mL, 0.74 mmol) were heated in a sealed tube at 150 °C for 12 h. After workup, the crude residue was purified through alumina (neutral, 175 mesh) column chromatography using hexane-EtOAc (85:15) as eluent; Yield 45% (49 mg); Yellow solid; m.p. = 104–106 °C; R_f 0.50 (1:1 hexane-EtOAc); IR (KBr) 3132–3064 (=C–H), 3005–2850 (C–H), 1728 (C=O), 1710–1512 (C=C), 1371 (C–H bend), 1309 (N–S=O), 1145 (S=O), 725 (=C–H bend) cm^{-1} ; ^1H NMR (400 MHz, CDCl_3) δ 8.74 (s, 1H), 8.06 (d, J = 7.5 Hz, 2H), 7.99 (d, J = 7.5 Hz, 2H), 7.71 (d, J = 3.8 Hz, 1H), 7.67–7.43 (m, 6H), 7.40 (dd, J = 3.0, 1.5 Hz, 1H), 6.67 (d, J = 3.8 Hz, 1H), 6.42 (dd, J = 3.0, 1.5 Hz, 1H), 6.35 (dd, J = 3.3, 2.5 Hz, 1H), 4.01 (s, 3H); ^{13}C NMR (100 MHz, CDCl_3) δ 166.0, 145.3, 142.1, 139.3, 139.0, 137.7, 134.8, 133.8, 131.0, 129.8, 129.6, 129.3, 129.1, 128.1, 127.1, 124.4, 117.5, 112.3, 110.1, 108.2, 52.9; HRMS (ESI) calcd for $[\text{C}_{25}\text{H}_{19}\text{N}_3\text{O}_6\text{S}_2+\text{Na}^+]$ 544.0607, found 544.0603.

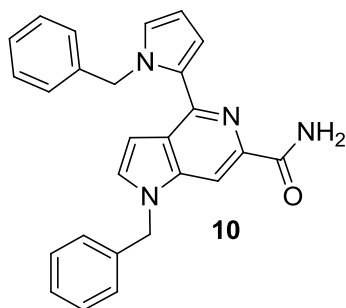


Methyl 1-benzyl-4-(1-benzyl-5-methyl-1H-

pyrrol-2-yl)-2-methyl-1H-pyrrolo[3,2-c]pyridine-6-carboxylate (3fa).

According to the general procedure mentioned above, **1f** (100 mg, 0.50 mmol), **2a** (32 mg, 0.25 mmol) and DIPEA (0.150 mL, 0.88 mmol) were heated in a sealed tube at 150 °C for 6 h. After workup, the crude residue was purified through alumina (neutral, 175 mesh) column chromatography using hexane-EtOAc (90:10) as eluent; Yield 64% (72 mg); Yellow liquid; R_f 0.55 (2:1 hexane-EtOAc); IR (KBr) 3027 (=C-H), 2949–2852 (C-H), 1727 (C=O), 1712–1539 (C=C), 1355 (C-H bend), 782 (=C-H bend) cm^{-1} ; ^1H NMR (400 MHz, CDCl_3) δ 7.88 (s, 1H), 7.43–7.26 (m, 3H), 7.19–7.01 (m, 3H), 6.99–6.90 (m, 2H), 6.89–6.82 (m, 2H), 6.80–6.66 (m, 2H), 6.12–6.02 (m, 1H), 5.92 (s, 2H), 5.33 (s, 2H), 3.87 (s, 3H), 2.38 (s, 3H), 2.22 (s, 3H); ^{13}C NMR (100 MHz, CDCl_3); ^{13}C NMR (100 MHz, CDCl_3) δ 167.5, 144.7, 141.4, 140.5, 139.9, 138.0, 136.5, 133.2, 130.4, 129.5, 129.0, 128.2, 127.7, 126.3, 126.1, 126.0, 112.3, 107.5, 105.1, 102.5, 52.3, 47.8, 46.8, 12.9, 12.7; HRMS (ESI) calcd for $[\text{C}_{29}\text{H}_{27}\text{N}_3\text{O}_2+\text{H}^+]$ 450.2176, found 450.2173.

2.4.2.3 Synthesis of 5-azaindole derivatives 10–16

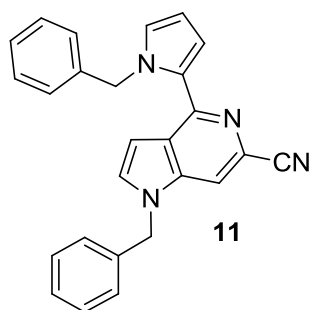


1-Benzyl-4-(1-benzyl-1H-pyrrol-2-yl)-1H-

pyrrolo[3,2-c]pyridine-6-carboxamide (10). In around-bottom flask (100 mL), *Methyl 1-benzyl-4-(1-benzyl-1H-pyrrol-2-yl)-1H-pyrrolo[3,2-c]pyridine-6-carboxylate (3aa*, 100 mg, 0.24 mmol) and KOH (14 mg, 0.24 mmol) was dissolved in methanol (5 mL) at room temperature under continuous stirring. Aqueous ammonia (25%, 0.350 mL, 9.40 mmol) was added to the mixture dropwise using a glass syringe over a period of 10 min. The reaction mixture was stirred at the room temperature for further 24 h. After the completion of the reaction, MeOH was evaporated under reduced pressure. MilliQ water (5 mL) and EtOAc (5 mL) was added to the residue and organic layer was separated. The aqueous phase was further extracted with EtOAc (5 × 3 mL). The combined organic layers were dried over anhydrous Na₂SO₄, filtered, and concentrated under reduced pressure. The residue was purified using EtOAc as eluent over neutral alumina (175 mesh) column chromatography; Yield 78% (150 mg); Yellow gummy liquid; R_f 0.50 (EtOAc); IR (KBr) 3431 (N–H), 3033 (=C–H), 2960–2852 (C–H), 1677 (C=O), 1562 (C–N bend), 1376–1360 (C–H bend), 1296–1029 (C–O), 726 (=C–H bend) cm^{−1}; ¹H NMR (400 MHz, CDCl₃) δ 8.07 (s, 1H), 7.38–7.19 (m, 7H), 7.16–7.06 (m, 3H), 6.95 (d, *J* = 3.0 Hz, 1H), 6.92–6.85 (m, 2H), 6.85–6.78 (m, 1H), 6.40 (dd, *J* = 3.0, 2.6 Hz, 1H), 5.59 (s, 2H), 5.38 (s, 2H), 4.89 (brs, 2H); ¹³C NMR (100 MHz, CDCl₃) δ 168.1, 144.1, 141.1, 140.0, 136.3, 131.0, 129.0, 129.0, 128.7, 128.1, 127.0, 127.0, 126.9, 126.1, 125.3, 124.9, 112.6, 108.8, 103.5,

103.0, 51.3, 50.2; MS (ESI) calcd for $[C_{26}H_{22}N_4O+H^+]$ 407.1866, found 407.2023.*

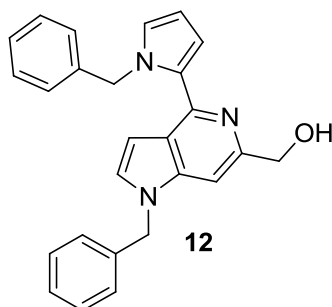
*The compound **10** is unstable in polar solvent to record a good HRMS.



1-Benzyl-4-(1-benzyl-1H-pyrrol-2-yl)-1H-

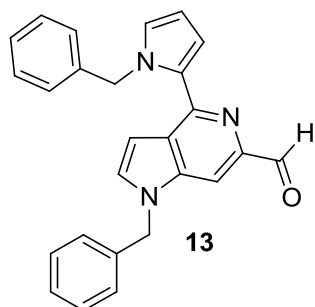
pyrrolo[3,2-c]pyridine-6-carbonitrile (11). An oven-dried single neck round-bottom flask (25 mL) was charged with 1-Benzyl-4-(1-benzyl-1H-pyrrol-2-yl)-1H-pyrrolo[3,2-c]pyridine-6-carboxamide **10** (40 mg, 0.098 mmol) and POCl₃ (5 mL) was added drop-wise using a glass syringe over a period of 20 min at room temperature. A reflux condenser was fixed to the round bottom flask and the reaction mixture was heated at 60 °C and stirred for overnight. After the completion of the reaction (monitored by TLC), the reaction mixture was diluted with toluene (5 mL) and the solvent was evaporated under reduced pressure. Saturated NaHCO₃ (10 mL) was added slowly to the reaction mixture to neutralize excess phosphorous oxychloride. The aqueous phase was extracted with EtOAc (5 × 3 mL). The combined organic layers were dried over anhydrous Na₂SO₄, filtered, and concentrated under reduced pressure. The residue was purified using hexane-EtOAc (90:10) as eluent over neutral alumina (175 mesh) column chromatography to afford **11**; Yield 66% (25 mg); colorless liquid; R_f 0.20 (2:1 hexane-EtOAc); IR (KBr) 3431 (N–H), 3031 (=C–H), 2960–2852 (C–H), 2223 (–C≡N stretch), 1588–1530 (C=C), 1376–1360 (C–H bend), 725 (=C–H bend) cm⁻¹; ¹H NMR (400 MHz, CDCl₃) δ 7.43 (s, 1H), 7.39–7.31 (m, 3H), 7.30 (d, *J* = 3.0 Hz, 1H), 7.22–7.02 (m, 7H), 6.94 (d, *J* = 3.0 Hz, 1H), 6.93–6.89 (m, 1H), 6.85 (dd, *J* = 3.5, 1.2 Hz, 1H), 6.31 (dd, *J* = 3.0, 2.4 Hz, 1H), 5.75 (s, 2H), 5.31 (s, 2H);

^{13}C NMR (100 MHz, CDCl_3) δ 147.3, 139.2, 135.5, 131.7, 129.5, 129.2, 128.5, 128.5, 128.4, 127.2, 127.0, 126.9, 126.6, 124.6, 123.1, 119.2, 114.1, 109.1, 108.4, 104.1, 52.1, 50.6; HRMS (ESI) calcd for $[\text{C}_{26}\text{H}_{20}\text{N}_4+\text{H}^+]$ 389.1761, found 389.1777.



(1-Benzyl-4-(1-benzyl-1H-pyrrol-2-yl)-1H-pyrrolo[3,2-c]pyridin-6-yl)methanol (**12**). In a two-neck round-bottom flask (50 mL), Methyl 1-benzyl-4-(1-benzyl-1H-pyrrol-2-yl)-1H-pyrrolo[3,2-c]pyridine-6-carboxylate (**3aa**, 250 mg, 0.59 mmol) was dissolved in dry THF (5 mL) under an inert atmosphere. The reaction mixture was cooled to 0 °C before addition of solid LiAlH_4 (68 mg, 1.78 mmol) in single portion. The reaction mixture was warmed to room temperature and further stirred for 20 min. After the consumption of ester **3aa**, as confirmed by TLC, the reaction mixture was quenched with saturated NH_4Cl (10 mL) solution and further diluted with EtOAc (10 mL). The aqueous layer was extracted using EtOAc (10 \times 3 mL). The combined organic extracts were dried over anhydrous Na_2SO_4 , filtered, evaporated under reduced pressure, and the crude residue was purified over neutral alumina (175 mesh) column chromatography using hexane-EtOAc (75:25) as eluent; Yield 94% (220 mg); colorless liquid; R_f 0.35 (2:1 hexane-EtOAc); IR (KBr) 3414 (O–H), 3028 (=C–H), 2958–2850 (C–H), 1695–1559 (C=C), 1357 (C–H bend), 1100–1023 (C–O stretch) cm^{-1} ; ^1H NMR (400 MHz, CDCl_3) δ 7.36–7.17 (m, 6H), 7.13 (d, J = 3.3 Hz, 1H), 7.07 (dd, J = 7.5, 8.0 Hz, 4H), 6.90 (s, 1H), 6.89–6.80 (m, 3H), 6.36 (dd, J = 3.0, 2.6 Hz, 1H), 5.65 (s, 2H), 5.28 (s, 2H), 4.63 (s, 2H), 3.24 (brs, 1H); ^{13}C NMR (100 MHz, CDCl_3) δ 149.6, 144.7, 141.6, 139.7,

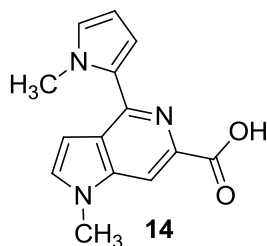
136.6, 131.1, 129.2, 129.0, 128.5, 128.0, 127.0, 126.8, 126.3, 125.2, 122.7, 112.6, 108.5, 103.0, 99.0, 64.7, 51.7, 50.1; HRMS (ESI) calcd for $[C_{26}H_{23}N_3O+H^+]$ 394.1914, found 394.1913.



1-Benzyl-4-(1-benzyl-1H-pyrrol-2-yl)-1H-

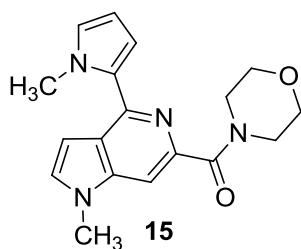
pyrrolo[3,2-c]pyridine-6-carbaldehyde (13). A solution of *(1-Benzyl-4-(1-benzyl-1H-pyrrol-2-yl)-1H-pyrrolo[3,2-c]pyridin-6-yl)methanol 12* (100 mg, 0.25 mmol) was prepared in dichloromethane (5 mL) in a round-bottom flask (100 mL) and solid MnO_2 (326 mg, 3.75 mmol) was added in a single portion. A double-walled reflux condenser was fixed to the round-bottom flask and reaction mixture was refluxed overnight. After the completion of reaction, solvent was evaporated under reduced pressure. The residual mixture was purified over neutral alumina (175 mesh) column chromatography using hexane-EtOAc (95:5) as eluent; Yield 70% (70 mg); Off white liquid; R_f 0.55 (2:1 hexane-EtOAc); IR (KBr) 3030 ($=C-H$), 2960–2852 ($C-H$), 1696 ($C=O$), 1606–1556 ($C=C$), 1358–1331 ($C-H$ bend), 1287–1079 ($C-O$), 725 ($=C-H$ bend) cm^{-1} ; 1H NMR (400 MHz, $CDCl_3$) δ 10.02 (s, 1H), 7.83 (s, 1H), 7.42–7.27 (m, 4H), 7.23–7.02 (m, 7H), 6.98–6.93 (m, 1H), 6.92–6.88 (m, 1H), 6.88–6.82 (m, 1H), 6.42–6.28 (m, 1H), 5.81 (s, 2H), 5.36 (s, 2H); ^{13}C NMR (100 MHz, $CDCl_3$) δ 194.3, 146.3, 145.1, 140.4, 139.5, 136.0, 132.3, 130.3, 129.1, 128.4, 128.3, 127.0*, 126.8, 126.2, 125.9, 113.3, 108.5, 103.7, 102.2, 51.9, 50.4; HRMS (ESI) calcd for $[C_{26}H_{21}N_3O+H^+]$ 392.1757, found 392.1756.

*higher intensity carbon



1-Methyl-4-(1-methyl-1H-pyrrol-2-yl)-1H-

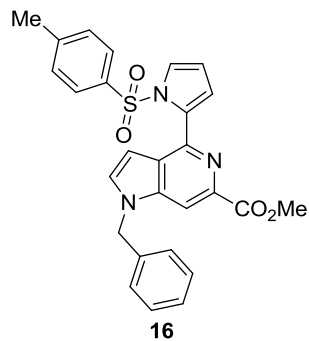
pyrrolo[3,2-c]pyridine-6-carboxylic acid (14). Around-bottom flask (50 mL) was charged with *Methyl 1-methyl-4-(1-methyl-1H-pyrrol-2-yl)-1H-pyrrolo[3,2-c]pyridine-6-carboxylate (3ca*, 200 mg, 0.74 mmol) dissolved in THF (3 mL). 1M aqueous LiOH solution (2.5 mL) was added at room temperature and the reaction mixture was stirred for 3 h at the same temperature (monitored by TLC). After the consumption of **3ca**, diethyl ether (10 mL) and saturated NaHCO₃ (10 mL) was added to the reaction mixture. The aqueous layer was separated and acidified to pH 4 (by dropwise addition of 6N HCl). The aqueous phase was extracted with EtOAc (5 × 10 mL). The combined organic layers were dried over anhydrous Na₂SO₄, filtered, and evaporated under reduced pressure to give crude product **14** which was utilized in the next step without further purification; Crude yield 90% (172 mg); Yellow oily liquid; R_f 0.10 (EtOAc); ¹H NMR (400 MHz, CDCl₃) δ 8.14 (s, 1H), 7.32 (d, *J* = 3.0 Hz, 1H), 6.90 (d, *J* = 3.0 Hz, 1H), 6.86 (m, 1H), 6.77 (dd, *J* = 3.5, 1.3 Hz, 1H), 6.29 (dd, *J* = 2.8, 2.4 Hz, 1H), 3.94 (s, 3H), 3.91 (s, 3H); ¹³C NMR (100 MHz, CDCl₃) δ 164.8, 142.8, 140.3, 135.8, 132.0, 128.2, 125.8, 124.5, 112.6, 107.3, 102.9, 102.7, 35.3, 32.3; HRMS (ESI) calcd for [C₁₄H₁₃N₃O₂+H⁺] 256.1081, found 256.1066.



(1-Methyl-4-(1-methyl-1H-pyrrol-2-yl)-1H-

pyrrolo[3,2-c]pyridin-6-yl)(morpholino)methanone (15). A two-neck

round-bottom flask (50 mL) was charged with unpurified **14** (100 mg, 0.39 mmol) dissolved in dry DMF (4 mL) under an inert atmosphere. The reaction mixture was cooled briefly to 0°C before addition of morpholine (0.13 mL, 1.57 mmol), *1-ethyl-3-(3-dimethylaminopropyl)carbodiimide* (300 mg, 1.57 mmol), hydroxybenzotriazole (212 mg, 1.57 mmol) and DIPEA (0.54 mL, 3.13 mmol) in a sequential manner under constant stirring. The reaction mixture was warmed to room temperature, stirred for further 16 h. After the consumption of **14** as confirmed by TLC, cold brine (10 mL) was added to the reaction mixture. The reaction mixture was extracted with EtOAc (10 × 3 mL) and the combined organic layers were dried over anhydrous Na₂SO₄, filtered, concentrated, and purified over neutral alumina (175 mesh) column chromatography using hexane-EtOAc (50:50) as eluent; Yield 49% (60 mg); White crystalline solid; m.p. = 95–96 °C; *R_f* 0.40 (1:1 hexane-EtOAc); IR (KBr) 3065 (=C–H), 2957–2850 (C–H), 1682 (C=O), 1641–1513 (C=C), 1371 (C–H bend), 723 (=C–H bend) cm⁻¹; ¹H NMR (400 MHz, CDCl₃) δ 7.65 (s, 1H), 7.17 (d, *J* = 3.0 Hz, 1H), 6.82 (d, *J* = 3.0 Hz, 1H), 6.80–6.77 (m, 1H), 6.76–6.71 (m, 1H), 6.25 (dd, *J* = 2.8, 2.4 Hz, 1H), 3.97 (s, 3H), 3.92–3.76 (m, 9H), 3.72–3.60 (m, 2H); ¹³C NMR (100 MHz, CDCl₃) δ 169.2, 144.2, 144.1, 141.1, 131.1, 130.9, 125.9, 123.4, 112.6, 107.6, 104.3, 102.8, 67.3, 67.0, 48.1, 43.1, 36.6, 32.9; HRMS (ESI) calcd for [C₁₈H₂₀N₄O₂+H⁺] 325.1659, found 325.1655.



Methyl 1-benzyl-4-(1-tosyl-1H-pyrrol-2-yl)-1H-pyrrolo[3,2-c]pyridine-6-carboxylate (16). A mixture of *N*-benzyl pyrrole-2-aldehyde **1a** (37 mg, 0.20 mmol) and *N*-tosyl pyrrole-2-aldehyde **1d** (50

mg, 0.20 mmol), glycine methyl ester hydrochloride **2a** (25 mg, 0.20 mmol) and DIPEA (0.12 mL, 0.70 mmol) was heated in a sealed tube at 150 °C for 6 h. The crude mixture was diluted with CH₂Cl₂ (10 mL) and washed with brine solution (10 mL). The aqueous layer was extracted with CH₂Cl₂ (3 × 10 mL). The combined organic layers were dried over anhydrous Na₂SO₄, filtered, concentrated, and purified over neutral alumina (175 mesh) column chromatography using hexane-EtOAc (80:20) as eluent; Yield 41% (40 mg); White crystalline solid; m.p. = 130–32 °C; R_f 0.22 (3:1 hexane-EtOAc); ¹H NMR (400 MHz, CDCl₃) δ 8.15 (s, 1H), 7.93 (d, *J* = 8.0 Hz, 2H), 7.34–7.09 (m, 9H), 6.54–6.47 (m, 1H), 6.45–6.37 (m, 1H), 6.29 (dd, *J* = 2.8, 2.4 Hz, 1H), 5.34 (s, 2H), 3.92 (s, 3H), 2.33 (s, 3H); ¹³C NMR (100 MHz, CDCl₃) δ 167.1, 144.8, 144.6, 139.9, 139.0, 136.3, 136.0, 132.1, 131.8, 129.6, 129.1, 128.34, 128.31, 128.2, 127.1, 123.7, 116.7, 111.9, 107.7, 103.4, 52.7, 50.4, 21.7; HRMS (ESI) calcd for [C₂₇H₂₃N₃O₄S+H⁺] 486.1409, found 486.1452.

2.4.2.4 Density Functional Theory Calculations

The density functional theoretical calculations are done at B3LYP/6-311++G** level of theory using Gaussian 09 D.01 program [20–22].

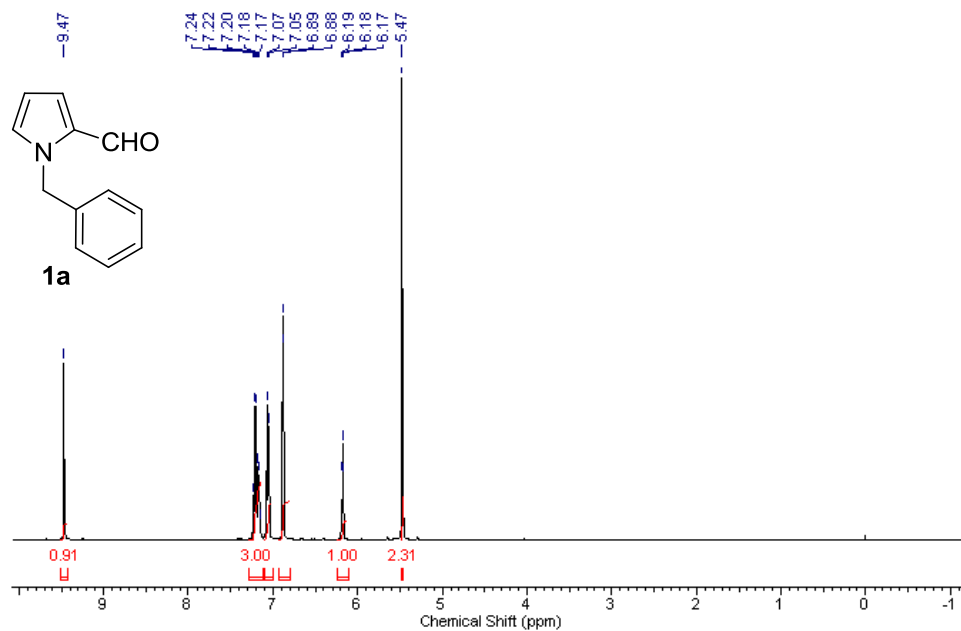
2.4.3 Copies of ^1H , ^{13}C NMR spectra for synthesized compounds

Figure 2.3 ^1H NMR spectrum of *1-benzyl-1H-pyrrole-2-carbaldehyde* (**1a**)

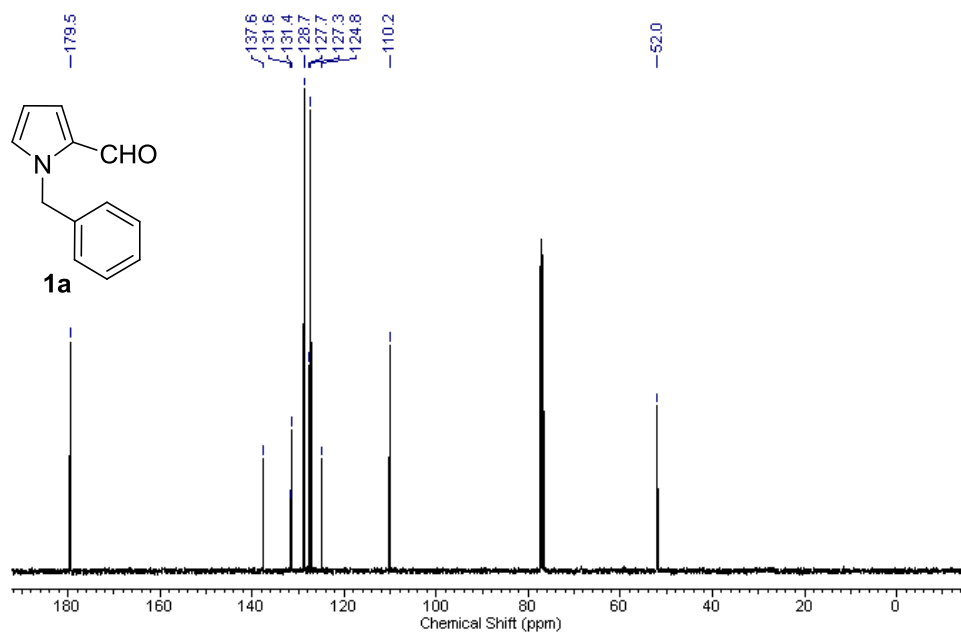


Figure 2.4 ^{13}C NMR spectrum of *1-benzyl-1H-pyrrole-2-carbaldehyde* (**1a**)

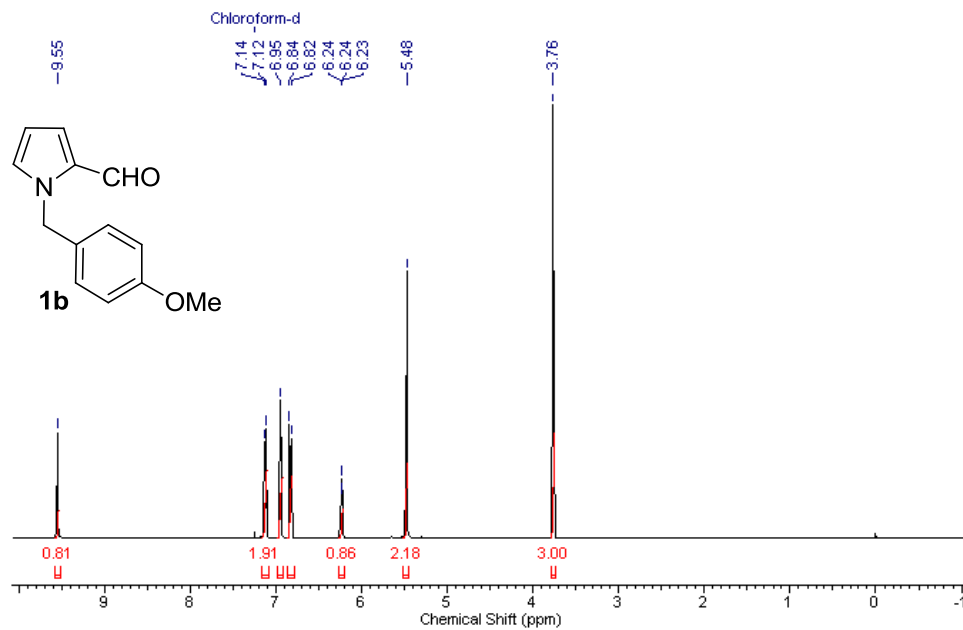


Figure 2.5 ¹H NMR spectrum of *1-(4-methoxybenzyl)-1H-pyrrole-2-carbaldehyde (1b)*

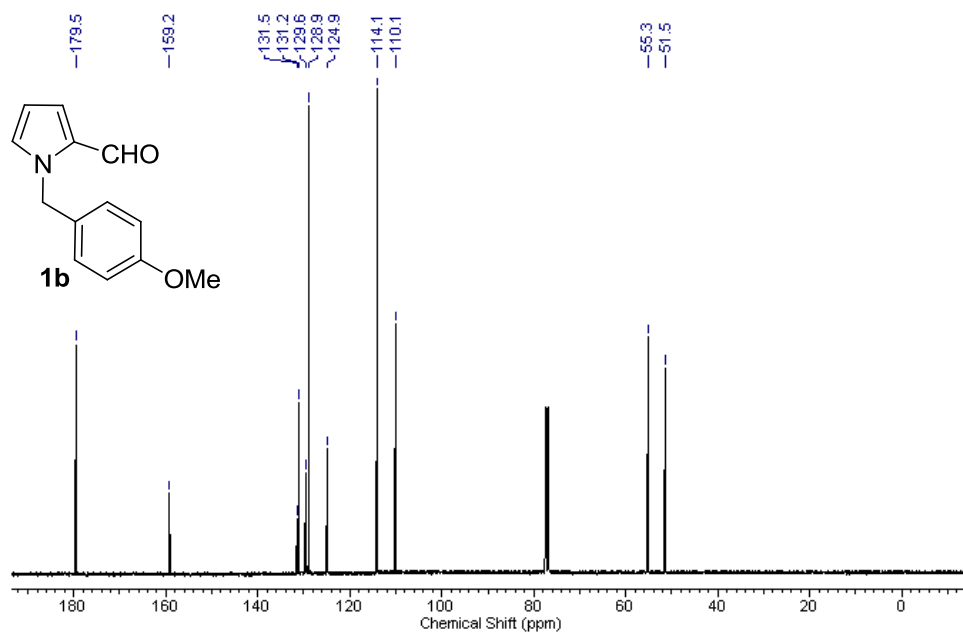


Figure 2.6 ¹³C NMR spectrum of *1-(4-methoxybenzyl)-1H-pyrrole-2-carbaldehyde (1b)*

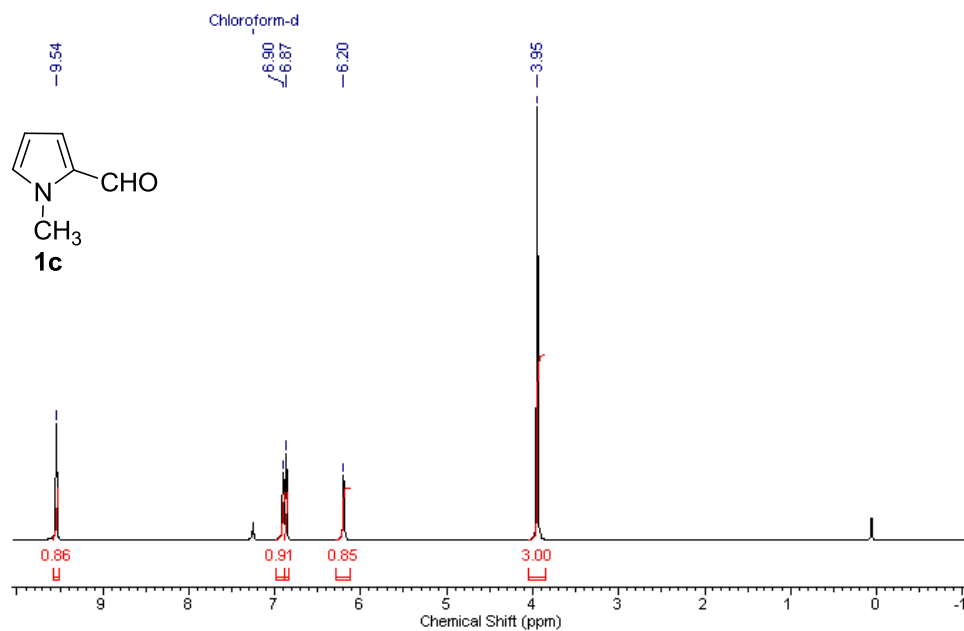


Figure 2.7 ¹H NMR spectrum of *1-methyl-1H-pyrrole-2-carbaldehyde* (**1c**)

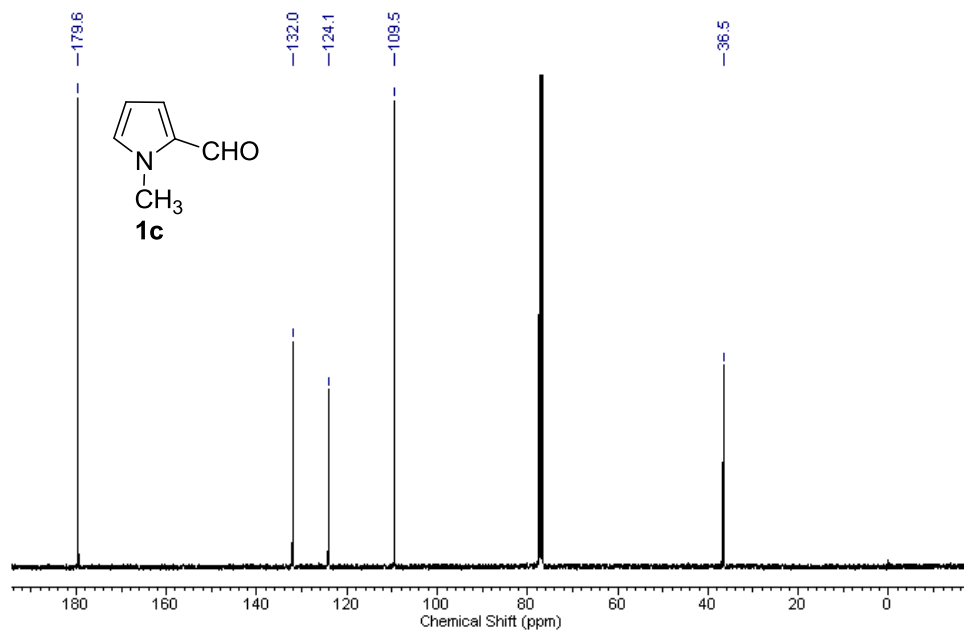


Figure 2.8 ¹³C NMR spectrum of *1-methyl-1H-pyrrole-2-carbaldehyde* (**1c**)

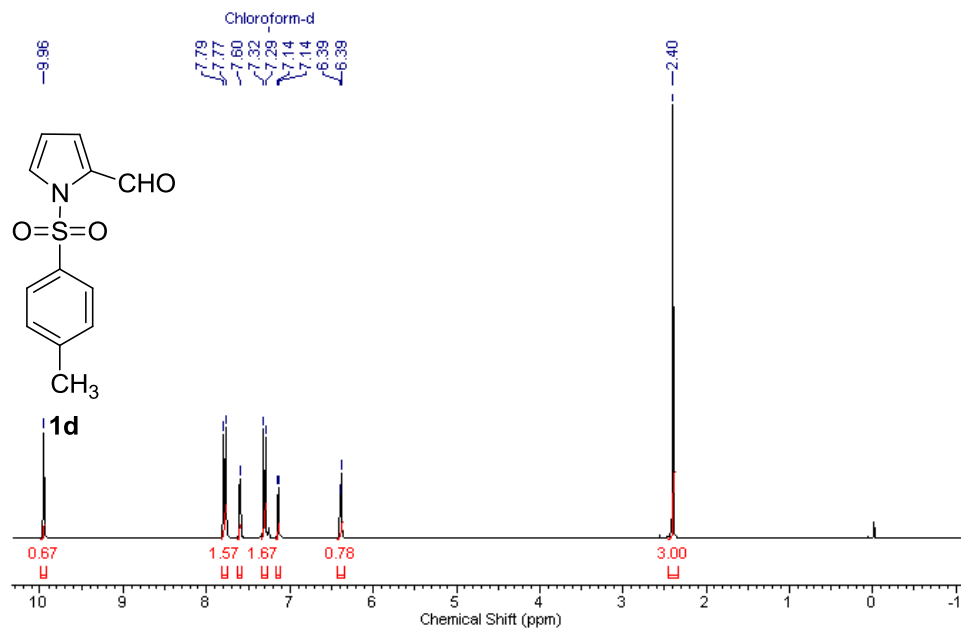


Figure 2.9 ¹H NMR spectrum of *1-tosyl-1H-pyrrole-2-carbaldehyde* (**1d**)

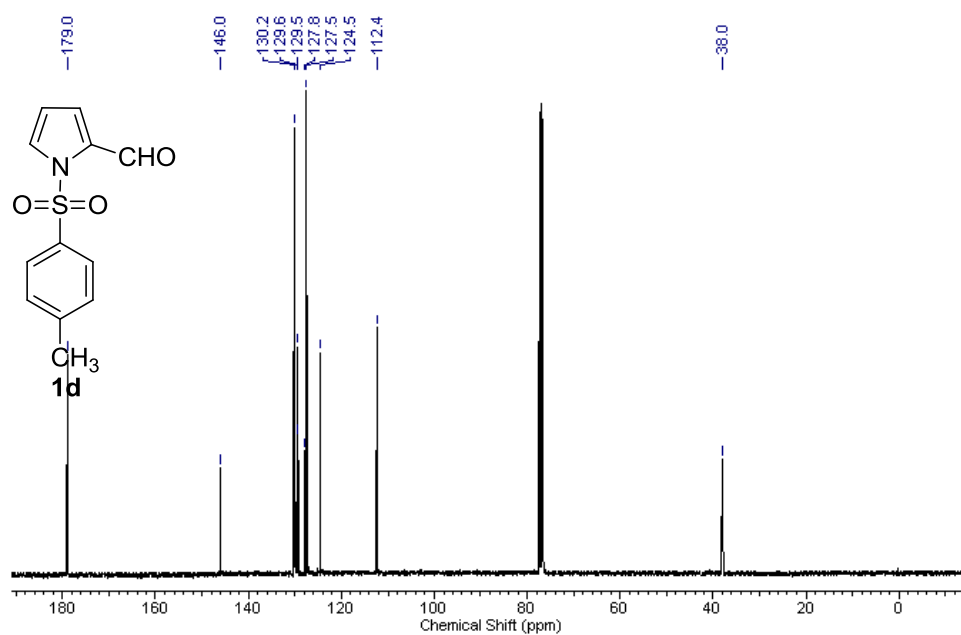


Figure 2.10 ¹³C NMR spectrum of *1-tosyl-1H-pyrrole-2-carbaldehyde* (**1d**)

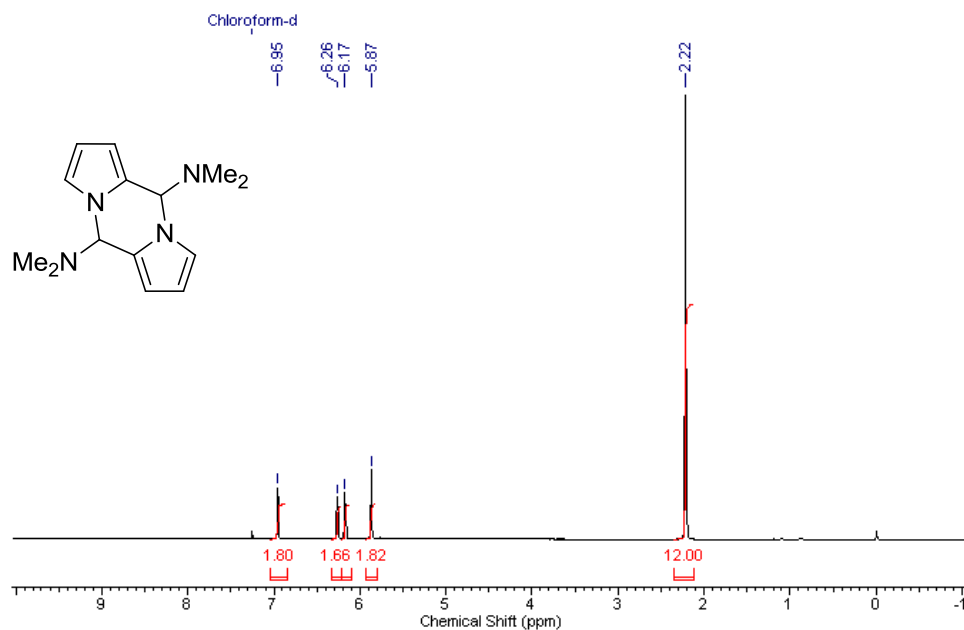


Figure 2.11 ¹H NMR spectrum of *N*₅,*N*₅,*N*₁₀,*N*₁₀-tetramethyl-5,10-dihydrodipyrrolo[1,2-*a*:1',2'-*d*]pyrazine-5,10-diamine

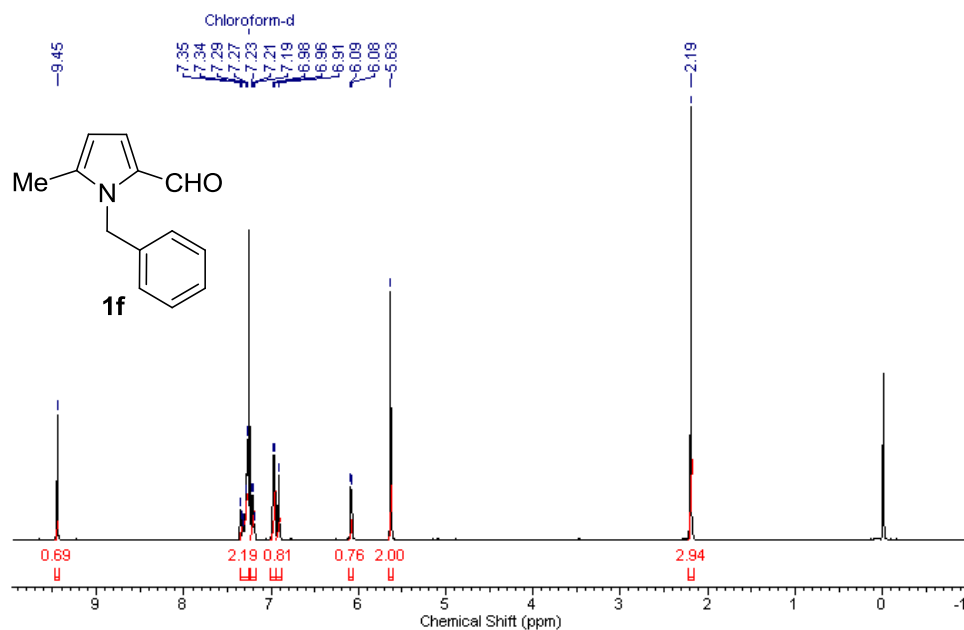


Figure 2.12 ¹H NMR spectrum of 1-benzyl-5-methyl-1H-pyrrole-2-carbaldehyde (**1f**)

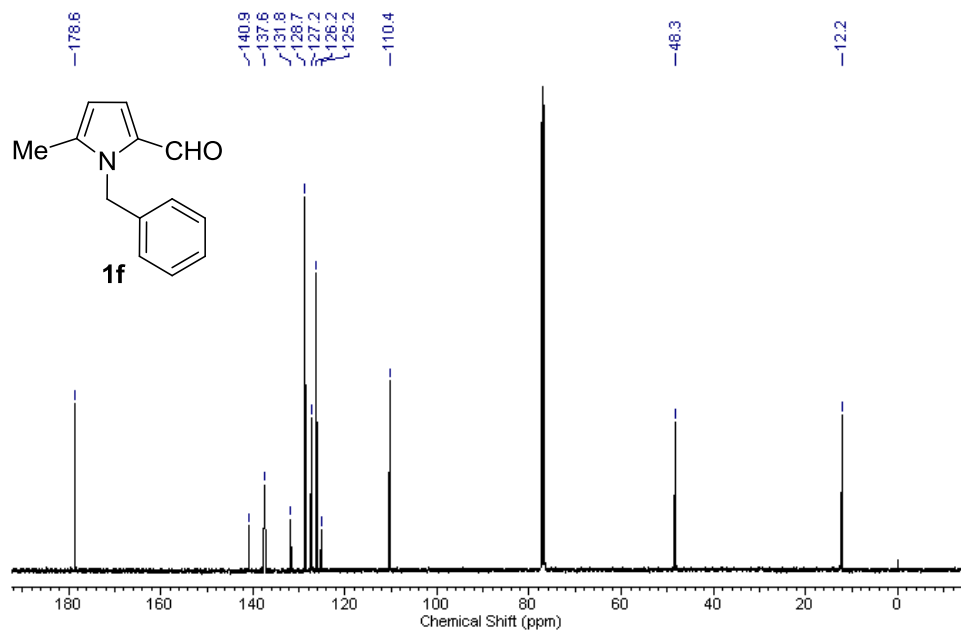


Figure 2.13 ¹³C NMR spectrum of *1-benzyl-5-methyl-1H-pyrrole-2-carbaldehyde* (**1f**)

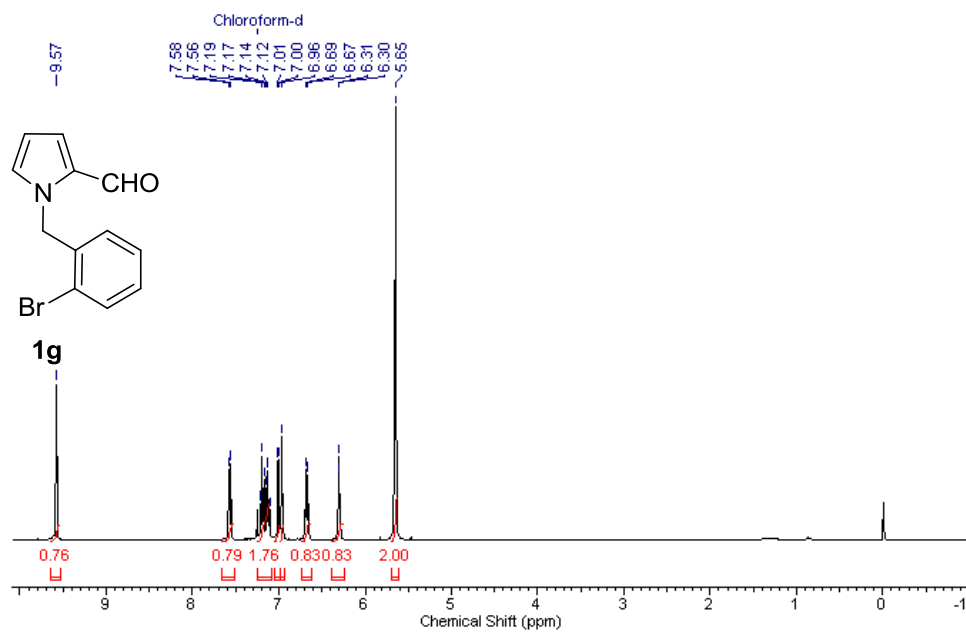


Figure 2.14 ¹H NMR spectrum of *1-(2-bromobenzyl)-1H-pyrrole-2-carbaldehyde* (**1g**)

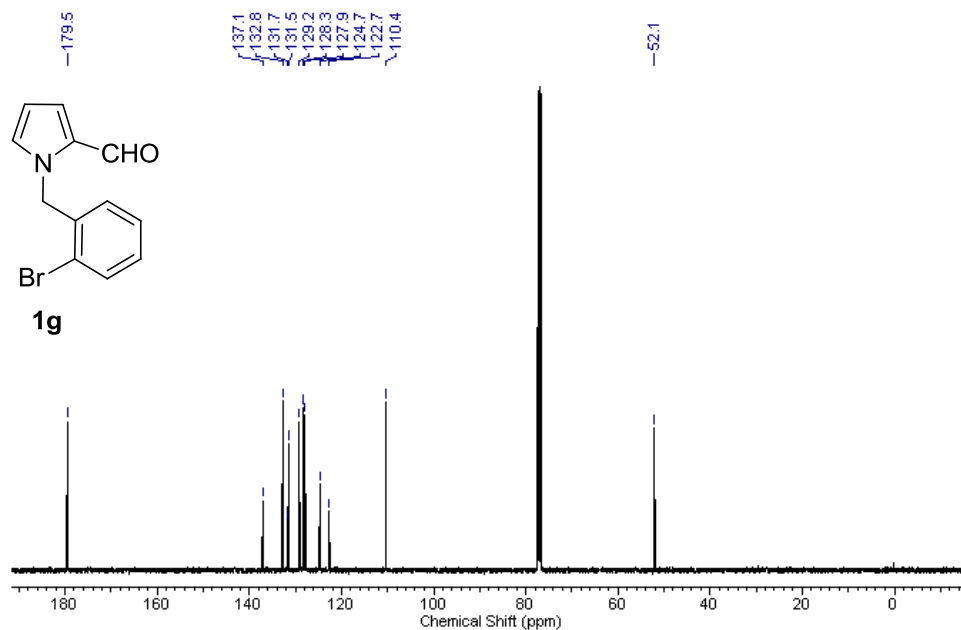


Figure 2.15 ¹³C NMR spectrum of *1-(2-bromobenzyl)-1H-pyrrole-2-carbaldehyde (1g)*

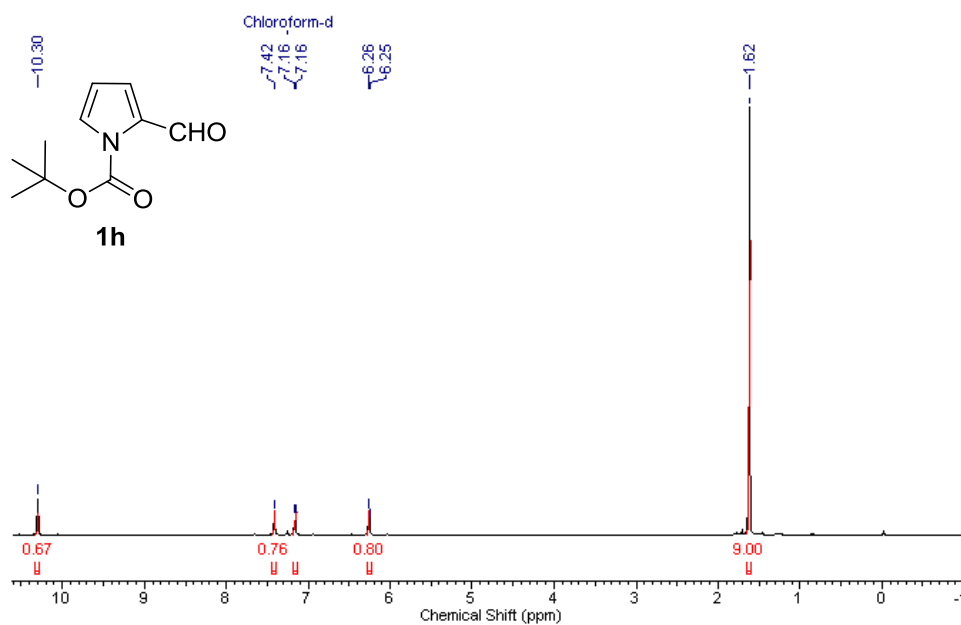


Figure 2.16 ¹H NMR spectrum of *tert-butyl 2-formyl-1H-pyrrole-1-carboxylate (1h)*

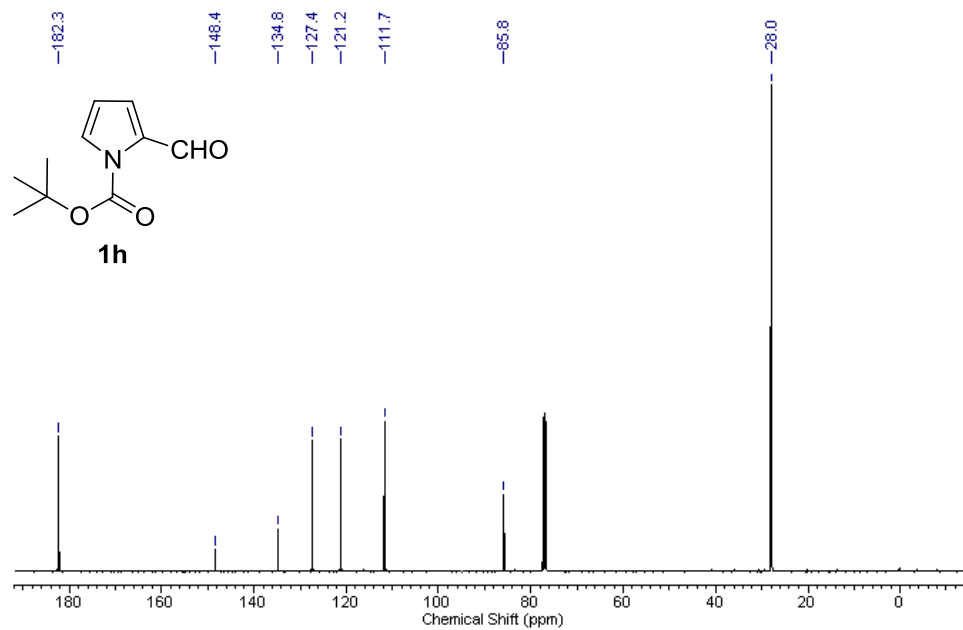


Figure 2.17 ^{13}C NMR spectrum of *tert*-butyl 2-formyl-1H-pyrrole-1-carboxylate (**1h**)

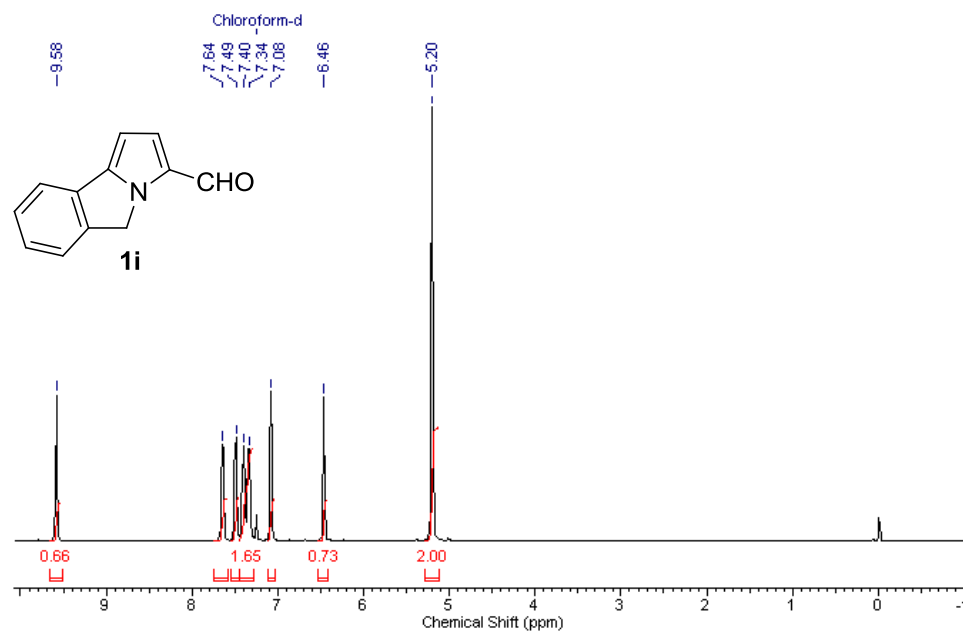


Figure 2.18 ^1H NMR spectrum of 5H-pyrrolo[2,1-a]isoindole-3-carbaldehyde (**1i**)

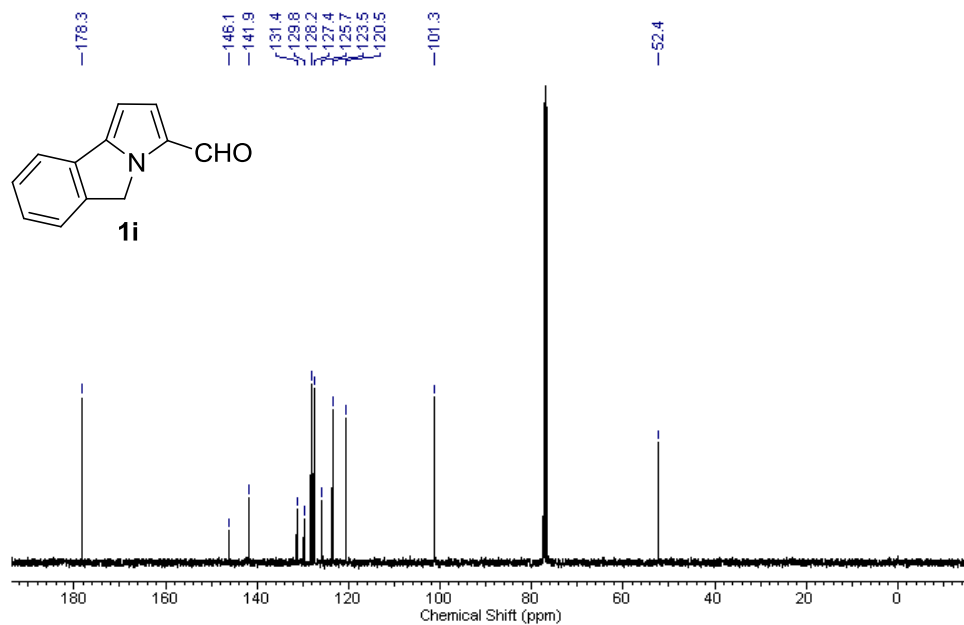


Figure 2.19 ¹³C NMR spectrum of *5H-pyrrolo[2,1-a]isoindole-3-carbaldehyde (1i)*

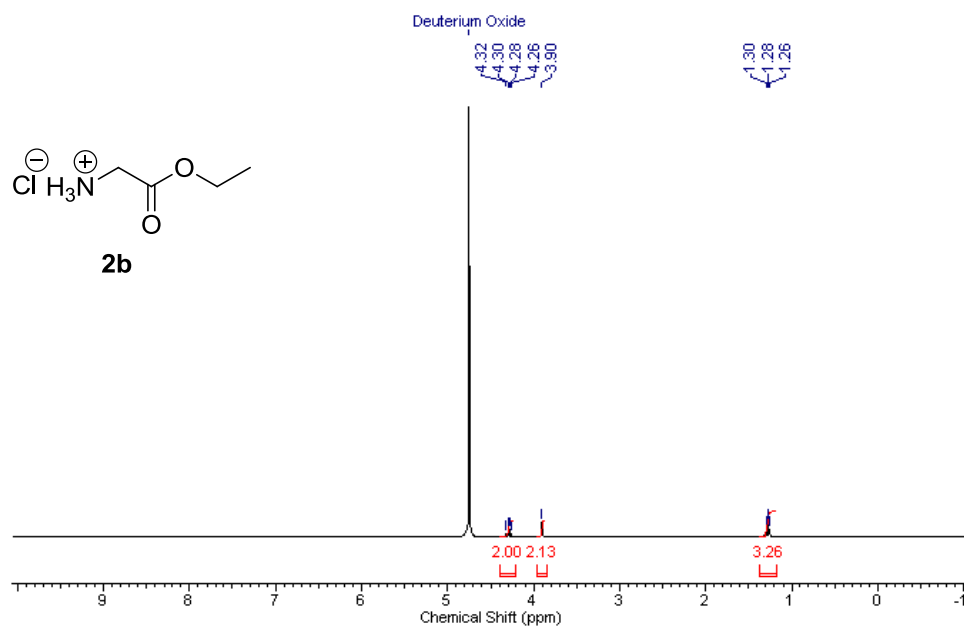


Figure 2.20 ¹H NMR spectrum of *glycine ethyl ester HCl salt (2b)*

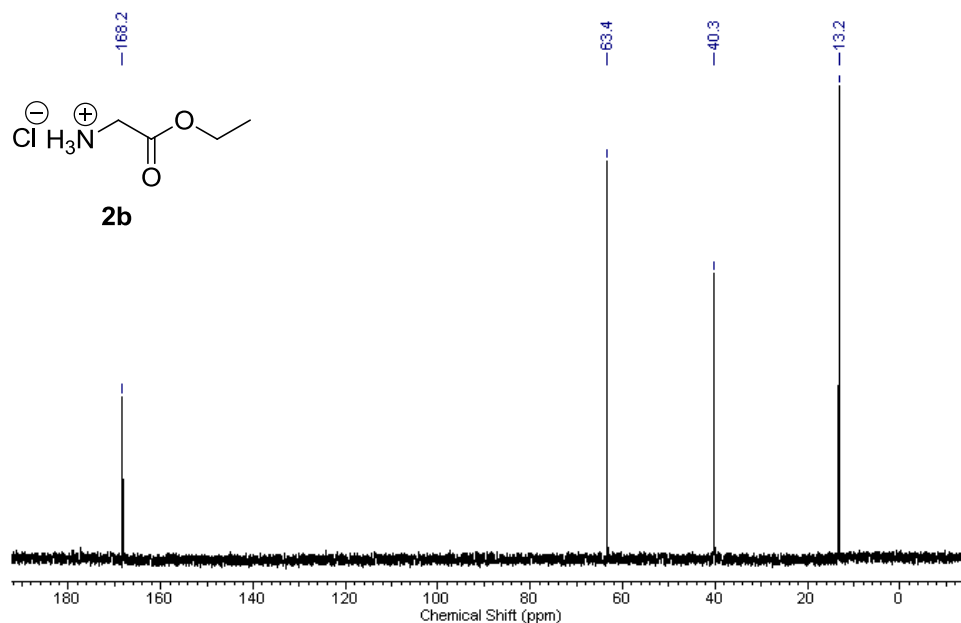


Figure 2.21 ¹³C NMR spectrum of *glycine ethyl ester HCl salt (2b)*

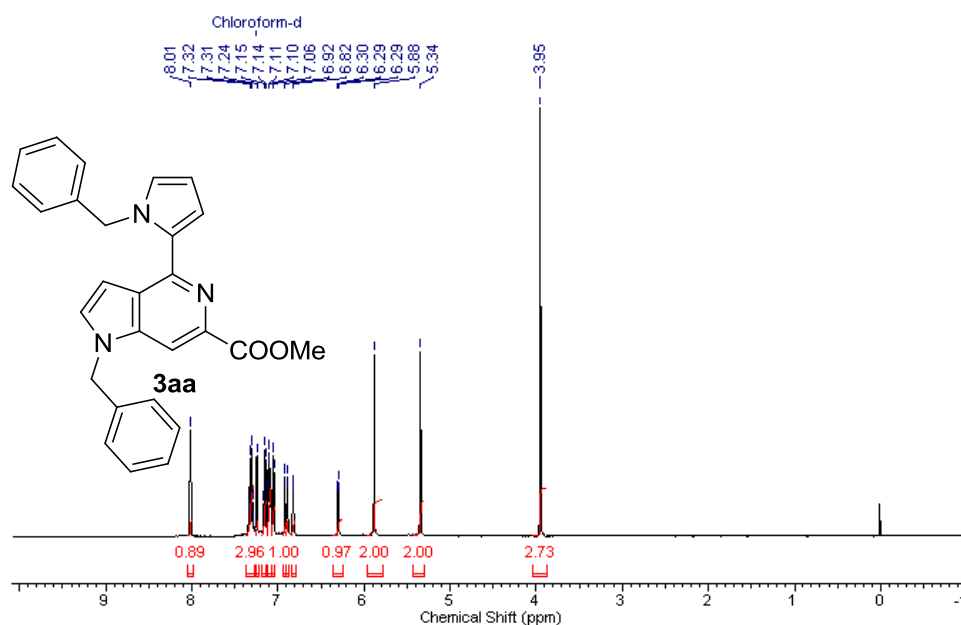


Figure 2.22 ¹H NMR spectrum (500 MHz) of *methyl 1-benzyl-4-(1-benzyl-1H-pyrrol-2-yl)-1H-pyrrolo[3,2-c]pyridine-6-carboxylate (3aa)*

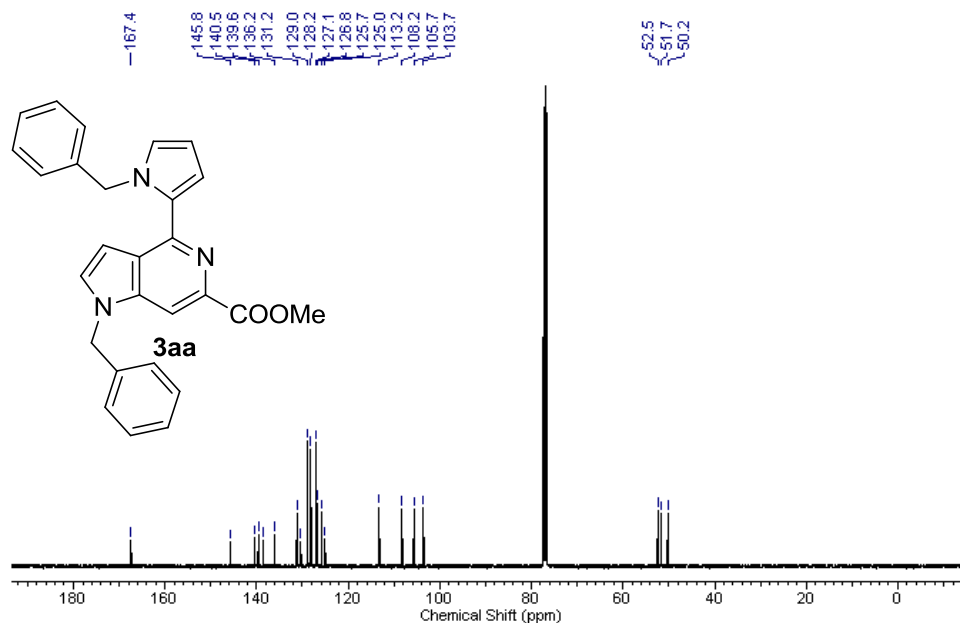


Figure 2.23 ¹³C NMR spectrum of *methyl 1-benzyl-4-(1-benzyl-1H-pyrrol-2-yl)-1H-pyrrolo[3,2-c]pyridine-6-carboxylate (3aa)*

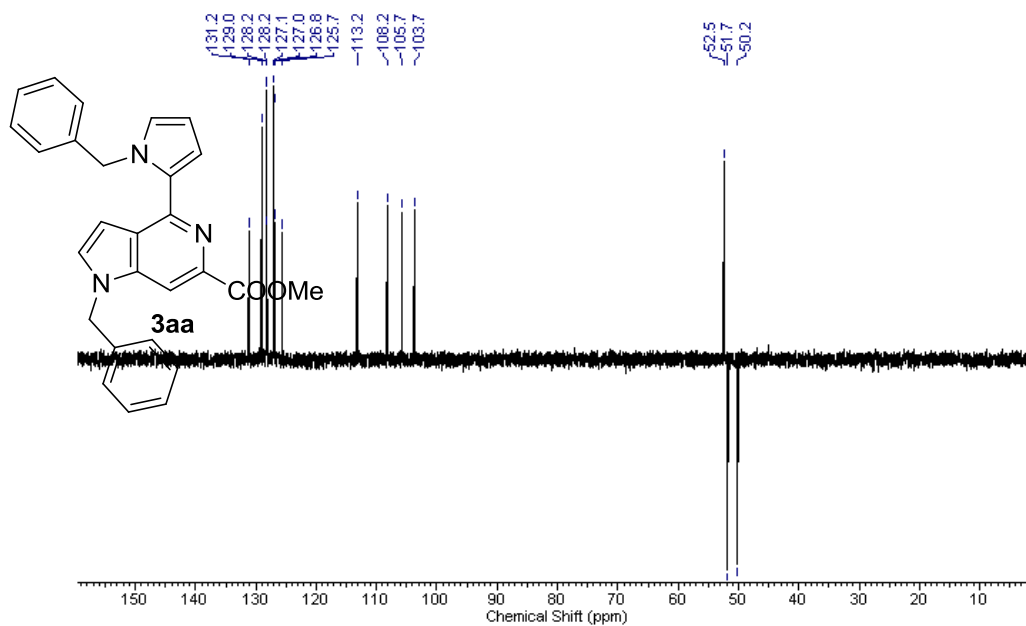


Figure 2.24 DEPT-135° spectrum of *methyl 1-benzyl-4-(1-benzyl-1H-pyrrol-2-yl)-1H-pyrrolo[3,2-c]pyridine-6-carboxylate (3aa)*

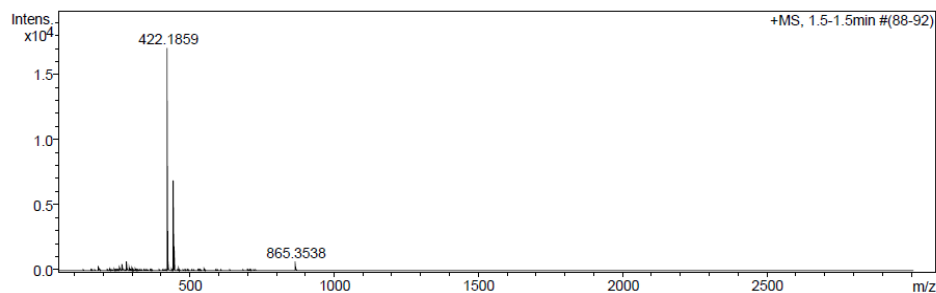


Figure 2.25 HRMS data of methyl 1-benzyl-4-(1-benzyl-1H-pyrrol-2-yl)-1H-pyrrolo[3,2-c]pyridine-6-carboxylate (**3aa**)

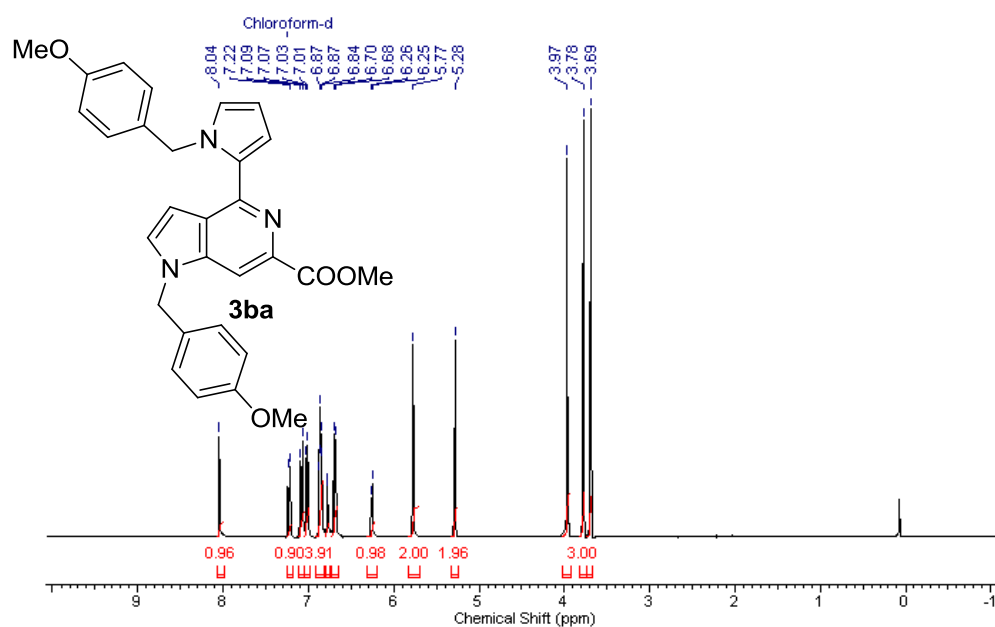


Figure 2.26 ¹H NMR spectrum of methyl 1-(4-methoxybenzyl)-4-(1-(4-methoxybenzyl)-1H-pyrrol-2-yl)-1H-pyrrolo[3,2-c]pyridine-6-carboxylate (**3ba**)

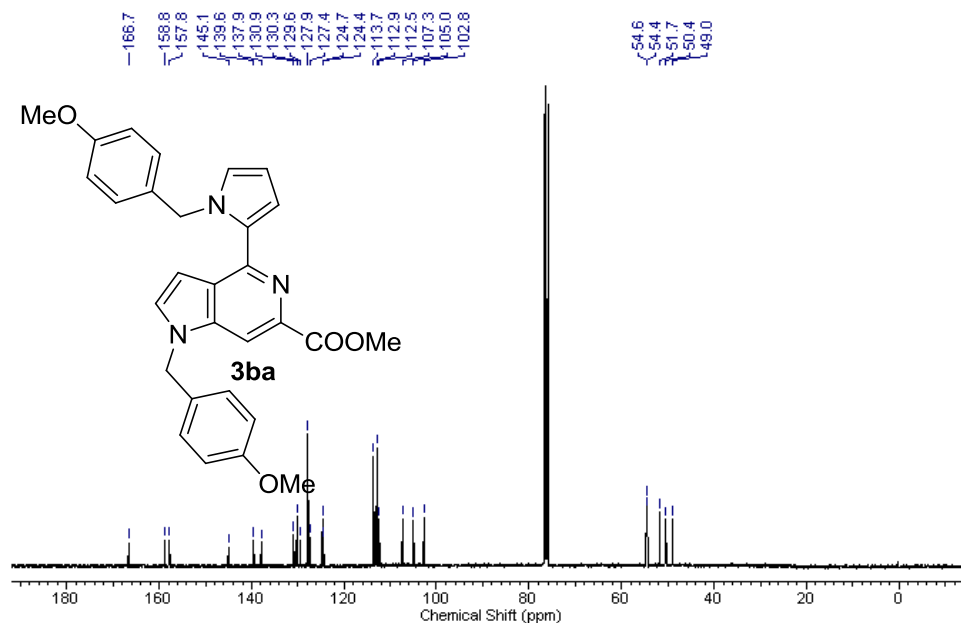


Figure 2.27 ¹³C NMR spectrum of *methyl 1-(4-methoxybenzyl)-4-(1-(4-methoxybenzyl)-1H-pyrrol-2-yl)-1H-pyrrolo[3,2-c]pyridine-6-carboxylate* (**3ba**)

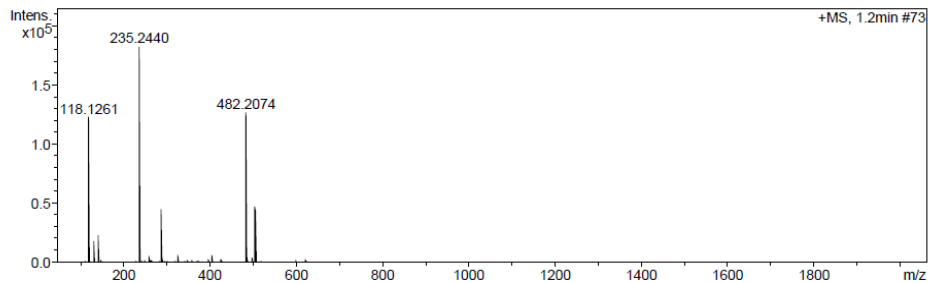


Figure 2.28 HRMS data of *methyl 1-(4-methoxybenzyl)-4-(1-(4-methoxybenzyl)-1H-pyrrol-2-yl)-1H-pyrrolo[3,2-c]pyridine-6-carboxylate* (**3ba**)

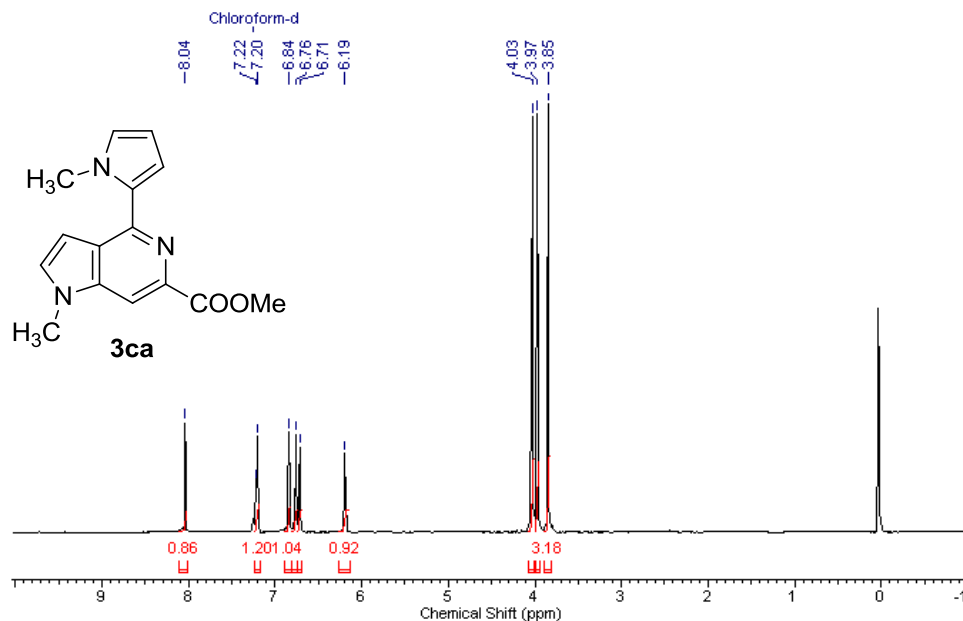


Figure 2.29 ^1H NMR spectrum of *methyl 1-methyl-4-(1-methyl-1H-pyrrol-2-yl)-1H-pyrrolo[3,2-c]pyridine-6-carboxylate (3ca)*

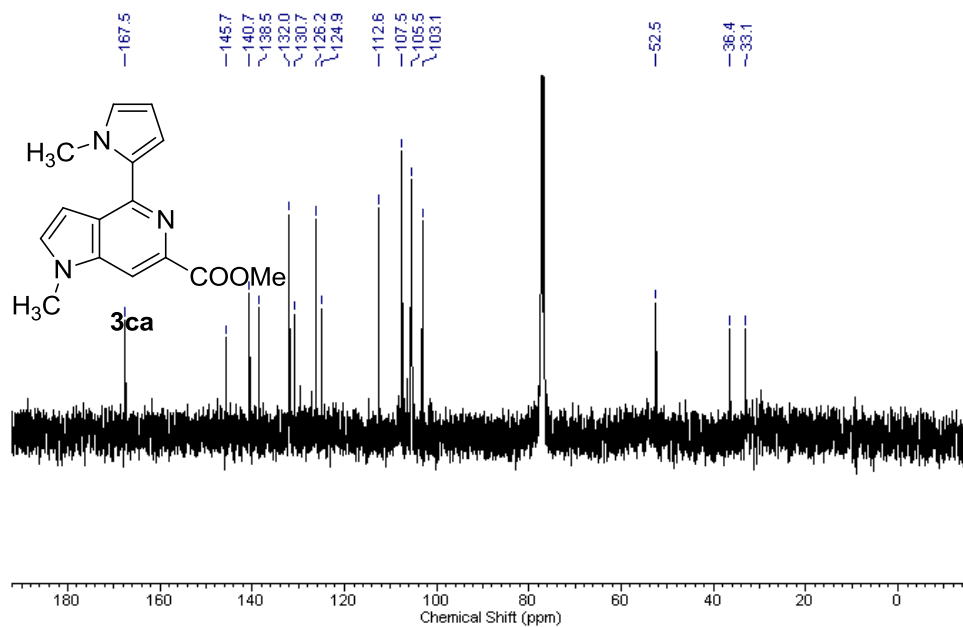


Figure 2.30 ^{13}C NMR spectrum of *methyl 1-methyl-4-(1-methyl-1H-pyrrol-2-yl)-1H-pyrrolo[3,2-c]pyridine-6-carboxylate (3ca)*

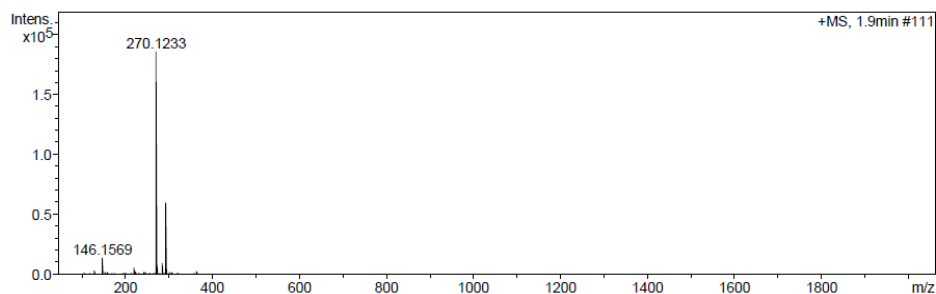


Figure 2.31 HRMS data of *methyl 1-methyl-4-(1-methyl-1H-pyrrol-2-yl)-1H-pyrrolo[3,2-c]pyridine-6-carboxylate (3ca)*

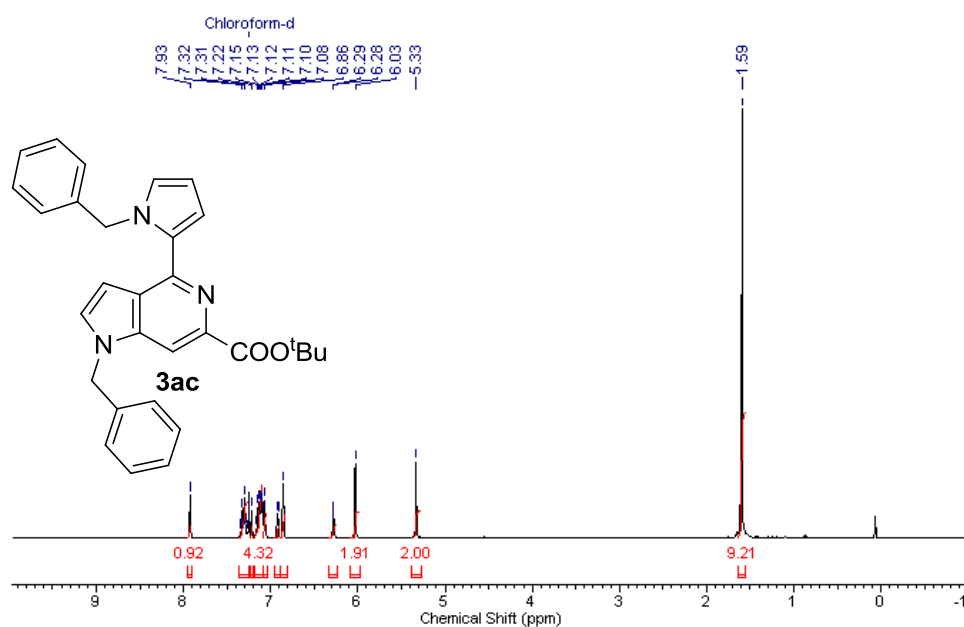


Figure 2.32 ^1H NMR spectrum of *tert-butyl 1-benzyl-4-(1-benzyl-1H-pyrrol-2-yl)-1H-pyrrolo[3,2-c]pyridine-6-carboxylate (3ac)*

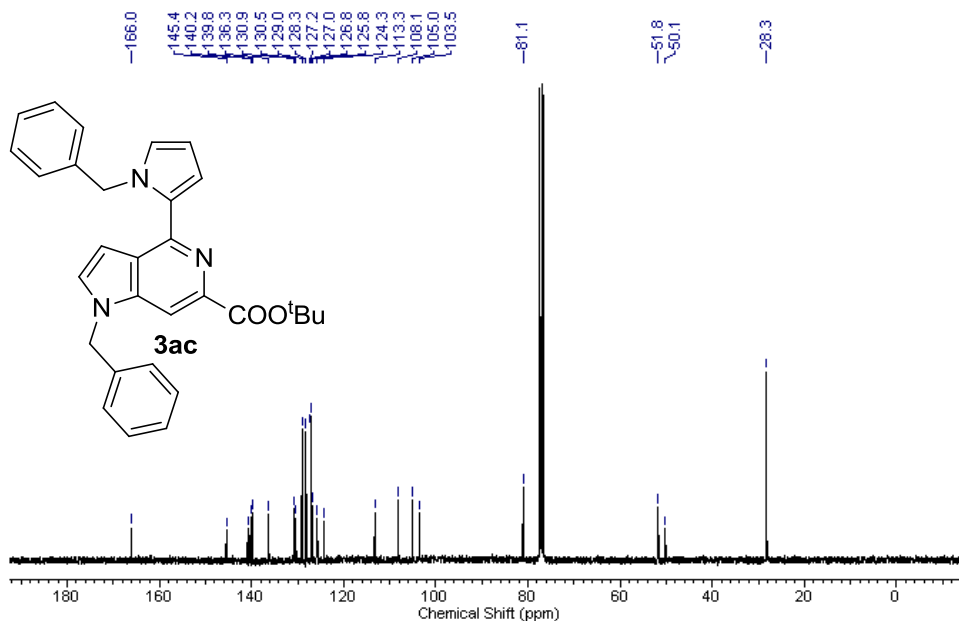


Figure 2.33 ¹³C NMR spectrum of *tert*-butyl 1-benzyl-4-(1-benzyl-1H-pyrrol-2-yl)-1H-pyrrolo[3,2-*c*]pyridine-6-carboxylate (**3ac**)

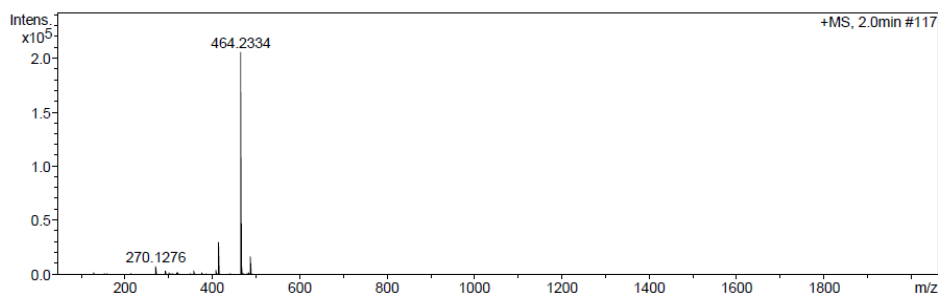


Figure 2.34 HRMS data of *tert*-butyl 1-benzyl-4-(1-benzyl-1H-pyrrol-2-yl)-1H-pyrrolo[3,2-*c*]pyridine-6-carboxylate (**3ac**)

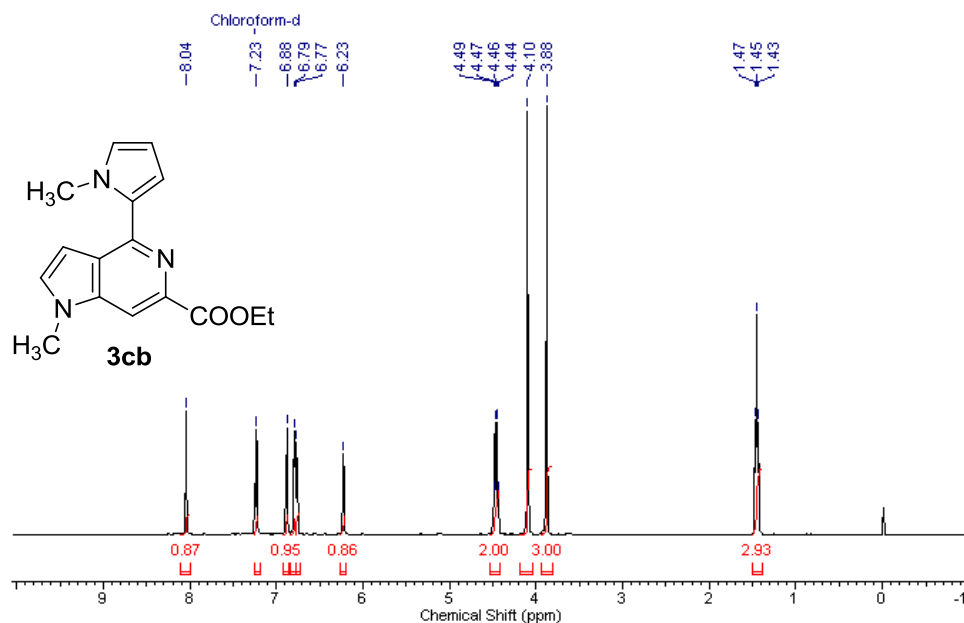


Figure 2.35 ¹H NMR spectrum of *ethyl 1-methyl-4-(1-methyl-1H-pyrrolo-2-yl)-1H-pyrrolo[3,2-c]pyridine-6-carboxylate (3cb)*

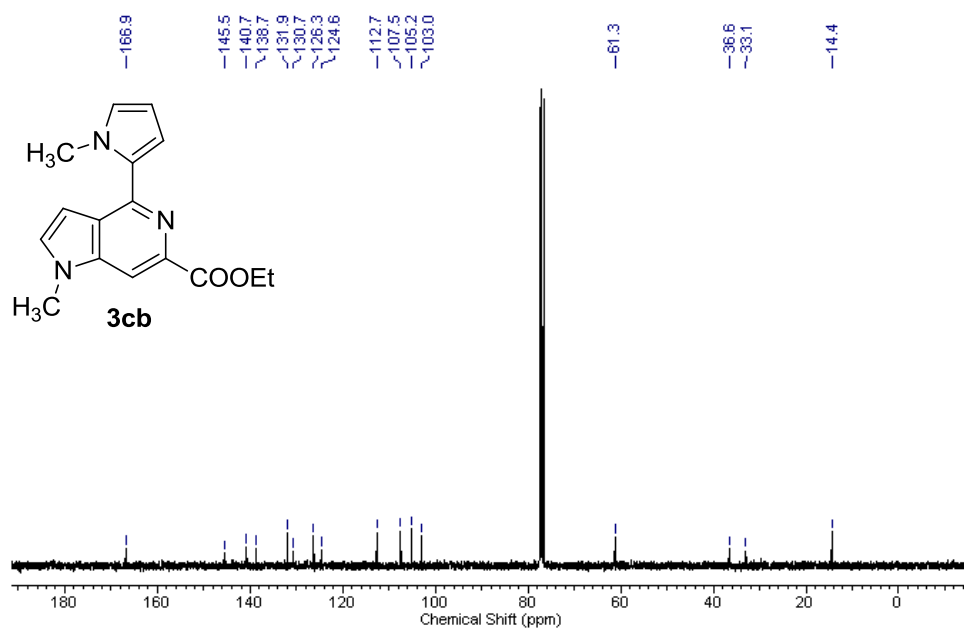


Figure 2.36 ¹³C NMR spectrum of *ethyl 1-methyl-4-(1-methyl-1H-pyrrolo-2-yl)-1H-pyrrolo[3,2-c]pyridine-6-carboxylate (3cb)*

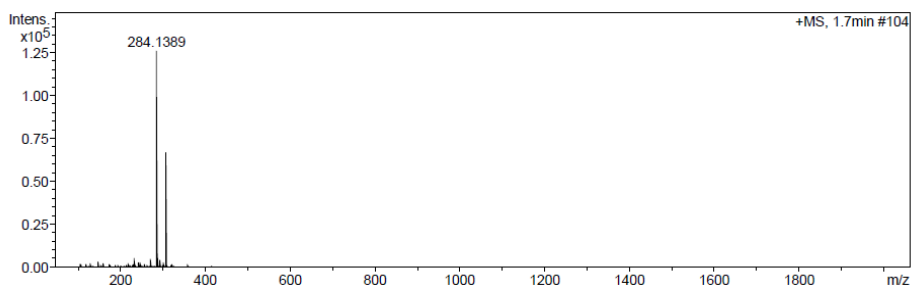


Figure 2.37 HRMS data of *ethyl 1-methyl-4-(1-methyl-1H-pyrrol-2-yl)-1H-pyrrolo[3,2-c]pyridine-6-carboxylate (3cb)*

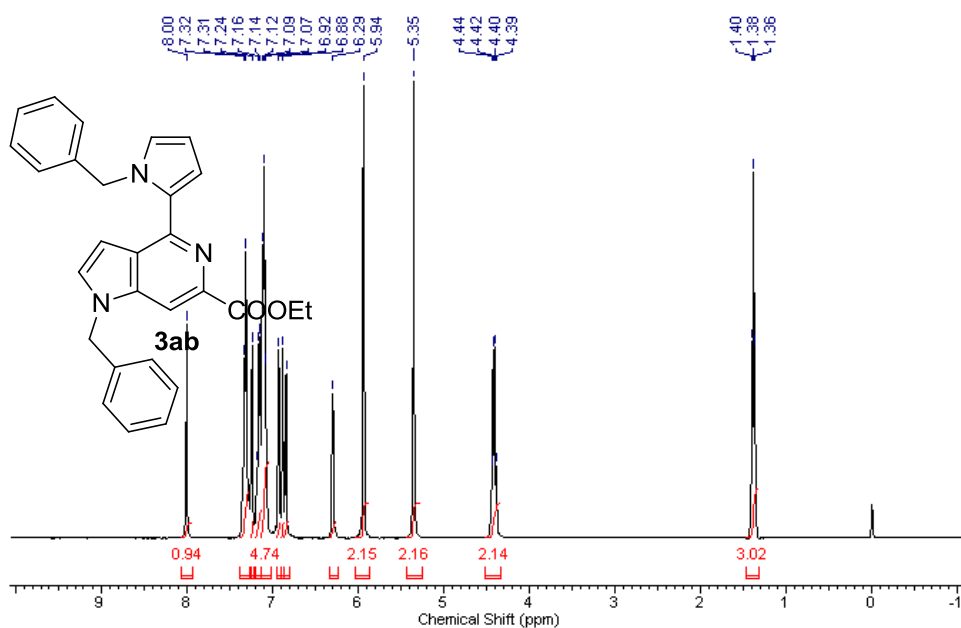


Figure 2.38 ^1H NMR spectrum of *ethyl 1-benzyl-4-(1-benzyl-1H-pyrrol-2-yl)-1H-pyrrolo[3,2-c]pyridine-6-carboxylate (3ab)*

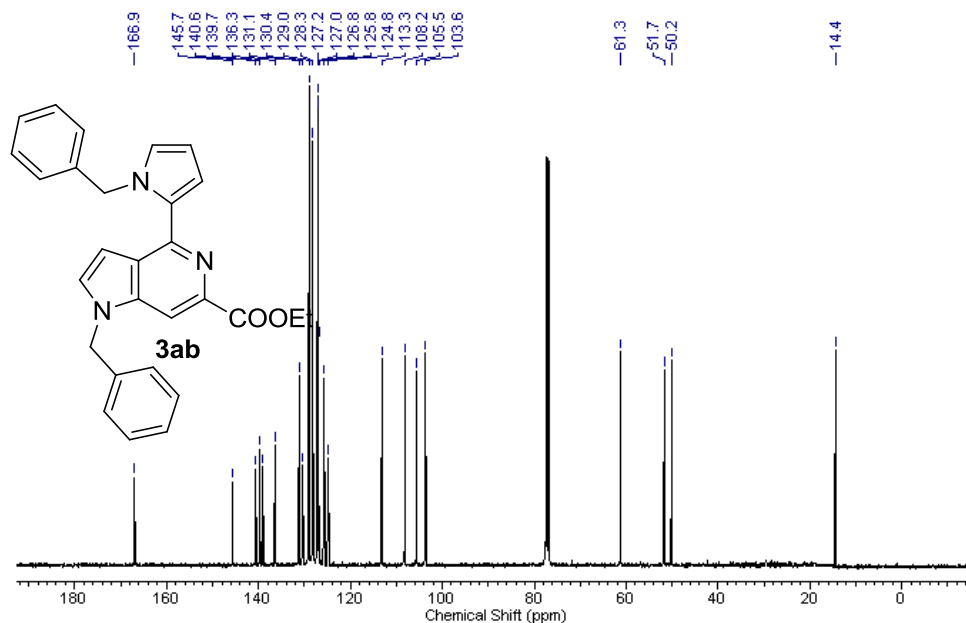


Figure 2.39 ¹³C NMR spectrum of *ethyl 1-benzyl-4-(1-benzyl-1H-pyrrol-2-yl)-1H-pyrrolo[3,2-c]pyridine-6-carboxylate (3ab)*

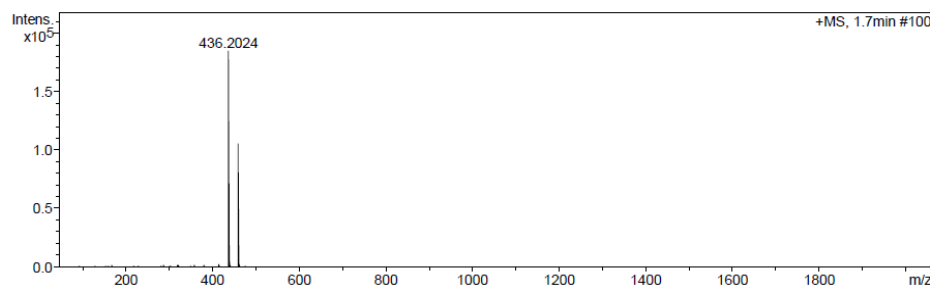


Figure 2.40 HRMS data of *ethyl 1-benzyl-4-(1-benzyl-1H-pyrrol-2-yl)-1H-pyrrolo[3,2-c]pyridine-6-carboxylate (3ab)*

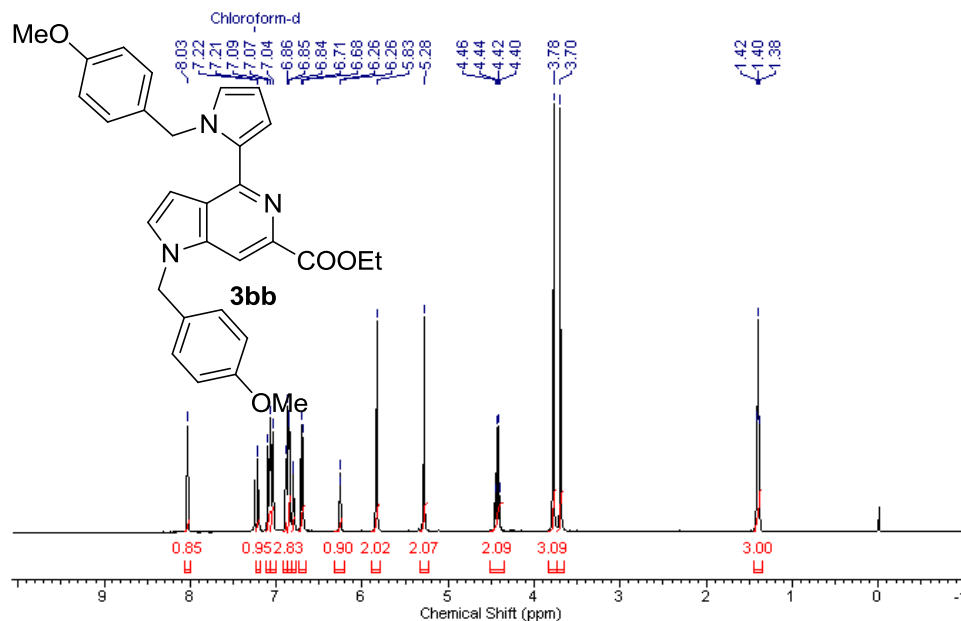


Figure 2.41 ¹H NMR spectrum of *ethyl 1-(4-methoxybenzyl)-4-(1-(4-methoxybenzyl)-1H-pyrrol-2-yl)-1H-pyrrolo[3,2-c]pyridine-6-carboxylate (3bb)*

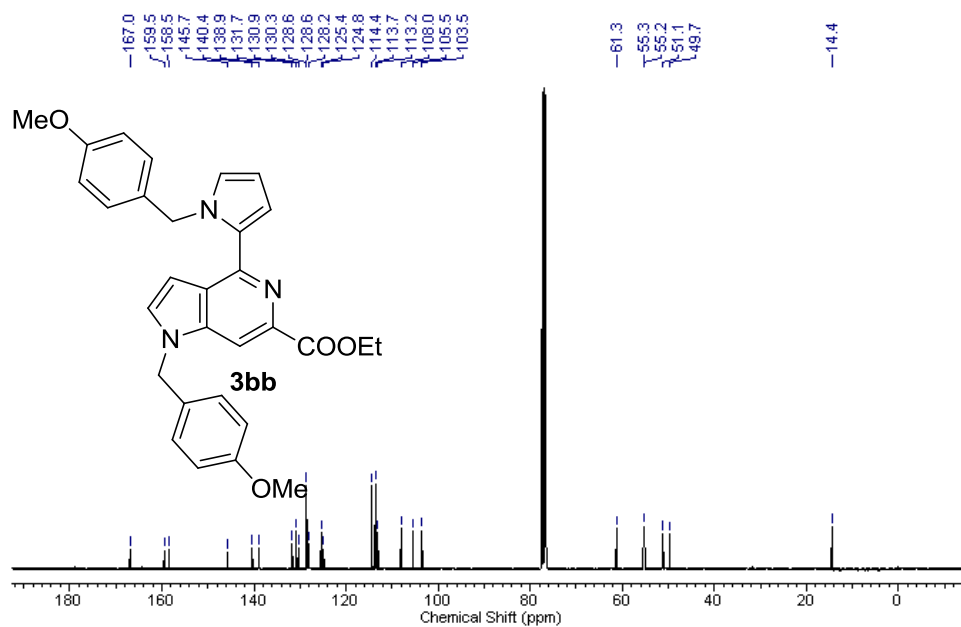


Figure 2.42 ¹³C NMR spectrum of *ethyl 1-(4-methoxybenzyl)-4-(1-(4-methoxybenzyl)-1H-pyrrol-2-yl)-1H-pyrrolo[3,2-c]pyridine-6-carboxylate (3bb)*

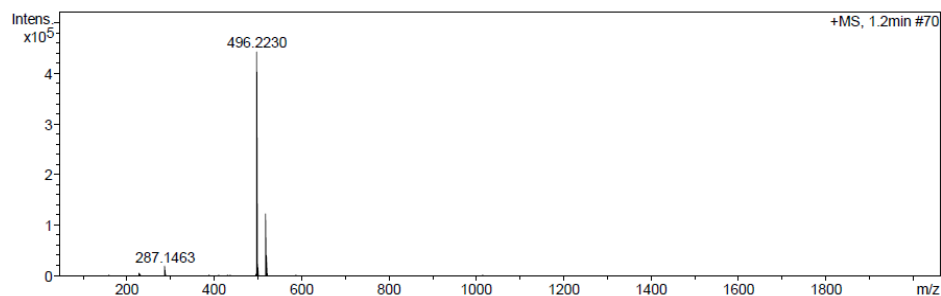


Figure 2.43 HRMS data of *ethyl 1-(4-methoxybenzyl)-4-(1-(4-methoxybenzyl)-1H-pyrrol-2-yl)-1H-pyrrolo[3,2-c]pyridine-6-carboxylate (3bb)*

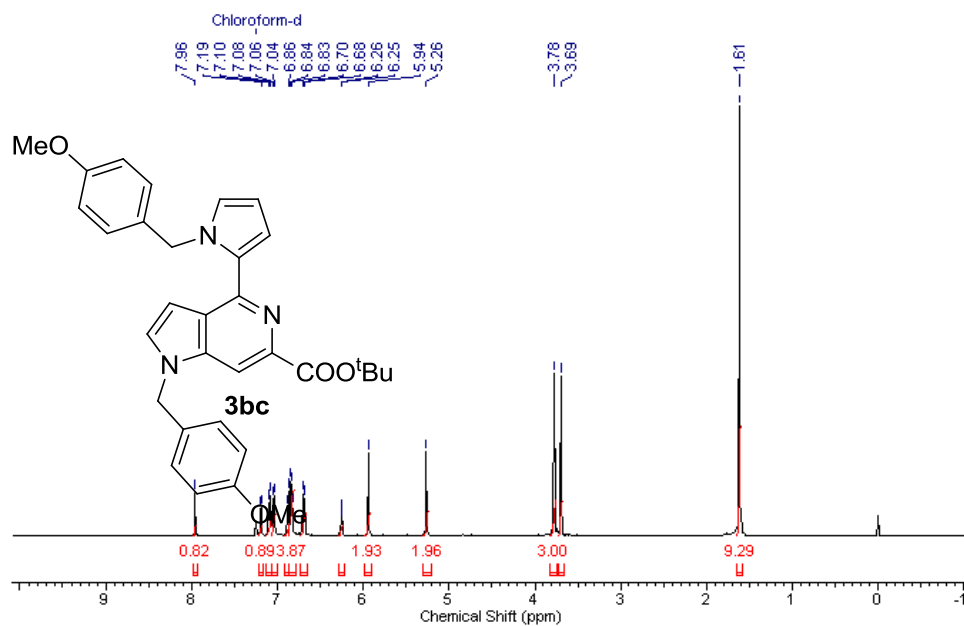


Figure 2.44 ^1H NMR spectrum of *tert-butyl 1-(4-methoxybenzyl)-4-(1-(4-methoxybenzyl)-1H-pyrrol-2-yl)-1H-pyrrolo[3,2-c]pyridine-6-carboxylate (3bc)*

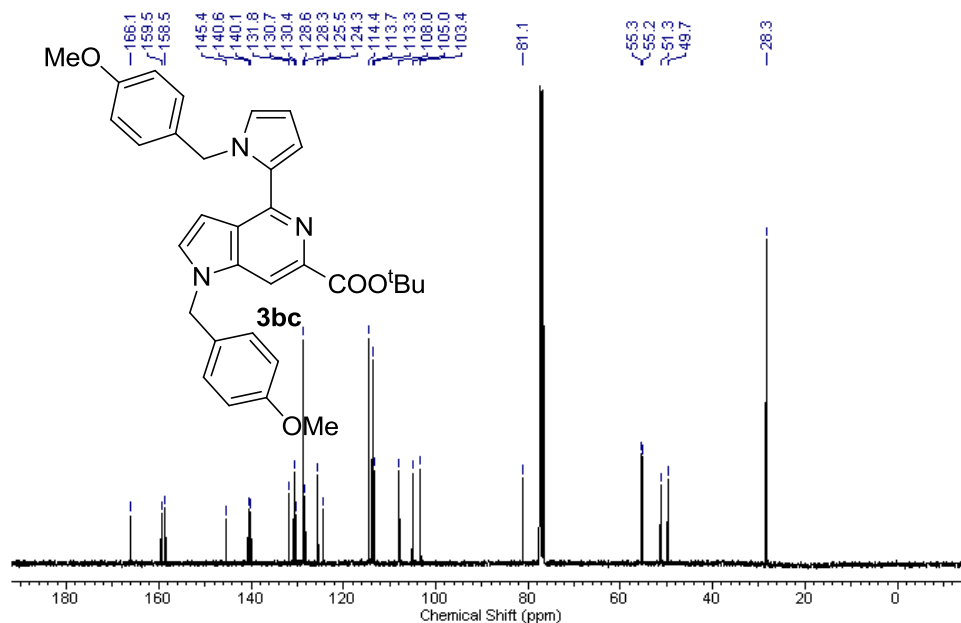


Figure 2.45 ^{13}C NMR spectrum of *tert*-butyl 1-(4-methoxybenzyl)-4-(1-(4-methoxybenzyl)-1*H*-pyrrol-2-yl)-1*H*-pyrrolo[3,2-*c*]pyridine-6-carboxylate (**3bc**)

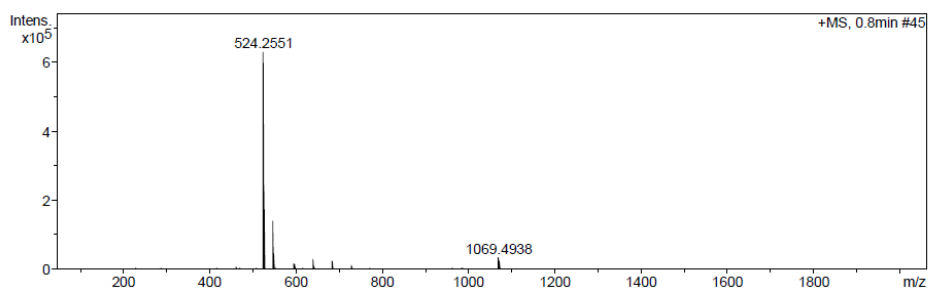


Figure 2.46 HRMS data of *tert*-butyl 1-(4-methoxybenzyl)-4-(1-(4-methoxybenzyl)-1*H*-pyrrol-2-yl)-1*H*-pyrrolo[3,2-*c*]pyridine-6-carboxylate (**3bc**)

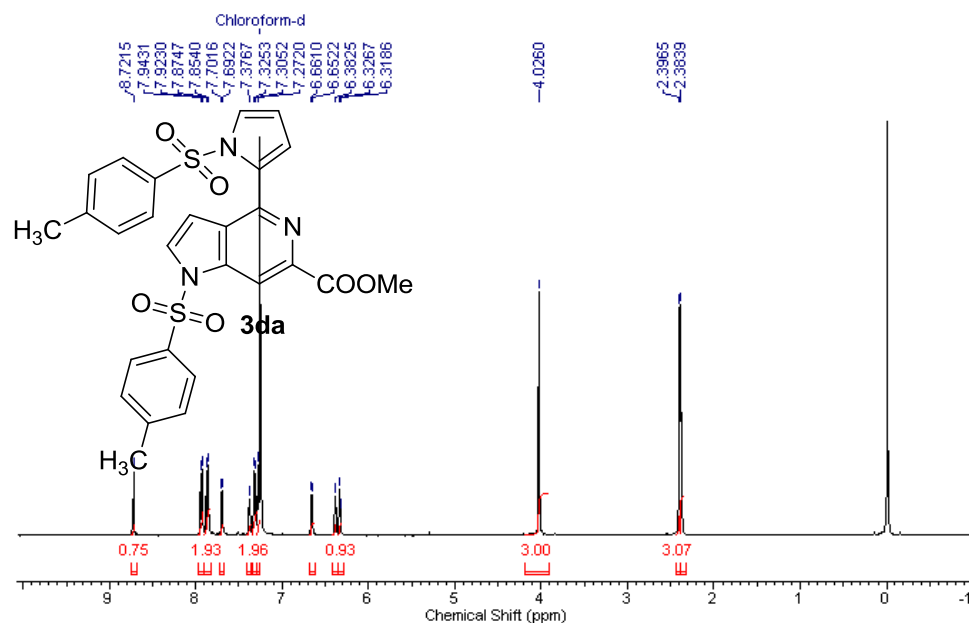


Figure 2.47 ¹H NMR spectrum of methyl 1-tosyl-4-(1-tosyl-1H-pyrrol-2-yl)-1H-pyrrolo[3,2-c]pyridine-6-carboxylate (3da)

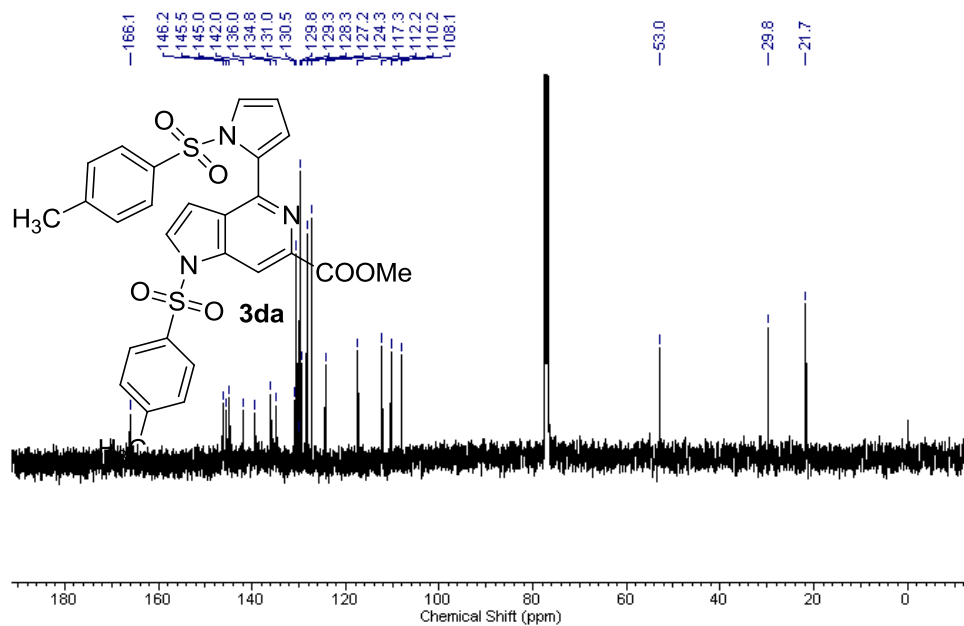


Figure 2.48 ¹³C NMR spectrum of methyl 1-tosyl-4-(1-tosyl-1H-pyrrol-2-yl)-1H-pyrrolo[3,2-c]pyridine-6-carboxylate (3da)

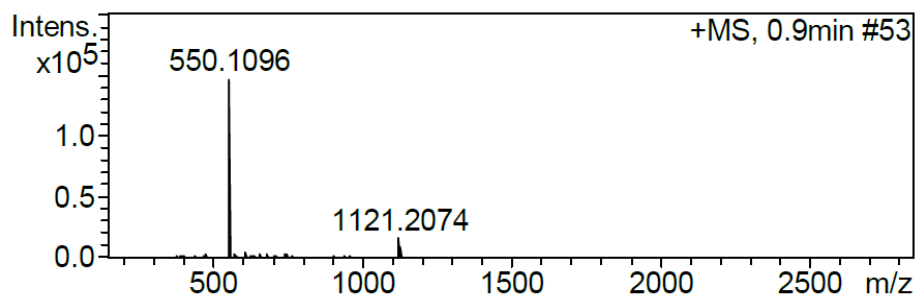


Figure 2.49 HRMS data of *Methyl 1-tosyl-4-(1-tosyl-1H-pyrrol-2-yl)-1H-pyrrolo[3,2-c]pyridine-6-carboxylate (3da)*

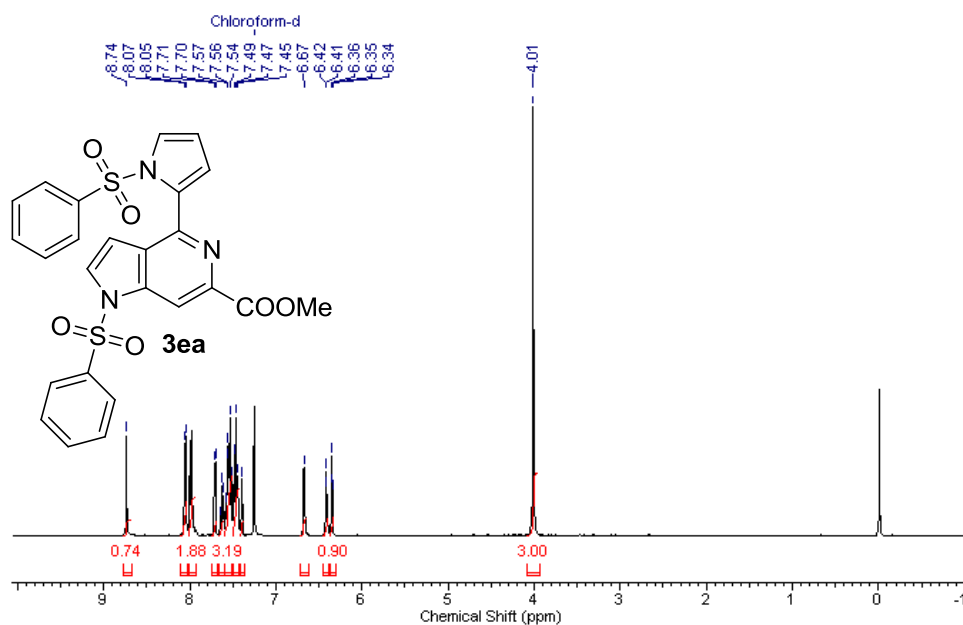


Figure 2.50 ^1H NMR spectrum of *methyl 1-(phenylsulfonyl)-4-(1-(phenylsulfonyl)-1H-pyrrol-2-yl)-1H-pyrrolo[3,2-c]pyridine-6-carboxylate (3ea)*

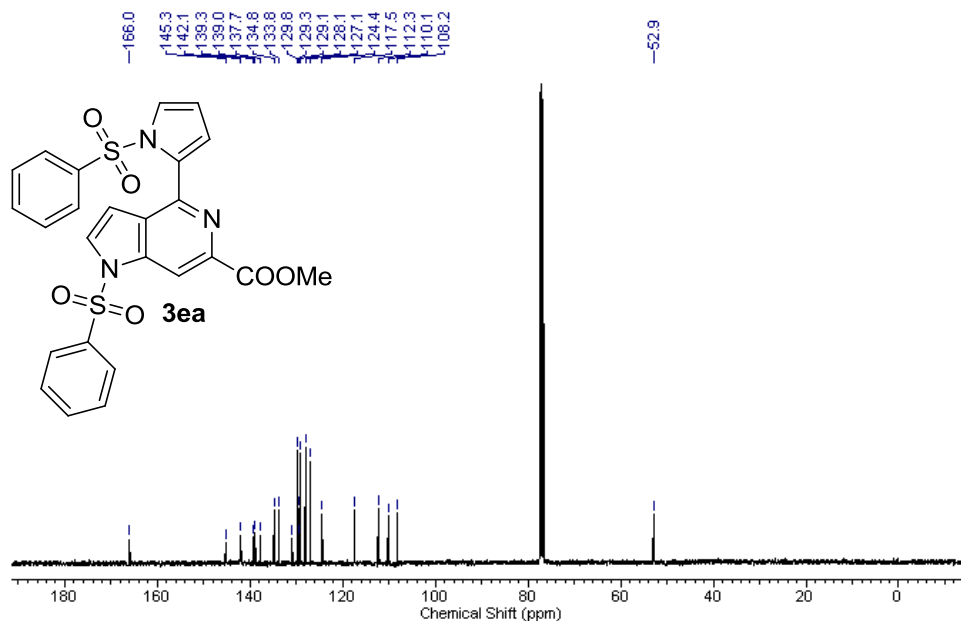


Figure 2.51 ¹³C NMR spectrum of *methyl 1-(phenylsulfonyl)-4-(1-(phenylsulfonyl)-1H-pyrrol-2-yl)-1H-pyrrolo[3,2-c]pyridine-6-carboxylate (3ea)*

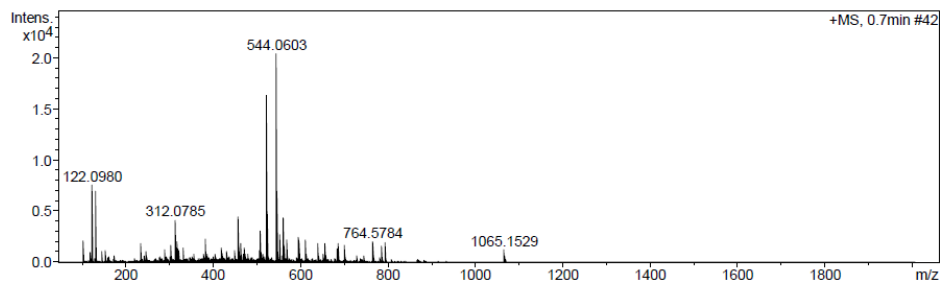


Figure 2.52 HRMS data of *methyl 1-(phenylsulfonyl)-4-(1-(phenylsulfonyl)-1H-pyrrol-2-yl)-1H-pyrrolo[3,2-c]pyridine-6-carboxylate (3ea)*

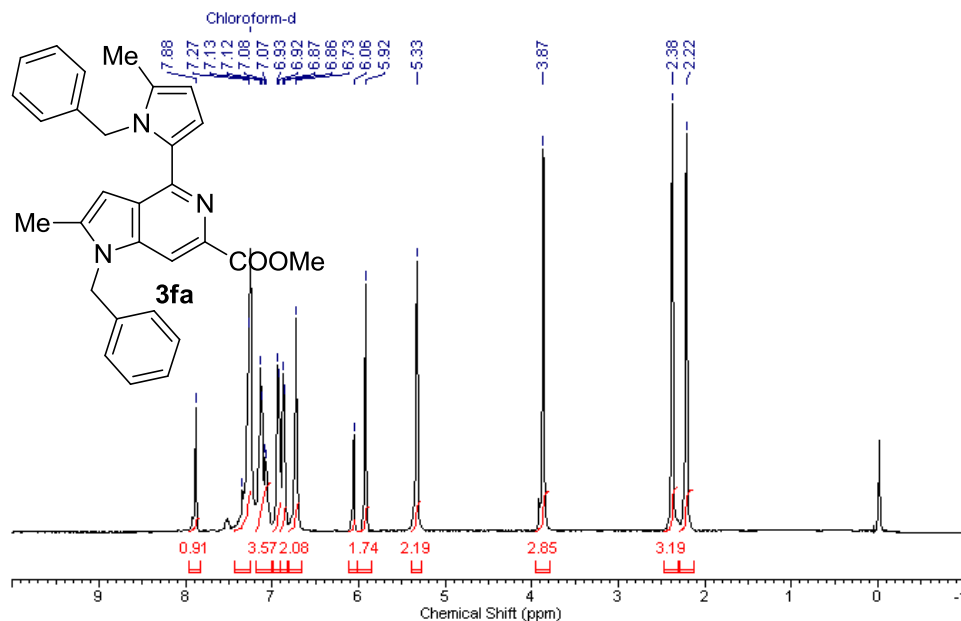


Figure 2.53 ¹H NMR spectrum of *methyl 1-benzyl-4-(1-benzyl-5-methyl-1H-pyrrol-2-yl)-2-methyl-1H-pyrrolo[3,2-c]pyridine-6-carboxylate (3fa)*

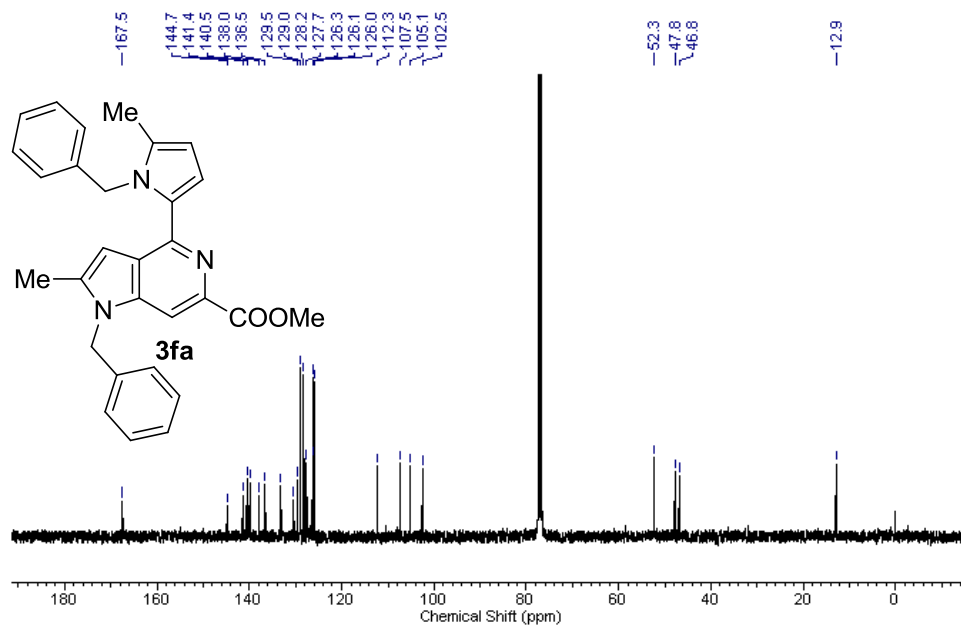


Figure 2.54 ¹³C NMR spectrum of *methyl 1-benzyl-4-(1-benzyl-5-methyl-1H-pyrrol-2-yl)-2-methyl-1H-pyrrolo[3,2-c]pyridine-6-carboxylate (3fa)*

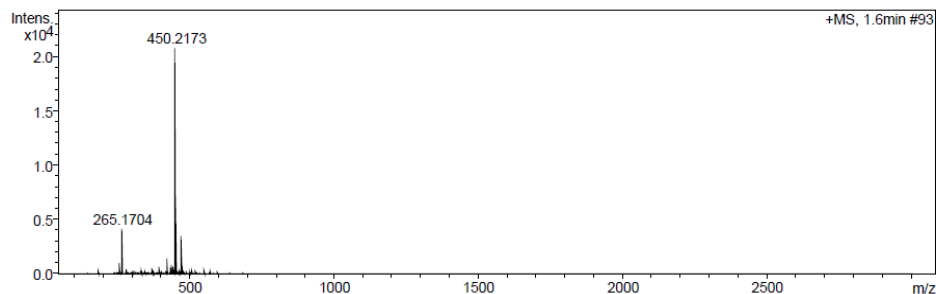


Figure 2.55 HRMS data of *methyl 1-benzyl-4-(1-benzyl-5-methyl-1H-pyrrol-2-yl)-2-methyl-1H-pyrrolo[3,2-c]pyridine-6-carboxylate (3fa)*

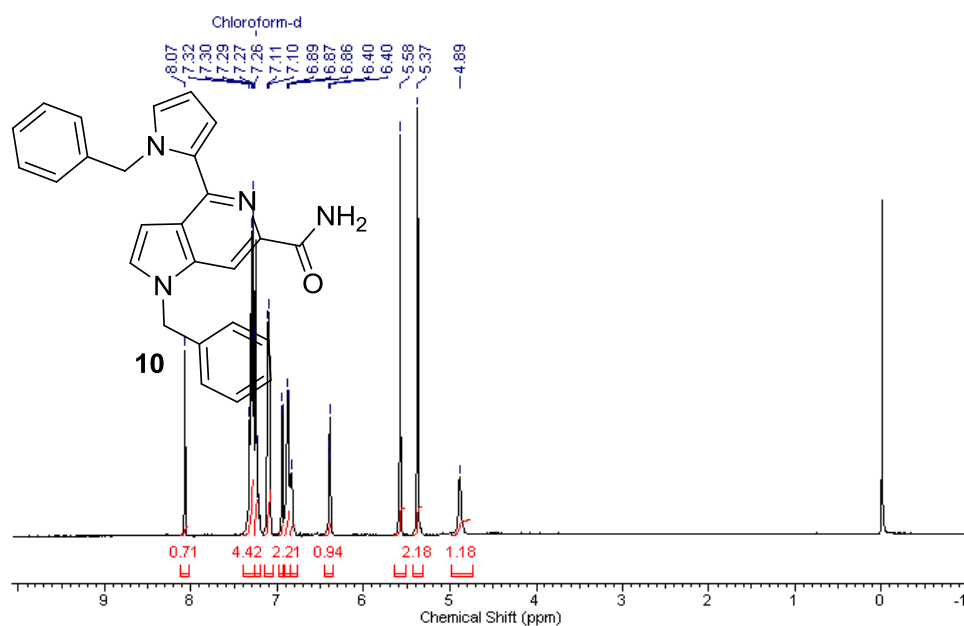


Figure 2.56 ^1H NMR spectrum of *1-benzyl-4-(1-benzyl-1H-pyrrol-2-yl)-1H-pyrrolo[3,2-c]pyridine-6-carboxamide (10)*

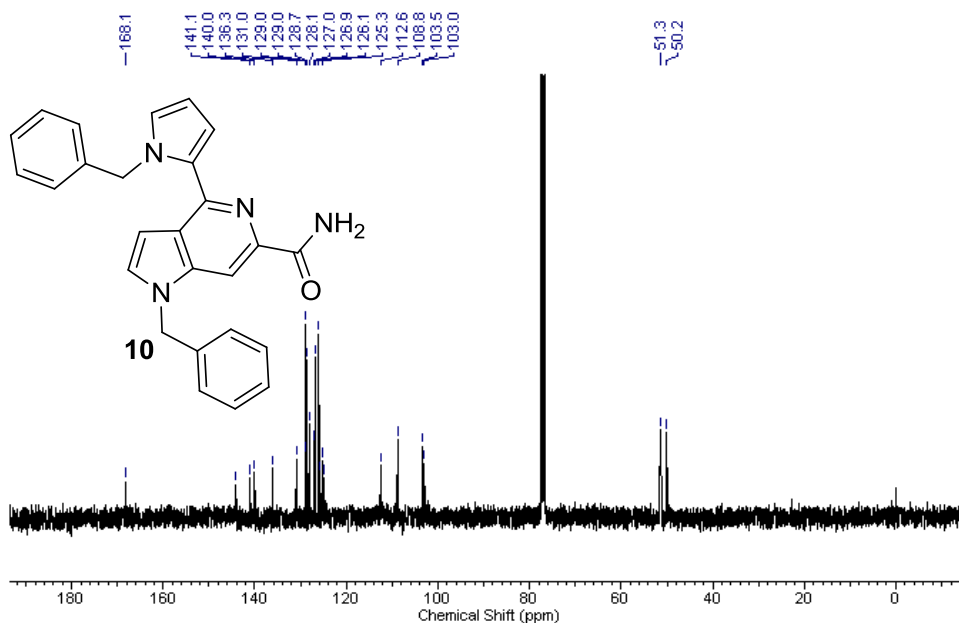


Figure 2.57 ^{13}C NMR spectrum of *1-benzyl-4-(1-benzyl-1H-pyrrol-2-yl)-1H-pyrrolo[3,2-c]pyridine-6-carboxamide (10)*

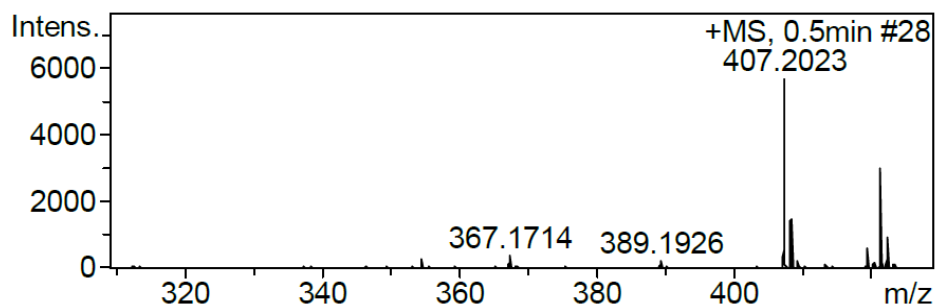


Figure 2.58 Mass data of *1-benzyl-4-(1-benzyl-1H-pyrrol-2-yl)-1H-pyrrolo[3,2-c]pyridine-6-carboxamide (10)*

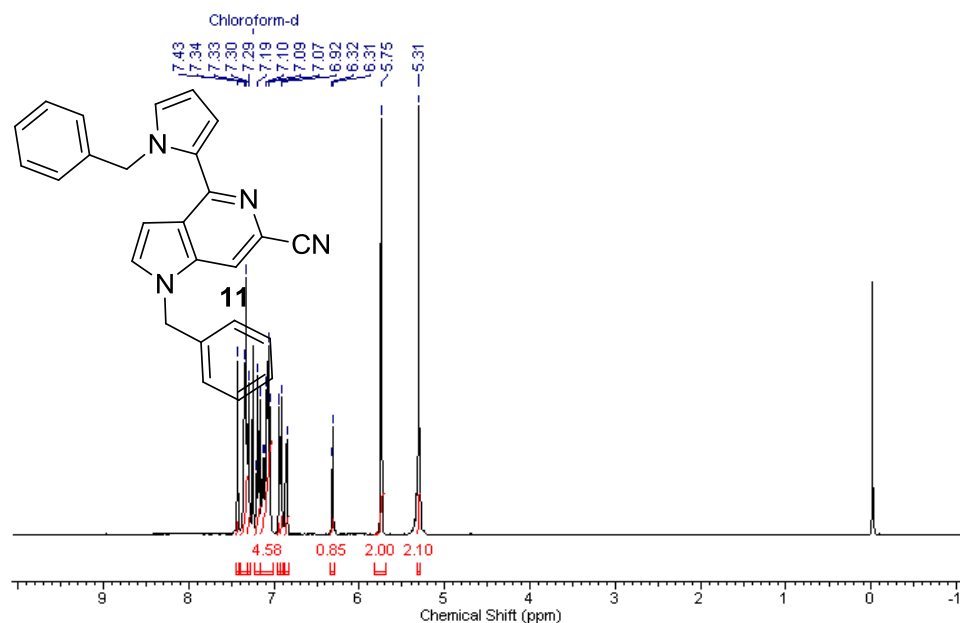


Figure 2.59 ¹H NMR spectrum of *1-benzyl-4-(1-benzyl-1H-pyrrol-2-yl)-1H-pyrrolo[3,2-c]pyridine-6-carbonitrile (**11**)*

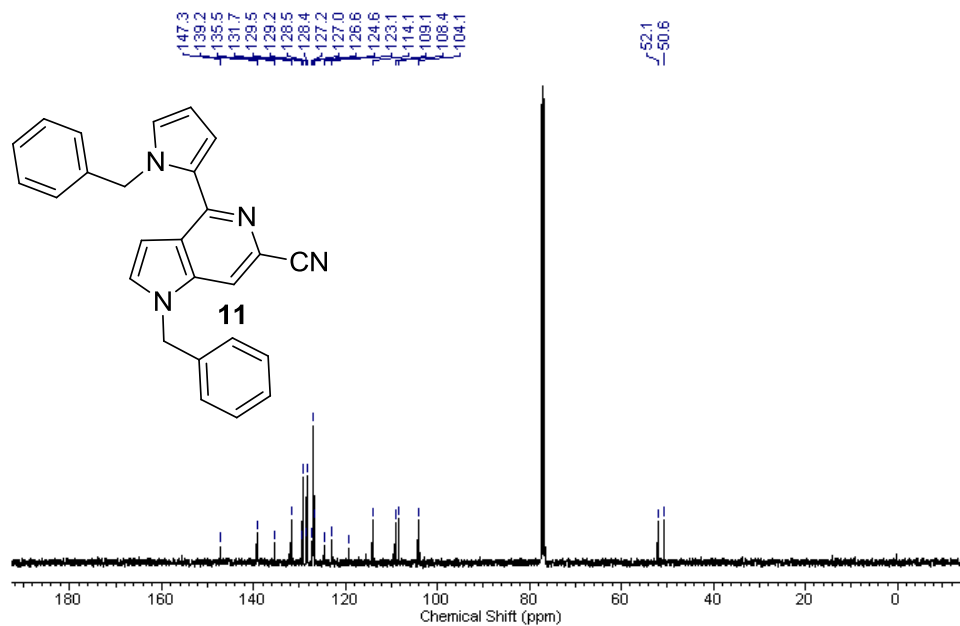


Figure 2.60 ¹³C NMR spectrum of *1-benzyl-4-(1-benzyl-1H-pyrrol-2-yl)-1H-pyrrolo[3,2-c]pyridine-6-carbonitrile (**11**)*

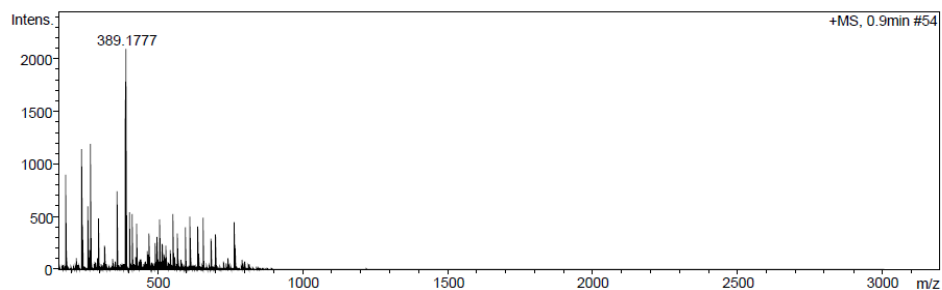


Figure 2.61 HRMS data of *1-Benzyl-4-(1-benzyl-1H-pyrrol-2-yl)-1H-pyrrolo[3,2-c]pyridine-6-carbonitrile (11)*

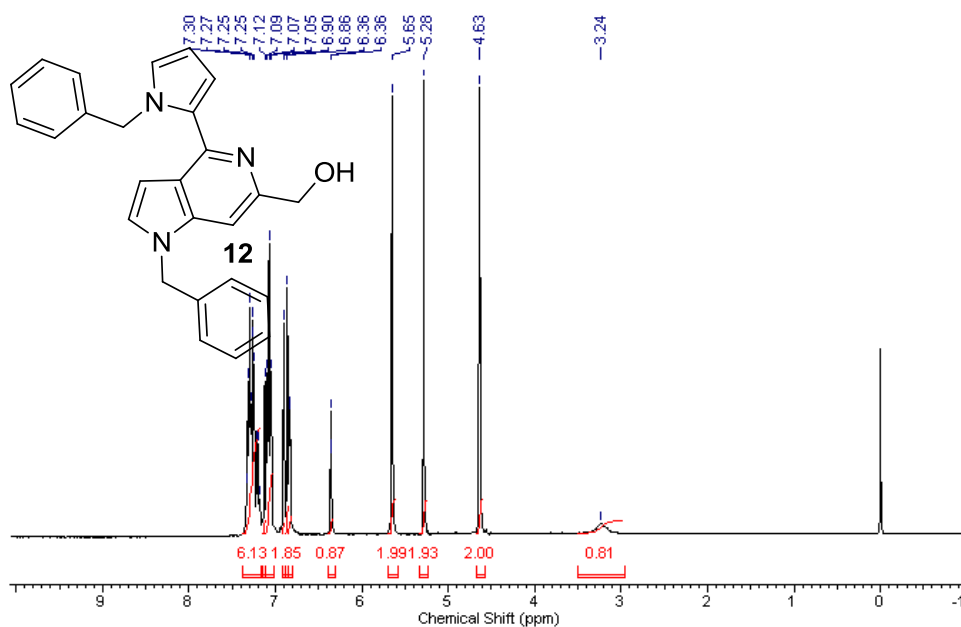


Figure 2.62 ^1H NMR spectrum of *1-benzyl-4-(1-benzyl-1H-pyrrol-2-yl)-1H-pyrrolo[3,2-c]pyridine-6-yl)methanol (12)*

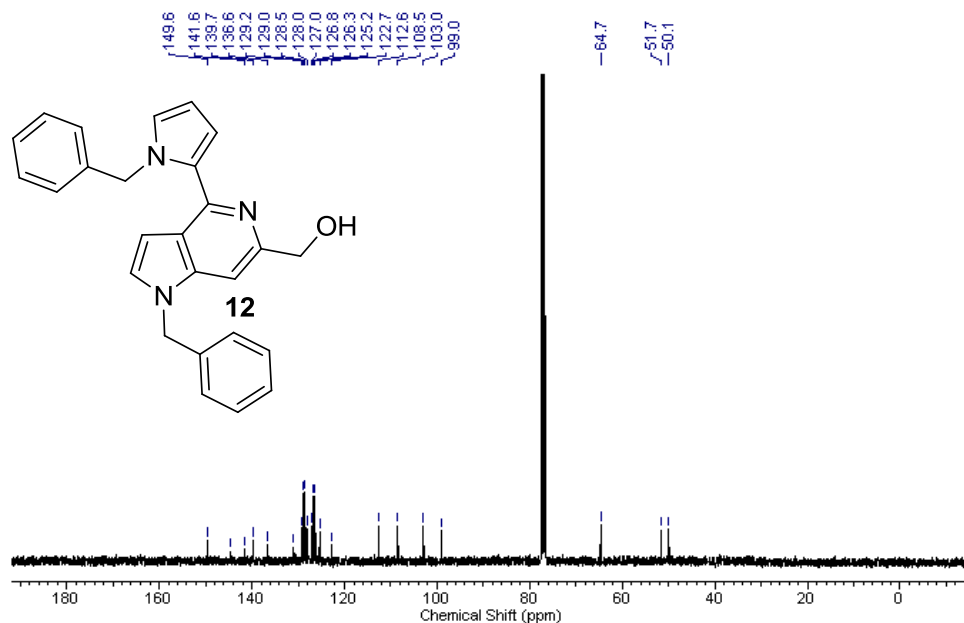


Figure 2.63 ^{13}C NMR spectrum of *1-benzyl-4-(1-benzyl-1H-pyrrol-2-yl)-1H-pyrrolo[3,2-c]pyridin-6-ylmethanol (12)*

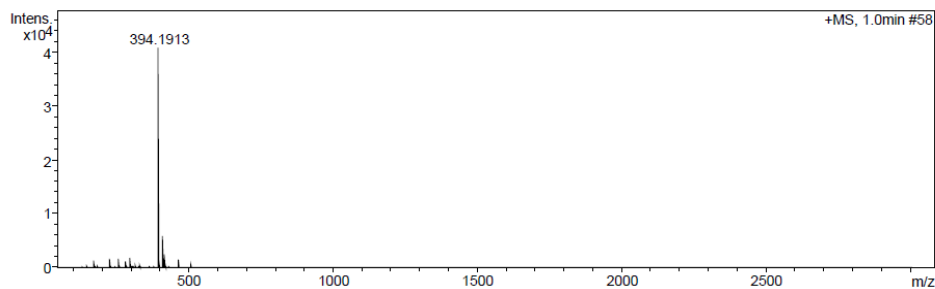


Figure 2.64 HRMS data of *1-benzyl-4-(1-benzyl-1H-pyrrol-2-yl)-1H-pyrrolo[3,2-c]pyridin-6-ylmethanol (12)*

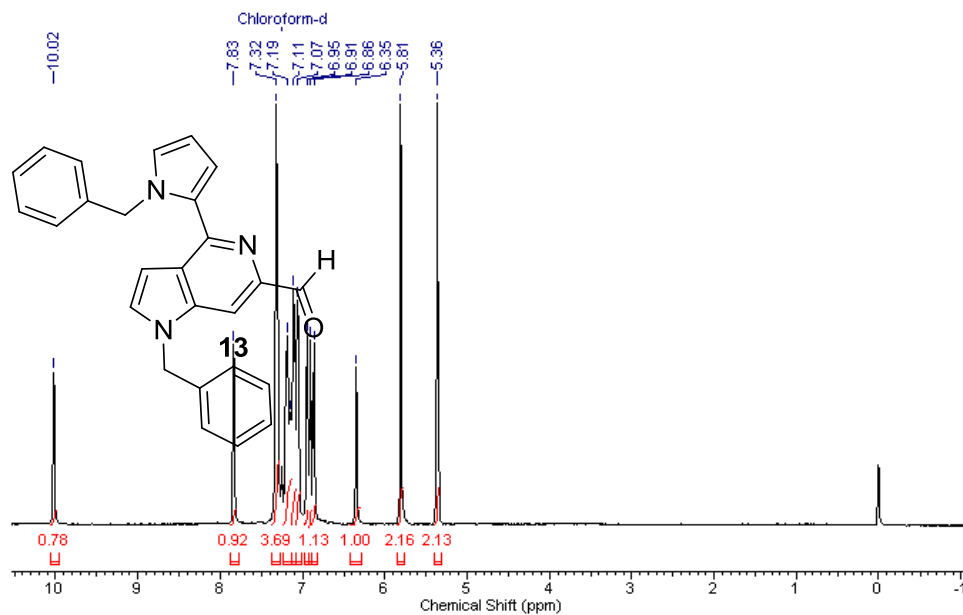


Figure 2.65 ¹H NMR spectrum of *1-benzyl-4-(1-benzyl-1H-pyrrol-2-yl)-1H-pyrrolo[3,2-c]pyridine-6-carbaldehyde* (**13**)

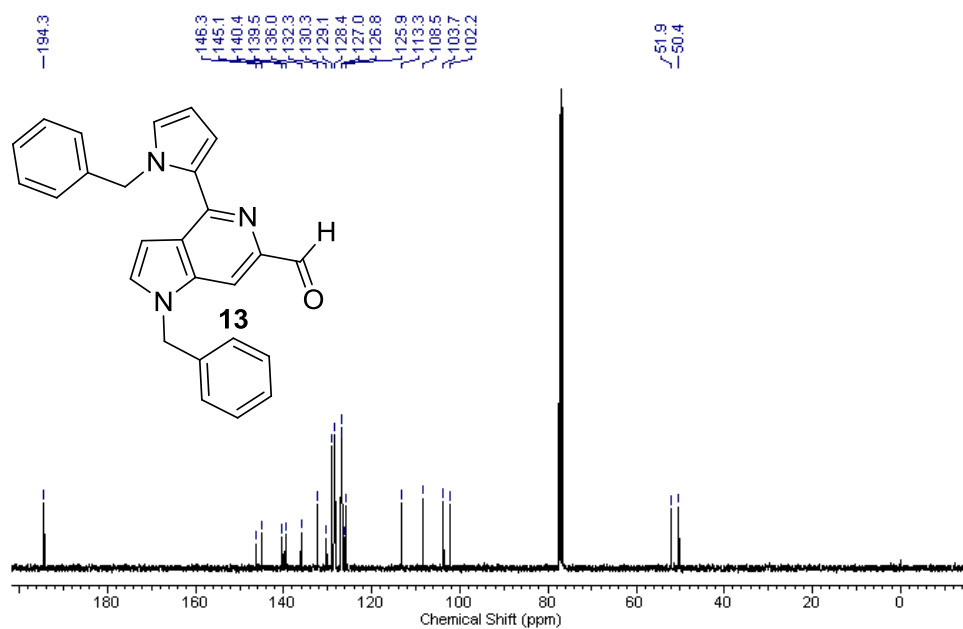


Figure 2.66 ¹³C NMR spectrum of *1-benzyl-4-(1-benzyl-1H-pyrrol-2-yl)-1H-pyrrolo[3,2-c]pyridine-6-carbaldehyde* (**13**)

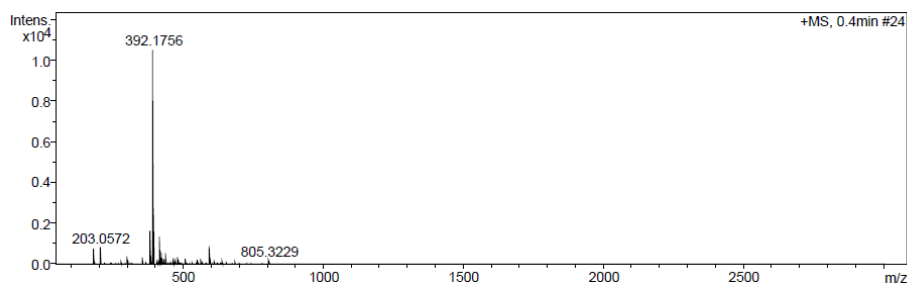


Figure 2.67 HRMS data of *1-benzyl-4-(1-benzyl-1H-pyrrol-2-yl)-1H-pyrrolo[3,2-c]pyridine-6-carbaldehyde (13)*

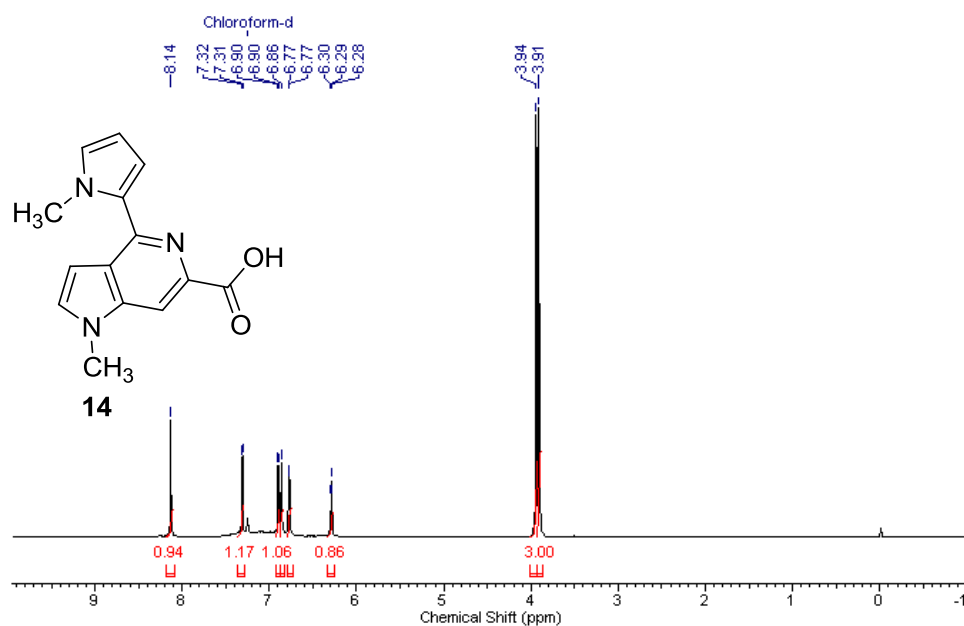


Figure 2.68 Crude ^1H NMR spectrum of *1-methyl-4-(1-methyl-1H-pyrrol-2-yl)-1H-pyrrolo[3,2-c]pyridine-6-carboxylic acid (14)*

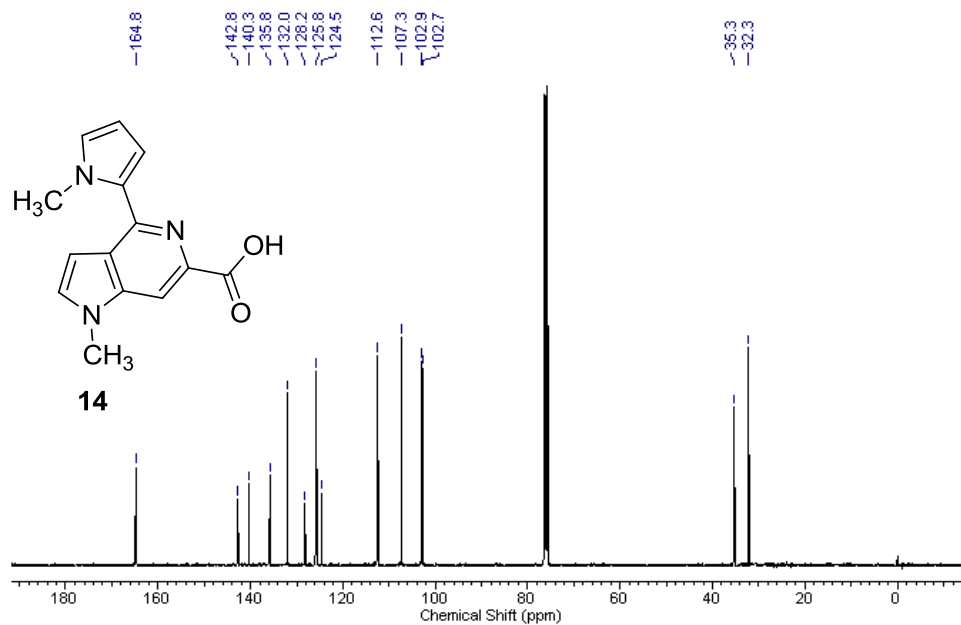


Figure 2.69 Crude ¹³C NMR spectrum of *1-methyl-4-(1-methyl-1H-pyrrol-2-yl)-1H-pyrrolo[3,2-c]pyridine-6-carboxylic acid (14)*

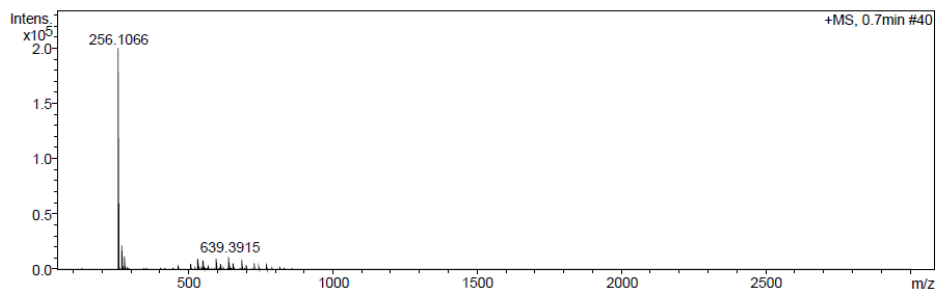


Figure 2.70 HRMS data of *1-methyl-4-(1-methyl-1H-pyrrol-2-yl)-1H-pyrrolo[3,2-c]pyridine-6-carboxylic acid (14)*

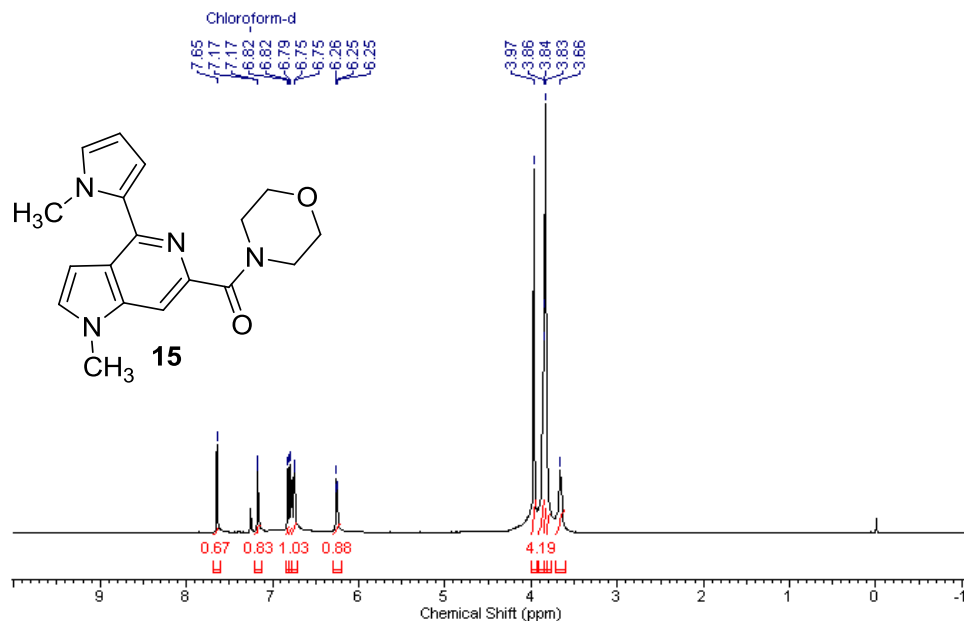


Figure 2.71 ¹H NMR spectrum of 1-methyl-4-(1-methyl-1H-pyrrol-2-yl)-1H-pyrrolo[3,2-c]pyridin-6-yl(morpholino)methanone (**15**)

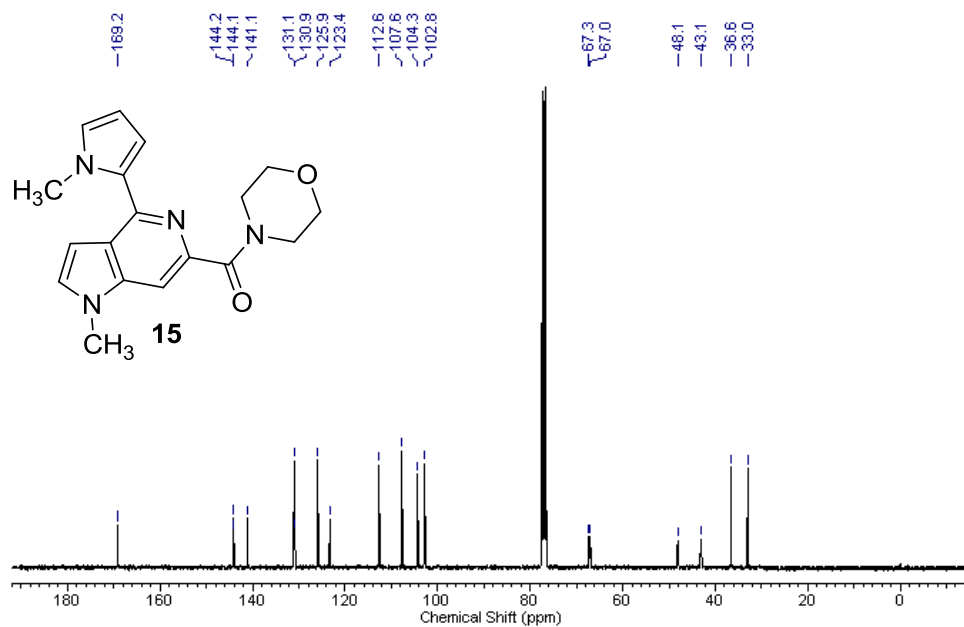


Figure 2.72 ¹³C NMR spectrum of 1-methyl-4-(1-methyl-1H-pyrrol-2-yl)-1H-pyrrolo[3,2-c]pyridin-6-yl(morpholino)methanone (**15**)

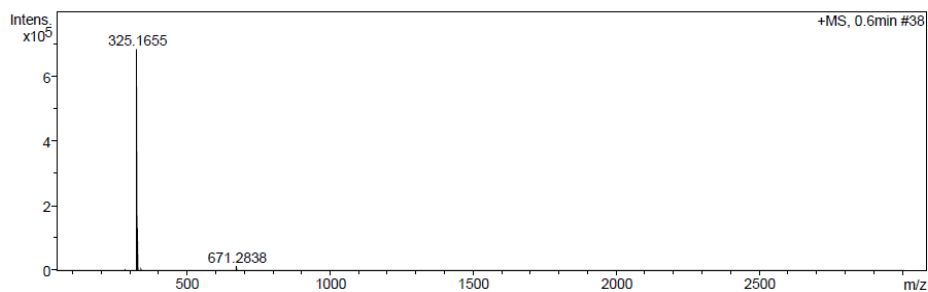


Figure 2.73 HRMS data of *1-methyl-4-(1-methyl-1H-pyrrol-2-yl)-1H-pyrrolo[3,2-c]pyridin-6-yl(morpholino)methanone (15)*

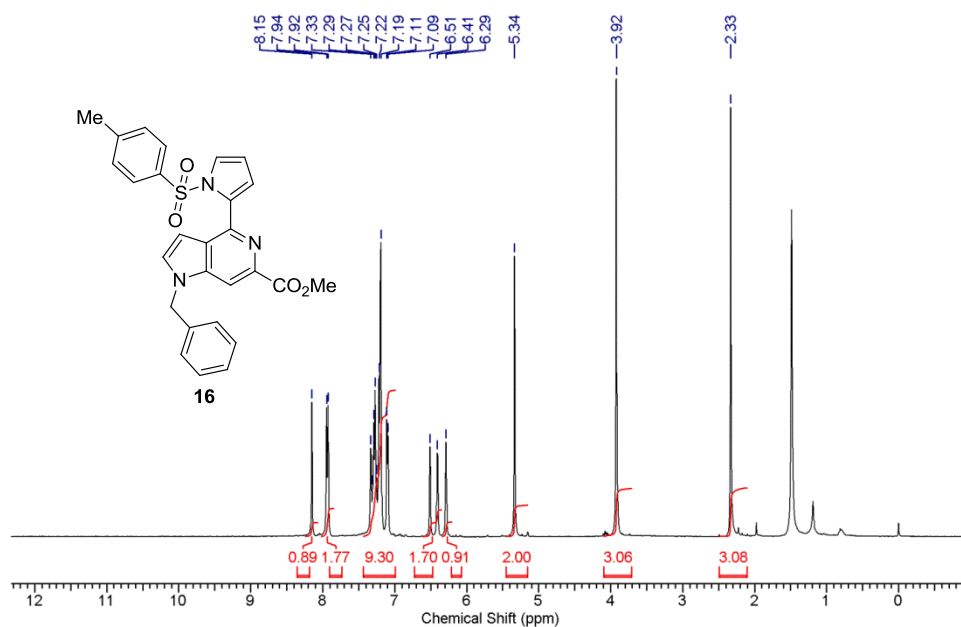


Figure 2.74 ^1H NMR spectrum of *methyl 1-benzyl-4-(1-tosyl-1H-pyrrol-2-yl)-1H-pyrrolo[3,2-c]pyridine-6-carboxylate (16)*

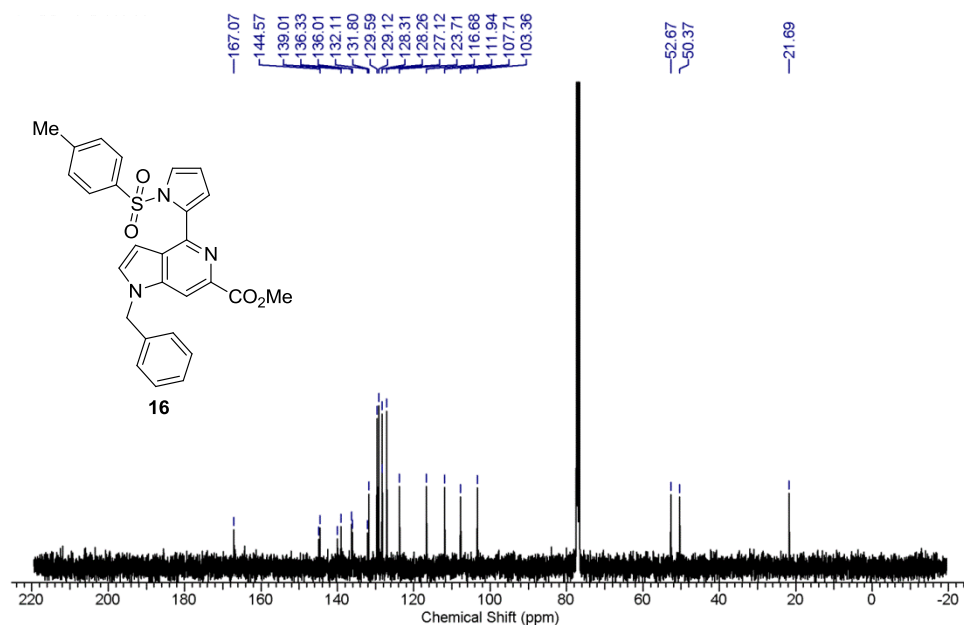


Figure 2.75 ^{13}C NMR spectrum of *methyl 1-benzyl-4-(1-tosyl-1H-pyrrol-2-yl)-1H-pyrrolo[3,2-c]pyridine-6-carboxylate (16)*

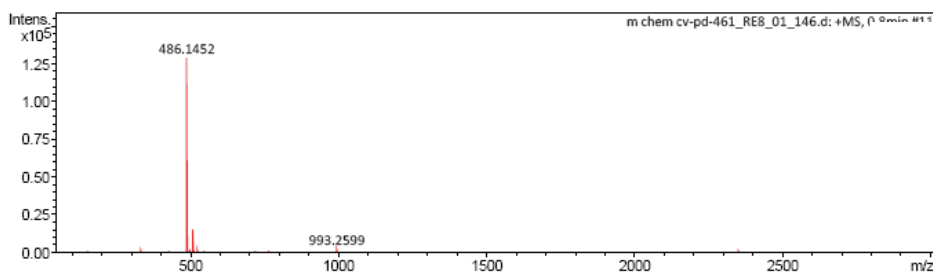


Figure 2.76 HRMS data of *methyl 1-benzyl-4-(1-tosyl-1H-pyrrol-2-yl)-1H-pyrrolo[3,2-c]pyridine-6-carboxylate (16)*

2.5 References

- [1] Anderson R.J., Hill J.B., Morris J.C. (2005), Concise total syntheses of variolin B and deoxyvariolin B, *J Org Chem*, 70, 6204–6212 (DOI: 10.1021/jo050523v)
- [2] Davies S.G., Fletcher A.M., Lee J.A., Lorkin T.J., Roberts P.M., Thomson J.E. (2013), Asymmetric synthesis of (–)-martinellic acid, *Org Lett*, 15, 2050–2053 (DOI: 10.1021/ol4007508)
- [3] Mérour J.Y., Buron F., Plé K., Bonnet P., Routier, S. (2014), The azaindole framework in the design of kinase inhibitors, *Molecules*, 19, 19935–19979 (DOI: 10.3390/molecules191219935)
- [4] Giblin G.M.P., Billinton A., Briggs M., Brown A.J., Chessell I.P., Clayton N.M., Eatherton A.J., Goldsmith P., Haslam C., Johnson M. R., Mitchell W.L., Naylor A., Perboni A., Slingsby B.P., Wilson A.W. (2009), Discovery of 1-[4-(3-chlorophenylamino)-1-methyl-1*H*-pyrrolo[3,2-*c*]pyridin-7-yl]-1-morpholin-4-ylmethanone (GSK554418A), a brain penetrant 5-azaindole CB₂agonist for the treatment of chronic pain, *J Med Chem*, 52, 5785–5788 (DOI: 10.1021/jm9009857)
- [5] Bastian J.A., Fisher M.J., Harper R.W., Lin H., McCowan J.R., Sall D.J., Smith G.F., Takeuchi K., Wiley M.R., Zhang M. (2004), European Patent EP000997465B1
- [6] Bryan M.C., Falsey J.R., Frohn M., Reichelt A., Yao G., Bartberger M.D., Bailis J.M., Zalameda L., San Miguel T., Doherty E.M., Allen J.G. (2013), N-substituted azaindoles as potent inhibitors of Cdc7 kinase, *Bioorg Med Chem Lett*, 23, 2056–2060 (DOI: 10.1016/j.bmcl.2013.02.007)

- [7] Chowdhury S., Sessions E.H., Pocas J.R., Grant W., Schröter T., Lin L., Ruiz C., Cameron M.D., Schürer S., LoGrasso P., Bannister T.D. (2011), Discovery and optimization of indoles and 7-azaindoles as Rho kinase (ROCK) inhibitors (part-I), *Bioorg Med Chem Lett*, 21, 7107–7112 (DOI: 10.1016/j.bmcl.2011.09.083)
- [8] Song J.J., Reeves J.T., Gallou F., Tan Z., Yee N.K., Senanayake, C.H. (2007), Organometallic methods for the synthesis and functionalization of azaindoles, *Chem Soc Rev*, 36, 1120–1132 (DOI: 10.1039/b607868k)
- [9] Popowycz F., Méroux J.Y., Joseph B. (2007), Synthesis and reactivity of 4-, 5- and 6-azaindoles, *Tetrahedron*, 63, 8689–8707 (DOI: 10.1016/j.tet.2007.05.078)
- [10] Shah S.K., Chen N., Guthikonda R.N., Mills S.G., Malkowitz L., Springer M.S., Gould S.L., DeMartino J.A., Carella A., Carver G., Holmes K. (2005), Synthesis and evaluation of CCR5 antagonists containing modified 4-piperidiny-2-phenyl-1-(phenylsulfonylamino)-butane, *Bioorg Med Chem Lett*, 15, 977–982 (DOI: 10.1016/j.bmcl.2004.12.044)
- [11] Wensbo D., Eriksson A., Jeschke T., Annby U., Gronowitz S., Cohen L.A. (1993), Palladium-catalysed synthesis of heterocondensed pyrroles, *Tetrahedron*, 34, 2823–2826 (DOI: 10.1016/S0040-4039(00)73572-6)
- [12] Roy P.J., Dufresne C., Lachance N., Leclerc J.P., Boisvert M., Wang Z., Leblanc Y. (2005), The Hemetsberger-Knittel synthesis of substituted 5-, 6-, and 7-azaindoles, *Synthesis*, 16, 2751–2757 (DOI: 10.1055/s-2005-872165)

- [13] Pires M.J., Poeira D.L., Purificacao S.I., Marques M.M.B. (2016), Synthesis of substituted 4-, 5-, 6-, and 7-azaindoles from aminopyridines via a cascade C–N cross-coupling/heck reaction, *Org Lett*, 18, 3250–3253 (DOI: 10.1021/acs.orglett.6b01500)
- [14] Purificação S.I., Pires M.J., Rippel R., Santos A.S., Marques M.M.B. (2017), One-pot synthesis of 1, 2-disubstituted 4-, 5-, 6-, and 7-azaindoles from amino-*o*-halopyridines via N-arylation/Sonogashira/cyclization reaction. *Org Lett*, 19, 5118–5121 (DOI: 10.1021/acs.orglett.7b02403)
- [15] Sun X., Wang C., Li Z., Zhang S., Xi Z. (2004), Zirconocene-mediated intermolecular coupling of one molecule of Si-tethered diyne with three molecules of organonitriles: one-pot formation of pyrrolo [3, 2-*c*] pyridine derivatives via cleavage of C:N triple bonds of organonitriles, *J Am Chem Soc*, 126, 7172–7173 (DOI: 10.1021/ja0497173)
- [16] Trejo A., Arzeno H., Browner M., Chanda S., Cheng S., Comer D.D., Dalrymple S.A., Dunten P., Lafargue J., Lovejoy B., Freire-Moar J. (2003), Design and synthesis of 4-azaindoles as inhibitors of p38 MAP kinase, *J Med Chem*, 46, 4702–4713 (DOI: 10.1021/jm0301787)
- [17] López-Pérez A., Adrio J., Carretero J.C. (2009), The phenylsulfonyl group as a temporal regiochemical controller in the catalytic asymmetric 1,3-dipolar cycloaddition of azomethine ylides, *Angew Chem Int Ed*, 121, 346–349 (DOI: 10.1002/ange.200805063)
- [18] Dekhane M., Potier P., Dodd R.H. (1993), A practical synthesis of 1*H*-pyrrolo[2,3-*c*]pyridine-5-carboxylic acid derivatives from

- pyrrole-2-carboxaldehydes, *Tetrahedron*, 49, 8139–8146 (DOI: 10.1016/S0040-4020(01)88033-9)
- [19] Outlaw V.K., d’Andrea F.B., Townsend C.A. (2015), One-pot synthesis of highly substituted *N*-fused heteroaromatic bicycles from azole aldehydes, *Org Lett*, 17, 1822–1825 (DOI: 10.1021/ol5036936)
- [20] Frisch M.J., Trucks G.W., Schlegel H.B., et al. Gaussian 09, Revision D.01, Gaussian, Inc., Wallingford, CT, 2009.
- [21] Becke A.D. (1988), Density-functional exchange-energy approximation with correct asymptotic behaviour, *Phys Rev A*, 38, 3098–3100 (DOI: 10.1103/PhysRevA.38.3098)
- [22] Lee C., Yang W., Parr R.G. (1988), Development of the Colle-Salvetti correlation-energy formula into a functional of the electron density, *Phys Rev B: Condens Matter Phys*, 37, 785–789 (DOI:10.1103/PhysRevB.37.785)

Chapter 3

Synthesis of 1-indolyl-3,5,8-substituted γ -carbolines: One-pot solvent-free protocol and biological evaluation

3.1 Introduction

Carbolines are privileged aza-heterocycles found in the core of several natural and synthetic compounds and are known for their biological applications. Among the four different isomers, 9*H*-pyrido[3,4-*b*]indole (β -carboline) is the most naturally abundant, present for instance, in the alkaloid harmine, a well-known selective inhibitor of monoamine oxidase-A (MAO-A) [1]. On the contrary, 5*H*-pyrido[4,3-*b*]indole (γ -carboline) are comparatively less examined, although these heterocycles have shown promising biological activities in preclinical and clinical studies (Figure 3.1) [2–6].

The pyrimidine- γ -carboline alkaloid ingenine B (isolated from an Indonesian sponge) exhibited pronounced cytotoxicity against a murine lymphoma cell line [7] and several isocanthine analogs are effective against cervical cancer (HeLa cells) [8]. Moreover, γ -carbolines are known for their well-established DNA intercalating [9] and anti-Alzheimer [10] properties.

The classical Graebe-Ullmann synthesis [11] of γ -carbolines, one of the very early protocols in the domain, is based on the thermal decomposition of *N*-pyridylbenzotriazoles. Later, the reaction conditions were modified to make this reaction more versatile and operationally simple such as by the use of microwave irradiation [12]. Meanwhile, the Fischer indole synthesis was successfully extended for the synthesis of significant biologically active tetrahydro- γ -carboline derivatives [13,14]. A systematic assessment of the above Graebe-Ullmann and Fischer synthesis protocols revealed that these reactions are associated with i) low

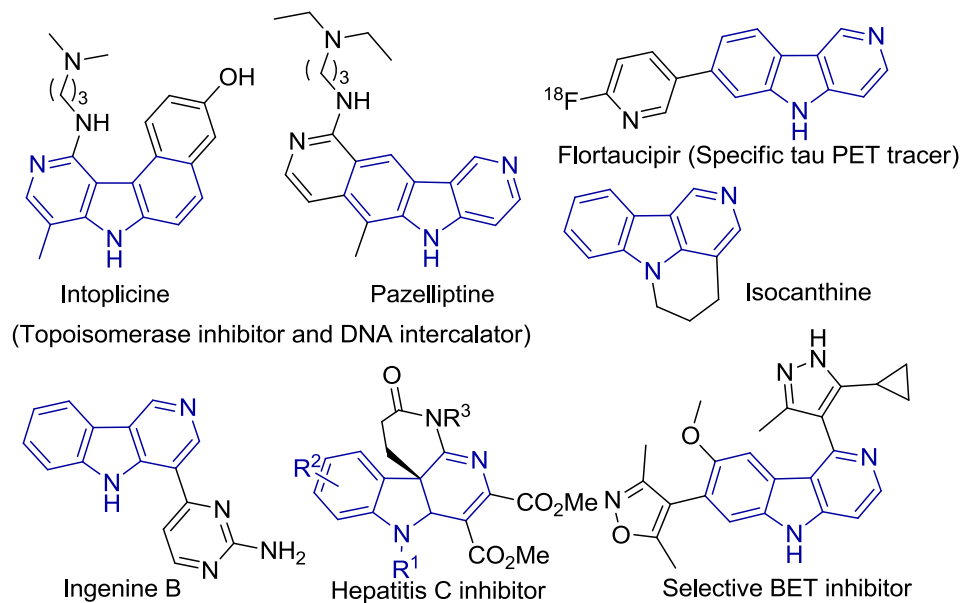
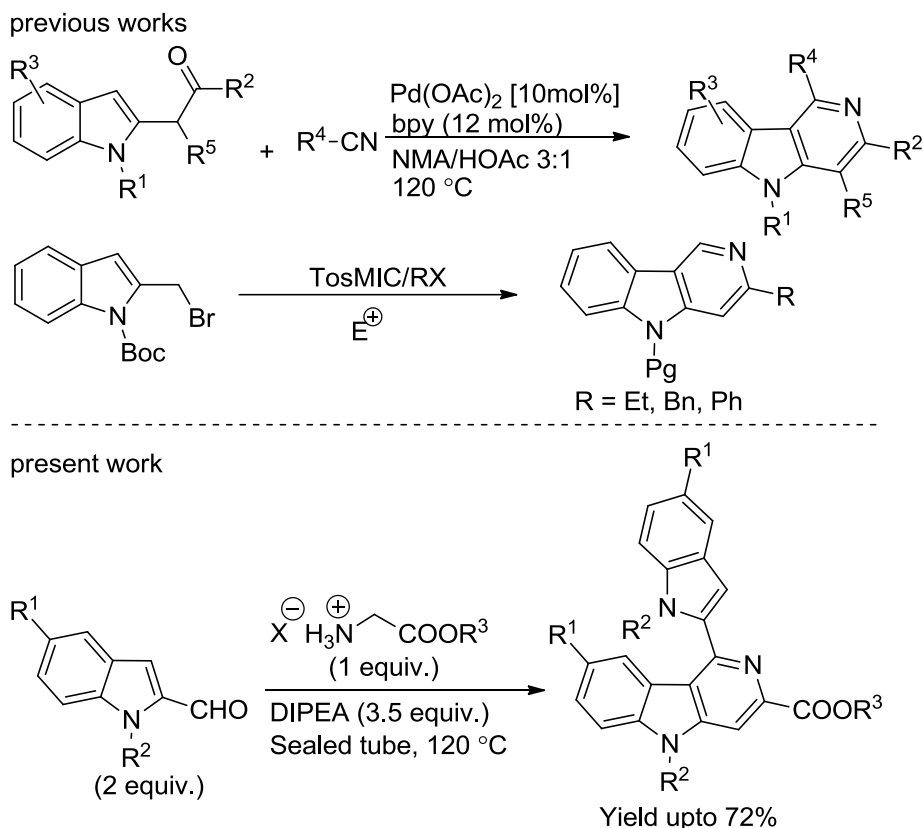


Figure 3.1 Selected examples of compounds containing γ -carboline core

product yield ii) limited scope including the use of a very specific set of substrates, and iii) involvement of extreme thermal conditions with the use of corrosive reagents. Much later, Larock and co-workers developed Pd/Cu-catalyzed imino-annulation of internal alkynes [15], which paved the way for transition-metal catalyzed cyclization as easy access to these scaffolds. Notably, the gold-catalyzed tandem cycloisomerization/Pictet–Spengler cyclization of 2-(4-aminobut-1-yn-1-yl)aniline [16], the Ru and Rh catalyzed [2+2+2] cycloadditions of yne-ynamides [17], and the Pd-catalyzed tandem coupling-cyclization [18] are significant works in the area (Scheme 3.1). However, the use of toxic and expensive metal catalysts has limited their development as environment-friendly synthetic protocols. More recently, an acid-catalyzed cyclization of α -indol-2-ylmethyl TosMIC (tosylmethyl isocyanide) derivatives to synthesize heterocycles [19] has been thoroughly studied (Scheme 3.1), including the synthesis of the carboline alkaloid ingenine B [20]. The iodine-catalyzed [3+3] cycloaddition of indolyl alcohol to enaminones [21] and thiourea-catalyzed iso-Pictet–Spengler reaction of isotryptamine with aldehydes [22], are some noteworthy contributions in the field.



Scheme 3.1 The synthetic strategy of present work in comparison with previous reports

A cascade or domino reaction is an interesting approach for the design efficient one-step transformation for complex molecule synthesis [23, 24]. Employing domino reactions to simplify cumbersome industrial processes can afford complex pharmaceutical products in an economical and environment-friendly manner [25]. Easy workup procedures and single-step purification reduce the efforts in synthesis of complex molecular architectures. Therefore, cascade reactions essential in synthetic organic chemistry, even with moderate yields [26]. Recently, Such reactions have claimed their much deserving place in drug designing and natural product synthesis [27]. In the literature, there is only a limited number of direct synthetic procedures to prepare γ -carboline till date [28], and this gives a cutting-edge advantage to our new protocol wherein a

solvent and metal-free direct access to the γ -carboline core from substituted indole-2-aldehydes and glycine ester salts has been discovered.

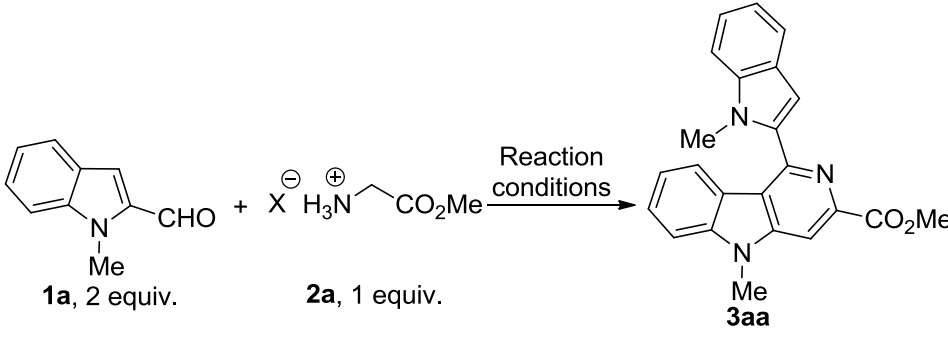
3.2 Results and Discussion

The base-catalyzed imination of aromatic aldehydes is a valuable method in organic synthesis to synthesize a variety of heterocyclic building blocks [29]. Among all the reported iminoesters, alkyl-*N*-arylidene glycinate have attracted much attention in recent years. For instance, the metal-catalyzed asymmetric [3+2] cycloaddition of ethyl *N*-benzylideneglycinate with electron-deficient alkenes has been reported to yield substituted pyrrolidines [30].

Recently, we reported the synthesis of substituted pyrrole-2-aldehydes to 5-azaindole transformation during a base-catalyzed imination reaction [31]. However, we envisioned that our methodology might be strategically applied towards synthesis of substituted γ -carbolines as C-3 nucleophilic attack is more favored in indoles than in pyrroles. In this chapter, we report an interesting observation for conversion of substituted indole-2-aldehydes **1** to 1-indolyl-3,5,8-substituted γ -carbolines **3** by a cascade imination-heterocyclisation pathway when treated with the salt glycine methyl ester hydrochloride (**2a**) in the presence of a base.

Earlier in the literature, it was reported that 1*H*-indole-2-carbaldehyde derivatives underwent condensation with *N*-arylideneglycinate to form pyrimidoindole derivatives [32]. However, when 1-methyl-1*H*-indole-2-carbaldehyde (**1a**) and glycine methyl ester hydrochloride salt (**2a**) were reacted in the presence of DIPEA (Hünig's base) at room temperature in a non-polar solvent such as toluene, only marginal amounts of the corresponding imine was observed, that could not be isolated (Table 3.1; entry 1). When the reaction mixture was further heated to reflux for 16 h, only traces of 1-indolyl 3,5,8-substituted γ -carboline **3aa** were formed that were still insufficient for complete

characterization. Intending to improve the yield of **3aa**, we screened various solvents, non-nucleophilic organic bases such as triethylamine and DBU, and several inorganic bases like K_2CO_3 , Cs_2CO_3 , and NaH (Table 3.1; entries 2–6).

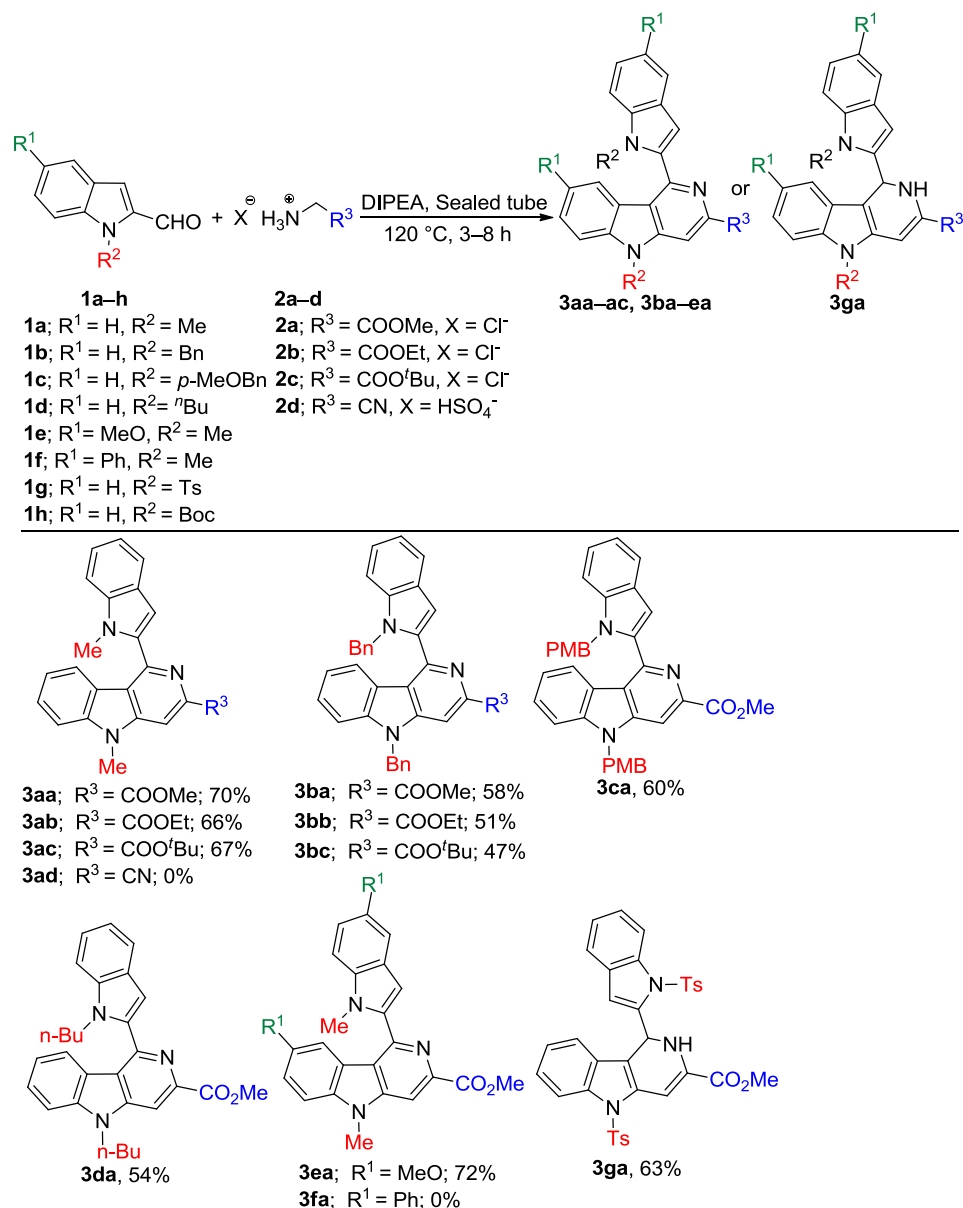
 <p>Reaction scheme showing the synthesis of 3aa from 1a and 2a under reaction conditions.</p> <p>1a, 2 equiv. 2a, 1 equiv. 3aa</p>						
Entry	mmol of 1a (conc.)	mmol of 2a (conc.)	Base (3.5 equiv., no of mmol, conc.)	Solvent (5mL)	Temp.	Yield
1	0.62 mmol (0.12 M)	0.31 mmol (0.06 M)	DIPEA (1.09 mmol, 0.21 M)	Toluene ^a	RT to reflux	Trace
2	0.62 mmol (0.12 M)	0.31 mmol (0.06 M)	Et ₃ N (1.09 mmol, 0.21 M)	Toluene ^a	RT to reflux	No product
3	0.62 mmol (0.12 M)	0.31 mmol (0.06 M)	DBU (1.09 mmol, 0.21 M)	Toluene ^a	RT to reflux	Trace
4	0.62 mmol (0.12 M)	0.31 mmol (0.06 M)	K_2CO_3 (1.09 mmol, 0.21 M)	Et ₂ O ^a	RT to reflux	No product

	M)	M)				
5	0.62 mmol (0.12 M)	0.31 mmol (0.06 M)	Cs ₂ CO ₃ (1.09 mmol, 0.21 M)	DMF ^a	RT to reflux	No product
6	0.62 mmol (0.12 M)	0.31 mmol (0.06 M)	NaH (1.09 mmol, 0.21 M)	THF ^a	RT to reflux	No product
7	0.62 mmol	0.31 mmol	DIPEA ^b	---	120 °C	70%

Table 3.1 Optimization of reaction conditions for the transformation of 1-methylindole-2-carbaldehyde (**1a**) to γ -carboline **3aa**: ^aReactions were monitored by TLC for 3 h at room temperature followed by reflux for 16 h in the appropriate solvent; ^bSolvent-free reaction carried out in a 25 mL borosilicate sealed tube in a preheated oil bath in an air atmosphere at 120 °C

After systematic screening of several reaction conditions, we found that heating at 120 °C of a neat mixture consisting of 1-methyl-1*H*-indole-2-carbaldehyde, (**1a**, 2.0 equiv.), glycine methyl ester HCl salt (**2a**, 1.0 equiv.), and DIPEA (3.5 equiv.) in a sealed tube for 6 h, led to the isolation of γ -carboline **3aa** in 70% yield (Table 3.1; entry 7). The product **3aa** was subsequently characterized by various spectroscopic techniques.

With the initial success at hand, the reaction was found to be equally effective with various glycine alkyl ester HCl salts **2a–2c** but failed to result in the formation of 1-indolyl-3-cyano-5-methyl γ -carboline derivative **3ad** when 2-aminoacetonitrile **2d** was utilized as the condensation component.



Scheme 3.2 Series of 1-indolyl-3,5,8-substituted γ -carboline **3aa–ac**, **3ba–ea** and 1-indolyl-1,2-dihydro-3,5-substituted γ -carboline **3ga** derivatives

Then, a range of 1,5-substituted indole-2-carboxaldehyde derivatives **1a–h** was synthesized to evaluate the scope of the reaction, further. Indole-2-carbaldehyde derivatives with electron-donating 1-substituent on the indole ring system **1a–e** were transformed in moderate to good yields into their corresponding γ -carboline derivatives **3aa–ac**, and **3ba–ea** due to an enhanced C-3 nucleophilicity of indole nucleus

(Scheme 3.3). The formation of the corresponding γ -carboline was confirmed unequivocally by single-crystal X-ray diffraction analysis of **3ac** (Figure 3.2).

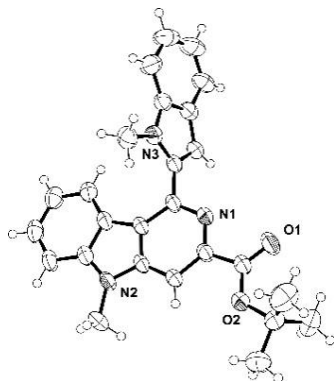


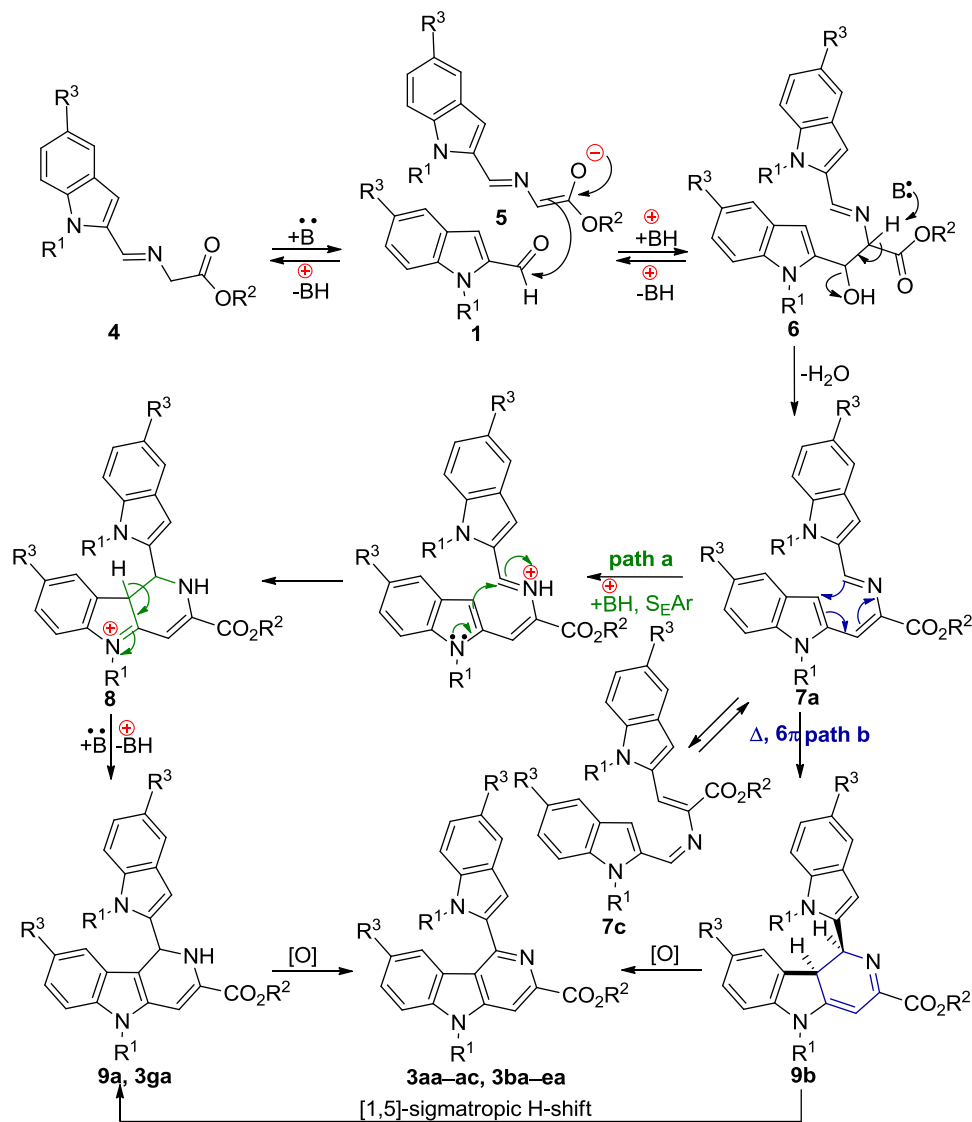
Figure 3.2 Single-crystal XRD structure of **3ac** (CCDC: 1897787)

The presence of two substituents in the 1,5-position of indole-2-carbaldehyde substrates such as **1e** (5-methoxy-1-methyl-1*H*-indole-2-carbaldehyde) and **1f** (1-methyl-5-phenyl-1*H*-indole-2-carbaldehyde) influenced the outcome of the heterocyclization reaction in different ways. For instance, 1-methyl-5-methoxy substituted compound **1e** was successfully transformed into 1-indolyl-3-carbomethoxy-5-methyl-8-methoxy γ -carboline (**3ea**) in 72% yield, whereas the 1-methoxy-5-phenyl-substituted indole carbaldehyde **1f** remained unreacted under optimized reaction condition and did not yield the expected 5-methyl-1-(1-methyl-5-phenyl-1*H*-indol-2-yl)-3-carbomethoxy-8-phenyl γ -carboline derivative **3fa**. The reason for this remains unclear but is likely due to the electron-withdrawing nature of the phenyl substituent at the 5-position in substrate **1f**. Indole substrates with a weak electron-withdrawing substituent in the 1-position such as *N*-tosyl in 1-tosyl-1*H*-indole-2-carbaldehyde (**1g**) did not affect the reaction course. The substrate was smoothly transformed into the corresponding 1-indolyl-3,5-substituted 1,2-dihydro- γ -carboline derivative **3ga** instead of completely aromatized γ -carboline when heated at 120 °C with glycine methyl ester hydrochloride and DIPEA for 8 h in a

sealed tube. However, electron-withdrawing 1-substituent such as *N*-Boc group in 1-*tert*-butyloxycarbonyl-1*H*-indole-2-carbaldehyde (**1h**), impeded the conversion to γ -carboline **3ha** (structure not shown) due to probable decomposition and decrease in nucleophilicity at 3-position in substrate **1h**.

The probable mechanistic explanation (Scheme 3.3) for the formation of γ -carboline derivatives **3aa–ac** and **3ba–ea** involves the initial formation of *trans*-iminoester **4** from *N*-protected indole-2-carboxaldehydes **1a–e** and **1g**, and glycine alkyl esters **2a–c**. The Hünig's base, DIPEA, helps abstract active methylene proton from iminoester **4** to generate enolate ion **5**, which undergoes nucleophilic addition with another molecule of aldehyde **1** to furnish iminoalcohol intermediate **6**. The iminoalcohol **6** undergoes dehydration under the reaction condition to give *E*-imine/*Z*-enamine **7a** or *Z*-imine/*E*-enamine **7c** intermediates irreversibly, which plays a decisive role in determining ring closure *via* either path a or path b.

In path a, protonation of the imine nitrogen in **7a** by the conjugate acid (+BH) leads to an electrophilic aromatic substitution at the 3-position of the indole unit to form a carbon-carbon bond in the intermediate **8**. A further proton abstraction in **8** by the base gives then gives the 1-indolyl-3,5-substituted 1,2-dihydro- γ -carboline intermediate **9a** or **3ga**. In path b, the intermediate **7a** cyclizes via a thermal 6- π electrocyclic reaction of the conjugated triene system to form the 1-indolyl-3,5-substituted 1,9 β -dihydro- γ -carboline **9b**, that may also undergo a [1,5]-sigmatropic hydrogen shift, to reinstall aromaticity of the indole ring, leading to the formation of **9a**. *In situ* oxidation of intermediates **9a** or **9b**, probably from the dissolved oxygen present in the reaction mixture, leads to the formation of 1-indolyl-3,5,8-substituted γ -carbolines **3aa–ac** and **3ba–ea**. We successfully isolated and characterized 1,2-dihydro γ -carboline derivative **3ga**, which again verifies the proposed mechanism.



Scheme 3.3 Plausible mechanism for the formation of 1,2-dihydro- γ -carboline derivative **3ga** and 1-indolyl-3,5,8-substituted γ -carbolines **3aa–ac** and **3ba–ea**

During the formation of carbolines, the substrates, **1a–e** and **1g** were exclusively transformed to γ -carbolines or 1,2-dihydro- γ -carbolines **9a** and no traces of any β -carboline regioisomers (**9c**) were observed, which proves that the heterocyclization reaction is highly regioselective (Figure 3.3). The γ -carbolines formed during the heterocyclization are isolated, and characterized unequivocally by various spectroscopic

techniques. Though transition states are important in understanding the mechanism of a reaction but finding such transitions states require higher computational resources which we do not have at our disposal. Therefore, we presume γ -carboline formation is thermodynamically favorable and to confirm the formation of thermodynamic product we have calculated the total energies of the products.

The exclusive formation of γ -carboline regioisomer is explained by proposing an intermediate **7a** before the heterocyclization reaction takes place. Indole ring A predominantly participates in electrophilic aromatic substitution on the intermediate **7a** over Michael's addition of indole ring B which is geometrically impossible.

Density functional theoretical calculations were carried out using the B3LYP/6-311++G** level of theory [33–35] to understand the reaction pathways (path a or path b) and regioselectivity for the formation of γ -carboline from **9a/9b** or β -carboline **9c** from **7a** or **7c** intermediates, respectively.

First, we have calculated the total energies of the two intermediates, **9a** and **9b**, formed from **7a** *via* two different pathways, as shown in scheme 3.3. The calculated total energies of the intermediates show that the intermediate **9a** generated *via* path a to be more stable (by 14.6 Kcal/mol) compared to the intermediate **9b** generated *via* path b. Therefore, we conclude that path a is preferable over path b based on the total energies of the intermediates (Scheme 3.3).

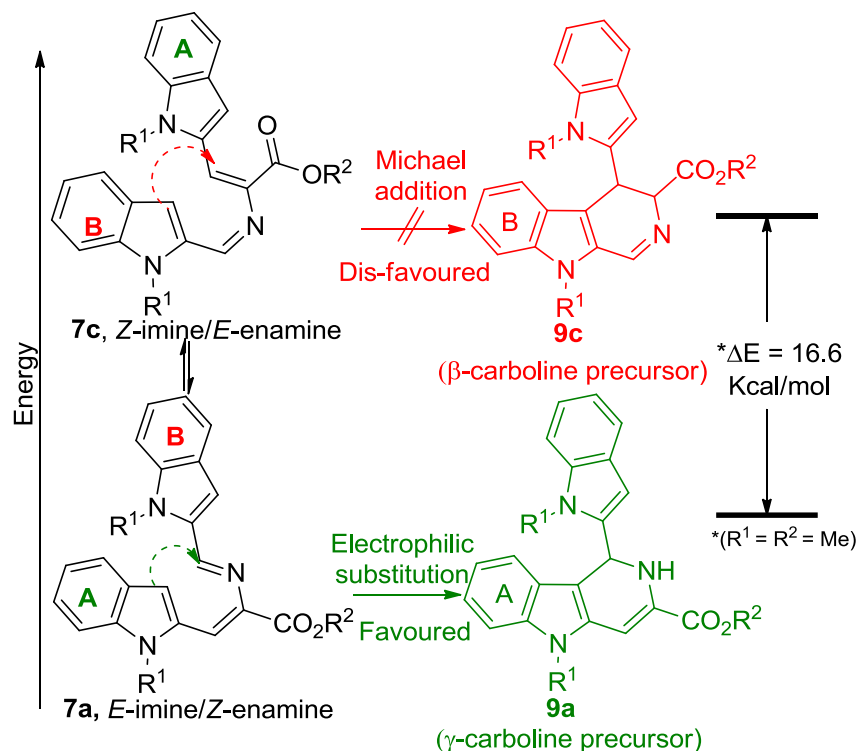


Figure 3.3 DFT relative energy calculation for the formation of γ -carboline **9a** over β -carboline **9c** regioisomer from **7a** using B3LYP/6-311++G** level of theory

Next, we have calculated the zero-point corrected total energies of the intermediates **9a**, **9b**, and **9c** to understand the regioselectivity of the formation of carbolines through electrophilic aromatic substitution (**9a**), thermal 6π -electrocyclization (**9b**) or Michael addition (**9c**) reactions (Scheme 3.3, Figure 3.3). Additionally, it is important to note that the intermediate **7a** (E-imine/Z-enamine) can exist in equilibrium with **7c** (Z-imine/E-enamine) (Figure 3.3). The calculated total energy values show that the product, 1,2-dihydro- γ -carboline, **9a** formed *via* electrophilic aromatic substitution is 16.6 Kcal/mol more stable over the product, 1,2-dihydro- β -carboline, **9c** formed *via* Michael addition reaction. This indicates that the γ -regioisomer **9a** is thermodynamically stable over β -regioisomer **9c** (Figure 3.3).

Interestingly, the γ -carboline derivatives were found to be highly fluorescent under UV light irradiation. A systematic literature survey

revealed that the structural core of carbolines had been widely exploited for the development of organic fluorescent entities, and in general, their UV absorbance ranges between 340 to 380 nm. For deeper insight into the optical properties of novel substituted γ -carbolines, absorption and emission studies were carried out in different organic solvents (Figure 3.4). The representative γ -carboline derivative *tert*-butyl-5-methyl-1-(1-methyl-1*H*-indol-2-yl)-5*H*-pyrido[4,3-*b*]indole-3-carboxylate (**3ac**) revealed similar absorption features with a shift in absorption maximum in different solvents. The highest absorption maximum (λ_{max}) was observed at 230 nm for **3ac** in DMSO (Figure 3.4, left side).

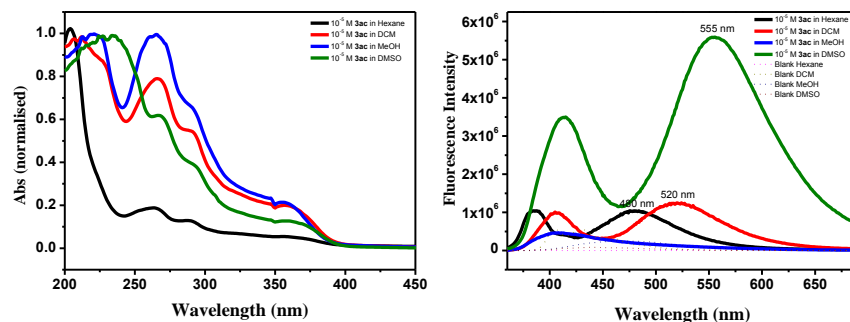


Figure 3.4 UV-vis absorption (left side) and emission (right side) spectra of **3ac** measured in different solvents

The fluorescence studies carried out for **3ac** in four different solvents revealed that emission maxima shifted bathochromically by almost 40 nm upon changing the solvent polarity, for instance, from non-polar hexane to moderately polar dichloromethane and then highly polar DMSO (Table 3.2, Figure 3.4). The fluorescence quenching of **3ac** in methanol is attributed to the partial protonation of the carboline unit's nitrogen atoms facilitated by polar-protic solvent [36].

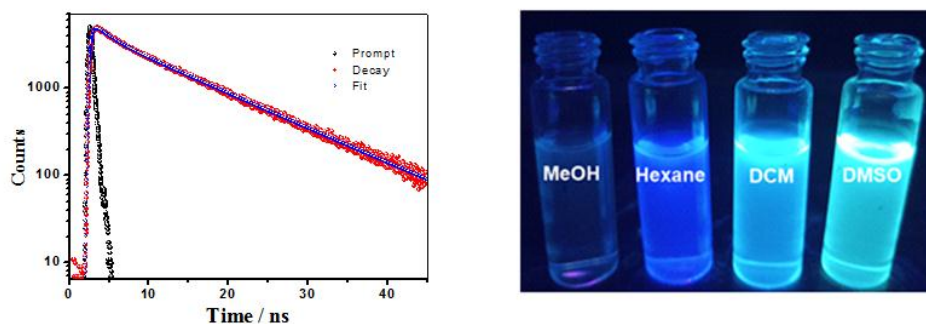


Figure 3.5 Fluorescence decay profile of **3ac** in DMSO (left side; λ_{exc} 360 nm) and 10^{-5} M solutions of compound **3ac** in four different solvents under UV chamber (right side)

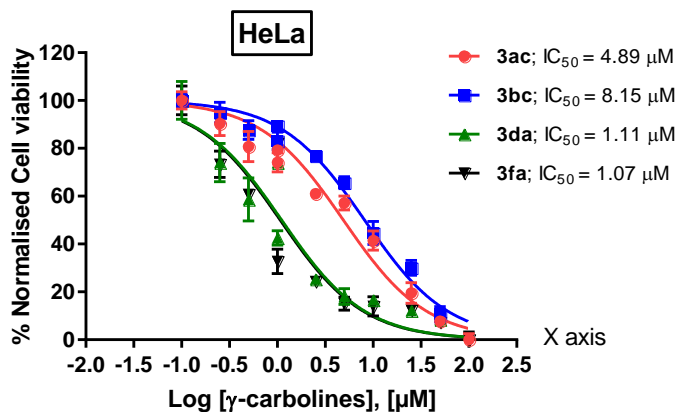
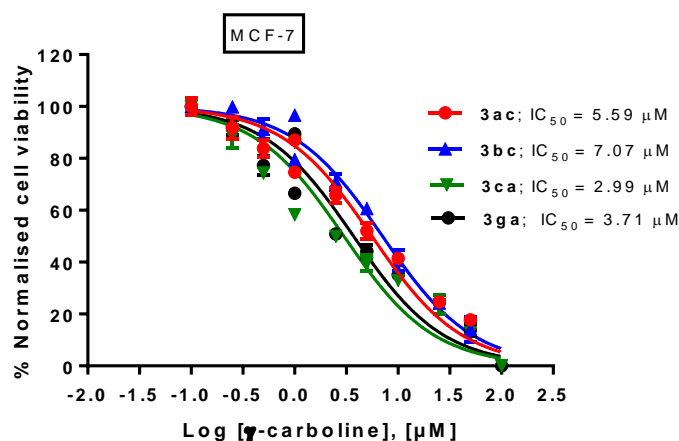
The fluorescence lifetimes were measured by time-correlated single-photon counting (TCSPC) experiments. The average fluorescence lifetime of compound **3ac** was found to be 8.35 nanoseconds (ns) and 4.73 ns in DMSO and DCM, respectively (Table 3.2, Figure 3.5).

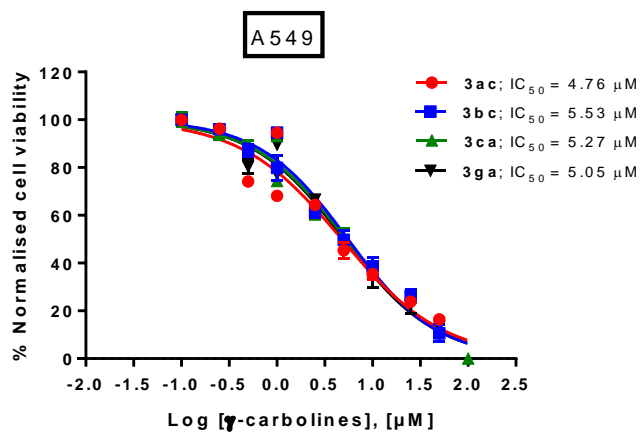
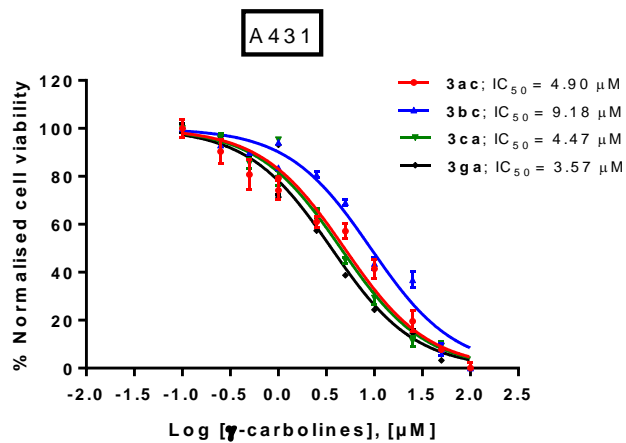
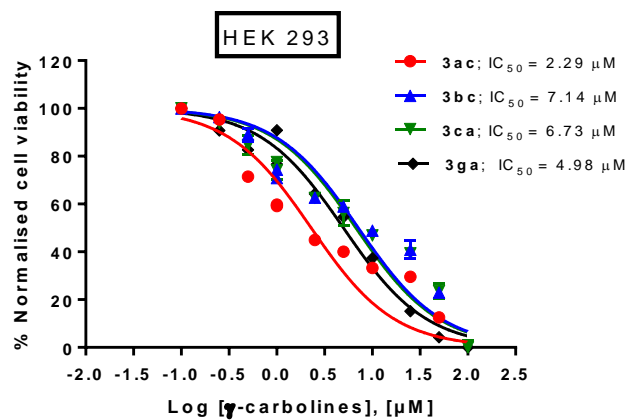
Solvent	λ_{abs} (nm)	ϵ ($10^3 \text{ M}^{-1} \text{ cm}^{-1}$)	λ_{em} (nm)	τ (ns)
Hexane	204, 262, 290, 355	0.78	386, 480	1.90
DCM	210, 266, 290, 356	1.01	405, 520	4.73
MeOH	220, 265, 290, 355	2.05	407, 422	0.99
DMSO	230, 266, 290, 357	1.67	413, 555	8.35

Table 3.2 Optical data for γ -carboline **3ac**

A panel of carboline derivatives **3ac**, **3bc**, **3ca**, and **3ga**, along with a standard drug, doxorubicin, were screened for their cytotoxicity against various cancer lines (Figure 3.6, Table 3.3) such as MCF-7 (breast cancer), A431 (skin cancer), A549 (lung cancer), HEK293 (human embryonic kidney cells), HeLa (cervical cancer), and macrophage or

immune cell line (RAW 264.7). The cancer cells were treated with increasing concentration of carboline derivatives **3ac**, **3bc**, **3ca**, **3ga** and doxorubicin (0.1 μM , 0.25 μM , 0.5 μM , 1 μM , 2.5 μM , 5 μM , 10 μM , 25 μM , 50 μM , 100 μM) and incubated for 48 h. Half-maximal inhibitory studies show that γ -carbolines are highly toxic to cancer cells in micromolar concentrations similar to doxorubicin, whereas they are non-cytotoxic (Figure 3.7) to human macrophages or immune cells.





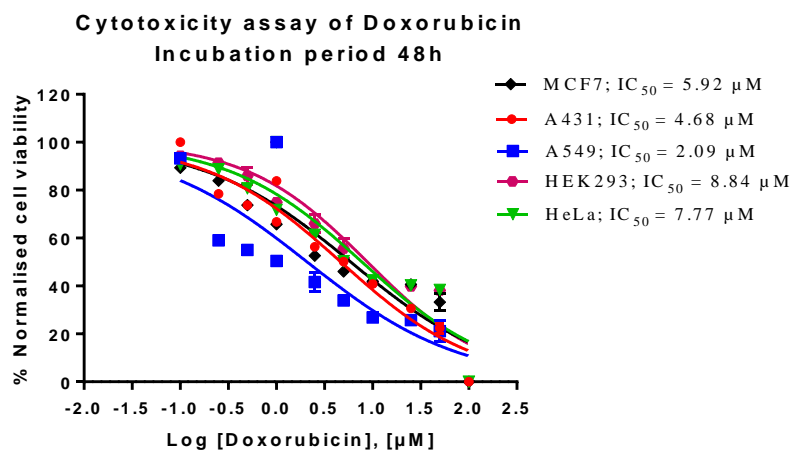


Figure 3.6 Dose vs response or IC_{50} curves for the representative γ -carboline, **3ac**, **3bc**, **3ca**, **3ga** and doxorubicin against cancer cell lines

Compound	IC_{50} in cancer cell lines (μM)				
	MCF7	A431	A549	HEK293	HeLa
γ -Carboline					
3ac	5.59	4.89	4.76	2.29	4.89
3bc	7.07	9.18	5.53	7.14	8.15
3ca	2.99	4.47	5.27	6.73	1.30
3ga	3.71	3.57	5.05	4.98	1.07
Doxorubicin	5.92	4.68	2.09	8.84	7.77

Table 3.3 IC_{50} values of γ -carboline **3ac**, **3bc**, **3ca**, **3ga** and doxorubicin in various cancer cell lines

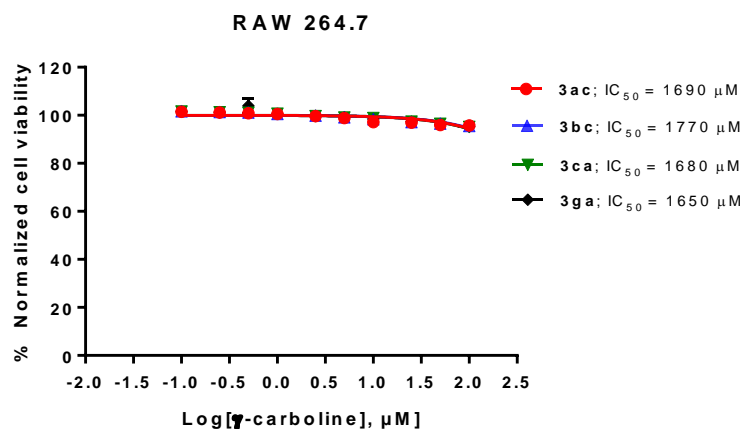


Figure 3.7 Dose vs response curve of γ -carbolines **3ac**, **3bc**, **3ca**, **3ga** in the macrophage cell line, RAW 264.7

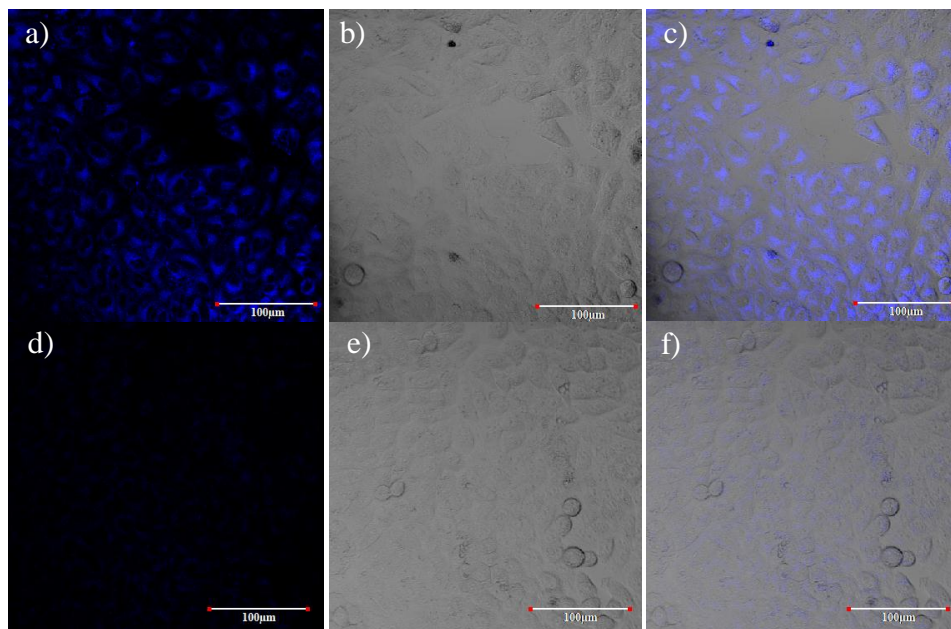


Figure 3.8 Laser scanning confocal microscopy studies ($\lambda_{\text{ex}} = 405 \text{ nm}$; collection range = 420–470 nm) for uptake of **3ac** in HeLa cells; a) Confocal fluorescent image of HeLa cells after 3 h incubation with 10 μM concentration of **3ac** (20X magnification, 2X zoom); b) DIC image of HeLa cells; c) Overlay of (a) and (b) indicating distribution of **3ac** in cytoplasm with distinct cell nucleus; d) Confocal image of HeLa cells

after 3 h incubation with 100 nM concentration of **3ac** (20X magnification, 2X zoom); e) DIC image of HeLa cells; f) Overlay of (d) and (e) showing nominal uptake of **3ac** in cytoplasm.

At last, to evaluate cell uptake of the novel γ -carboline for fluorescence imaging, live-cell imaging experiments were performed. In brief, HeLa cells were incubated with **3ac** (10 μ M and 100 nM) and the cellular uptake were examined using confocal microscopy (λ_{ex} = 405 nm; λ_{em} = 420–470 nm). Compound **3ac** showed excellent cytosolic uptake in cancer cells when incubated at a 10 μ M concentration, whereas only little uptake was observed at a concentration of 100 nM (Figure 3.8).

3.3 Conclusion

In summary, we have developed an operationally simple one-pot synthetic protocol for the synthesis of highly substituted γ -carboline derivatives. The metal- and solvent-free method provides direct access to complex molecular structures in good yield from inexpensive substrates. The optical and biological evaluations carried out for representative γ -carbolines revealed promising photophysical and anticancer properties of the core framework for developing novel theranostic applications to diagnose and treat cancer in the future.

3.4 Experimental section

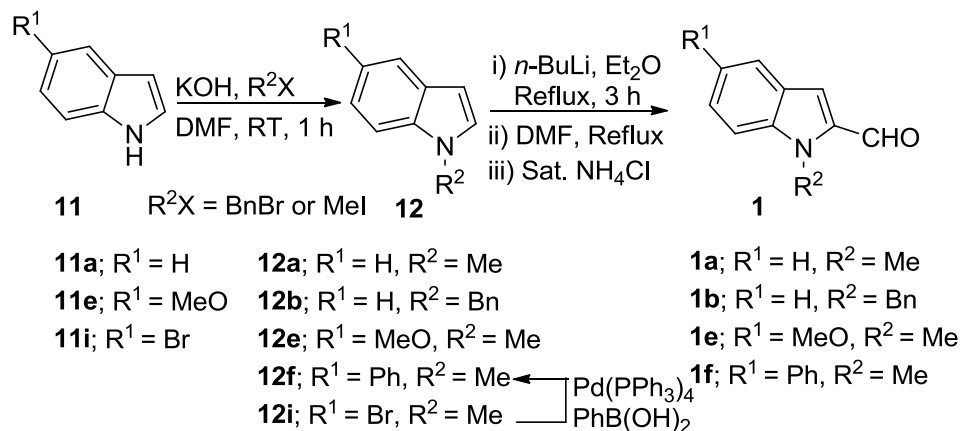
3.4.1 General information

All reactions were carried out in oven-dried glassware with magnetic stirring. Starting materials and other reagents were obtained from a commercial supplier and used without further purification. Compounds **1a–b**, **1d**, **1g–h**, **12a–b**, **12e–f**, **12i**, **14d**, **14g**, and **15** were prepared by methods reported in the literature [37–48]. NMR spectra were recorded on

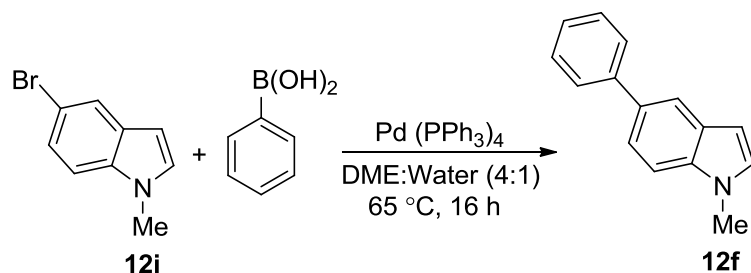
Avance III 400 Ascend Bruker. CDCl_3 and D_2O were used as NMR solvents. Chemical shifts (δ) were reported as part per million (ppm), and TMS was used as an internal reference. High-resolution mass spectra were recorded through Bruker Daltonik High-Performance LC-MS (Electrospray Ionization Quadrupole time-of-flight) spectrometer. X-ray structure analysis was carried out at a Single crystal X-ray diffractometer Bruker KAPPA APEXII. Melting points (m.p.) are uncorrected and were measured on the Veego melting point apparatus (Capillary method). Analytical thin-layer chromatography (TLC) was carried out on silica gel plates (silica gel 60 F254 aluminum supported plates), and the spots were visualized with a UV lamp (254 nm and 365 nm) or using chemical staining with Brady's reagent, KMnO_4 , ninhydrin, iodine, and bromocresol. Column chromatography was performed using silica gel (100–200 mesh or 230–400 mesh) and neutral alumina (175 mesh). DMF, DCM, DMA, Toluene, and Acetonitrile were dried using CaH_2 and distilled over flame-dried 4\AA molecular sieves. THF and Et_2O were dried over Na/benzophenone and stored over flame-dried 4\AA molecular sieves under an inert atmosphere prior to use. Organic bases, including DIPEA, Et_3N , and DBU, were stored over anhydrous KOH pellets.

3.4.2 Experimental details and characterization data

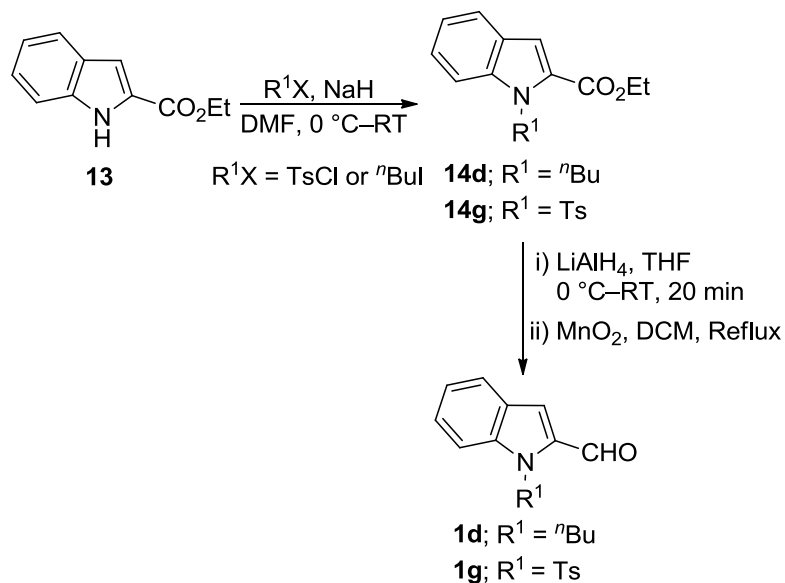
3.4.2.1 Synthesis of precursors or indole substrates 1a–h



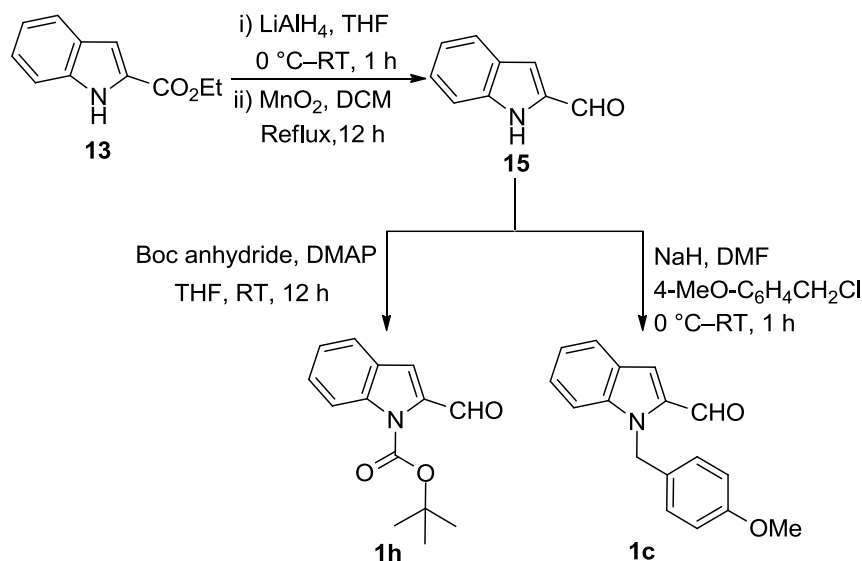
Scheme 3.4 Synthesis of *N*-substituted indole-2-carboxaldehyde derivatives **1a**, **1b**, **1e**, and **1f**



Scheme 3.5 Preparation of **12f** by Suzuki (sp^2C - sp^2C) reaction



Scheme 3.6 Synthesis of *N*-substituted indole-2-carboxaldehyde derivatives **1d** and **1g**



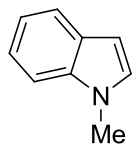
Scheme 3.7 Synthesis of *N*-substituted indole-2-carboxaldehydes **1c** and **1h**

A. Synthesis of *N*-substituted indole-2-carboxaldehyde derivatives 1a, 1b, 1e, and 1f

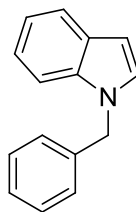
(a) General procedure for the synthesis of *N*-substituted indoles 12a–b, 12e and 12i

Crushed potassium hydroxide (5.0 equiv.) was dissolved in *N,N*-dimethyl formamide (5 mL) in a two-neck round-bottom flask (50 mL) by stirring for 5 min at room temperature. 5-Substituted indole, **11a**, **11e**, or **11i** (1.0 equiv.) was added to the reaction mixture in one portion and stirred for another 5 min under an inert atmosphere. Subsequently, the reaction mixture was cooled to $0\text{ }^\circ\text{C}$, and benzyl bromide or methyl iodide (2.0 equiv.) was added using a glass syringe dropwise over a period of 5 min. The reaction mixture was warmed to room temperature, monitored by TLC, and stirred for another 1 h. After the completion of the reaction, the reaction mixture was quenched with cold brine (10 mL) and extracted with EtOAc ($3 \times 10\text{ mL}$). The combined organic layers was dried over anhydrous Na_2SO_4 , filtered, and concentrated under reduced pressure. The

crude residue was purified over silica gel (230–400 mesh) column chromatography using hexane:EtOAc solvent mixture as eluent to afford **12a–b**, **12e**, and **12i**.

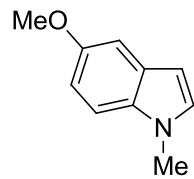
**12a**

1-Methyl-1H-indole (12a). According to the general procedure mentioned above, methyl iodide (1.06 mL, 17.08 mmol) was added to a mixture of KOH (2.40 g, 42.68 mmol) and indole (**11a**, 1.0 g, 8.54 mmol) in DMF (5 mL) drop-wise and reaction was stirred at room temperature for 1 h. After workup, the crude residue was purified over silica gel (230–400 mesh) column chromatography using hexane-EtOAc (99.0:1.0) as eluent. Yield 92% (1.03 g); Off white liquid; R_f 0.50 (9:1 hexane-EtOAc); ^1H NMR (400 MHz, CDCl_3) δ 7.62 (d, J = 7.8 Hz, 1H), 7.30 (d, J = 7.5 Hz, 1H), 7.21 (dd, J = 7.8, 7.3 Hz, 1H), 7.10 (dd, J = 7.5, 7.3 Hz, 1H), 7.01 (d, J = 3.0 Hz, 1H), 6.47 (d, J = 3.0 Hz, 1H), 3.74 (s, 1H); ^{13}C NMR (100 MHz, CDCl_3) δ 136.8, 128.8, 128.5, 121.5, 120.9, 119.3, 109.2, 100.9, 32.8.

**12b**

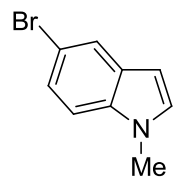
1-Benzyl-1H-indole (12b). According to the general procedure mentioned above, benzyl bromide (68 μL , 5.12 mmol) was added to a mixture of KOH (0.957 g, 17.07 mmol) and indole **11a** (0.500 g, 4.27 mmol) in DMF (3 mL) drop-wise and reaction was stirred at room temperature for 2 h. After workup, the crude residue was purified over silica gel (230–400 mesh) column chromatography using hexane as eluent. Yield 93% (0.824 g); Pale green liquid; R_f 0.60 (9:1 hexane-EtOAc); ^1H NMR (400 MHz, CDCl_3) δ 7.65 (d, J = 7.8 Hz, 1H), 7.32–7.20 (m, 4H),

7.16 (ddd, $J = 7.6, 7.0, 0.7$ Hz), 7.13–7.06 (m, 4H), 6.55 (d, $J = 3.0$ Hz, 1H), 5.31 (s, 2H); ^{13}C NMR (100 MHz, CDCl_3) δ 137.6, 136.3, 128.8, 128.7, 128.3, 127.6, 126.8, 121.7, 121.0, 119.6, 109.7, 101.7, 50.1.



12e 5-Methoxy-1-methyl-1H-indole (**12e**). According to the

general procedure mentioned above, methyl iodide (169 μL , 2.72 mmol) was added to a mixture of KOH (0.380 g, 6.79 mmol) and 5-methoxy indole **11e** (0.20 g, 1.36 mmol) in DMF (3 mL) drop-wise and reaction was stirred at room temperature for 30 min. After workup, the crude residue was purified over silica gel (230–400 mesh) column chromatography using hexane-EtOAc (98:2) as eluent. Yield 99% (0.216 g); White solid; R_f 0.40 (9:1 hexane-EtOAc); ^1H NMR (400 MHz, CDCl_3) δ 7.22 (d, $J = 8.8$ Hz, 1H), 7.13–7.09 (m, 1H), 7.02 (d, $J = 2.5$ Hz, 1H), 6.94–6.87 (m, 1H), 6.42 (d, $J = 2.5$ Hz, 1H), 3.86 (s, 3H), 3.76 (s, 3H); ^{13}C NMR (100 MHz, CDCl_3) δ 154.0, 132.2, 129.3, 128.8, 111.9, 109.9, 102.6, 100.4, 55.9, 33.0.

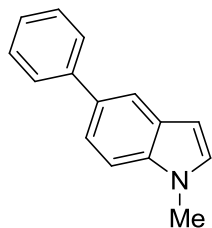


12i 5-Bromo-1-methyl-1H-indole (**12i**). According to the general

procedure mentioned above, methyl iodide (317 μL , 5.10 mmol) was added to a mixture of KOH (0.71 g, 12.75 mmol) and 5-bromo indole **11i** (0.50 g, 2.55 mmol) in DMF (3 mL) drop-wise and reaction was stirred at room temperature for 1 h. After workup, the crude residue was purified over silica gel (230–400 mesh) column chromatography using hexane-EtOAc (98:2) as eluent. Yield 99% (0.525 g); Pale yellow liquid; R_f 0.45 (9:1 hexane-EtOAc); ^1H NMR (400 MHz, CDCl_3) δ 7.75 (d, $J = 1.5$ Hz,

1H), 7.30 (dd, $J = 8.8, 1.5$ Hz, 1H), 7.18 (d, $J = 8.8$ Hz, 1H), 7.04 (d, $J = 3.0$ Hz, 1H), 6.43 (d, $J = 3.0$ Hz, 1H), 3.76 (s, 3H); ^{13}C NMR (100 MHz, CDCl_3) δ 135.4, 130.2, 130.0, 124.3, 123.3, 112.7, 110.7, 100.6, 33.0.

(b) Preparation of 12f by Suzuki (sp^2C - sp^2C) reaction

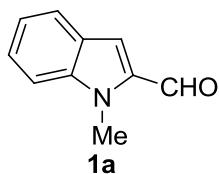


12f *1-Methyl-5-phenyl-1H-indole* (**12f**). 5-Bromo-1-methyl-

1H-indole **12i**, (0.200 g, 0.95 mmol) and phenyl boronic acid (0.14 g, 1.14 mmol) were dissolved in a mixture (4:1) of dimethoxyethane (DME) and milli-Q water in a two-neck round-bottom flask (100 mL) and the solution was degassed (by bubbling N_2 gas for 30 min). K_3PO_4 (403 mg, 1.90 mmol) and $\text{Pd}(\text{PPh}_3)_4$ (23 mg, 0.02 mmol) were added to the reaction mixture at room temperature in one portion. The reaction mixture was heated at 65 °C using oil bath under an inert atmosphere, monitored by TLC for 16 h. After the completion of the reaction, the reaction mixture was quenched with brine (5 mL) and extracted with EtOAc (3×10 mL). The combined organic layers were dried over anhydrous Na_2SO_4 , filtered, and concentrated under reduced pressure. The crude residue was purified over silica gel (230–400 mesh) column chromatography using hexane:EtOAc (96:4) as eluent to afford **12f**. Yield 81% (0.160 g); White solid; R_f 0.55 (9:1 hexane-EtOAc); ^1H NMR (400 MHz, CDCl_3) δ 7.87 (d, $J = 1.2$ Hz, 1H), 7.68 (d, $J = 7.8$ Hz, 2H), 7.51 (dd, $J = 8.3, 1.2$ Hz, 1H), 7.46 (dd, $J = 7.8, 7.6$ Hz, 2H), 7.40 (d, $J = 8.3$ Hz, 1H), 7.33 (dd, $J = 7.3, 7.3$ Hz, 1H), 7.09 (d, $J = 2.8$ Hz, 1H), 6.56 (d, $J = 2.8$ Hz, 1H), 3.82 (s, 3H); ^{13}C NMR (100 MHz, CDCl_3) δ 142.7, 136.3, 132.9, 129.5, 129.0, 128.7, 127.5, 126.3, 121.5, 119.5, 109.5, 101.4, 33.0.

(c) General procedure for the synthesis of *N*-substituted indole-2-carboxaldehydes **1a–b, **1e**, and **1f****

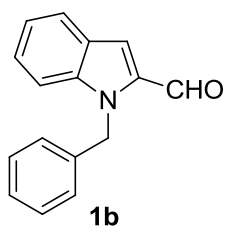
N-Substituted indole, **12a–b**, **12e** or **12f** (1.0 equiv.) was dissolved in anhydrous diethyl ether (10 mL) in a two neck round bottom flask (50 mL) fitted with a double-walled condenser, under an inert atmosphere at room temperature. *n*-BuLi (1.2 equiv.) was added to the reaction mixture using a glass syringe in a dropwise manner at the same temperature over a period of 10 min. The reaction mixture was further heated to reflux for 3 h on a preheated oil bath and allowed to cool to ambient temperature. Anhydrous DMF (1.5 equiv.) was added to the *N*-substituted 2-lithiated indole anion and heated to reflux further for another 5 h. Saturated ammonium chloride (20 mL) was added to the reaction mixture at room temperature, and the aqueous layer was extracted with EtOAc (3 × 10 mL). The combined organic layers was dried over anhydrous Na₂SO₄, filtered, and concentrated under reduced pressure. The crude residue was purified using hexane: EtOAc as eluent over silica gel column chromatography to afford **1a–b**, **1e**, **1f**.



1-Methyl-1H-indole-2-carbaldehyde (1a). According to the general procedure mentioned above, 1-methyl-1*H*-indole (**12a**, 1.0 g, 7.62 mmol) was dissolved in dry diethyl ether (10 mL) under an inert atmosphere. *n*-BuLi (5.71 mL, 9.17 mmol, 1.6 M in hexane) was added dropwise at room temperature, and the reaction mixture was heated to reflux for 3 h.

The reaction mixture was allowed to cool to room temperature, and DMF (0.88 mL, 11.43 mmol) was added. The reaction mixture was further heated to reflux for 5 h and allowed to cool to room temperature. Saturated ammonium chloride (20 mL) was added to the reaction mixture, and the

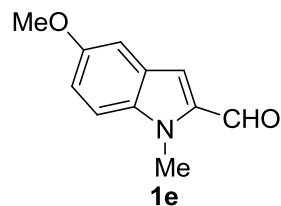
aqueous layer was extracted with EtOAc (3×10 mL). The combined organic layers was dried over anhydrous Na_2SO_4 , filtered, concentrated, and purified over silica gel (230–400 mesh) column chromatography using hexane-EtOAc (98:2) as eluent. Yield 79% (0.946 g); Pale yellow liquid; R_f 0.50 (8:2 hexane-EtOAc); ^1H NMR (400 MHz, CDCl_3) δ 9.88 (s, 1H), 7.73 (d, $J = 8.0$ Hz, 1H), 7.50–7.34 (m, 2H), 7.24 (s, 1H), 7.18 (dd, $J = 7.8, 7.6$ Hz, 1H), 4.09 (s, 3H); ^{13}C NMR (100 MHz, CDCl_3) δ 182.9, 140.9, 135.7, 126.9, 126.3, 123.4, 120.9, 117.5, 110.4, 31.5.



1-Benzyl-1H-indole-2-carbaldehyde (1b). According to the general procedure, 1-benzyl-1H-indole (**2b**, 0.75 g, 3.62 mmol) was dissolved in dry diethyl ether (7.5 mL) under an inert atmosphere. *n*-BuLi (2.70 mL, 4.34 mmol, 1.6 M in hexane) was added dropwise at room temperature, and the reaction mixture was heated to reflux for 3 h.

The reaction mixture was allowed to cool to room temperature, followed by the addition of DMF (0.40 mL, 5.43 mmol). The reaction mixture was further heated to reflux for 5 h and allowed to cool to room temperature. Saturated ammonium chloride (20 mL) was added, and the aqueous layer was extracted with EtOAc (3×10 mL). The combined organic layers was dried over anhydrous Na_2SO_4 , filtered, concentrated, and purified over silica gel (230–400 mesh) column chromatography using hexane-EtOAc (98:2) as eluent. Yield 83% (0.710 g); Yellow liquid; R_f 0.60 (8:2 hexane-EtOAc); ^1H NMR (400 MHz, CDCl_3) δ 9.90 (s, 1H), 7.76 (d, $J = 8.0$ Hz, 1H), 7.42–7.34 (m, 2H), 7.33 (s, 1H), 7.28–7.14 (m, 4H), 7.12–7.05 (m, 2H), 5.83 (s, 2H); ^{13}C NMR (100 MHz, CDCl_3) δ 182.7, 140.7, 137.8*, 135.4, 128.6, 127.4, 127.2, 126.6, 123.5, 121.2, 118.3, 111.1, 48.0.

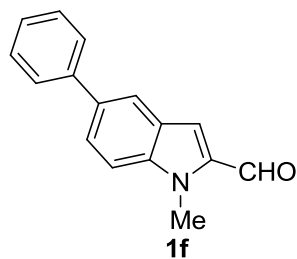
*Higher intensity carbon



5-Methoxy-1-methyl-1H-indole-2-carbaldehyde (1e).

According to the general procedure, 5-methoxy-1-methyl-1*H*-indole, **12e**, (0.200 g, 1.24 mmol) was dissolved in dry diethyl ether (5 mL) under an inert atmosphere. *n*-BuLi (0.93 mL, 1.49 mmol, 1.6 M in hexane) was added dropwise at room temperature, and the reaction mixture was heated to reflux for 3 h.

The reaction mixture was allowed to cool to room temperature, and DMF (0.14 mL, 1.86 mmol) was added to the reaction mixture. The reaction mixture was further heated to reflux for 5 h and cooled to ambient temperature before the addition of saturated ammonium chloride (10 mL) solution. The aqueous layer was extracted with EtOAc (3 × 10 mL), and the combined organic layers was dried over anhydrous Na₂SO₄. The organic layer was filtered, concentrated, and purified over silica gel (230–400 mesh) column chromatography using hexane-EtOAc (90:10) as eluent. Yield 58% (0.137 g); Off white solid; *R*_f 0.35 (8:2 hexane-EtOAc); ¹H NMR (400 MHz, CDCl₃) δ 9.83 (s, 1H), 7.28 (d, *J* = 8.8 Hz, 1H), 7.13 (s, 1H), 7.12–7.06 (m, 2H), 4.05 (s, 3H), 3.85 (s, 3H); ¹³C NMR (100 MHz, CDCl₃) δ 182.7, 154.8, 136.6, 135.9, 126.5, 119.0, 116.5, 111.4, 102.7, 55.7, 31.7.



1-Methyl-5-phenyl-1H-indole-2-carbaldehyde (1f).

According to the general procedure, 1-methyl-5-phenyl-1*H*-indole (**12f**,

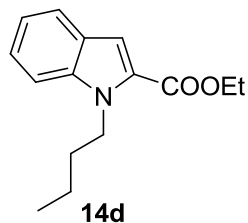
0.13 g, 0.63 mmol) was dissolved in dry diethyl ether (5 mL) under an inert atmosphere. *n*-BuLi (0.47 mL, 0.75 mmol, 1.6 M in hexane) was added dropwise at room temperature, and the reaction mixture was heated to reflux for 3 h. The reaction mixture was allowed to cool to room temperature, and DMF (0.07 mL, 0.95 mmol) was added to the reaction mixture and further heated to reflux for 5 h. Saturated ammonium chloride solution (10 mL) was added to the mixture after cooling to room temperature. The aqueous layer was extracted with EtOAc (3 × 10 mL), and the combined organic layers was dried over anhydrous Na₂SO₄. The organic layer was filtered, concentrated, and purified over silica gel (230–400 mesh) column chromatography using hexane-EtOAc (96:4) as eluent. Yield 68% (0.100 g); White solid; *R*_f 0.50 (9:1 hexane-EtOAc); ¹H NMR (400 MHz, CDCl₃) δ 9.90 (s, 1H), 7.95–7.88 (m, 1H), 7.69 (dd, *J* = 8.8, 1.5 Hz, 1H), 7.66–7.59 (m, 2H), 7.50–7.41 (m, 3H), 7.34 (dd, *J* = 7.5, 7.3 Hz, 1H), 7.29 (s, 1H), 4.12 (s, 3H); ¹³C NMR (100 MHz, CDCl₃) δ 182.9, 141.5, 140.4, 136.3, 134.5, 128.9, 127.3, 127.0, 126.9, 126.8, 121.5, 117.7, 110.7, 31.8.

B. Synthesis of *N*-substituted indole-2-carboxaldehyde derivatives **1d and **1g****

(a) General procedure for the synthesis of *N*-substituted ethyl-1*H*-indole-2-carboxylate **14d and **14g****

In a round bottom flask (50 mL), sodium hydride (NaH, 2.0 equiv.) was added to dry DMF (2 mL), and the suspension was cooled to 0 °C under an inert atmosphere. Ethyl indole-2-carboxylate, **13** (1.0 equiv.) was added to the suspension in one portion, and the reaction mixture was stirred for 5 min at the same temperature. Alkyl or tosyl halide (1.5 equiv.) was added to the reaction mixture dropwise via a glass syringe, and the reaction mixture was allowed to warm to room temperature and stirred further until **13** was consumed completely.

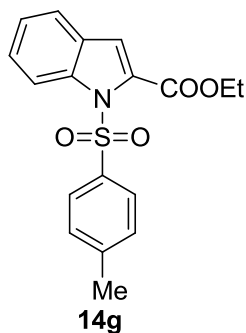
EtOAc (5 mL) was added to the reaction mixture, followed by cold brine (5 mL). The aqueous layer was extracted with EtOAc (3×5 mL), and the combined organic layers was dried over anhydrous Na_2SO_4 , filtered, and concentrated under reduced pressure. The crude residue was purified using hexane: EtOAc as eluent over silica gel (230–400 mesh) column chromatography.



Ethyl 1-butyl-1H-indole-2-carboxylate (**14d**).

According to the general procedure, NaH (46 mg, 1.06 mmol, 55–60% in mineral oil) was added to dry DMF (2 mL) in a 50 mL round bottom flask, and the suspension was cooled to 0 °C under an inert atmosphere. Ethyl indole-2-carboxylate (100 mg, 0.53 mmol) was added to the suspension in one portion, and the reaction mixture was stirred for 5 min at the same temperature. n-Butyl iodide (91 μL , 0.80 mmol) was added dropwise to the reaction mixture and stirred at room temperature for a further 5 min.

After the completion of the reaction as confirmed by TLC, EtOAc (5 mL) was added to the reaction mixture followed by cold brine solution (5 mL). The aqueous layer was further extracted with EtOAc (3×5 mL) and the combined organic layers was dried over anhydrous Na_2SO_4 . The organic layer was filtered, concentrated and purified over silica gel (230–400 mesh) column chromatography using hexane-EtOAc (98:2) as eluent. Yield 98% (0.125 g); Colorless liquid; R_f 0.45 (9:1 hexane-EtOAc); ^1H NMR (400 MHz, CDCl_3) δ 7.67 (d, $J = 8.0$ Hz, 1H), 7.40 (d, $J = 7.8$ Hz, 1H), 7.36–7.28 (m, 2H), 7.14 (dd, $J = 7.8, 7.0$ Hz, 1H), 4.57 (t, $J = 7.5$ Hz, 2H), 4.38 (q, $J = 7.0$ Hz, 2H), 1.86–1.71 (m, 2H), 1.45–1.31 (m, 5H), 0.95 (t, $J = 7.3$ Hz, 3H); ^{13}C NMR (100 MHz, CDCl_3) δ 162.1, 139.1, 127.5, 126.0, 124.8, 122.6, 120.4, 110.5, 110.4, 60.5, 44.6, 32.8, 20.2, 14.4, 13.9.



Ethyl 1-tosyl-1H-indole-2-carboxylate (**14g**).

According to the general procedure, NaH (46 mg, 1.06 mmol, 55–60% in mineral oil) was added to dry DMF (2 mL) in a 50 mL round bottom flask, and the suspension was cooled to 0 °C under an inert atmosphere. Ethyl indole-2-carboxylate (100 mg, 0.53 mmol) was added in one portion, and the reaction mixture was stirred for 5 min at the same temperature. Tosyl chloride (0.152 g, 0.80 mmol) was added in one portion to the reaction mixture and stirred further at room temperature overnight.

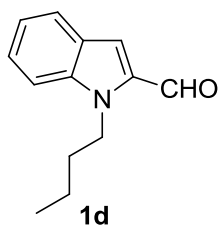
After the completion of the reaction, as confirmed by TLC, EtOAc (5 mL) was added to the reaction mixture followed by cold brine (5 mL). The aqueous layer was further extracted with EtOAc (3 × 5 mL) and the combined organic layers was dried over anhydrous Na₂SO₄. The organic layer was filtered, concentrated and purified over silica gel (230–400 mesh) column chromatography using hexane-EtOAc (90:10) as eluent. Yield 98% (0.180 g); Colorless liquid; *R_f* 0.50 (8:2 hexane-EtOAc); ¹H NMR (400 MHz, CDCl₃) δ 8.10 (d, *J* = 8.5 Hz, 1H), 7.91 (d, *J* = 8.0 Hz, 2H), 7.55 (d, *J* = 7.8 Hz, 1H), 7.42 (dd, *J* = 8.5, 7.8 Hz, 1H), 7.30–7.20 (m, 3H), 7.14 (s, 1H), 4.41 (q, *J* = 7.0 Hz, 2H), 2.36 (s, 3H), 1.39 (t, *J* = 7.0 Hz, 3H); ¹³C NMR (100 MHz, CDCl₃) δ 161.4, 144.9, 138.2, 135.7, 131.9, 129.6, 128.2, 127.4, 126.9, 124.1, 122.4, 116.5, 115.4, 62.0, 21.6, 14.1.

(b) General procedure for synthesis of *N*-substituted indole-2-carboxaldehyde 1d and 1g

N-substituted ethyl indole-2-carboxylate **14d** or **14g** (1.0 equiv.) was dissolved in dry THF and cooled to 0 °C under an inert atmosphere. Lithium aluminium hydride (LiAlH₄, 3.0 equiv.) was added in one portion to the mixture with constant stirring. The reaction mixture was allowed to warm at room temperature and continued to stir for a further 20 min.

After the completion of the reaction, a saturated ammonium chloride solution (5 mL) was added cautiously to quench the reaction. The aqueous layer was extracted with EtOAc (3 × 10 mL), and the combined organic layers were dried over anhydrous Na₂SO₄. The organic layer was filtered, concentrated, and used as such in the next step without further purification.

The crude residue was dissolved in dichloromethane (10 mL), MnO₂ (15.0 equiv.) was added in one portion, and the reaction mixture was heated to reflux for 12–48 h. After the completion of the reaction, CH₂Cl₂ was evaporated under reduced pressure, and the crude residue was purified through silica gel (230–400 mesh) column chromatography using the hexane-EtOAc mixture as eluent.

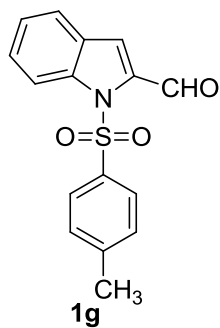


1-Butyl-1H-indole-2-carbaldehyde (**1d**). According to the general procedure, **14d** (125 mg, 0.51 mmol) was dissolved in dry THF (3 mL) in a round bottom flask (50 mL) under an inert atmosphere. The solution was cooled to 0 °C, and LiAlH₄ (59 mg, 1.53 mmol) was added in one portion to the reaction mixture. The reaction mixture was allowed to warm to room temperature and stirred for another 20 min.

After the completion of the reaction, a saturated ammonium chloride solution (5 mL) was added cautiously to quench the reaction. The

aqueous layer was extracted with EtOAc (3×10 mL), and the combined organic layers was dried over anhydrous Na_2SO_4 . The organic layer was filtered, concentrated, and used as such in the next step without further purification.

The crude residue was dissolved in dichloromethane (10 mL), MnO_2 (652 mg, 7.50 mmol) was added in one portion and the reaction mixture was heated to reflux for 24 h. After the completion of reaction, CH_2Cl_2 was evaporated under reduced pressure and the crude residue was purified through silica gel (230–400 mesh) column chromatography using hexane-EtOAc (90:10) as eluent. Yield 98% (100 mg); White gummy solid; R_f 0.55 (4:1 hexane-EtOAc); ^1H NMR (400 MHz, CDCl_3) δ 9.80 (s, 1H), 7.66 (d, $J = 8.0$ Hz, 1H), 7.38–7.29 (m, 2H), 7.18 (s, 1H), 7.13–7.05 (m, 1H), 4.49 (t, $J = 7.3$ Hz, 2H), 1.75–1.63 (m, 2H), 1.34–1.22 (m, 2H), 0.86 (t, $J = 7.3$ Hz, 3H); ^{13}C NMR (100 MHz, CDCl_3) δ 181.5, 139.3, 134.4, 125.7, 125.4, 122.4, 119.8, 116.8, 109.7, 43.5, 31.6, 19.1, 12.8.



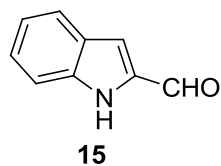
1-Tosyl-1H-indole-2-carboxylate (1g). According to the general procedure, **14g** (180 mg, 0.52 mmol) was dissolved in dry THF (3 mL) in a round bottom flask (50 mL) under an inert atmosphere. The solution was cooled to 0 °C, and LiAlH_4 (60 mg, 1.56 mmol) was added in one portion, and the reaction mixture was allowed to warm to room temperature with constant stirring for another 20 min.

After the completion of the reaction, a saturated ammonium chloride solution (5 mL) was added cautiously to quench the reaction. The aqueous layer was extracted with EtOAc (3×10 mL), and the combined

organic layers was dried over anhydrous Na_2SO_4 . The organic layer was filtered, concentrated, and used as such in the next step without further purification.

The crude residue was dissolved in dichloromethane (10 mL), MnO_2 (649 mg, 7.46 mmol) was added in one portion and the reaction mixture was heated to reflux for 48 h. After the completion of the reaction, CH_2Cl_2 was evaporated under reduced pressure and the crude residue was purified through silica gel (230–400 mesh) column chromatography using hexane-EtOAc (90:10) as eluent. Yield 89% (132 mg); White gummy solid; R_f 0.40 (4:1 hexane-EtOAc); ^1H NMR (400 MHz, CDCl_3) δ 10.5 (s, 1H), 8.22 (d, $J = 7.5$ Hz, 1H), 7.65 (d, $J = 8.3$ Hz, 2H), 7.61 (d, $J = 7.3$ Hz, 1H), 7.51 (dd, $J = 7.5, 7.5$ Hz, 1H), 7.46 (s, 1H), 7.30 (dd, $J = 7.5, 7.3$ Hz, 1H), 7.18 (d, $J = 8.3$ Hz, 2H), 2.32 (s, 3H); ^{13}C NMR (100 MHz, CDCl_3) δ 183.4, 145.6, 138.5, 137.8, 134.7, 130.0, 128.8, 128.2, 126.7, 124.8, 123.6, 118.9, 115.4, 21.6.

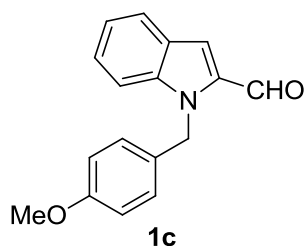
C. Synthesis of *N*-substituted indole-2-carboxaldehydes **1c** and **1h**



1H-indole-2-carbaldehyde (**15**). Ethyl indole-2-carboxylate **13**, (200 mg, 1.06 mmol) was dissolved in dry THF under an inert atmosphere, and the solution was cooled to 0 °C before the addition of LiAlH_4 (120 mg, 3.17 mmol) in a single portion. The reaction mixture was allowed to warm to room temperature and stirred for another 1 h.

After the completion of the reaction, as confirmed by TLC, the reaction mixture was quenched using saturated ammonium chloride (10 mL), and the aqueous layer was extracted with EtOAc (3×10 mL). The combined organic layers was dried over anhydrous Na_2SO_4 , filtered, and concentrated under reduced pressure.

The crude residue was dissolved in CH_2Cl_2 (10 mL), MnO_2 (1.382 gms, 15.90 mmol) was added to the solution at room temperature in one portion and the reaction mixture was heated to reflux for 12 h. After the completion of the reaction, the crude reaction mixture was filtered through celite and recrystallized using 10% CH_2Cl_2 in hexane. Yield 88% (105 mg); Yellow crystalline solid; R_f 0.60 (4:1 hexane-EtOAc); ^1H NMR (400 MHz, CDCl_3) δ 9.85 (s, 1H), 9.66 (s, 1H), 7.75 (d, J = 8.0 Hz, 1H), 7.48 (d, J = 7.5 Hz, 1H), 7.40 (dd, J = 8.0, 7.3 Hz, 1H), 7.29 (s, 1H), 7.18 (dd, J = 7.5, 7.3 Hz, 1H); ^{13}C NMR (100 MHz, CDCl_3) δ 182.4, 138.3, 136.0, 127.43, 127.35, 123.5, 121.3, 115.3, 112.7.

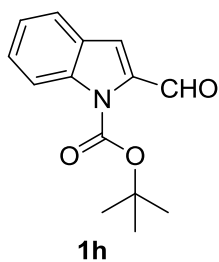


1-(4-Methoxybenzyl)-1H-indole-2-carbaldehyde

(**1c**). Under an inert atmosphere, indole-2-carbaldehyde **15** (135 mg, 0.93 mmol) was dissolved in dry DMF (3 mL) in a single neck round bottom flask (50 mL). The mixture was cooled to 0 °C, and sodium hydride (56 mg, 1.40 mmol, 60% in mineral oil) was added in a single portion with stirring. The reaction mixture was allowed to warm to room temperature and stirred for further 5 minutes. 4-Methoxy benzyl chloride (250 μL , 1.86 mmol) was added dropwise to the reaction mixture at room temperature, and the reaction was stirred for another 1 h.

After the completion of the reaction, cold brine solution (5 mL) was added cautiously to quench the reaction. The aqueous layer was extracted with EtOAc (3×10 mL) and the combined organic layers were dried over anhydrous Na_2SO_4 . The organic layer was filtered, concentrated and purified through silica gel (230–400 mesh) column chromatography using hexane-EtOAc (95:5) as eluent. Yield 81% (200 mg); White solid; R_f 0.45 (9:1 hexane-EtOAc); ^1H NMR (400 MHz, CDCl_3) δ 9.90 (s, 1H),

7.75 (d, $J = 8.2$ Hz, 1H), 7.46–7.34 (m, 2H), 7.31 (s, 1H), 7.18 (dd, $J = 7.8, 6.8$ Hz, 1H), 7.08 (d, $J = 8.5$ Hz, 2H), 6.78 (d, $J = 8.5$ Hz, 2H), 5.76 (s, 2H), 3.73 (s, 3H); ^{13}C NMR (100 MHz, CDCl_3) δ 182.7, 158.9, 140.6, 135.3, 129.9, 128.1, 127.2, 126.6, 123.5, 121.2, 118.4, 114.0, 111.1, 55.2, 47.4.



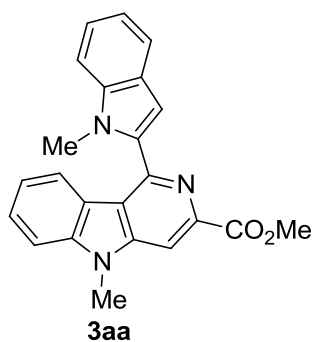
Tert-butyl 2-formyl-1H-indole-1-carboxylate (1h). A

stirred solution of indole-2-carbaldehyde **15**, (75 mg, 0.52 mmol), trimethylamine (86 μL , 0.62 mmol), and dimethyl aminopyridine (6 mg, 0.05 mmol) in dry THF (3 mL) was cooled to 0 $^{\circ}\text{C}$, and Boc anhydride (145 μL , 0.62 mmol) was added dropwise to the mixture using a glass syringe under an inert atmosphere. The reaction mixture was allowed to warm to room temperature and stirred overnight.

After the completion of the reaction, the reaction mixture was concentrated under reduced pressure and the crude product was purified through silica gel (230–400 mesh) column chromatography using hexane-EtOAc (95:5.0) as eluent. Yield 94% (120 mg); White gummy solid; R_f 0.50 (9:1 hexane-EtOAc); ^1H NMR (400 MHz, CDCl_3) δ 10.43 (s, 1H), 8.16 (d, $J = 7.8$ Hz, 1H), 7.67 (d, $J = 7.5$ Hz, 1H), 7.48 (dd, $J = 7.8, 7.8$ Hz, 1H), 7.43 (s, 1H), 7.29 (dd, $J = 7.8, 7.5$ Hz, 1H), 1.71 (s, 9H); ^{13}C NMR (100 MHz, CDCl_3) δ 184.2, 149.9, 137.94, 137.9, 128.3, 127.6, 123.9, 123.2, 116.5, 116.1, 85.6, 28.2.

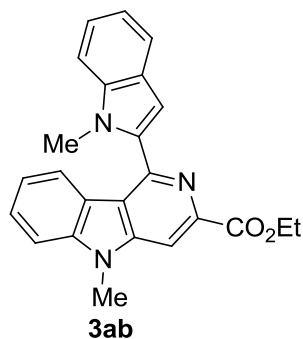
3.4.2.2 General procedure for the synthesis of 1-indolyl-3,5,8-substituted γ -carbolines **3aa–ac**, **3ba–ea** and 1-indolyl-1,2-dihydro-3,5-substituted γ -carbolines **3ga** derivatives

A mixture of *N*-substituted indole-2-aldehyde (**1a–h**, 2.0 mmol), glycine alkyl ester hydrochloride (**2a–c**, 1.0 mmol), and DIPEA (3.5 mmol) was heated in a sealed tube for 3–8 h at 120 °C. After the completion of the reaction, as evident by TLC, the reaction mixture was diluted with dichloromethane (CH₂Cl₂, 10 mL) and washed with cold brine (10 mL). The aqueous layer was again extracted with CH₂Cl₂ (3 × 10 mL). Organic layers were pooled and dried over anhydrous Na₂SO₄, filtered, concentrated under reduced pressure, and purified over neutral alumina gel (175 mesh) column chromatography, using a mixture of ethyl acetate and hexane as eluent to afford products **3aa–ac**, **3ba–ea**, and **3ga**.

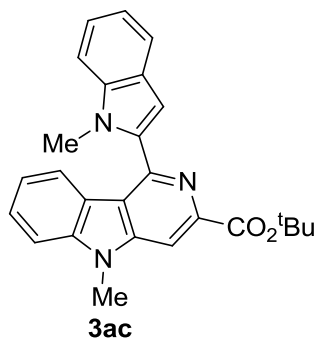


Methyl 5-methyl-1-(1-methyl-1H-indol-2-yl)-5H-pyrido[4,3-b]indole-3-carboxylate (**3aa**). According to the general procedure mentioned above, **1a** (0.100 g, 0.62 mmol), **2a** (39 mg, 0.31 mmol) and DIPEA (190 μL, 1.09 mmol) were heated in a sealed tube at 120 °C for 6 h. After workup, the crude reaction mixture was purified through alumina (neutral, 175 mesh) column chromatography using hexane-EtOAc (80:20) as eluent; Yield 70% (80 mg); Yellow solid; m.p. = 210–212 °C; *R_f* 0.35 (2:1 hexane-EtOAc); IR (KBr) 3055 (=C–H), 2956–2854 (C–H), 1734 (C=O), 1687–1534 (C=C), 1407–1376 (C–H bend), 782 (=C–H bend) cm^{−1}; ¹H NMR (400 MHz, CDCl₃) δ 8.31 (s, 1H), 7.82 (d, *J* = 8.0 Hz, 1H), 7.74 (d, *J* = 8.0 Hz, 1H), 7.56 (dd, *J* = 8.0, 7.3 Hz, 1H), 7.51 (d, *J* = 8.3 Hz, 1H), 7.45 (d, *J* = 8.3 Hz, 1H), 7.33 (dd, *J* = 8.0, 7.8 Hz, 1H), 7.19 (dd, *J* = 7.5, 7.5 Hz, 1H), 7.15 (dd, *J* = 7.6, 7.5 Hz, 1H), 6.99 (s, 1H), 4.05 (s, 3H), 4.00 (s, 3H), 3.75 (s, 3H); ¹³C NMR (100 MHz, CDCl₃) δ 166.9, 146.3, 145.8, 142.9, 142.2, 138.3, 137.6, 128.1, 127.9,

123.1, 122.4, 121.3, 121.2, 121.1, 120.8, 119.8, 109.8, 109.1, 105.7, 104.3, 53.0, 31.0, 29.6; HRMS (ESI) calcd for $[C_{23}H_{19}N_3O_2+H^+]$ 370.1550, found 370.1515.

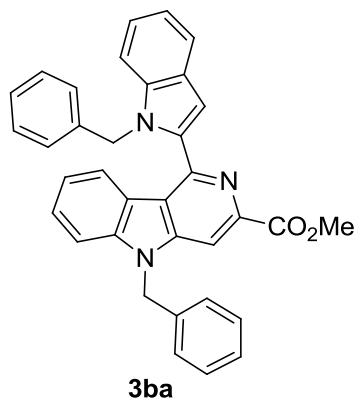


Ethyl 5-methyl-1-(1-methyl-1H-indol-2-yl)-5H-pyrido[4,3-b]indole-3-carboxylate (3ab). According to the general procedure mentioned above, **1a** (0.100 g, 0.62 mmol), **2b** (43 mg, 0.31 mmol) and DIPEA (190 μ L, 1.09 mmol) were heated in a sealed tube at 120 $^{\circ}$ C for 6 h. After workup, the crude reaction mixture was purified through alumina (neutral, 175 mesh) column chromatography using hexane-EtOAc (85:15) as eluent; Yield 66% (78 mg); Yellow solid; m.p. = 175–177 $^{\circ}$ C; R_f 0.40 (2:1 hexane-EtOAc); IR (KBr) 3058 (=C–H), 2988–2851 (C–H), 1735 (C=O), 1704–1536 (C=C), 1409–1375 (C–H bend), 780 (=C–H bend) cm^{-1} ; ^1H NMR (400 MHz, CDCl_3) δ 8.27 (s, 1H), 7.89 (d, J = 8.0 Hz, 1H), 7.73 (d, J = 7.8 Hz, 1H), 7.56 (dd, J = 7.8, 7.3 Hz, 1H), 7.50 (d, J = 8.0 Hz, 1H), 7.46 (d, J = 8.0 Hz, 1H), 7.33 (dd, J = 7.8, 7.8 Hz, 1H), 7.19 (m, 2H), 7.01 (s, 1H), 4.53 (q, J = 7.0 Hz, 2H), 3.99 (s, 3H), 3.79 (s, 3H), 1.48 (t, J = 7.0 Hz, 3H); ^{13}C NMR (100 MHz, CDCl_3) δ 166.3, 146.3, 145.9, 143.2, 142.2, 138.3, 137.6, 128.0, 127.8, 123.1, 122.4, 121.2, 121.1, 120.9, 120.8, 119.8, 109.8, 109.1, 105.5, 104.4, 61.9, 31.1, 29.5, 14.5; HRMS (ESI) calcd for $[C_{24}H_{21}N_3O_2+H^+]$ 384.1707, found 384.1672.



Tert-butyl 5-methyl-1-(1-methyl-1H-indol-2-yl)-5H-pyrido[4,3-b]indole-3-carboxylate (3ac). According to the general procedure mentioned above, **1a** (0.100 g, 0.62 mmol), **2c** (52 mg, 0.31 mmol) and DIPEA (190 μ L, 1.09 mmol) were heated in a sealed tube at 120 $^{\circ}$ C for 8 h. After workup, the crude reaction mixture was purified through alumina (neutral, 175 mesh) column chromatography using hexane-EtOAc (90:10) as eluent; Yield 67% (85 mg); Yellow solid; m.p. = 200–202 $^{\circ}$ C; R_f 0.60 (2:1 hexane-EtOAc); IR (KBr) 3053 (=C–H), 2972–2852 (C–H), 1729 (C=O), 1686–1532 (C=C), 1412–1365 (C–H bend), 781 (=C–H bend) cm^{-1} ; ^1H NMR (400 MHz, CDCl_3) δ 8.14 (s, 1H), 8.07 (d, J = 8.0 Hz, 1H), 7.73 (d, J = 7.8 Hz, 1H), 7.55 (dd, J = 7.5, 7.5 Hz, 1H), 7.52–7.43 (m, 2H), 7.33 (dd, J = 8.0, 7.3 Hz, 1H), 7.23–7.11 (m, 2H), 7.06 (s, 1H), 3.97 (s, 3H), 3.88 (s, 3H), 1.69 (s, 9H); ^{13}C NMR (100 MHz, CDCl_3) δ 165.2, 146.2, 146.1, 144.3, 142.2, 138.4, 137.7, 127.8, 127.7, 123.1, 122.4, 121.2, 120.9*, 120.3, 119.7, 109.8, 109.0, 104.7, 104.6, 81.9, 31.2, 29.5, 28.3; HRMS (ESI) calcd for $[\text{C}_{26}\text{H}_{25}\text{N}_3\text{O}_2+\text{H}^+]$ 412.2020, found 412.2012.

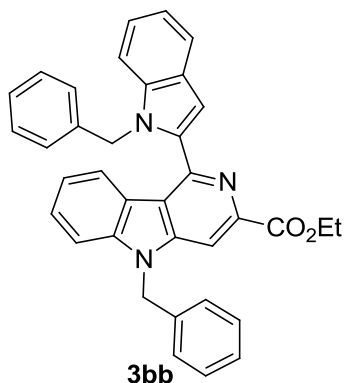
*Higher intensity carbon



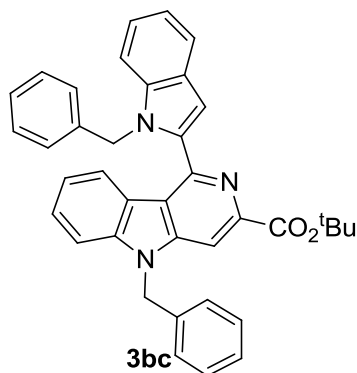
Methyl 5-benzyl-1-(1-benzyl-1H-indol-2-yl)-

5H-pyrido[4,3-b]indole-3-carboxylate (3ba). According to the general procedure mentioned above, **1b** (100 mg, 0.42 mmol), **2a** (26 mg, 0.21 mmol) and DIPEA (95 μ L, 0.74 mmol) were heated in a sealed tube at 120 $^{\circ}$ C for 6 h. After workup, the crude reaction mixture was purified through alumina (neutral, 175 mesh) column chromatography using hexane-EtOAc (85:15) as eluent; Yield 58% (63 mg); Yellow solid; m.p. = 168–170 $^{\circ}$ C; R_f 0.60 (2:1 hexane-EtOAc); IR (ATR) 3062 (=C–H), 2920–2850 (C–H), 1710 (C=O), 1667–1528 (C=C), 1467–1315 (C–H bend), 787–694 (=C–H bend) cm^{-1} ; ^1H NMR (400 MHz, CDCl_3) δ 8.20 (s, 1H), 8.13 (d, J = 8.0 Hz, 1H), 7.75 (d, J = 7.5 Hz, 1H), 7.48 (dd, J = 7.5, 7.3 Hz, 1H), 7.41 (m, 2H), 7.35–7.23 (m, 4H), 7.20 (d, J = 7.5 Hz, 1H), 7.16 (d, J = 8.0 Hz, 1H), 7.14–7.08 (m, 3H), 6.99–6.89 (m, 5H), 5.67 (s, 2H), 5.60 (s, 2H), 3.98 (s, 3H); ^{13}C NMR (100 MHz, CDCl_3) δ 166.8, 146.5, 145.8, 142.9, 141.7, 138.3, 138.1, 136.9, 135.6, 129.0, 128.1*, 128.0, 127.9, 126.7, 126.6, 126.3, 123.3, 122.7, 121.3, 121.13, 121.06, 121.0, 120.0, 110.6, 109.6, 105.7, 105.5, 52.9, 47.7, 46.8; HRMS (ESI) calcd for $[\text{C}_{35}\text{H}_{27}\text{N}_3\text{O}_2+\text{H}^+]$ 522.2176, found 522.2160.

*Higher intensity carbon

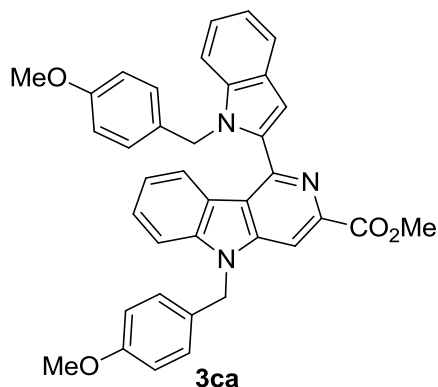


Ethyl 5-benzyl-1-(1-benzyl-1H-indol-2-yl)-5H-pyrido[4,3-b]indole-3-carboxylate (3bb). According to the general procedure mentioned above, **1b** (0.100 g, 0.62 mmol), **2b** (43 mg, 0.31 mmol) and DIPEA (190 μ L, 1.09 mmol) were heated in a sealed tube at 120 $^{\circ}$ C for 6 h. After workup, the crude reaction mixture was purified through alumina (neutral, 175 mesh) column chromatography using hexane-EtOAc (80:20) as eluent; Yield 51% (85 mg); Reddish yellow liquid; R_f 0.40 (2:1 hexane-EtOAc); IR (KBr) 3059 (=C-H), 2965–2860 (C-H), 1722 (C=O), 1609–1574 (C=C), 1423–1383 (C-H bend), 799 (=C-H bend) cm^{-1} ; ^1H NMR (400 MHz, CDCl_3) δ 8.21–8.14 (m, 2H), 7.75 (d, J = 7.5 Hz, 1H), 7.47 (dd, J = 7.8, 7.3 Hz, 1H), 7.40 (m, 2H), 7.35–7.23 (m, 4H), 7.20 (d, J = 7.3 Hz, 1H), 7.16 (d, J = 7.3 Hz, 1H), 7.14–7.08 (m, 3H), 7.02–6.89 (m, 5H), 5.72 (s, 2H), 5.59 (s, 2H), 4.45 (q, J = 7.1 Hz, 2H), 1.40 (t, J = 7.1 Hz, 3H); ^{13}C NMR (100 MHz, CDCl_3) δ 166.2, 146.5, 145.9, 143.2, 141.7, 138.4, 138.1, 136.9, 135.7, 129.0, 128.2, 128.1, 128.0, 127.8, 126.7, 126.6, 126.4, 123.3, 122.7, 121.2, 121.1, 121.0, 120.9, 120.0, 110.6, 109.6, 105.52, 105.48, 61.8, 47.7, 46.8, 14.4; HRMS (ESI) calcd for $[\text{C}_{36}\text{H}_{29}\text{N}_3\text{O}_2 + \text{H}^+]$ 536.2333, found 536.2349.



Tert-butyl 5-benzyl-1-(1-benzyl-1H-indol-2-

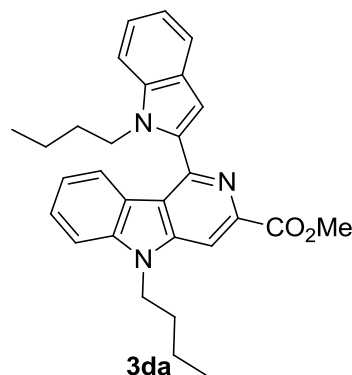
yl)-5H-pyrido[4,3-b]indole-3-carboxylate (3bc). According to the general procedure mentioned above, **1b** (0.100 g, 0.62 mmol), **2c** (52 mg, 0.31 mmol) and DIPEA (190 μ L, 1.09 mmol) were heated in a sealed tube at 120 $^{\circ}$ C for 8 h. After workup, the crude reaction mixture was purified through alumina (neutral, 175 mesh) column chromatography using hexane-EtOAc (85:15) as eluent; Yield 47% (82 mg); Yellow solid; m.p. = 148–150 $^{\circ}$ C; R_f 0.60 (2:1 hexane-EtOAc); IR (ATR) 3062 (=C–H), 2926–2848 (C–H), 1706 (C=O), 1665–1531 (C=C), 1495–1323 (C–H bend), 782–694 (=C–H bend) cm^{-1} ; ^1H NMR (400 MHz, CDCl_3) δ 8.28 (d, J = 8.0 Hz, 1H), 8.06 (s, 1H), 7.75 (d, J = 7.8 Hz, 1H), 7.47 (dd, J = 7.5, 7.3 Hz, 1H), 7.43–7.36 (m, 2H), 7.34–7.22 (m, 4H), 7.21–7.15 (m, 2H), 7.15–7.10 (m, 3H), 7.02–6.93 (m, 5H), 5.86 (s, 2H), 5.58 (s, 2H), 1.63 (s, 9H); ^{13}C NMR (100 MHz, CDCl_3) δ 165.2, 146.4, 146.1, 144.5, 141.7, 138.6, 138.1, 137.0, 135.8, 129.0, 128.2, 128.0, 127.84, 127.75, 126.7, 126.5, 126.4, 123.3, 122.7, 121.2, 121.1, 120.9, 120.4, 120.0, 110.6, 109.6, 105.7, 104.9, 81.8, 47.5, 46.8, 28.2; HRMS (ESI) calcd for $[\text{C}_{38}\text{H}_{33}\text{N}_3\text{O}_2+\text{H}^+]$ 564.2646, found 564.2644.



Methyl 5-(4-methoxybenzyl)-1-(1-(4-

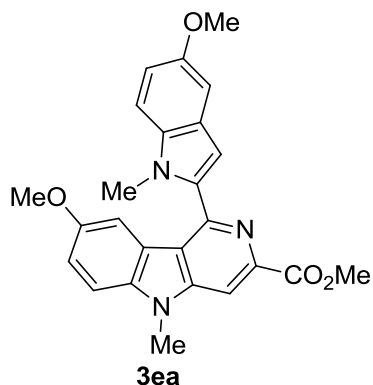
methoxybenzyl)-1H-indol-2-yl)-5H-pyrido[4,3-b]indole-3-carboxylate

(**3ca**). According to the general procedure mentioned above, **1c** (100 mg, 0.38 mmol), **2a** (24 mg, 0.19 mmol) and DIPEA (120 μ L, 0.66 mmol) were heated in a sealed tube at 120 $^{\circ}$ C for 3 h. After workup, the crude reaction mixture was purified through alumina (neutral, 175 mesh) column chromatography using hexane-EtOAc (85:15) as eluent; Yield 60% (66 mg); Yellow solid; m.p. = 106–108 $^{\circ}$ C; R_f 0.60 (2:1 hexane-EtOAc); IR(ATR) 3056 (=C–H), 2952–2835 (C–H), 1737 (C=O), 1664–1512 (C=C), 1457–1348 (C–H bend), 1106–989 (C–O), 819–695 (=C–H bend) cm^{-1} ; ^1H NMR (400 MHz, CDCl_3) δ 8.22 (s, 1H), 8.04 (d, J = 8.0 Hz, 1H), 7.73 (d, J = 7.8 Hz, 1H), 7.51–7.39 (m, 3H), 7.27 (d, J = 7.3 Hz, 1H), 7.18 (dd, J = 7.5, 7.0 Hz, 1H), 7.12 (dd, J = 7.3, 7.3 Hz, 1H), 7.07 (d, J = 8.5 Hz, 2H), 7.06 (s, 1H), 6.85 (d, J = 8.8 Hz, 2H), 6.83 (d, J = 8.8 Hz, 2H), 6.45 (d, J = 8.5 Hz, 2H), 5.55 (s, 2H), 5.54 (s, 2H), 3.99 (s, 3H), 3.76 (s, 3H), 3.52 (s, 3H); ^{13}C NMR (100 MHz, CDCl_3) δ 166.9, 159.4, 158.4, 146.6, 145.7, 142.9, 141.7, 138.0, 137.0, 130.4, 128.1, 127.95, 127.92, 127.75, 127.68, 123.3, 122.6, 121.2, 121.1, 121.04, 121.01, 119.9, 114.5, 113.5, 110.6, 109.6, 105.7, 105.3, 55.3, 55.1, 52.9, 47.2, 46.4; HRMS (ESI) calcd for $[\text{C}_{37}\text{H}_{31}\text{N}_3\text{O}_4 + \text{H}^+]$ 582.2387, found 582.2373.



Methyl 5-butyl-1-(1-butyl-1H-indol-2-yl)-5H-pyrido[4,3-b]indole-3-carboxylate (3da). According to the general procedure mentioned above, **1d** (0.100 g, 0.49 mmol), **2a** (31 mg, 0.25 mmol) and DIPEA (114 μ L, 0.88 mmol) were heated in a sealed tube at 120 $^{\circ}$ C for 3 h. After workup, the crude reaction mixture was purified through alumina (neutral, 175 mesh) column chromatography using hexane-EtOAc (85:15) as eluent; Yield 54% (61 mg); Yellow liquid; R_f 0.60 (2:1 hexane-EtOAc); IR (KBr) 3064 (=C-H), 2972–2854 (C-H), 1726 (C=O), 1621–1570 (C=C), 1462–1317 (C-H bend), 796 (=C-H bend) cm^{-1} ; ^1H NMR (400 MHz, CDCl_3) δ 8.27 (s, 1H), 8.00 (d, J = 8.0 Hz, 1H), 7.72 (d, J = 7.5 Hz, 1H), 7.59–7.45 (m, 3H), 7.30 (dd, J = 7.6, 7.5 Hz, 1H), 7.18 (dd, J = 8.2, 7.2 Hz, 1H), 7.13 (dd, J = 8.2, 7.3 Hz, 1H), 6.97 (s, 1H), 4.43 (t, J = 6.8 Hz, 2H), 4.34 (t, J = 7.0 Hz, 2H), 4.05 (s, 3H), 2.00–1.87 (m, 2H), 1.71–1.60 (m, 2H), 1.52–1.39 (m, 2H), 1.16–1.04 (m, 2H), 0.99 (t, J = 7.0 Hz, 3H), 0.62 (t, J = 7.3 Hz, 3H); ^{13}C NMR (100 MHz, CDCl_3) δ 167.1, 146.8, 145.4, 142.7, 141.6, 137.7, 136.9, 127.92, 127.87, 123.3, 122.2, 121.3, 120.9, 120.8*, 119.6, 110.2, 109.3, 105.6, 104.7, 52.9, 43.9, 43.4, 32.2, 31.1, 20.6, 20.0, 13.9, 13.5; HRMS (ESI) calcd for $[\text{C}_{29}\text{H}_{31}\text{N}_3\text{O}_2 + \text{H}^+]$ 454.2489, found 454.2559.

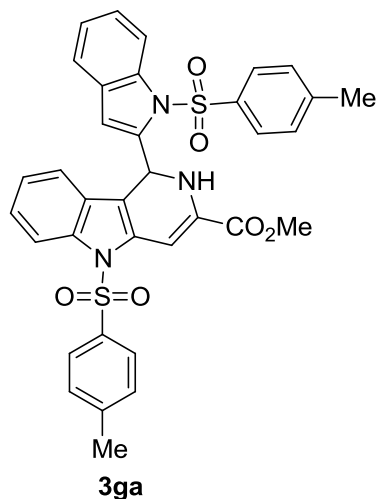
*Carbon merged



Methyl 8-methoxy-1-(5-methoxy-1-methyl-

1H-indol-2-yl)-5-methyl-5H-pyrido[4,3-b]indole-3-carboxylate (3ea).

According to the general procedure mentioned above, **1e** (70 mg, 0.37 mmol), **2a** (23 mg, 0.18 mmol) and DIPEA (110 μ L, 0.63 mmol) were heated in a sealed tube at 120 $^{\circ}$ C for 3 h. After workup, the crude reaction mixture was purified through alumina (neutral, 175 mesh) column chromatography using hexane-EtOAc (85:15) as eluent; Yield 72% (55 mg); Yellow solid; m.p. = 160–162 $^{\circ}$ C; R_f 0.60 (2:1 hexane-EtOAc); IR (ATR) 3070 (=C–H), 2957–2850 (C–H), 1701 (C=O), 1660–1528 (C=C), 1485–1329 (C–H bend), 1105–991 (C–O), 810–688 (=C–H bend) cm^{-1} ; ^1H NMR (400 MHz, CDCl_3) δ 8.26 (s, 1H), 7.40 (d, J = 9.8 Hz, 1H), 7.32 (d, J = 8.8 Hz, 1H), 7.21–7.16 (m, 2H), 7.15 (d, J = 2.0 Hz, 1H), 6.97 (dd, J = 9.0 Hz, 2.3 Hz, 1H), 6.91 (s, 1H), 4.05 (s, 3H), 3.96 (s, 3H), 3.89 (s, 3H), 3.71 (s, 3H), 3.55 (s, 3H); ^{13}C NMR (100 MHz, CDCl_3) δ 167.0, 154.8, 154.3, 146.3, 145.8, 142.6, 137.9, 137.2, 133.8, 128.1, 121.2, 120.8, 117.7, 112.8, 110.4, 109.9, 105.8, 105.0, 103.8, 102.5, 55.8, 55.7, 53.0, 31.1, 29.6; HRMS (ESI) calcd for $[\text{C}_{25}\text{H}_{23}\text{N}_3\text{O}_4+\text{H}^+]$ 430.1761, found 430.1764.



Methyl 5-tosyl-1-(1-tosyl-1H-indol-2-yl)-2,5-dihydro-1H-pyrido[4,3-b]indole-3-carboxylate (3ga). According to the general procedure mentioned above, **1g** (0.100 g, 0.33 mmol), **2a** (21 mg, 0.17 mmol) and DIPEA (101 μ L, 0.58 mmol) were heated in a sealed tube at 120 $^{\circ}$ C for 8 h. After workup, the crude reaction mixture was purified through alumina (neutral, 175 mesh) column chromatography using hexane-EtOAc (90:10) as eluent; Yield 63% (70 mg); Yellow solid; m.p. = 205–207 $^{\circ}$ C; R_f 0.60 (2:1 hexane-EtOAc); IR (ATR) 3413 (N–H), 3062 (=C–H), 2956–2850 (C–H), 1706 (C=O), 1633–1489 (C=C), 1448–1350 (C–H bend), 1307 (N–S=O), 1145 (S=O), 812–687 (=C–H bend) cm^{-1} ; ^1H NMR (400 MHz, CDCl_3) δ 8.16 (dd, J = 8.0, 8.0 Hz, 2H), 7.73 (d, J = 8.5 Hz, 2H), 7.70 (d, J = 8.5 Hz, 2H), 7.32–7.26 (m, 3H), 7.24–7.19 (m, 3H), 7.18–7.14 (m, 2H), 7.09 (d, J = 2.0 Hz, 1H), 6.98 (dd, J = 7.5, 7.3 Hz, 1H), 6.59 (d, J = 2.0 Hz, 1H), 6.38 (d, J = 7.8 Hz, 1H), 5.90 (s, 1H), 5.64 (s, 1H), 3.83 (s, 3H), 2.41 (s, 3H), 2.37 (s, 3H); ^{13}C NMR (100 MHz, CDCl_3) δ 163.9, 145.4, 145.0, 139.4, 137.7, 137.4, 136.3, 135.2, 135.0, 132.6, 130.1, 129.9, 128.8, 127.7, 126.8, 126.3, 125.2, 124.4, 124.0, 123.8, 121.2, 117.5, 114.9, 114.8, 113.1, 110.6, 94.4, 52.6, 47.9, 21.7, 21.6; HRMS* (ESI) calcd for $[\text{C}_{35}\text{H}_{27}\text{N}_3\text{O}_6\text{S}_2 + \text{H}^+]$ 650.1414, found 650.1386.

*HRMS peak corresponds to dehydrogenated (aromatized) form of **3ga**.

3.4.2.3 UV calibration of γ -carboline **3ac** in organic solvents

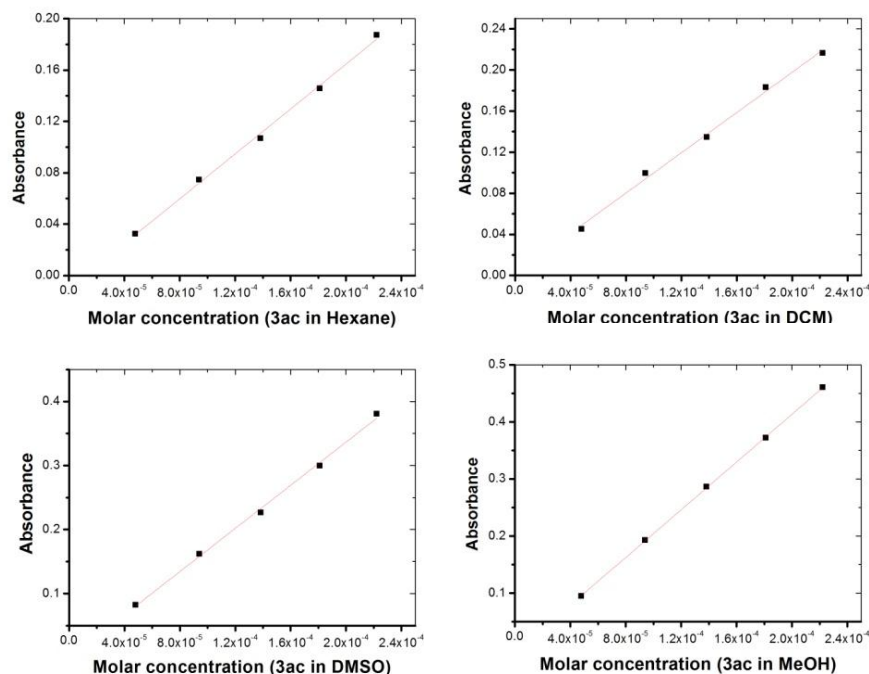


Figure 3.9 UV calibration curve for γ -carboline **3ac** in different solvents

3.4.2.4 *In vitro* cytotoxicity studies

3.4.2.4.1 Cytotoxicity analysis in cancer and macrophage cells

Cancer (MCF7, A431, A549, HEK293 or HeLa cell lines) or RAW264.7 cells were seeded in a 96-well plate (4,200 cells/well) and allowed to form a monolayer for a period of 48 h. Old medium was replaced with fresh medium (0.2 mL) containing an increasing concentration of γ -carboline derivatives **3ac**, **3bc**, **3ca**, **3ga** and doxorubicin (0.1 μ M, 0.25 μ M, 0.5 μ M, 1 μ M, 2.5 μ M, 5 μ M, 10 μ M, 25 μ M, 50 μ M, 100 μ M) and incubated for 48 h or 3 h, respectively. Spent medium in each well were discarded, and cells were rinsed with PBS (3×0.2 mL) followed by treatment with 0.5% crystal violet (0.05 mL) for 20 minutes at room temperature. Cells were rinsed with PBS (3×0.2 mL), methanol (0.20 mL) was added to each well and incubated for 20 minutes.

The absorbance from each well proportional to the live cell was measured using Synergy H1 multimode plate reader (BioTek Instruments, Inc., Winooski, VT, USA) at an excitation and emission wavelength of 530 nm and 590 nm, respectively.

Dose vs response curves were obtained from a plot of semi-log[conc] vs intensity of fluorescence emission, and IC₅₀ (concentration at which 50% of the enzymatic activity is inhibited) was calculated for carboline derivative or doxorubicin using GraphPad Prism, version 7.02 for Windows (GraphPad Software, San Diego, CA).

3.4.2.4.2 HeLa cell uptake study of γ -carboline **3ac**

A live-cell imaging experiment was performed with HeLa cells. The HeLa cells were plated in a 4-well confocal dish (cell count \approx 100 cells per well) and incubated for 48 h at 37 °C under 5% CO₂. After 3 h of incubation with carboline derivative **3ac** (10 nM, 100 nM, 1 μ M, 10 μ M, and 100 μ M), cellular uptake and distribution were monitored by using confocal microscopy (λ_{ex} = 405 nm; λ_{em} range = 420–470 nm).

3.4.2.5 Density Functional Theory Calculations

All the calculations have been carried out using the Becke's three-parameter hybrid exchange functional and Lee–Yang–Parr's correlation functional (B3LYP) and 6-311++G**(d,p) basis sets as implemented in the Gaussian 09 program. The calculated total (E) and relative (ΔE) energies for **7a**, **7c**, **9a**, **9b** and **9c** are as follows:

Compound	Electronic energy + ZPE (hartrees)	Relative Energy (Kcal/mol)
<i>E</i> -Imine/ <i>Z</i> -enamine precursor (7a)	−1203.7126	7.78
<i>Z</i> -Imine/ <i>E</i> -enamine precursor (7c)	−1203.6972	17.44
1,2-Dihydro- γ -carboline (9a)	−1203.7250	0.00
1,6-Dihydro- γ -carboline (9b)	−1203.7018	14.55
1,2-Dihydro- β -carboline (9c)	−1203.6986	16.56

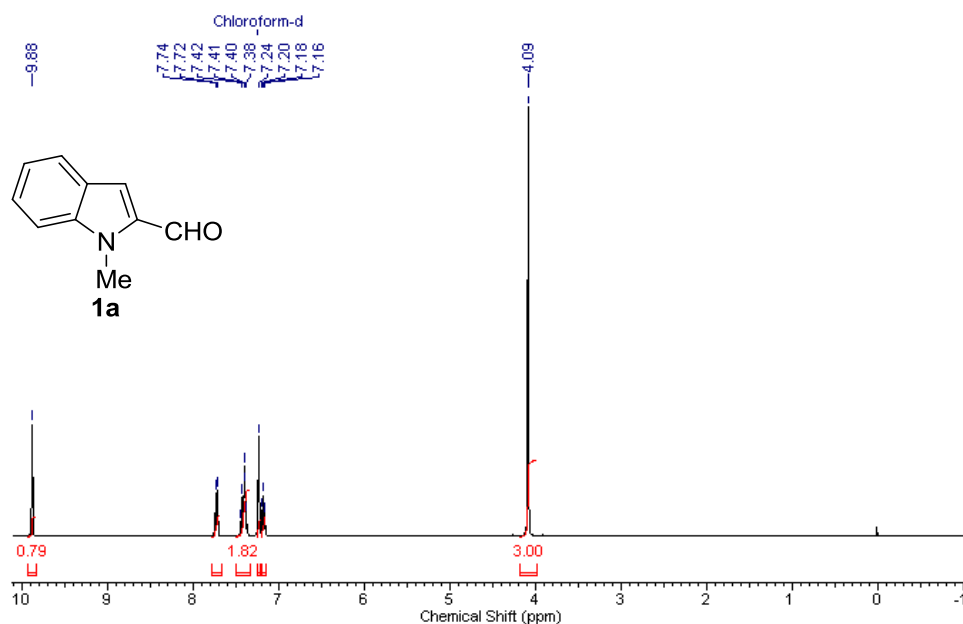
3.4.3 Copies of ^1H , ^{13}C NMR spectra for synthesized compounds

Figure 3.10 ^1H NMR spectrum of *1-methyl-1H-indole-2-carbaldehyde* (**1a**)

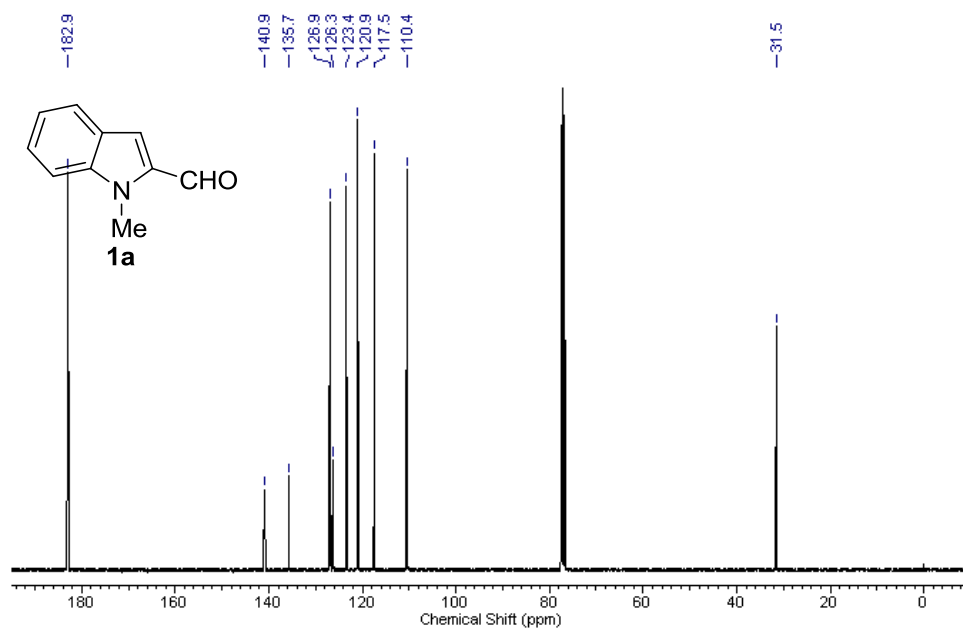
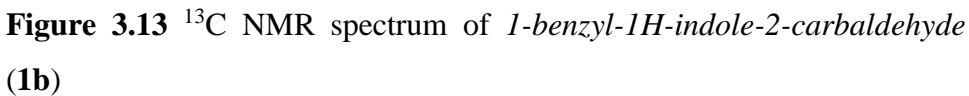
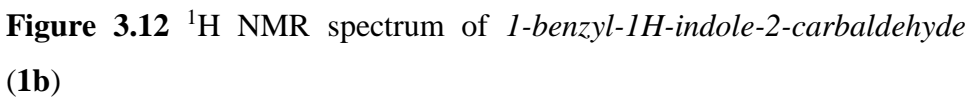


Figure 3.11 ^{13}C NMR spectrum of *1-methyl-1H-indole-2-carbaldehyde* (**1a**)



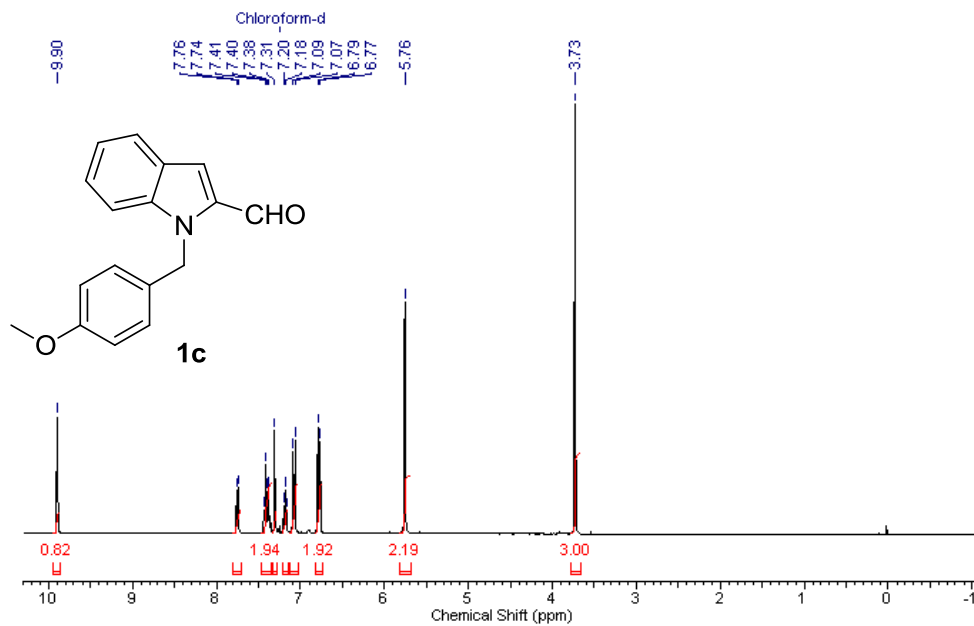


Figure 3.14 ¹H NMR spectrum of *1-(4-methoxybenzyl)-1H-indole-2-carbaldehyde (1c)*

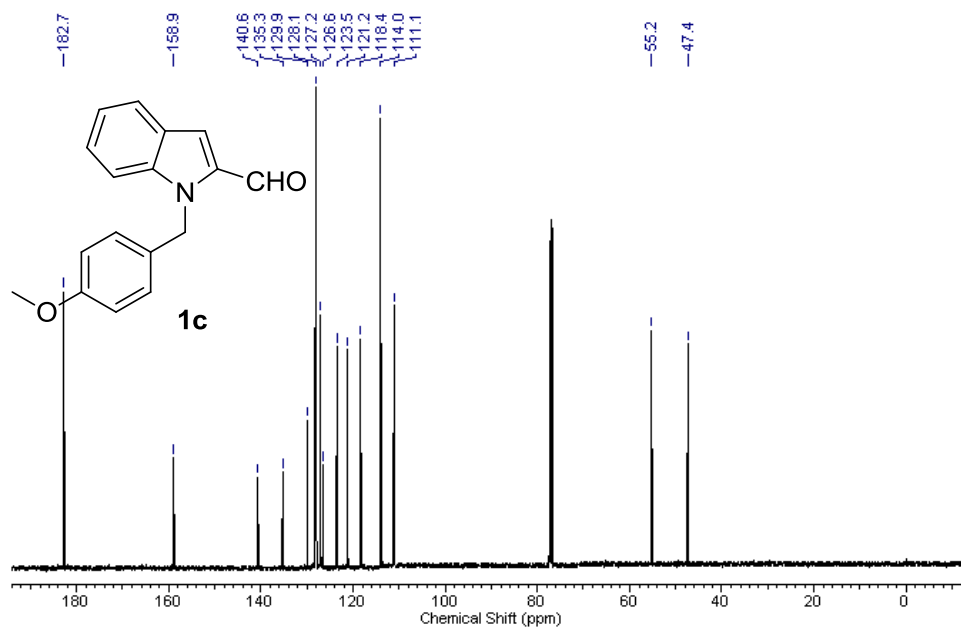


Figure 3.15 ¹³C NMR spectrum of *1-(4-methoxybenzyl)-1H-indole-2-carbaldehyde (1c)*

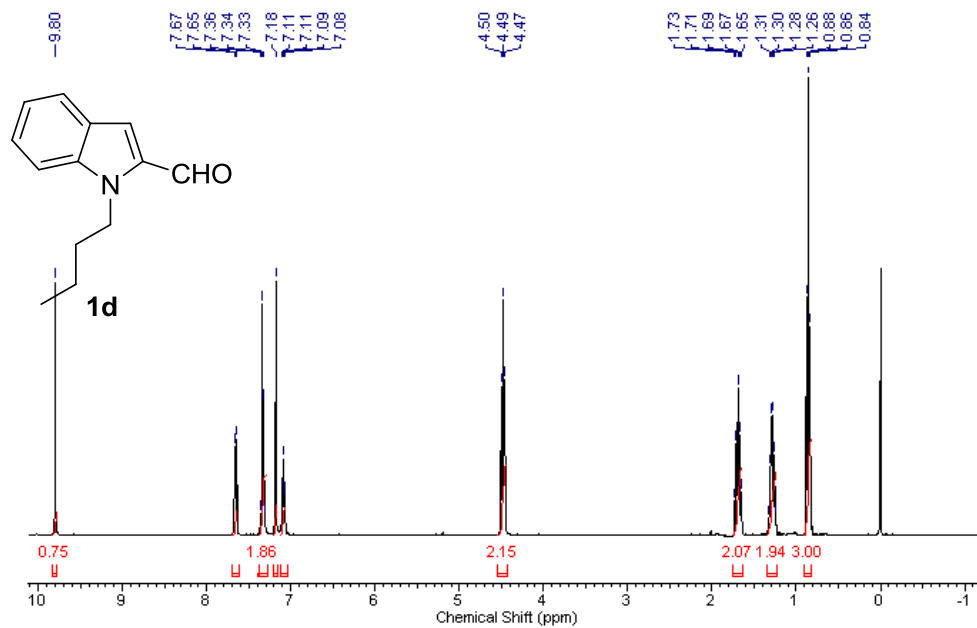


Figure 3.16 ^1H NMR spectrum of 1-butyl-1H-indole-2-carbaldehyde (**1d**)

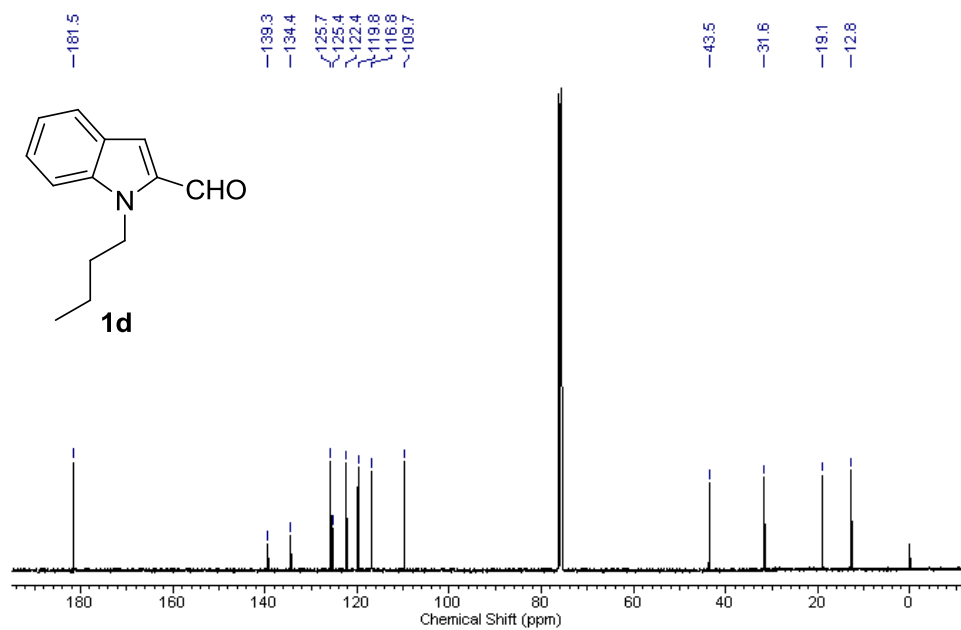


Figure 3.17 ^{13}C NMR spectrum of 1-butyl-1H-indole-2-carbaldehyde (**1d**)

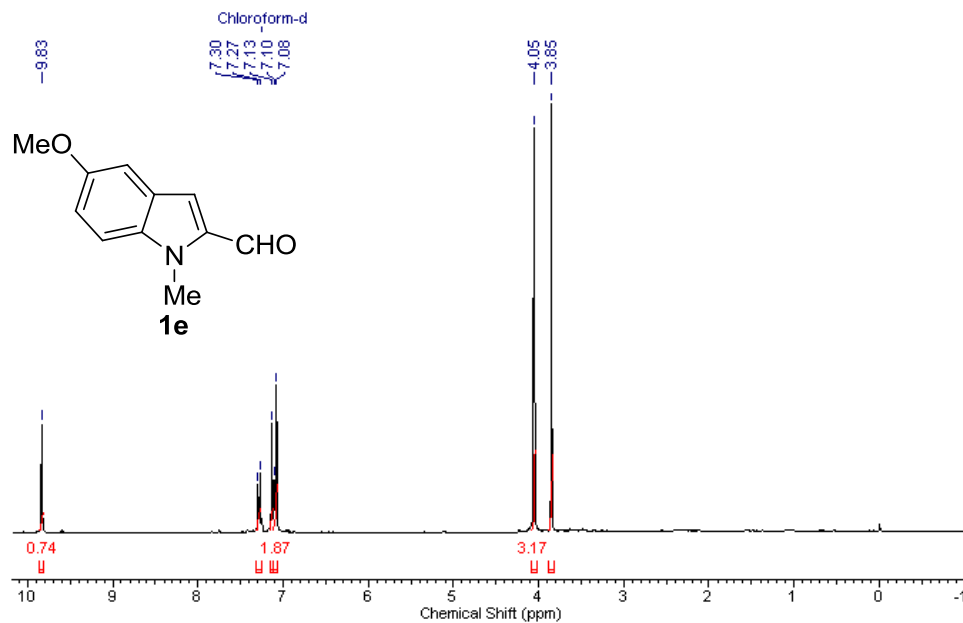


Figure 3.18 ¹H NMR spectrum of 5-methoxy-1-methyl-1H-indole-2-carbaldehyde (**1e**)

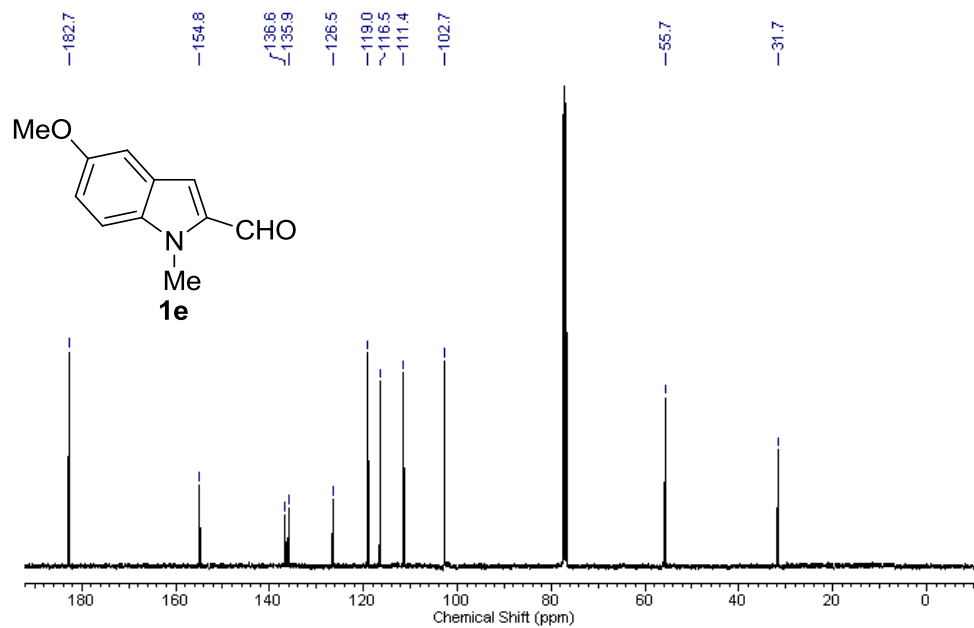


Figure 3.19 ¹³C NMR spectrum of 5-methoxy-1-methyl-1H-indole-2-carbaldehyde (**1e**)

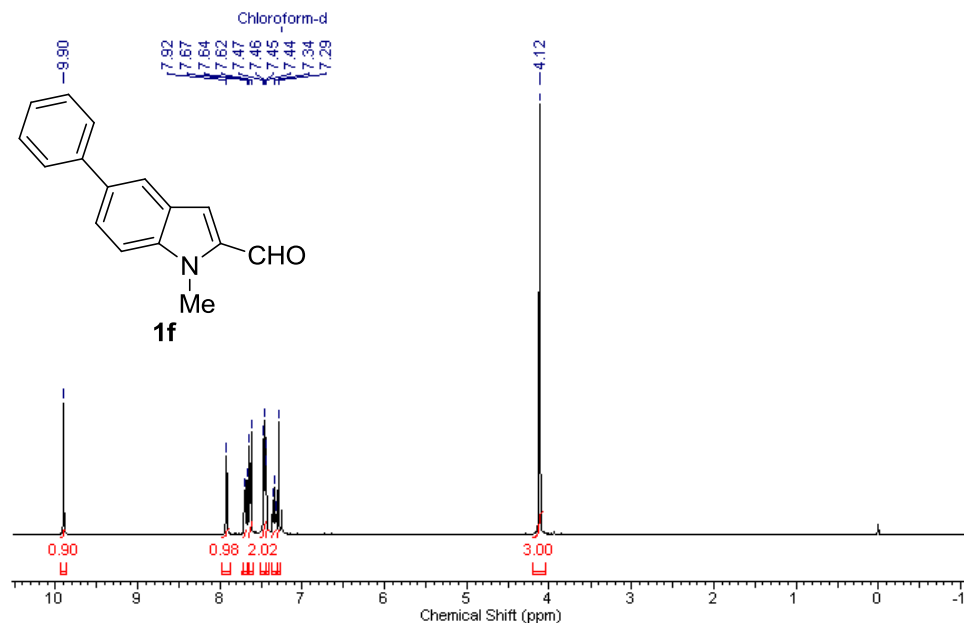


Figure 3.20 ^1H NMR spectrum of 1-methyl-5-phenyl-1H-indole-2-carbaldehyde (**1f**)

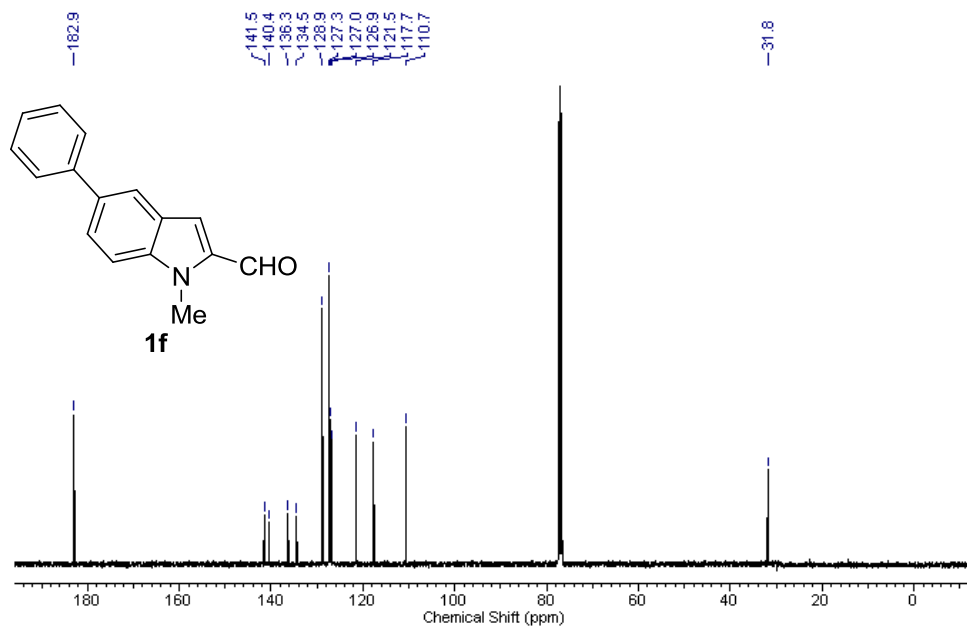


Figure 3.21 ^{13}C NMR spectrum of 1-methyl-5-phenyl-1H-indole-2-carbaldehyde (**1f**)

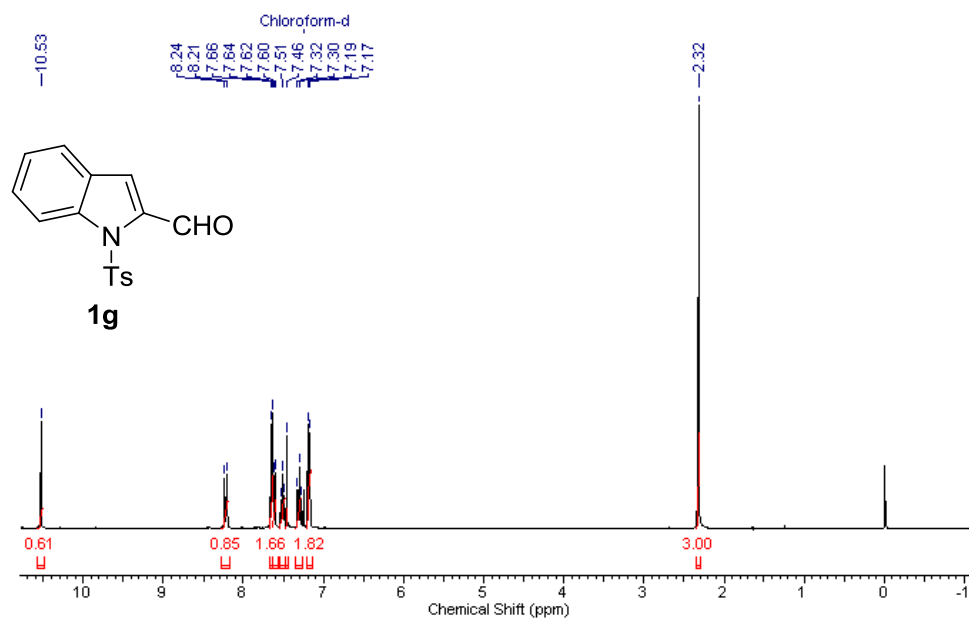


Figure 3.22 ¹H NMR spectrum of *1-tosyl-1H-indole-2-carboxylate* (**1g**)

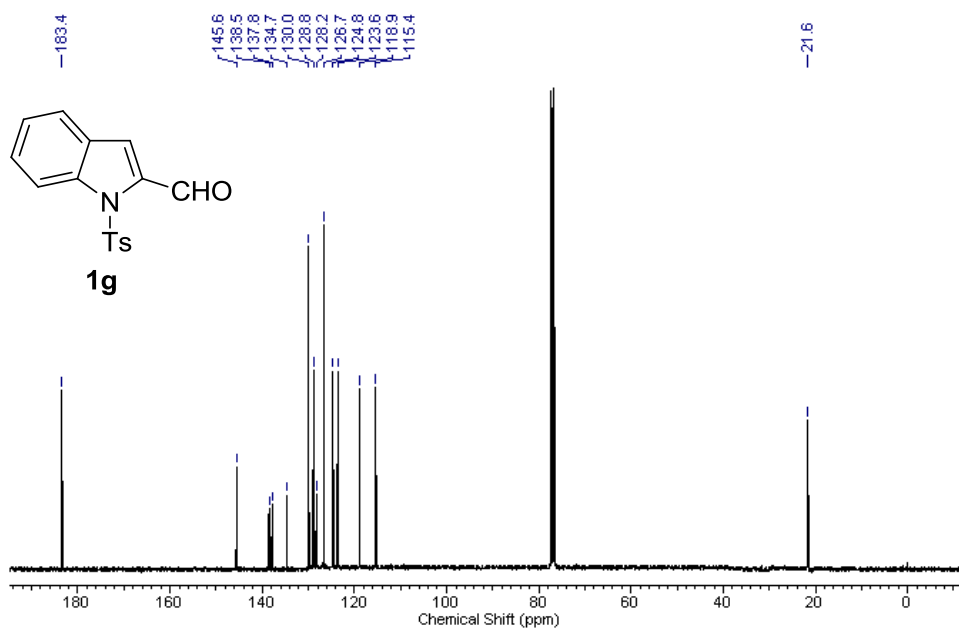


Figure 3.23 ¹³C NMR spectrum of *1-tosyl-1H-indole-2-carboxylate* (**1g**)

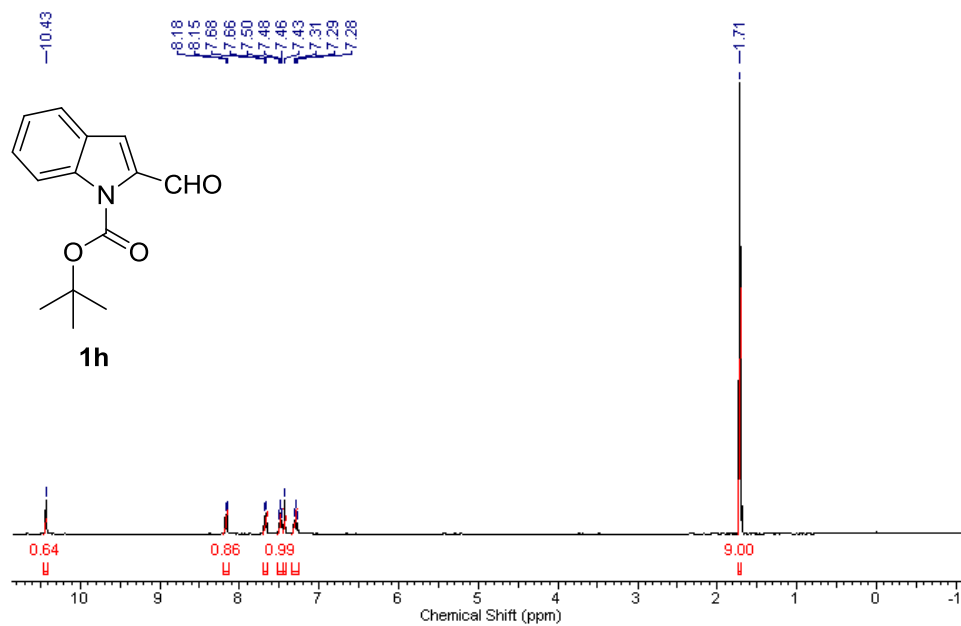


Figure 3.24 ¹H NMR spectrum of *tert*-butyl 2-formyl-1*H*-indole-1-carboxylate (**1h**)

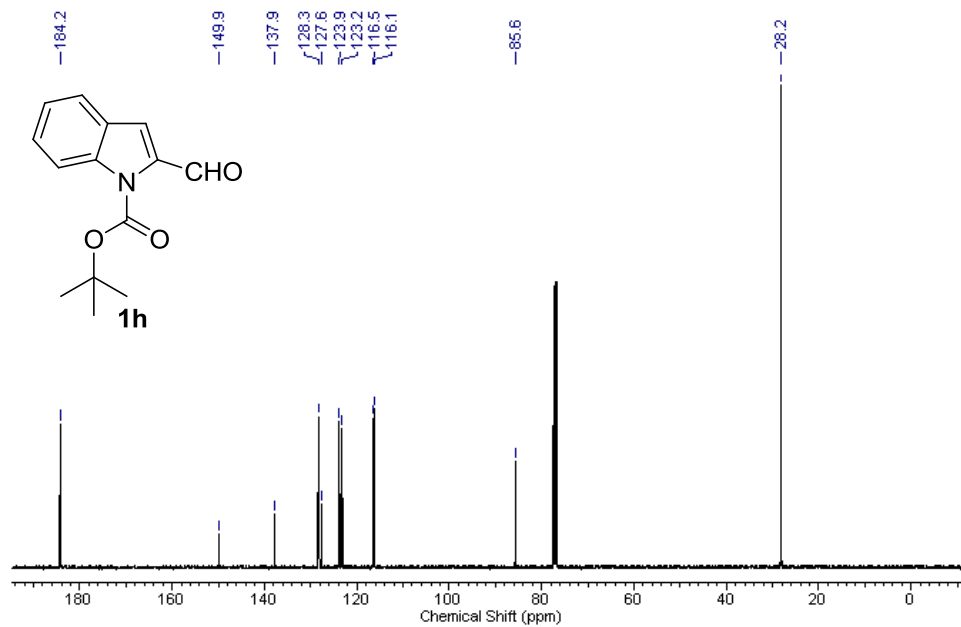


Figure 3.25 ¹³C NMR spectrum of *tert*-butyl 2-formyl-1*H*-indole-1-carboxylate (**1h**)

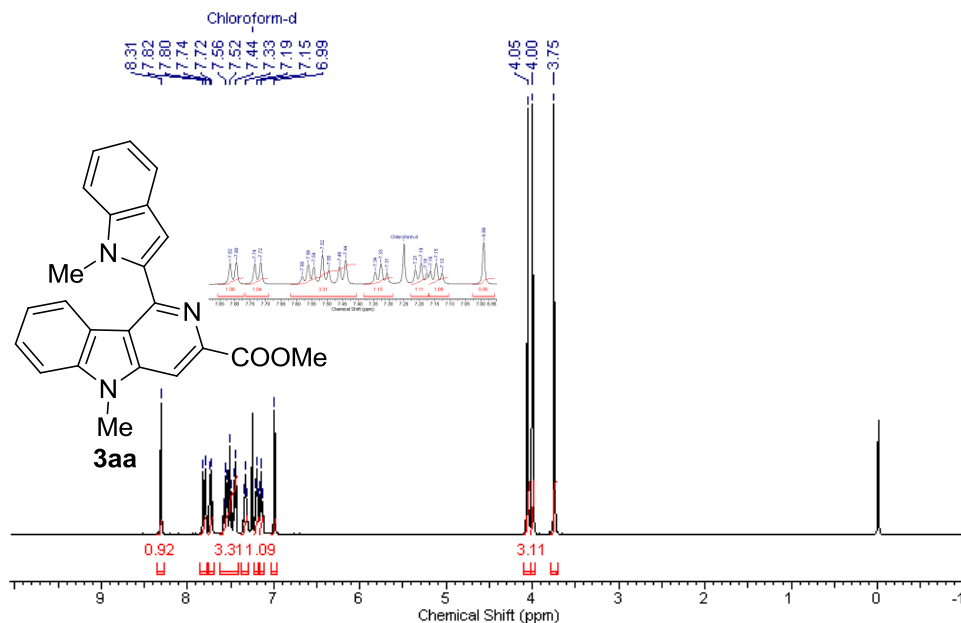


Figure 3.26 ¹H NMR spectrum of methyl 5-methyl-1-(1-methyl-1H-indol-2-yl)-5H-pyrido[4,3-b]indole-3-carboxylate (**3aa**)

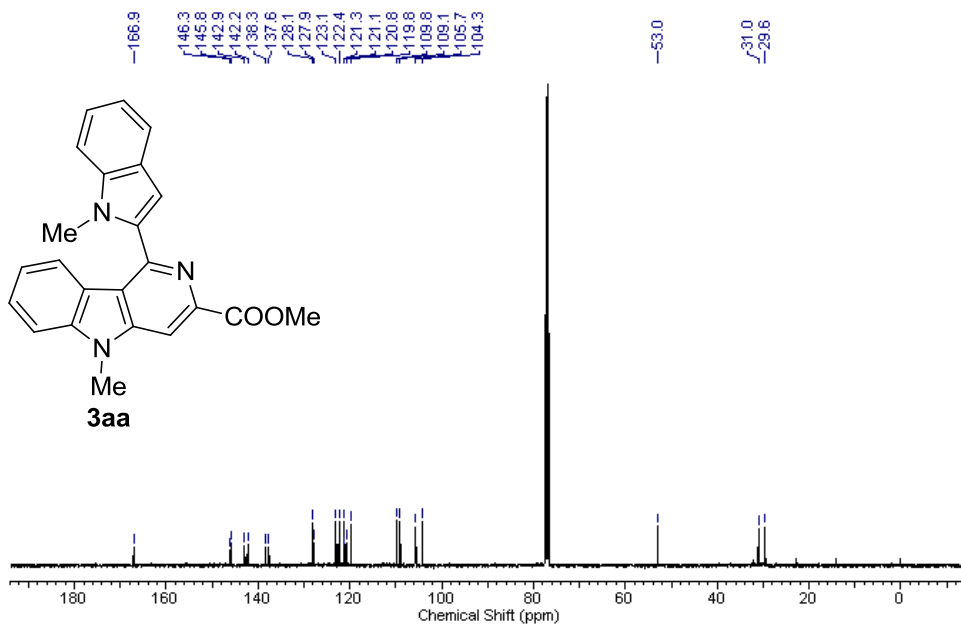


Figure 3.27 ¹³C NMR spectrum of methyl 5-methyl-1-(1-methyl-1H-indol-2-yl)-5H-pyrido[4,3-b]indole-3-carboxylate (**3aa**)

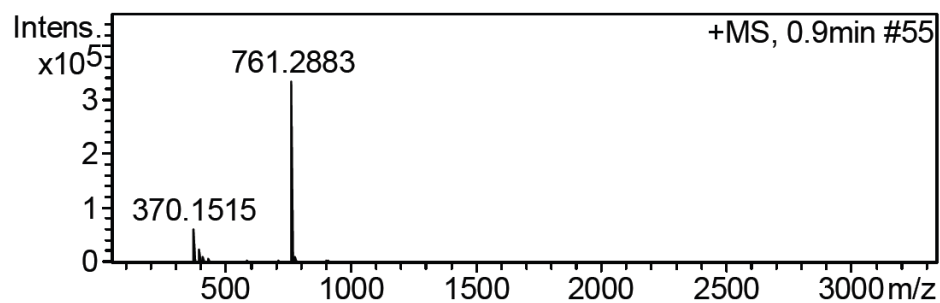


Figure 3.28 HRMS of methyl 5-methyl-1-(1-methyl-1H-indol-2-yl)-5H-pyrido[4,3-b]indole-3-carboxylate (**3aa**)

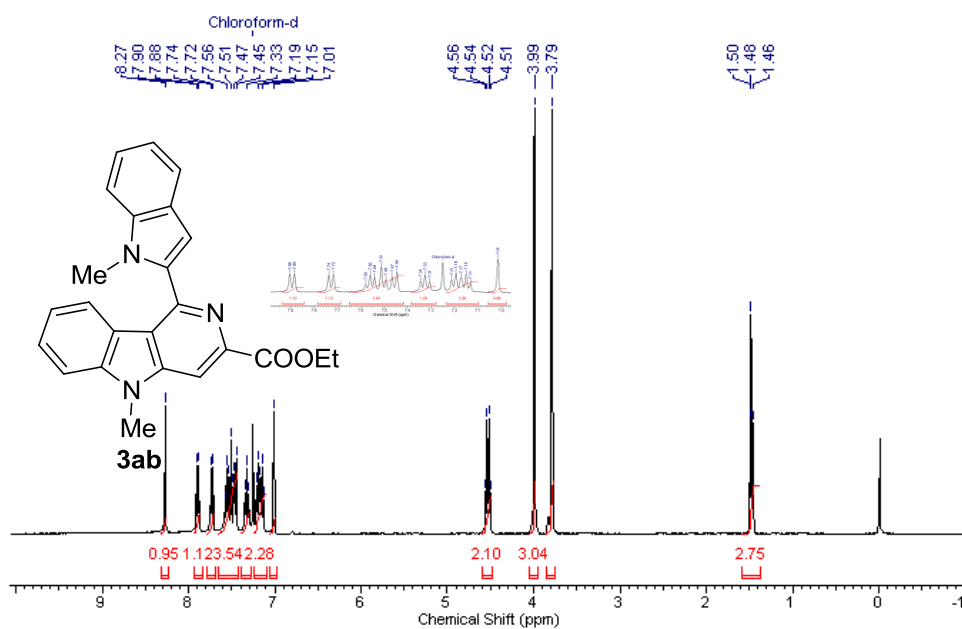


Figure 3.29 ¹H NMR spectrum of ethyl 5-methyl-1-(1-methyl-1H-indol-2-yl)-5H-pyrido[4,3-b]indole-3-carboxylate (**3ab**)

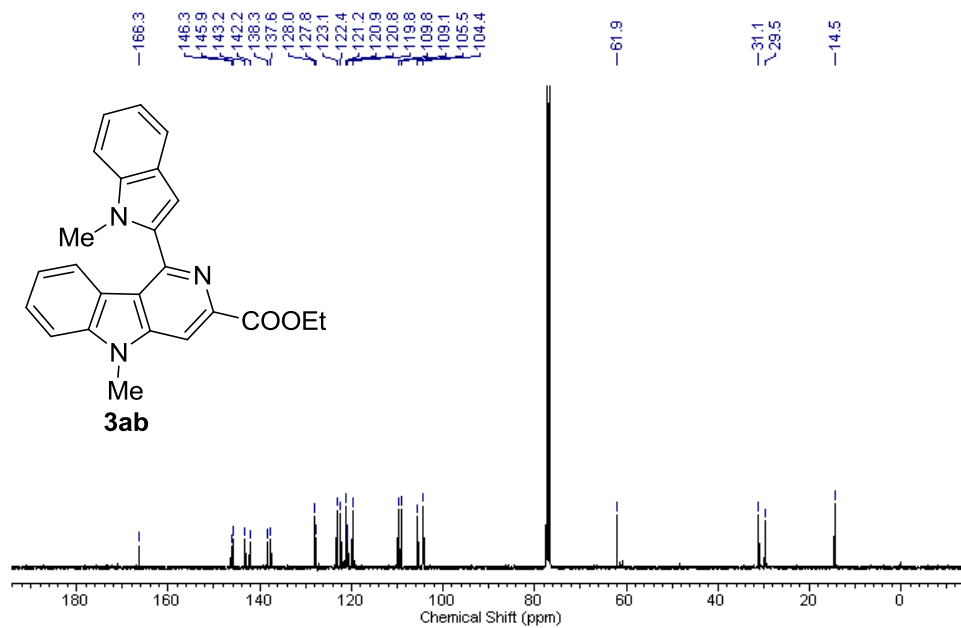


Figure 3.30 ¹³C NMR spectrum of ethyl 5-methyl-1-(1-methyl-1H-indol-2-yl)-5H-pyrido[4,3-b]indole-3-carboxylate (**3ab**)

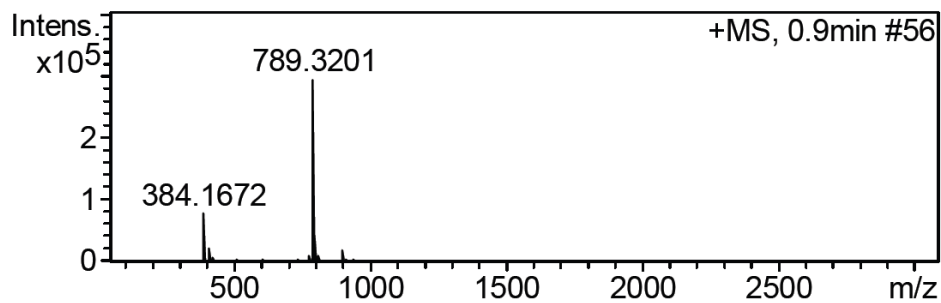


Figure 3.31 HRMS of ethyl 5-methyl-1-(1-methyl-1H-indol-2-yl)-5H-pyrido[4,3-b]indole-3-carboxylate (**3ab**)

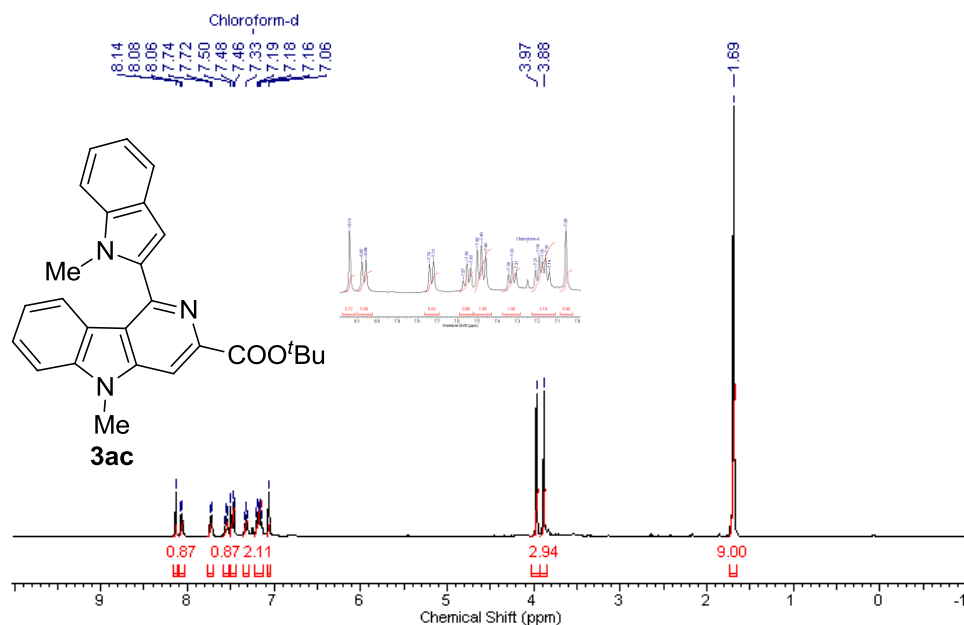


Figure 3.32 ¹H NMR spectrum of *tert*-butyl 5-methyl-1-(1-methyl-1*H*-indol-2-yl)-5*H*-pyrido[4,3-*b*]indole-3-carboxylate (**3ac**)

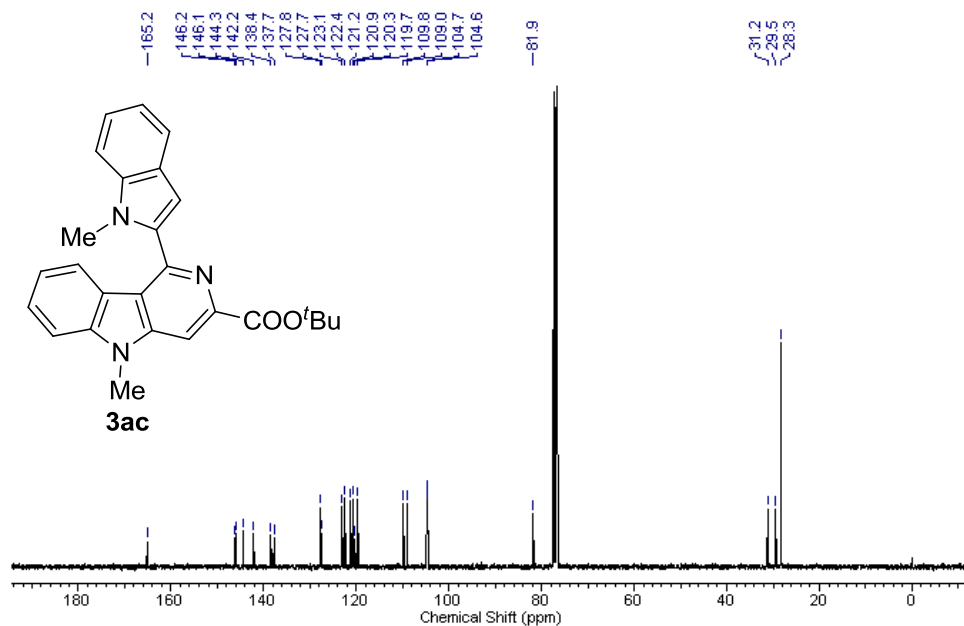


Figure 3.33 ¹³C NMR spectrum of *tert*-butyl 5-methyl-1-(1-methyl-1*H*-indol-2-yl)-5*H*-pyrido[4,3-*b*]indole-3-carboxylate (**3ac**)

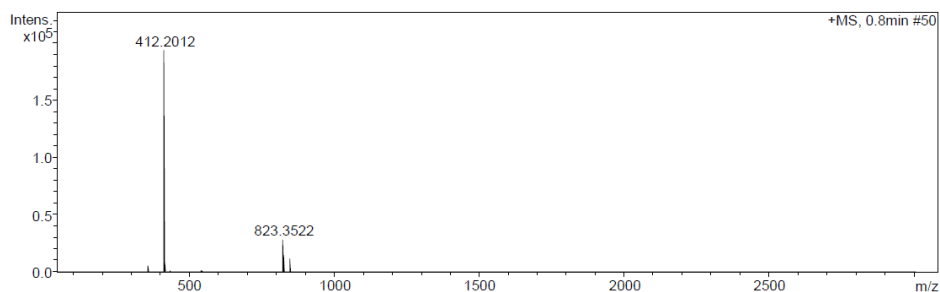


Figure 3.34 HRMS of *tert*-butyl 5-methyl-1-(1-methyl-1H-indol-2-yl)-5H-pyrido[4,3-b]indole-3-carboxylate (**3ac**)

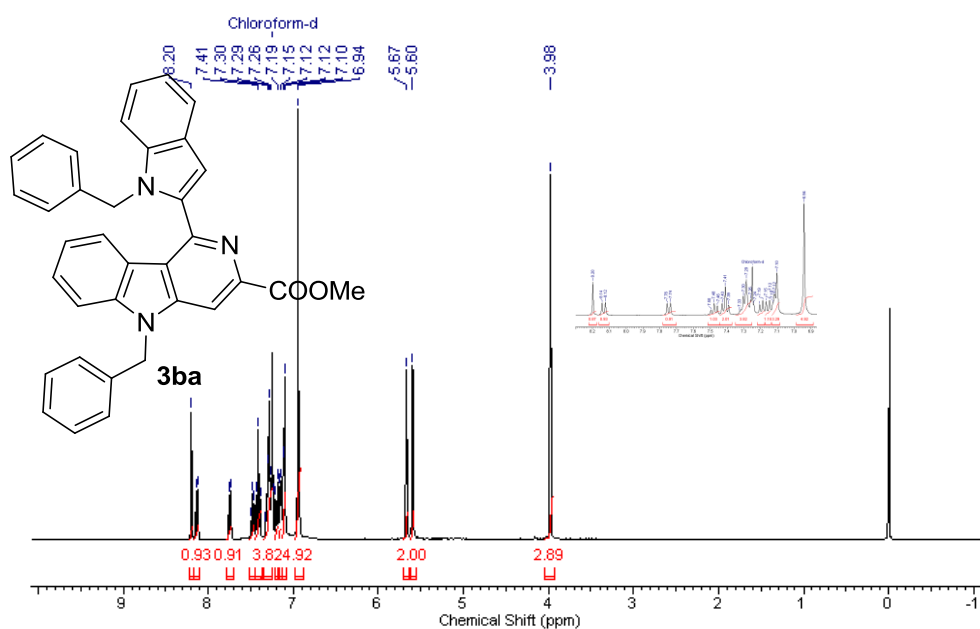


Figure 3.35 ¹H NMR spectrum of methyl 5-benzyl-1-(1-benzyl-1H-indol-2-yl)-5H-pyrido[4,3-b]indole-3-carboxylate (**3ba**)

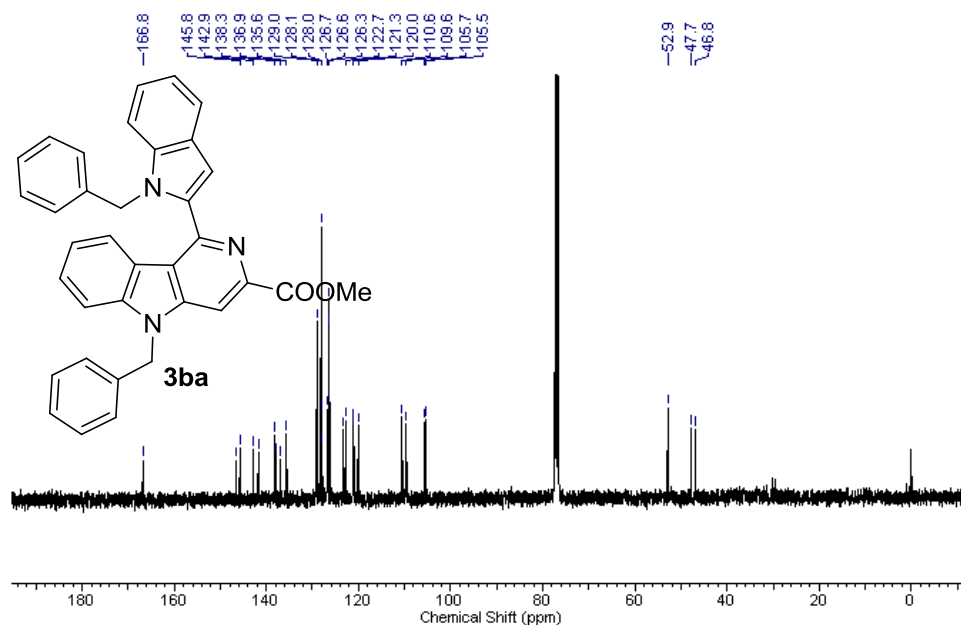


Figure 3.36 ^{13}C NMR spectrum of methyl 5-benzyl-1-(1-benzyl-1H-indol-2-yl)-5H-pyrido[4,3-b]indole-3-carboxylate (**3ba**)

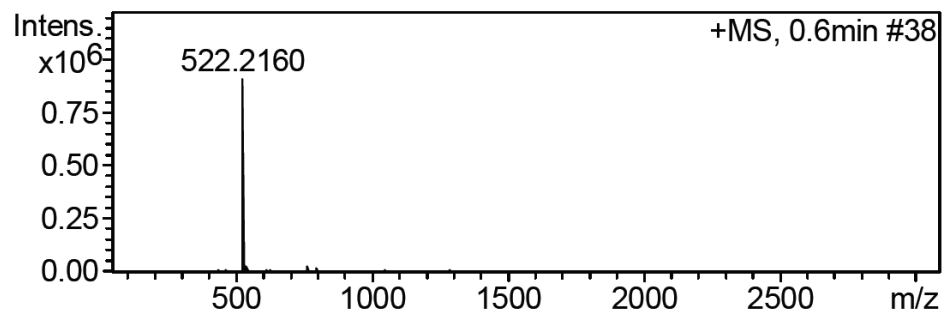


Figure 3.37 HRMS of methyl 5-benzyl-1-(1-benzyl-1H-indol-2-yl)-5H-pyrido[4,3-b]indole-3-carboxylate (**3ba**)

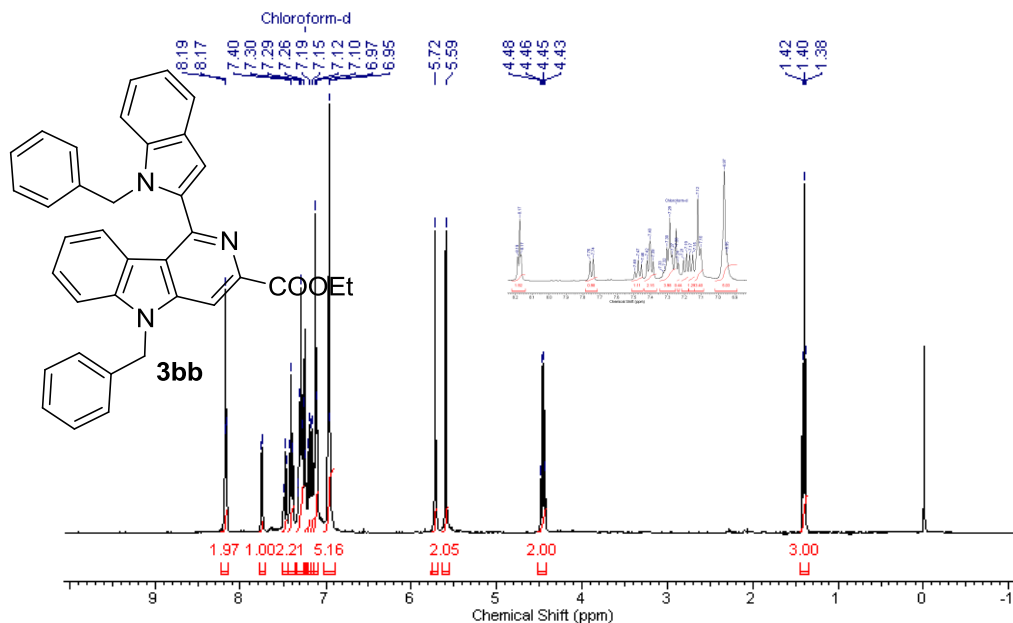


Figure 3.38 ¹H NMR spectrum of *ethyl 5-benzyl-1-(1-benzyl-1H-indol-2-yl)-5H-pyrido[4,3-b]indole-3-carboxylate (3bb)*

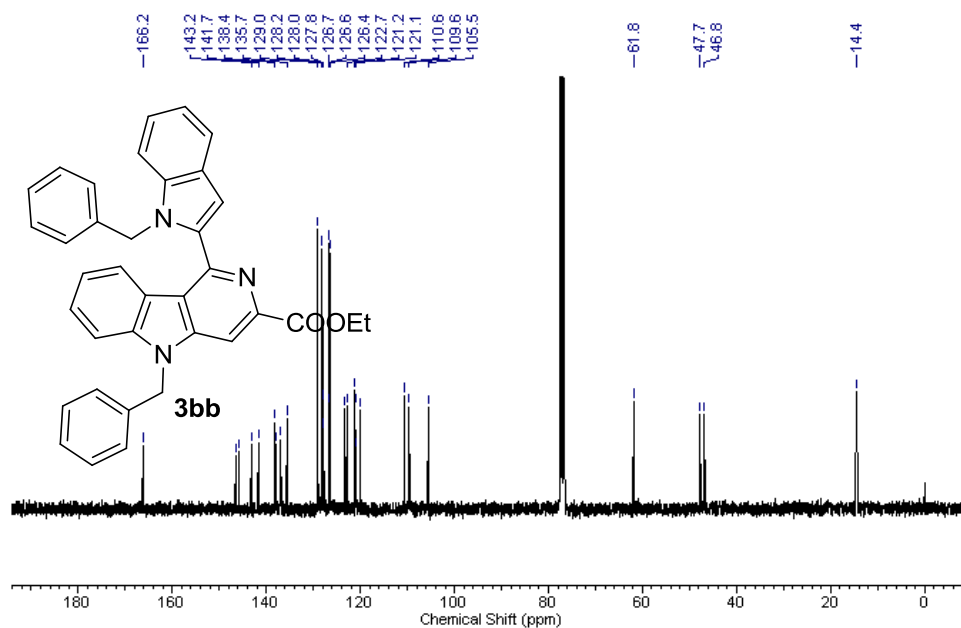


Figure 3.39 ¹³C NMR spectrum of *ethyl 5-benzyl-1-(1-benzyl-1H-indol-2-yl)-5H-pyrido[4,3-b]indole-3-carboxylate (3bb)*

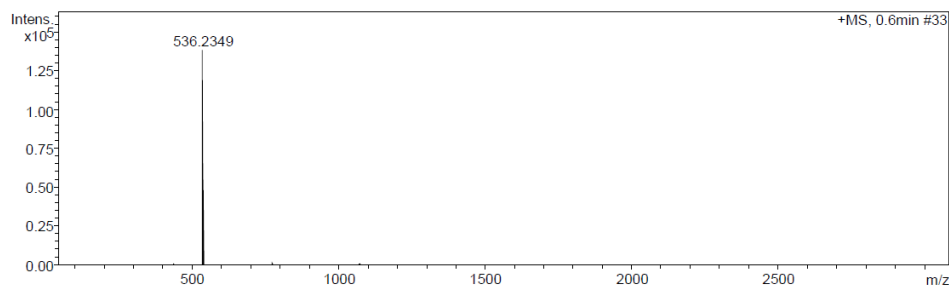


Figure 3.40 HRMS of *ethyl 5-benzyl-1-(1-benzyl-1H-indol-2-yl)-5H-pyrido[4,3-b]indole-3-carboxylate (3bb)*

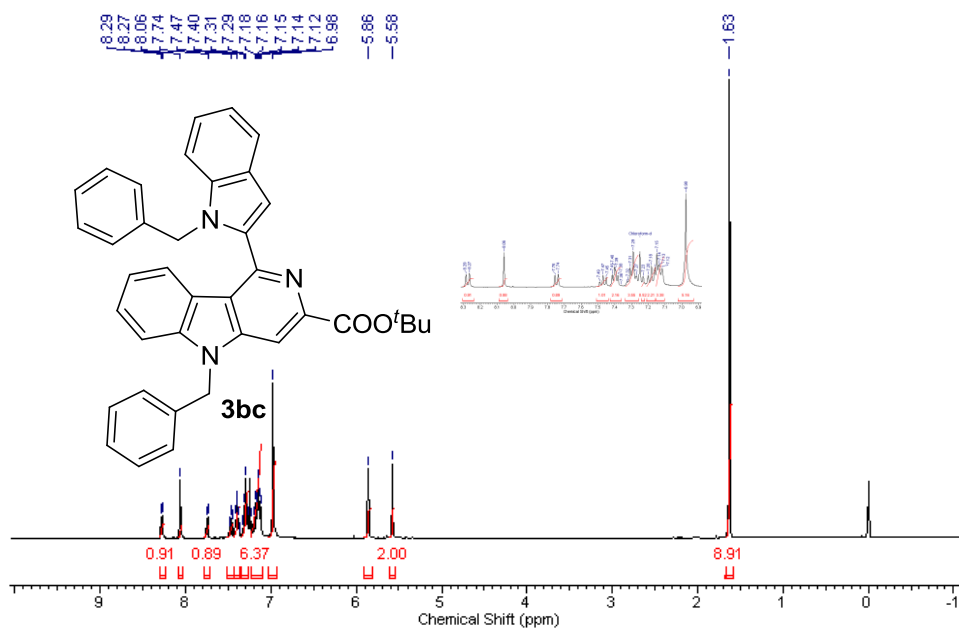


Figure 3.41 ¹H NMR spectrum of *tert-butyl 5-benzyl-1-(1-benzyl-1H-indol-2-yl)-5H-pyrido[4,3-b]indole-3-carboxylate (3bc)*

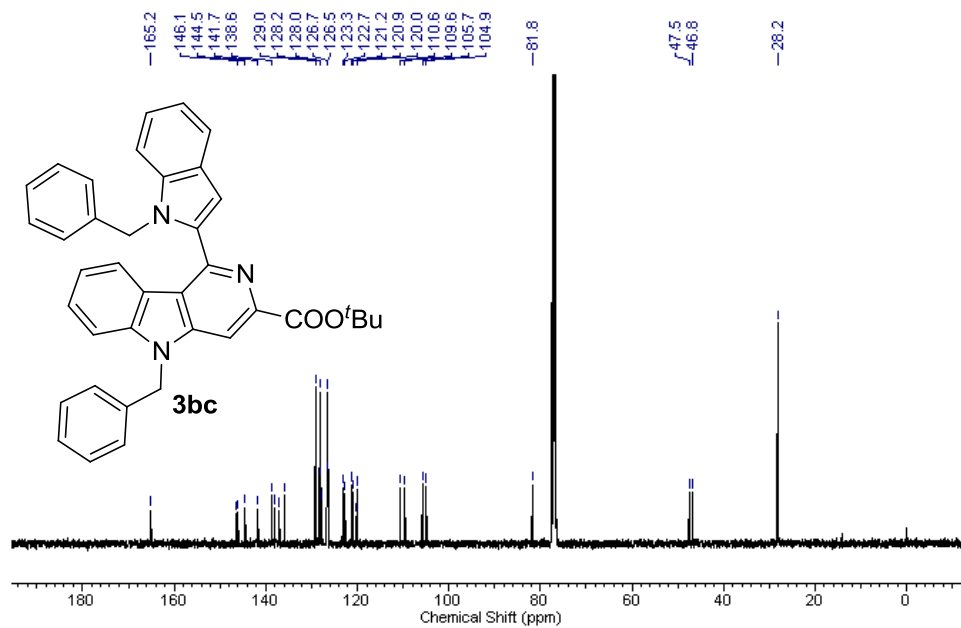


Figure 3.42 ^{13}C NMR spectrum of *tert*-butyl 5-benzyl-1-(1-benzyl-1*H*-indol-2-yl)-5*H*-pyrido[4,3-*b*]indole-3-carboxylate (**3bc**)

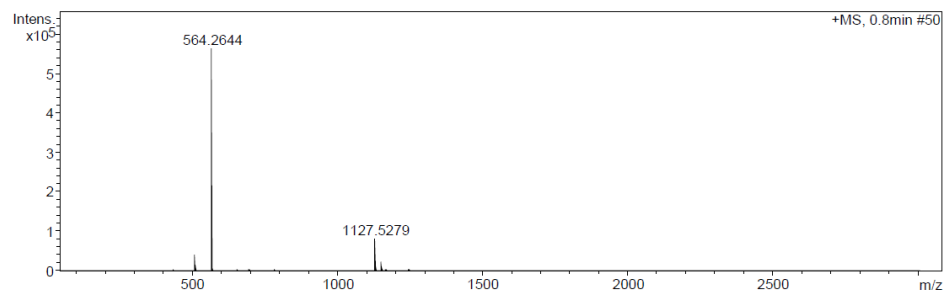


Figure 3.43 HRMS of *tert*-butyl 5-benzyl-1-(1-benzyl-1*H*-indol-2-yl)-5*H*-pyrido[4,3-*b*]indole-3-carboxylate (**3bc**)

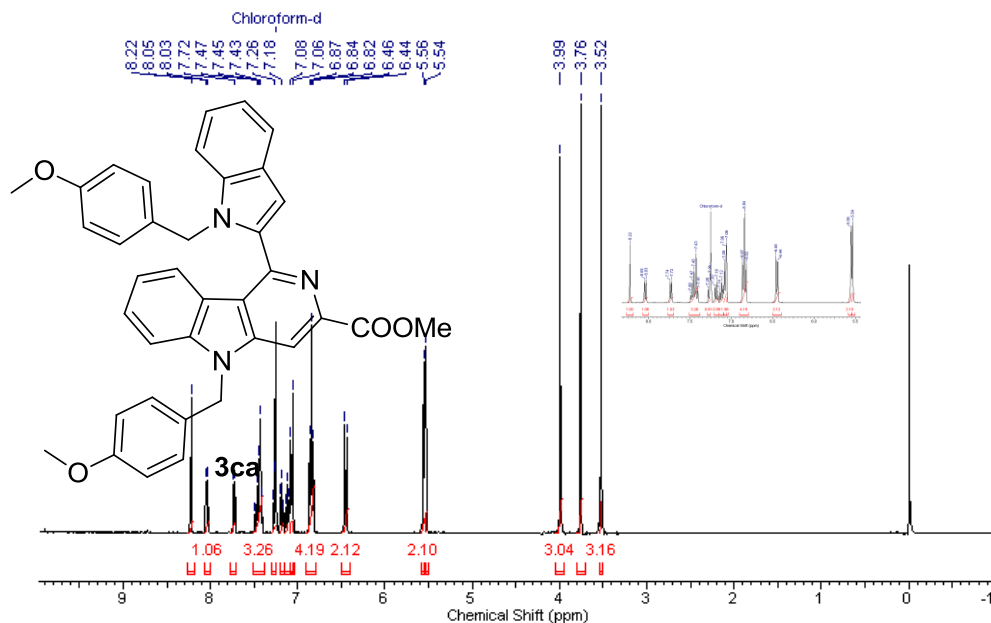


Figure 3.44 ^1H NMR spectrum of *methyl 5-(4-methoxybenzyl)-1-(1-(4-methoxybenzyl)-1H-indol-2-yl)-5H-pyrido[4,3-b]indole-3-carboxylate (3ca)*

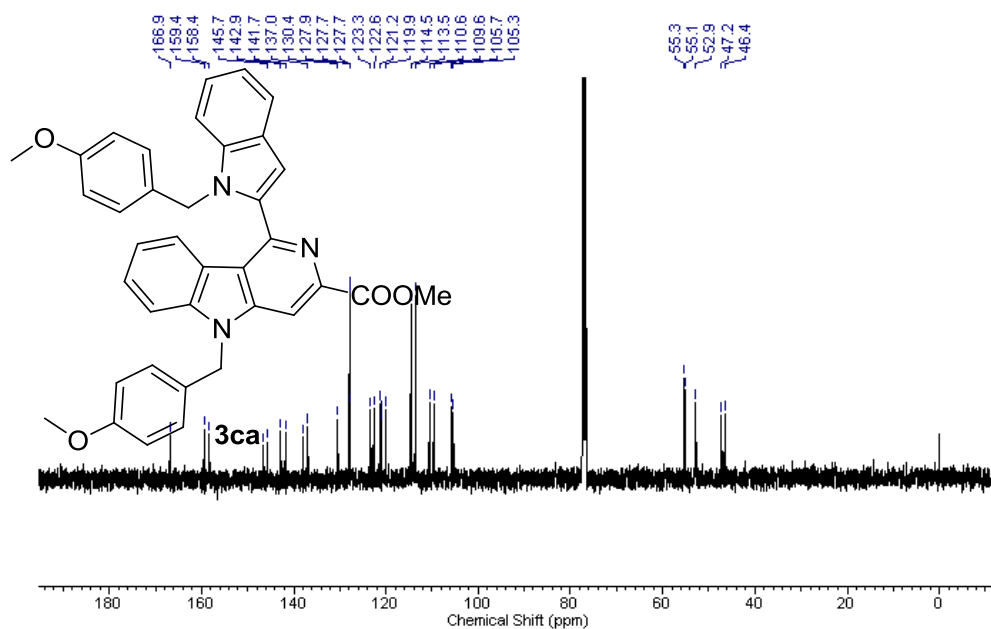


Figure 3.45 ^{13}C NMR spectrum of *methyl 5-(4-methoxybenzyl)-1-(1-(4-methoxybenzyl)-1H-indol-2-yl)-5H-pyrido[4,3-b]indole-3-carboxylate (3ca)*

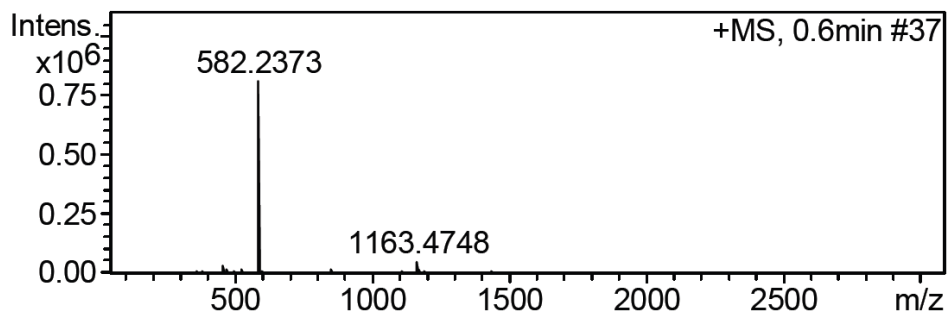


Figure 3.46 HRMS of *methyl 5-(4-methoxybenzyl)-1-(1-(4-methoxybenzyl)-1H-indol-2-yl)-5H-pyrido[4,3-b]indole-3-carboxylate (3ca)*

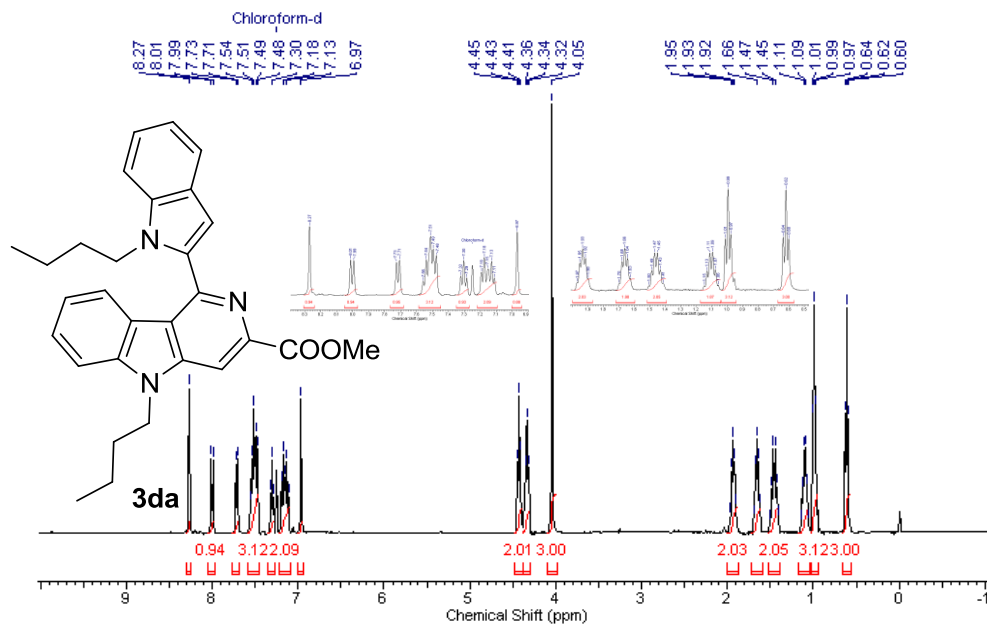


Figure 3.47 ¹H NMR spectrum of *methyl 5-butyl-1-(1-butyl-1H-indol-2-yl)-5H-pyrido[4,3-b]indole-3-carboxylate (3da)*

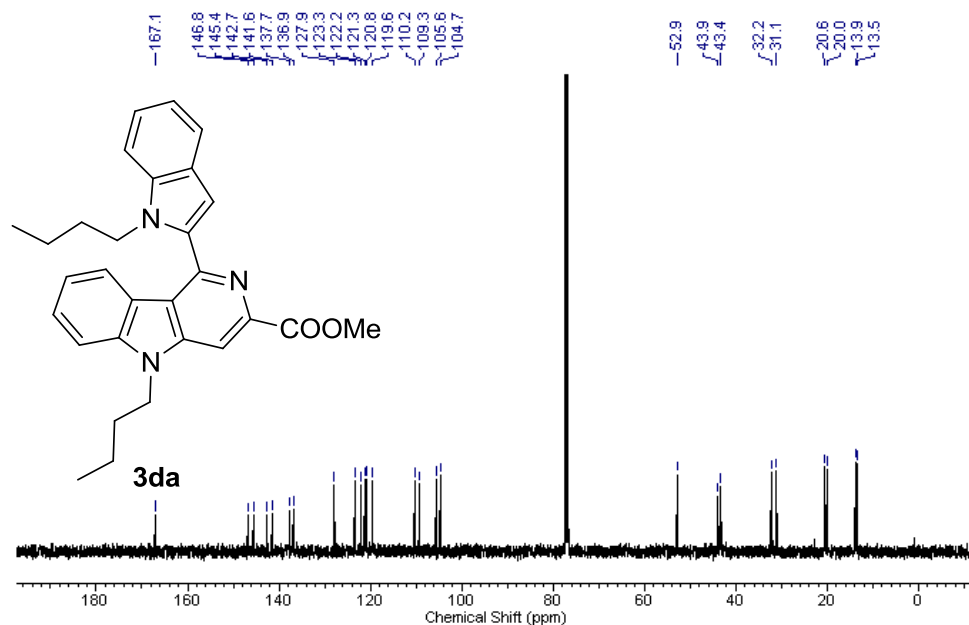


Figure 3.48 ¹³C NMR spectrum of methyl 5-butyl-1-(1-butyl-1H-indol-2-yl)-5H-pyrido[4,3-b]indole-3-carboxylate (**3da**)

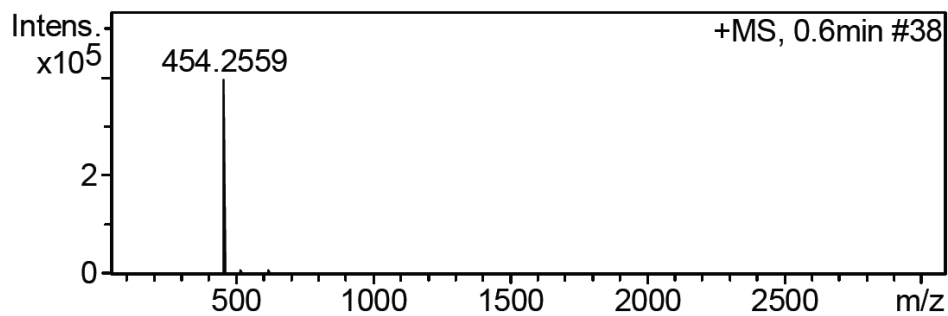


Figure 3.49 HRMS of methyl 5-butyl-1-(1-butyl-1H-indol-2-yl)-5H-pyrido[4,3-b]indole-3-carboxylate (**3da**)

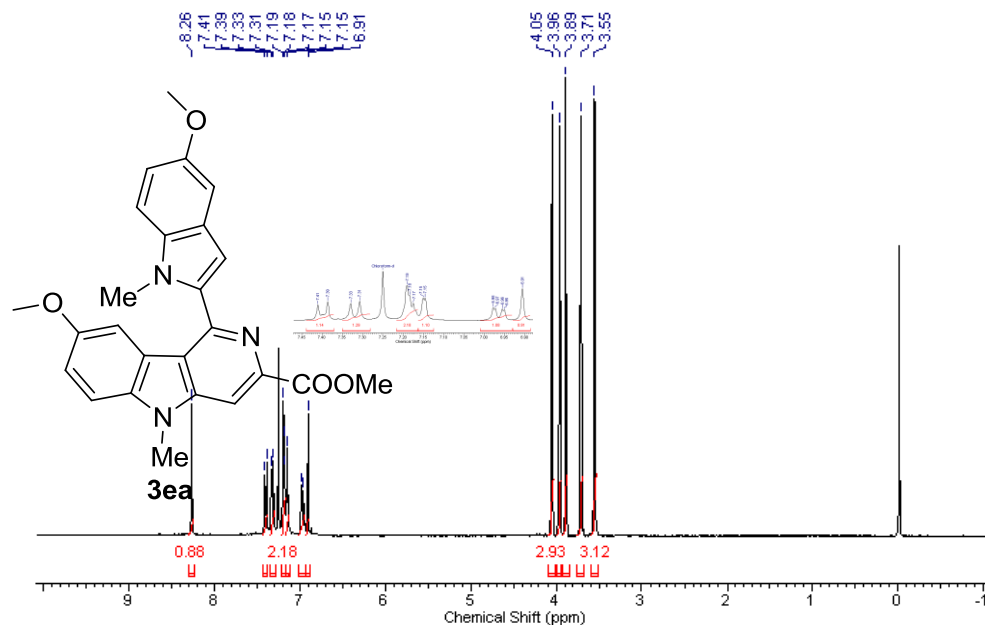


Figure 3.50 ^1H NMR spectrum of *methyl 8-methoxy-1-(5-methoxy-1-methyl-1H-indol-2-yl)-5-methyl-5H-pyrido[4,3-b]indole-3-carboxylate (3ea)*

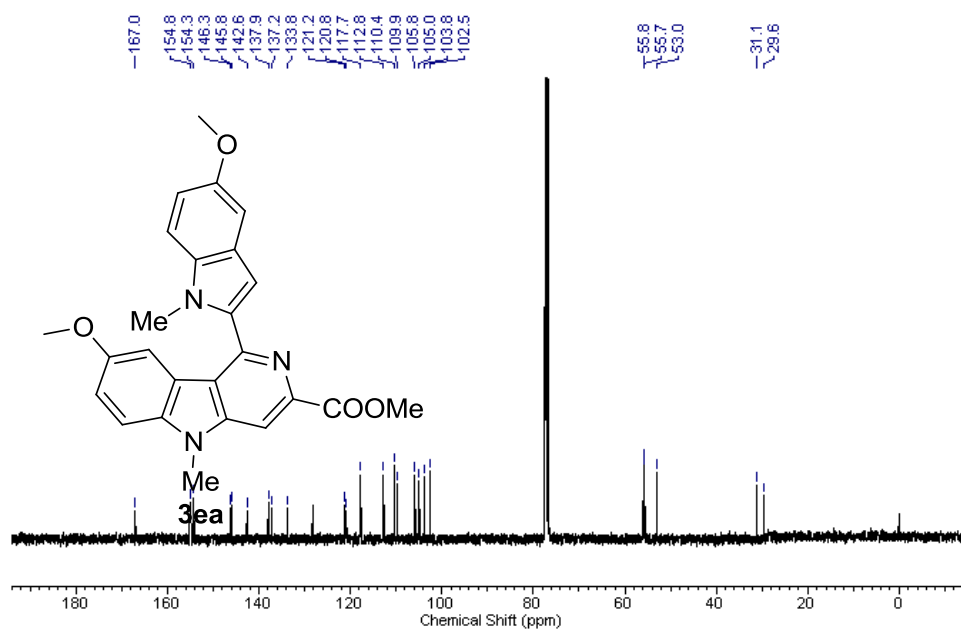


Figure 3.51 ^{13}C NMR spectrum of *methyl 8-methoxy-1-(5-methoxy-1-methyl-1H-indol-2-yl)-5-methyl-5H-pyrido[4,3-b]indole-3-carboxylate (3ea)*

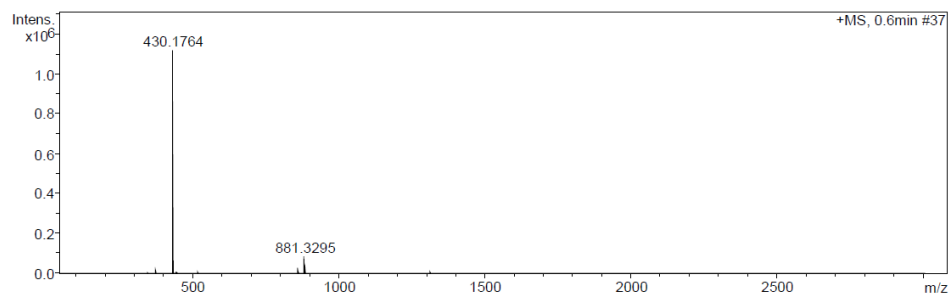


Figure 3.52 HRMS of methyl 8-methoxy-1-(5-methoxy-1-methyl-1H-indol-2-yl)-5-methyl-5H-pyrido[4,3-b]indole-3-carboxylate (3ea)

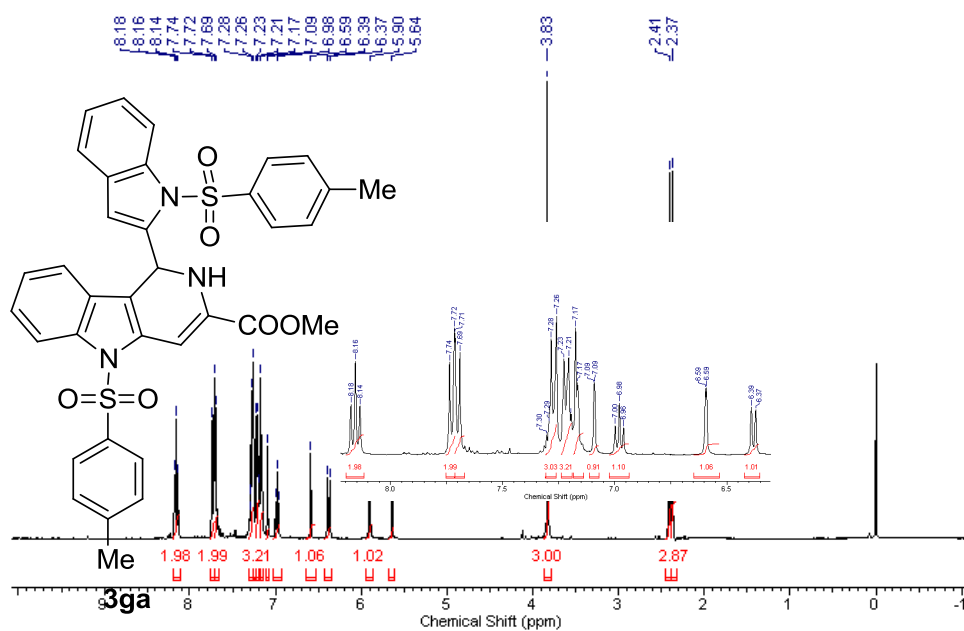


Figure 3.53 ¹H NMR spectrum of methyl 5-tosyl-1-(1-tosyl-1H-indol-2-yl)-2,5-dihydro-1H-pyrido[4,3-b]indole-3-carboxylate (3ga)

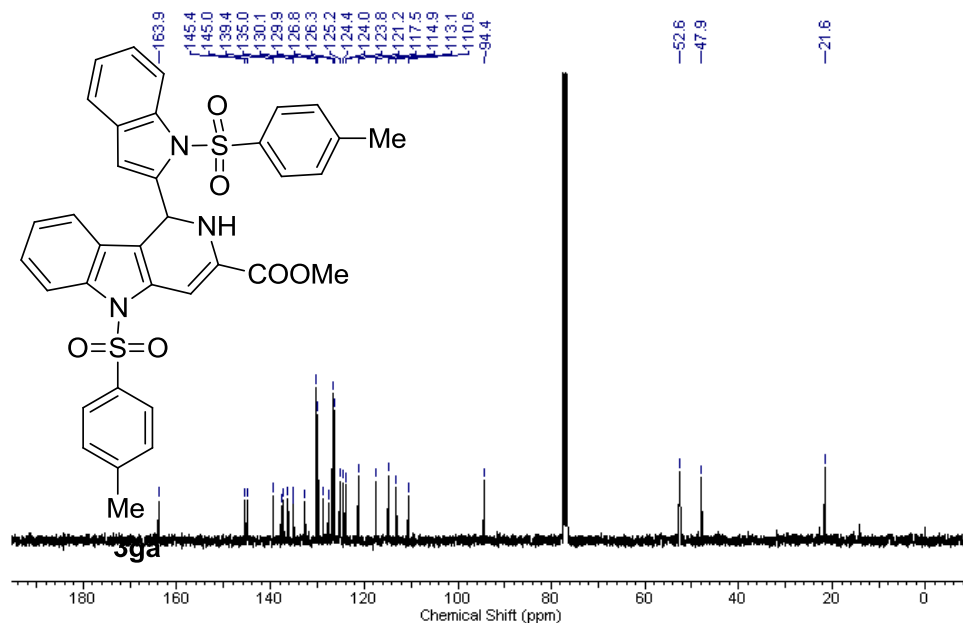


Figure 3.54 ^{13}C NMR spectrum of methyl 5-tosyl-1-(1-tosyl-1H-indol-2-yl)-2,5-dihydro-1H-pyrido[4,3-b]indole-3-carboxylate (**3ga**)

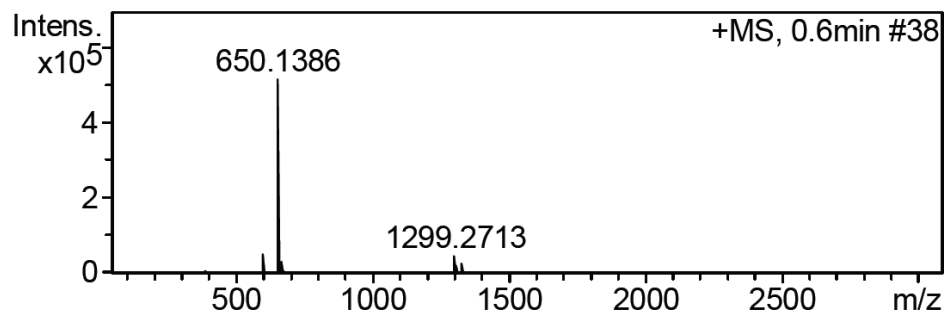


Figure 3.55 HRMS of methyl 5-tosyl-1-(1-tosyl-1H-indol-2-yl)-2,5-dihydro-1H-pyrido[4,3-b]indole-3-carboxylate (**3ga**)

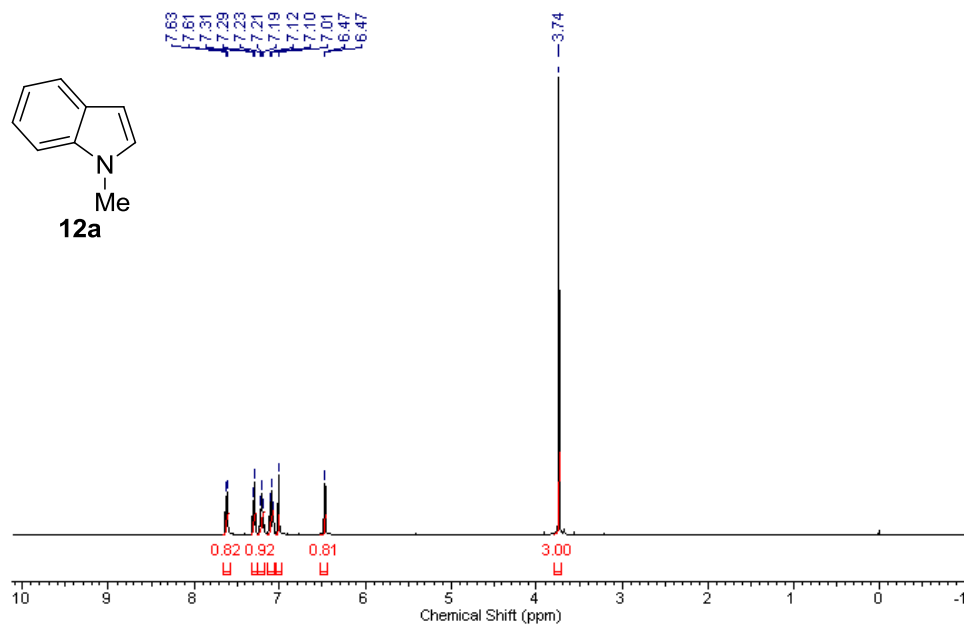


Figure 3.56 ^1H NMR spectrum of *1-methyl-1H-indole* (**12a**)

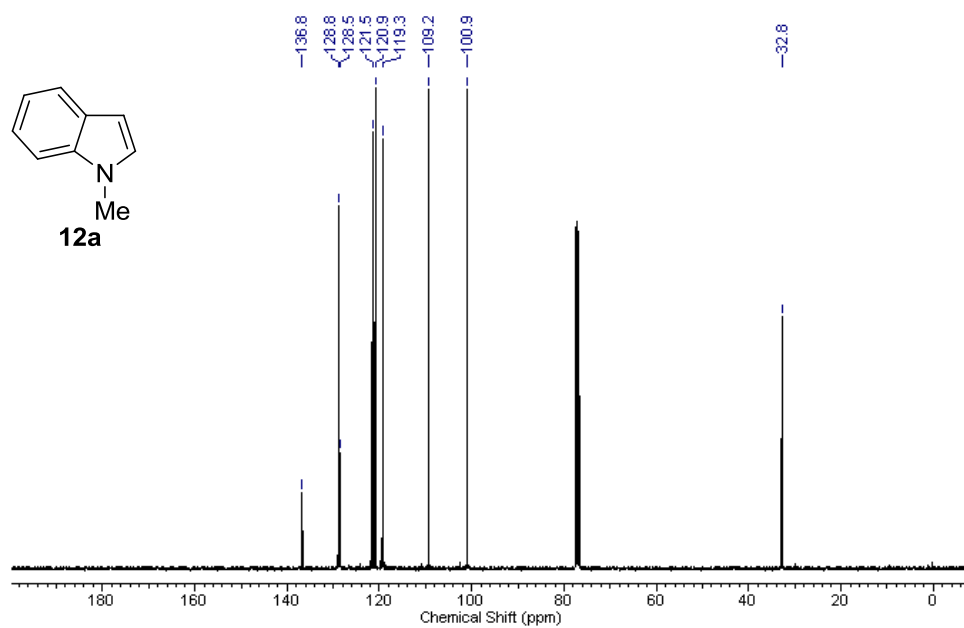


Figure 3.57 ^{13}C NMR spectrum of *1-methyl-1H-indole* (**12a**)

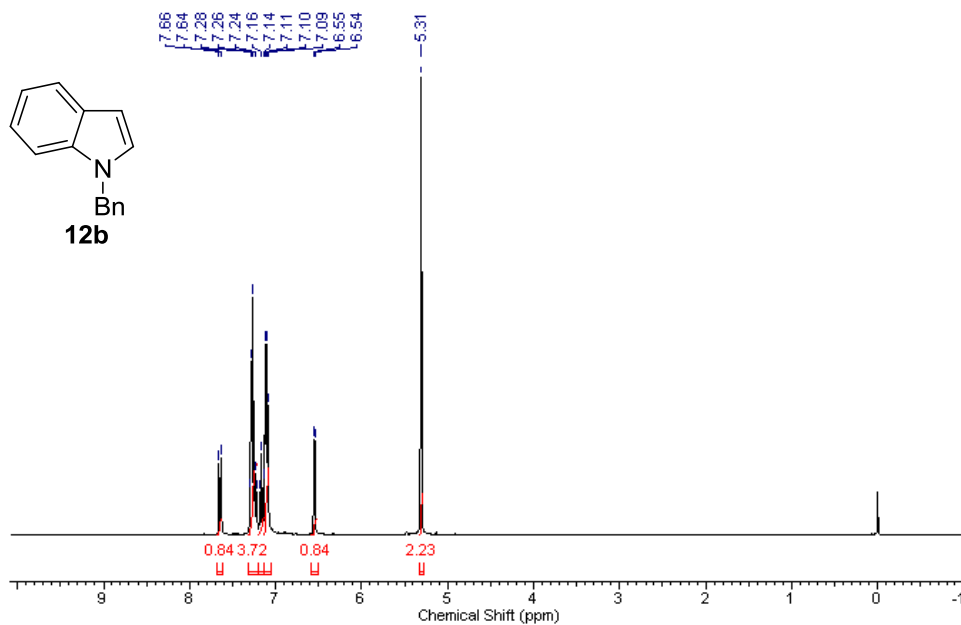


Figure 3.58 ^1H NMR spectrum of 1-benzyl-1H-indole (**12b**)

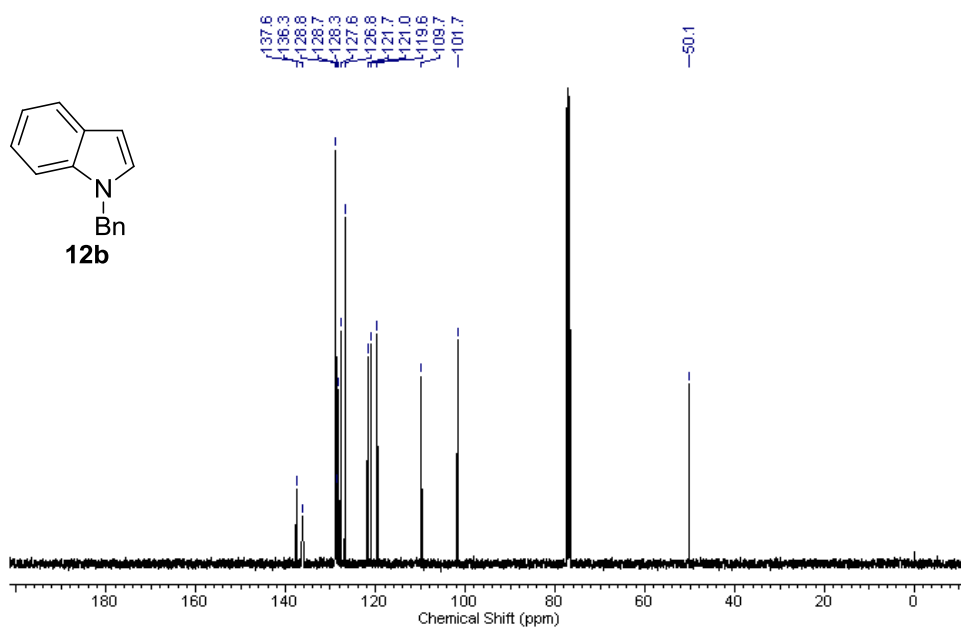


Figure 3.59 ^{13}C NMR spectrum of 1-benzyl-1H-indole (**12b**)

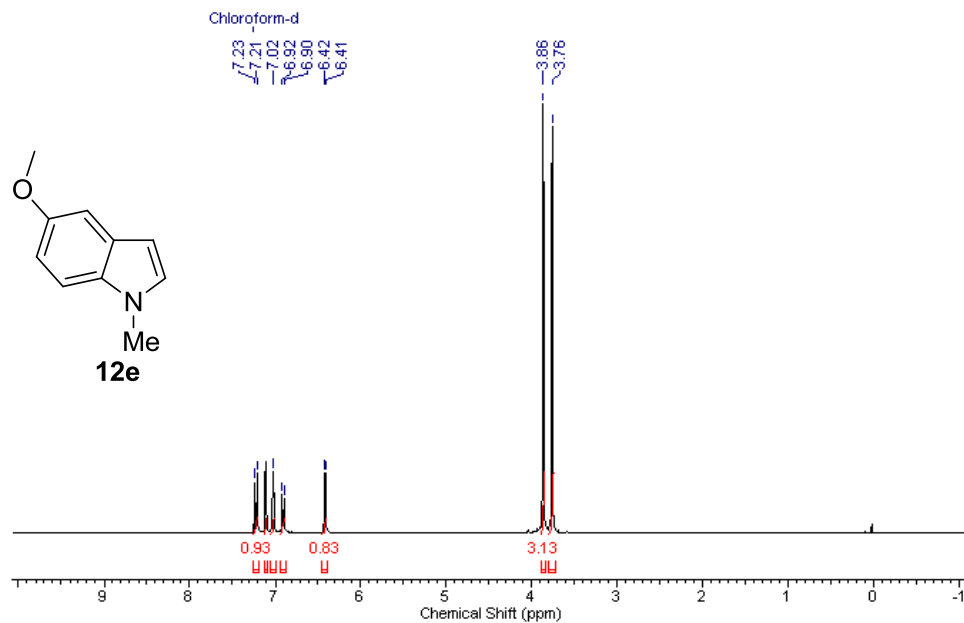


Figure 3.60 ¹H NMR spectrum of 5-methoxy-1-methyl-1H-indole (**12e**)

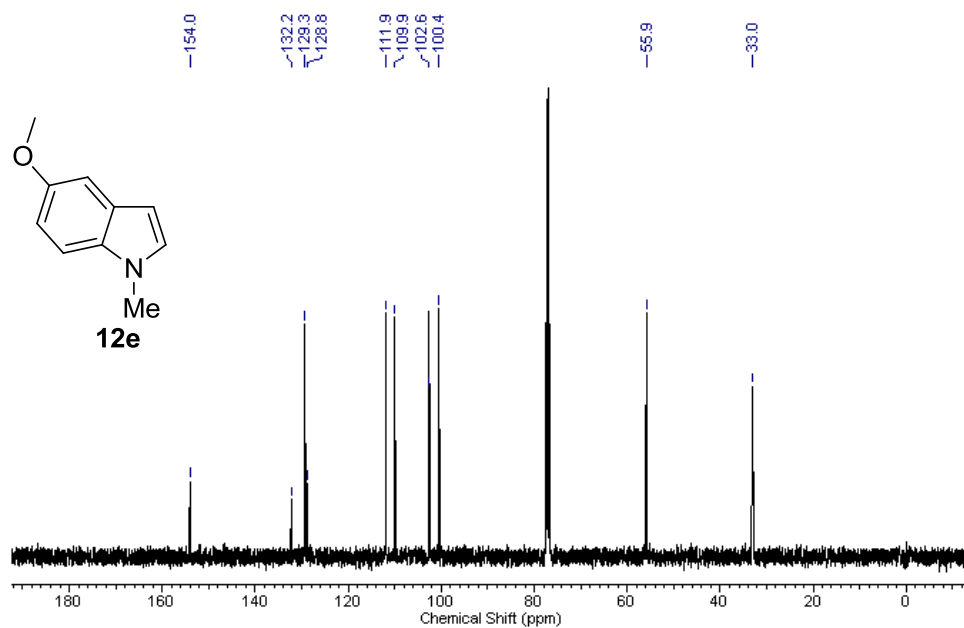


Figure 3.61 ¹³C NMR spectrum of 5-methoxy-1-methyl-1H-indole (**12e**)

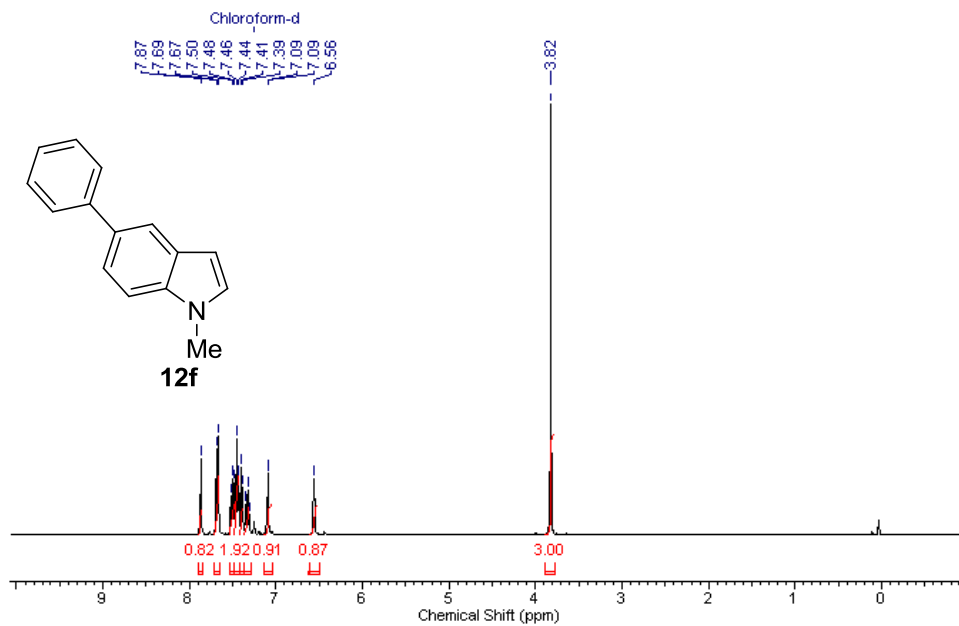


Figure 3.62 ¹H NMR spectrum of 1-methyl-5-phenyl-1H-indole (**12f**)

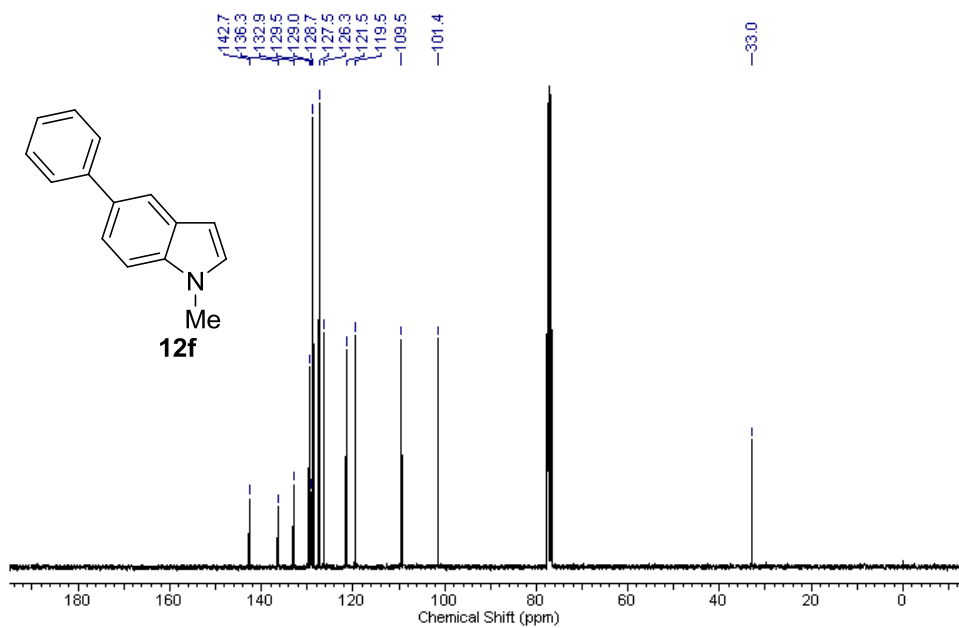


Figure 3.63 ¹³C NMR spectrum of 1-methyl-5-phenyl-1H-indole (**12f**)

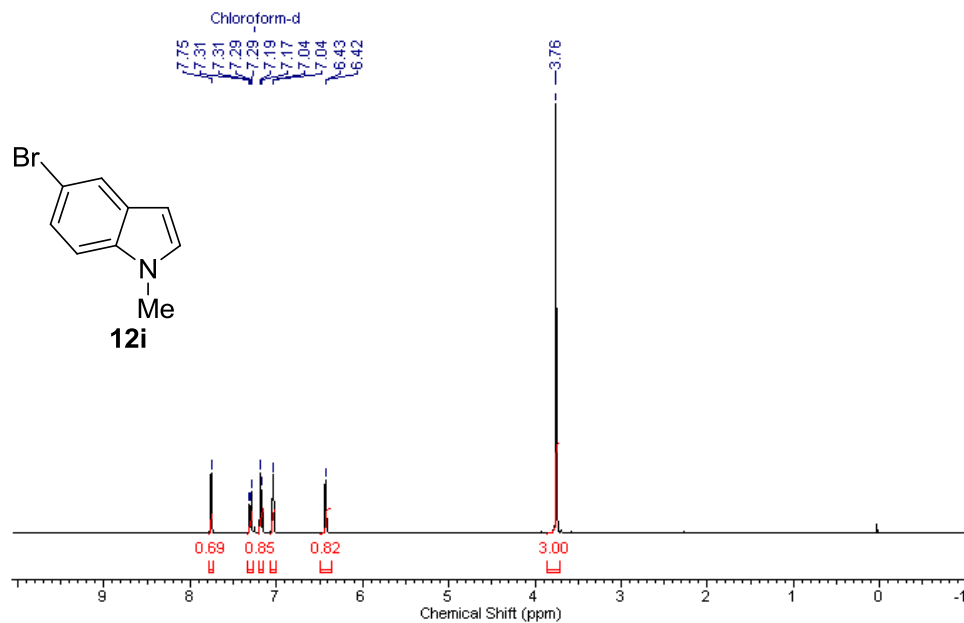


Figure 3.64 ¹H NMR spectrum of 5-bromo-1-methyl-1H-indole (**12i**)

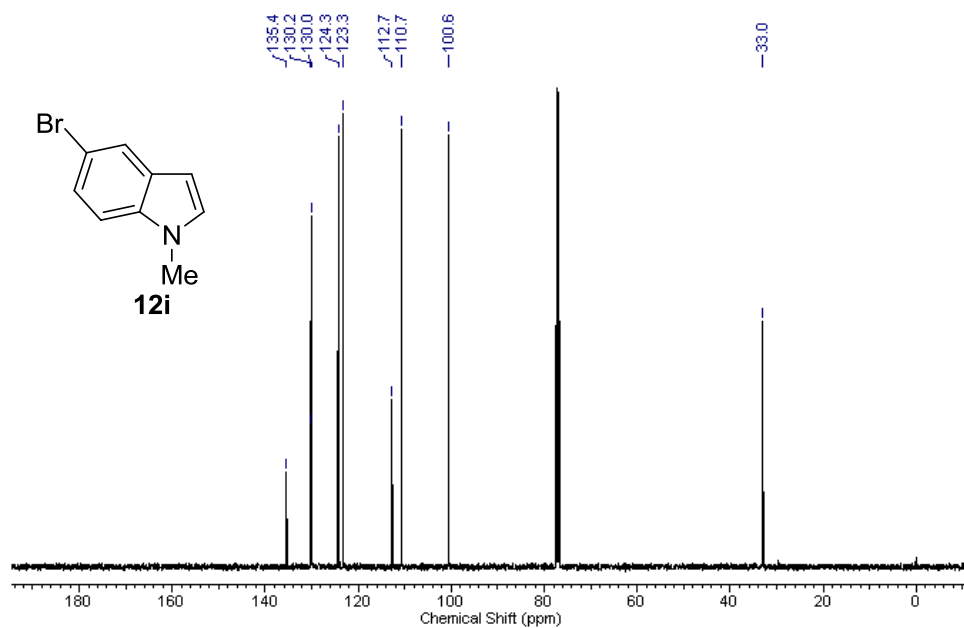


Figure 3.65 ¹³C NMR spectrum of 5-bromo-1-methyl-1H-indole (**12i**)

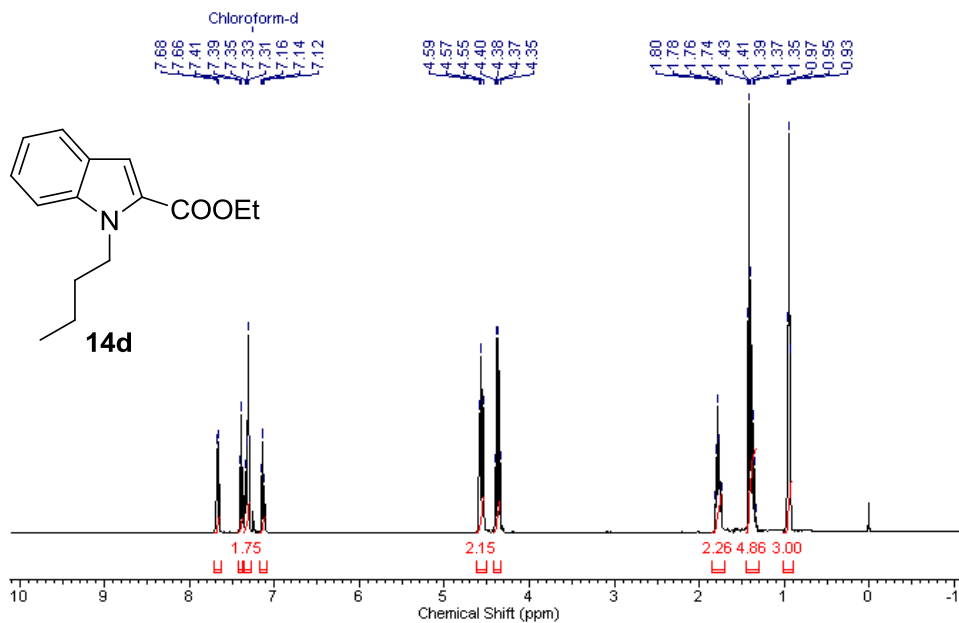


Figure 3.66 ¹H NMR spectrum of *ethyl 1-butyl-1H-indole-2-carboxylate* (**14d**)

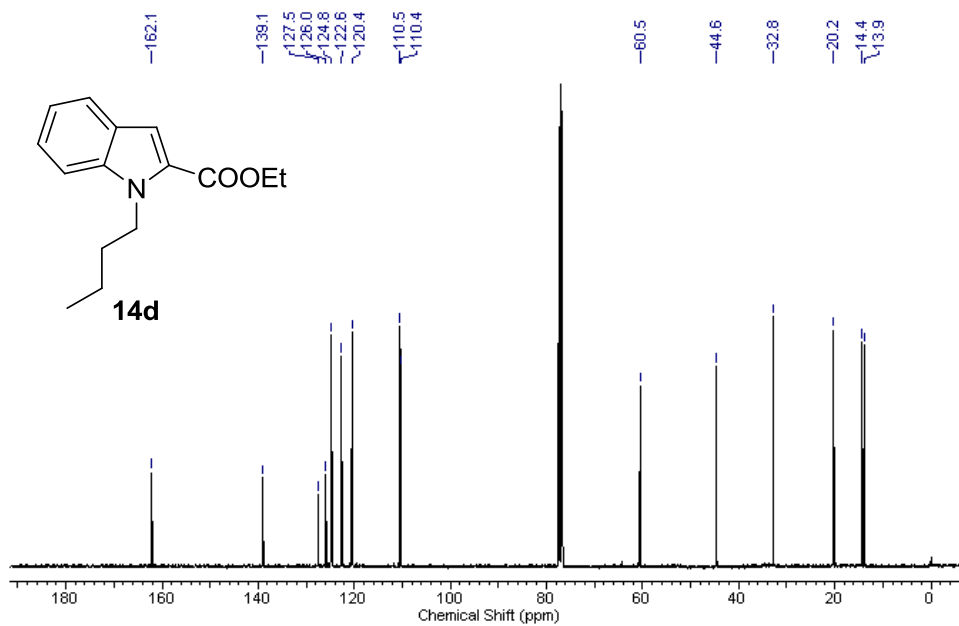


Figure 3.67 ¹³C NMR spectrum of *ethyl 1-butyl-1H-indole-2-carboxylate* (**14d**)

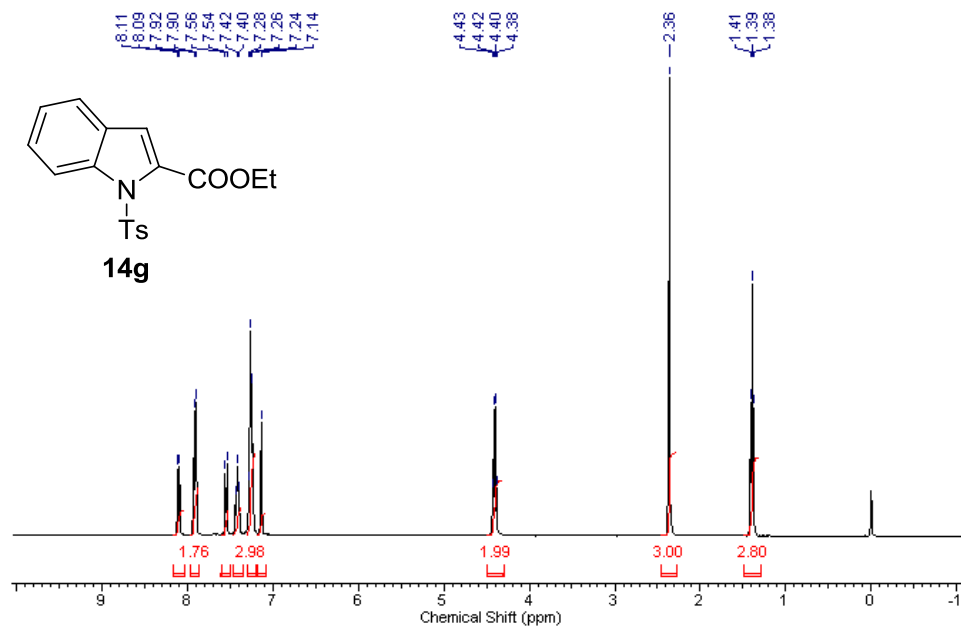


Figure 3.68 ¹H NMR spectrum of *ethyl 1-tosyl-1H-indole-2-carboxylate* (**14g**)

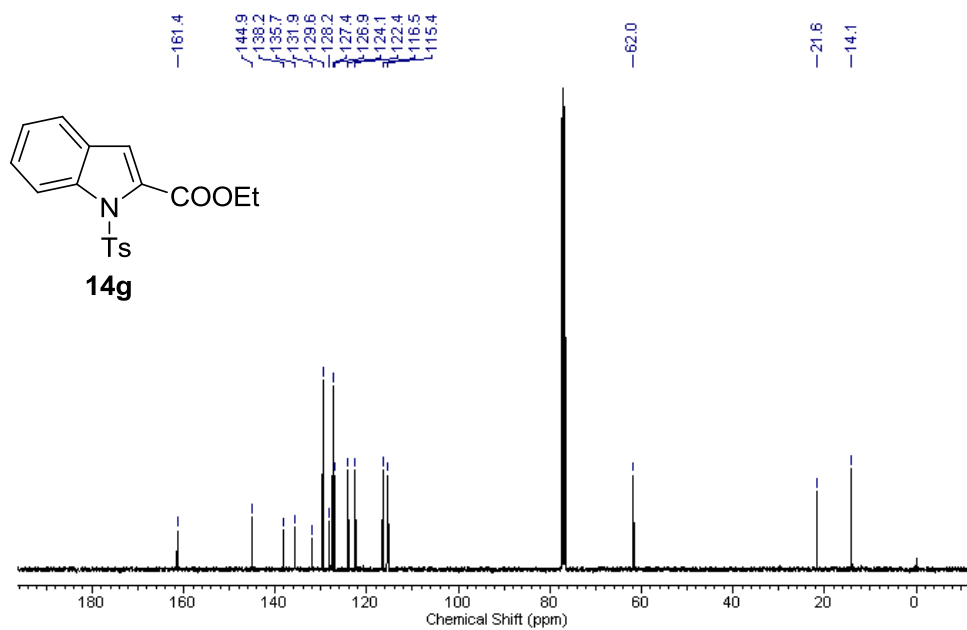


Figure 3.69 ¹³C NMR spectrum of *ethyl 1-tosyl-1H-indole-2-carboxylate* (**14g**)

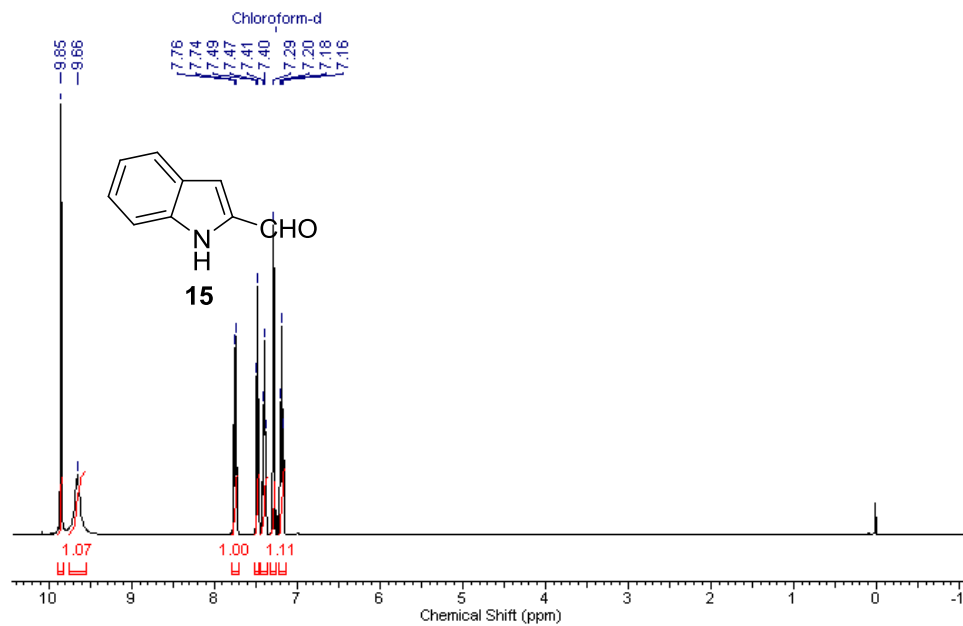


Figure 3.70 ¹H NMR spectrum of 1H-indole-2-carbaldehyde (15)

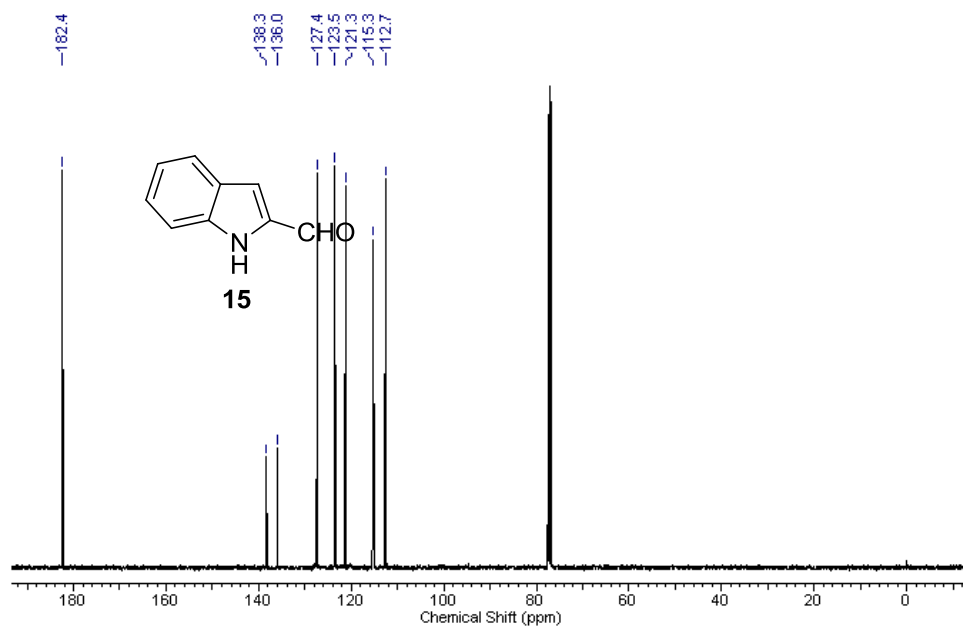


Figure 3.71 ¹³C NMR spectrum of 1H-indole-2-carbaldehyde (15)

3.5 References

- [1] Reniers J., Robert S., Frederick R., Masereel B., Vincent S., Wouters J. (2011), Synthesis and evaluation of β -carboline derivatives as potential monoamine oxidase inhibitors, *Bioorg Med Chem*, 19, 134–144 (DOI: 10.1016/j.bmc.2010.11.041)
- [2] Alekseyev R.S., Kurkin A.V., Yurovskaya M.A. (2009), γ -Carbolines and their hydrogenated derivatives 1 aromatic γ -carbolines: Methods of synthesis, chemical and biological properties, *Chem Heterocycl Comp*, 45, 889–925 (DOI: 10.1007/s10593-009-0373-9)
- [3] Pontecorvo M.J., Devous Sr M.D., Navitsky M., Lu M., Salloway S., Schaerf F.W., Jennings D., Arora A.K., McGeehan A., Lim N.C., Xiong H. (2017), Relationships between flortaucipir PET tau binding and amyloid burden, clinical diagnosis, age and cognition, *Brain*, 140, 748–763 (DOI: 10.1093/brain/aww334)
- [4] Snyder J.K., Wei W.G., Strosberg A.D., Kota S., Takahashi V. (2010), Small molecule inhibitors of Hepatitis C virus, *International Patent WO 2011/056630 A2*.
- [5] Guerquin-Kern J.L., Coppey M., Carrez D., Brunet A.C., Nguyen C.H., Rivalle C., Slodzian G., Croisy A. (1997), Complementary advantages of fluorescence and SIMS microscopies in the study of cellular localization of two new antitumor drugs, *Micros Res Tech*, 36, 287–295 (DOI: 10.1002/(SICI)1097-0029(19970215)36:4<287::AID-JEMT6>3.0.CO;2-J)
- [6] Ran X., Zhao Y., Liu L., Bai L., Yang C.Y., Zhou B., Meagher J.L., Chinnaswamy K., Stuckey J.A., Wang S. (2015) Structure-based design of γ -carboline analogues as potent and specific BET bromodomain inhibitors, *J Med Chem*, 58, 4927–4939 (DOI: 10.1021/acs.jmedchem.5b00613)
- [7] Ibrahim S.R., Mohamed G.A., Zayed M.F., Sayed H.M. (2015), Ingenines A and B, two new alkaloids from the Indonesian sponge

- Acanthostrongylophora ingens, Drug Res, 65, 361–365 (DOI: 10.1055/s-0034-1384577)
- [8] Naik P.N., Khan A., Kusurkar R.S. (2013), Intramolecular Diels–Alder reaction for the synthesis of tetracyclic carbazoles and isocanthines, Tetrahedron, 69, 10733–10738 (DOI: 10.1016/j.tet.2013.10.054)
- [9] Jia T., Wang J., Guo P., Yu J. (2015), Characterizations of cationic γ -carboline binding with double-stranded DNA by spectroscopic methods and AFM imaging, Org Biomol Chem, 13, 1234–1242 (DOI: 10.1039/C4OB01905A)
- [10] Otto R., Penzis R., Gaube F., Winckler T., Appenroth D., Fleck C., Tränkle C., Lehmann J., Enzensperger C. (2014), Beta and gamma carboline derivatives as potential anti-Alzheimer agents: A comparison, Eur J Med Chem, 87, 63–70 (DOI: 10.1016/j.ejmech.2014.09.048)
- [11] Shuvalov V.Y., Shestakov A.N., Kulakova L.A., Kuratova A.K., Vorontsova M.A., Sagitullina G.P. (2019), Synthesis of 4-nitro- γ -carbolines by Graebe–Ullmann reaction, Chem Heterocycl Comp, 55, 844–850 (DOI: 10.1007/s10593-019-02547-w)
- [12] Alekseev R.S., Kurkin A.V., Yurovskaya M.A. (2012), Use of the Graebe–Ullmann reaction in the synthesis of 8-methyl- γ -carboline and isomeric aromatic aza- γ -carbolines, Chem Heterocycl Comp, 48, 1235–1250 (DOI: 10.1007/s10593-012-1127-7)
- [13] Harbert C.A., Plattner J.J., Welch W.M., Weissman A., Koe B.K. (1980), Neuroleptic activity in 5-aryltetrahydro- γ -carbolines, J Med Chem, 23, 635–643 (DOI: 10.1021/jm00180a011)
- [14] Butler K.V., Kalin J., Brochier C., Vistoli G., Langley B., Kozikowski, A.P. (2010), Rational design and simple chemistry yield a superior, neuroprotective HDAC6 inhibitor, tubastatin A, J Am Chem Soc, 132, 10842–10846 (DOI: 10.1021/ja102758v)

- [15] Zhang H., Larock R.C. (2002), Synthesis of β - and γ -carbolines by the palladium/copper-catalyzed coupling and copper-catalyzed or thermal cyclization of terminal acetylenes, *Tetrahedron Lett*, 43, 1359–1362 (DOI: 10.1016/S0040-4039(02)00005-9)
- [16] Subba Reddy B.V., Swain M., Reddy S.M., Yadav J.S., Sridhar B. (2012), Gold-catalyzed domino cycloisomerization/Pictet–Spengler reaction of 2-(4-aminobut-1-yn-1-yl) anilines with aldehydes: synthesis of tetrahydropyrido [4,3-*b*] indole scaffolds, *J Org Chem*, 77, 11355–11361 (DOI: 10.1021/jo302068e)
- [17] Nissen F., Richard V., Alayrac C., Witulski B. (2011), Synthesis of β - and γ -carbolines via ruthenium and rhodium catalysed [2+ 2+ 2] cycloadditions of yne-ynamides with methylcyanoformate, *Chem Commun*, 47, 6656–6658 (DOI: 10.1039/C1CC11298H)
- [18] Wang T.T., Zhang D., Liao W.W. (2018), Versatile synthesis of functionalized β - and γ -carbolines via Pd-catalyzed C–H addition to nitriles/cyclization sequences, *Chem Commun*, 54, 2048–2051 (DOI: 10.1039/C8CC00040A)
- [19] Gutiérrez S., Sucunza D., Vaquero J.J. (2018), γ -Carboline synthesis by heterocyclization of TosMIC derivatives, *J Org Chem*, 83, 6623–6632 (DOI: 10.1021/acs.joc.8b00906)
- [20] Chepyshev S.V., Lujan-Montelongo J.A., Chao A., Fleming F.F. (2017), Alkenyl isocyanide conjugate additions: A rapid route to γ -carbolines, *Angew Chem, Int Ed*, 129, 4374–4377 (DOI: 10.1002/ange.201612574)
- [21] Hao W.J., Wang S.Y., Ji S.J. (2013), Iodine-catalyzed cascade formal [3+ 3] cycloaddition reaction of indolyl alcohol derivatives with enaminones: Constructions of functionalized spirodihydrocarbolines, *ACS Catal*, 3, 2501–2504 (DOI: 10.1021/cs400703u)

- [22] Lee Y., Klausen R.S., Jacobsen E.N. (2011), Thiourea-catalyzed enantioselective iso-Pictet–Spengler reactions, *Org Lett*, 13, 5564–5567 (DOI: 10.1021/ol202300t)
- [23] Toure B.B., Hall D.G. (2009), Natural product synthesis using multicomponent reaction strategies, *Chem Rev*, 109, 4439–4486 (DOI: 10.1021/cr800296p)
- [24] Held F.E., Guryev A.A., Fröhlich T., Hampel F., Kahnt A., Hutterer C., Steingruber M., Bahsi H., von Bojničić-Kninski C., Mattes D.S., Foertsch T.C. (2017), Facile access to potent antiviral quinazoline heterocycles with fluorescence properties via merging metal-free domino reactions, *Nat Commun*, 8, pp. 15071 (DOI: 10.1038/ncomms15071 (2017))
- [25] Tietze L.F., Rackelmann N. (2004), Domino reactions in the synthesis of heterocyclic natural products and analogs, *Pure Appl Chem*, 76, 1967–1983 (DOI: 10.1351/pac200476111967)
- [26] Tietze L.F., Modi A. (2000), Multicomponent domino reactions for the synthesis of biologically active natural products and drugs, *Med Res Rev*, 20, 304–322 (DOI: 10.1002/1098-1128(200007)20:4<304::AID-MED3>3.0.CO;2-8)
- [27] Nicolaou K.C., Edmonds D.J., Bulger P.G. (2006), Cascade reactions in total synthesis, *Angew Chem, Int Ed*, 45, 7134–7186 (DOI: 10.1002/anie.200601872)
- [28] Dai J., Dan W., Zhang Y., Wang J. (2018), Recent developments on synthesis and biological activities of γ -carboline, *Eur J Med Chem*, 157, 447–461 (DOI: 10.1016/j.ejmech.2018.08.015)
- [29] Martin S.F. (2009), Recent applications of imines as key intermediates in the synthesis of alkaloids and novel nitrogen heterocycles, *Pure Appl Chem*, 81, 195–204 (DOI: 10.1351/PAC-CON-08-07-03)
- [30] López-Pérez A., Adrio J., Carretero J.C. (2009), The phenylsulfonyl group as a temporal regiochemical controller in the catalytic

- asymmetric 1, 3-dipolar cycloaddition of azomethine ylides, *Angew Chem Int Ed*, 121, 346–349 (DOI: 10.1002/ange.200805063)
- [31] Dudhe P., Venkatasubbaiah K., Pathak B., Chelvam V. (2020), Serendipitous base catalysed condensation–heteroannulation of iminoesters: A regioselective route to the synthesis of 4, 6-disubstituted 5-azaindoles, *Org Biomol Chem*, 18, 1582–1587 (DOI: 10.1039/C9OB02657F)
- [32] Das T., Kayet A., Mishra R., Singh V.K. (2016), Highly fluorescent 1, 2-dihydropyrimido [1,6- α] indole: An efficient metal-free synthesis and photophysical study, *Chem Commun*, 52, 11231–11234 (DOI: 10.1039/C6CC05378E)
- [33] Frisch M.J., Trucks G.W., Schlegel H.B., et al., (2009), Gaussian 09, Revision D.01, Gaussian, Inc., Wallingford, CT
- [34] Becke A.D. (1988), Density-functional exchange-energy approximation with correct asymptotic behavior, *Phys Rev A*, 38, 3098–3100 (DOI: 10.1103/PhysRevA.38.3098)
- [35] Lee C., Yang W., Parr R.G. (1988), *Phys Rev B: Condens Matter Mater Phys*, 37, 785–789
- [36] Zhao G.J., Liu J.Y., Zhou L.C., Han K.L. (2007), Site-selective photoinduced electron transfer from alcoholic solvents to the chromophore facilitated by hydrogen bonding: A new fluorescence quenching mechanism, *J Phys Chem B*, 111, 8940–8945 (DOI: 10.1021/jp0734530)
- [37] Clerici F., Gelmi M.L., Rossi L.M. (1987), N-arylsulfonylamidines. II: A new synthesis of ketones from N-tosylamidines and organolithium compounds, *Synthesis (Stuttgart)*, 11, 1025–1027 (DOI: 10.1055/s-1987-28159)
- [38] Biswas S., Singh V., Batra S. (2010), Morita–Baylis–Hillman reaction of indole-2-carboxaldehyde: New vistas for indole-annulated systems, *Tetrahedron*, 66, 7781–7786 (DOI: 10.1016/j.tet.2010.07.078)

- [39] Meguellati A., Ahmed-Belkacem A., Yi W., Haudecoeur R., Crouillère M., Brillet R., Pawlotsky J.M., Boumendjel A., Peuchmaur M. (2014), B-ring modified aurones as promising allosteric inhibitors of hepatitis C virus RNA-dependent RNA polymerase, *Eur J Med Chem*, 80, 579–592 (DOI: 10.1016/j.ejmech.2014.04.005)
- [40] Karadeolian A., Kerr M.A. (2010), Total synthesis of (+)-isatisine A, *J Org Chem*, 75, 6830–6841 (DOI: 10.1021/jo101209y)
- [41] Carlier P.R., Lam P.C.H., Wong D.M. (2002), Catalytic asymmetric synthesis of protected tryptophan regioisomers, *J Org Chem*, 67, 6256–6259 (DOI: 10.1021/jo025964i)
- [42] Santaniello, E. (1979), N-alkylation of pyrrole and indole catalyzed by crown ethers, *Synthesis*, 8, 617–618 (DOI: 10.1055/s-1979-28783)
- [43] Kiguchi T., Kuninobu N., Takahashi Y., Yoshida Y., Naito T. (1989), One-pot synthesis of indoles from 1-benzyl-2, 3-dihydroindoles, *Synthesis (Stuttgart)*, 10, 778–781 (DOI: 10.1055/s-1989-28358)
- [44] Jiang X., Tiwari A., Thompson M., Chen Z., Cleary T.P., Lee T.B. (2001), A practical method for N-methylation of indoles using dimethyl carbonate, *Org Proc Res Dev*, 5, 604–608 (DOI: 10.1021/op0102215)
- [45] Quasdorf K.W., Riener M., Petrova K.V., Garg N.K. (2009), Suzuki–Miyaura coupling of aryl carbamates, carbonates, and sulfamates, *J Am Chem Soc*, 131, 17748–17749 (DOI: 10.1021/ja906477r)
- [46] Nowacki M., Wojciechowski K. (2018), Transition-metal-free [3+ 3] annulation of indol-2-ylmethyl carbanions to nitroarenes, a novel synthesis of indolo [3, 2-b] quinolines (quindolines), *Beilstein J Org Chem*, 14, 194–202 (DOI: 10.3762/bjoc.14.14)
- [47] McNulty J., Keskar K., Bordón C., Yolken R., Jones-Brando L. (2014), Total synthesis of the cyanobacterial metabolite nostodione A: discovery of its antiparasitic activity against *Toxoplasma gondii*, *Chem Commun*, 50, 8904–8907 (DOI: 10.1039/C4CC03904A)

- [48] Pérez-Serrano L., Casarrubios L., Dominguez G., González-Pérez P., Pérez-Castells J. (2002), Synthesis of enynoindoles via vinyl and ethynyl indoles, *Synthesis*, 13, 1810–1812 (DOI: 10.1055/s-2002-33921)

Chapter 4

One-pot synthesis of furo[3,2-*c*]pyridines and benzofuro[3,2-*c*]pyridines: Development of isatin molecular hybrids for treatment of tuberculosis

4.1 Introduction

In the global tuberculosis report-2020, World Health Organisation (WHO) admits that despite all the efforts to eradicate tuberculosis (TB), the number of TB cases is falling very slowly compared to WHO's target in its initiative called 'End TB strategy'. Tuberculosis is the leading cause of death from a single infectious agent surpassing HIV/AIDS. The emerging drug-resistance is also reflected in the increased death toll. In the calendar year of 2019, an estimated 1.4 million TB-related deaths have been recorded, with an over 10% increase in multidrug-resistant TB cases [1].

Mycobacterium tuberculosis (Mtb) strains resistant to the conventional anti-TB drugs, isoniazid (INH) and rifampicin, are termed as multidrug-resistant TB (MDR-TB) strains. Extensively drug-resistant TB (XDR-TB) is a severe case of multidrug resistance in which pathogens are resistant to all fluoroquinolone and other second-line anti-TB injectable drugs such as amikacin, kanamycin, or capreomycin. Both MDR-TB and XDR-TB do not respond to the standard anti-TB drugs and are emerging threats to the success of anti-TB programs [2]. More recently, two new drugs, bedaquiline (BDQ) and delamanid (DLM) have been introduced to counter these drug-resistant pathogens. Unfortunately, the controversies related to bedaquiline uses have introduced an urgent need to develop new chemical entities with improved efficacy and alternative working principles.

There is a rapid increase in drug resistance of Mtb, mainly due to its bacterial cell wall's complex structure. The outermost layer of the bacterial cell wall in Mtb is made up of complex fatty acids called mycolic acid (MA). The mycolic acid layer makes a hydrophobic protective layer around the bacteria and is critical for its viability and virulence. The biosynthetic pathway for MA is a validated target for many first and second-line anti-TB drugs. For instance, isoniazid (INH) pro-drug interactions with NAD (nicotinamide adenine dinucleotide) inhibit enoyl-ACP reductase, an important enzyme in MA synthesis. This was a key strategy against Mtb for several decades. Unfortunately, a mutation in the *inhA* gene and its promoter region has complicated the situation by conferring resistance to INH and the second-line TB drug ethionamide (ETH) [3].

In Mtb, more than 20 enzymes together make a multi-enzyme complex for the biosynthesis of MA. Hence, this pathway is crucial for developing new TB drugs, especially in the context of the emergence of drug resistance. Polyketide synthetase 13 (Pks13) performs the final assembly step of the mycolic acid synthesis, and recently it has emerged as a novel drug target for the treatment of MDR-TB and XDR-TB [4].

Furopyridines and benzofuropyridines are less explored heterocycles in comparison to their iso-structural analogs indoles and carbolines. In a typical furopyridine ring, an electron-rich five-membered furan ring is fused with another electron-deficient six-membered pyridine ring. This unusual structural framework confers the structural motif with unique chemical properties and makes them challenging to synthesize in the laboratory. The first and the most apparent synthetic strategy involves forming a furan ring from a suitable pyridine substrate. However, the use of i) specific pyridine substrates as building blocks, ii) expensive heavy metal catalysts for coupling reactions, and iii) multiple synthetic and purification steps leading to limited yields of the desired product confines

the overall scope of the strategy. Alternatively, a few research groups have thoroughly investigated pyridine ring formation over a furan derivative [5]. The synthetic protocol developed by Shiotani and Morita [6], Friedlander-type [7], and Combes-type reactions of 2-amino furan derivatives [8] has been extensively used to synthesize biologically active compounds of this class. In the last two decades, the furopyridine core has been exploited much in a variety of synthetic drug molecules such as anti-mycobacterial agents [9], MCH-1 antagonists [10], and kinase inhibitors [11]. Therefore, it is pertinent to look for alternative protocols for the synthesis of furopyridines and related compounds.

4.2 Results and discussion

Chemical architecture-wise inhibitors of Pks13, including the most potent TAM16 (MIC 0.09 μ M), belong to benzofuran-5-ol core (Figure 4.1), which can be obtained only by multi-step synthetic procedures [12]. Moreover, Fumagalli *et al.* [9] have identified a few new furopyridine derivatives targeting the same protein due to their structural similarity and almost identical physicochemical properties.

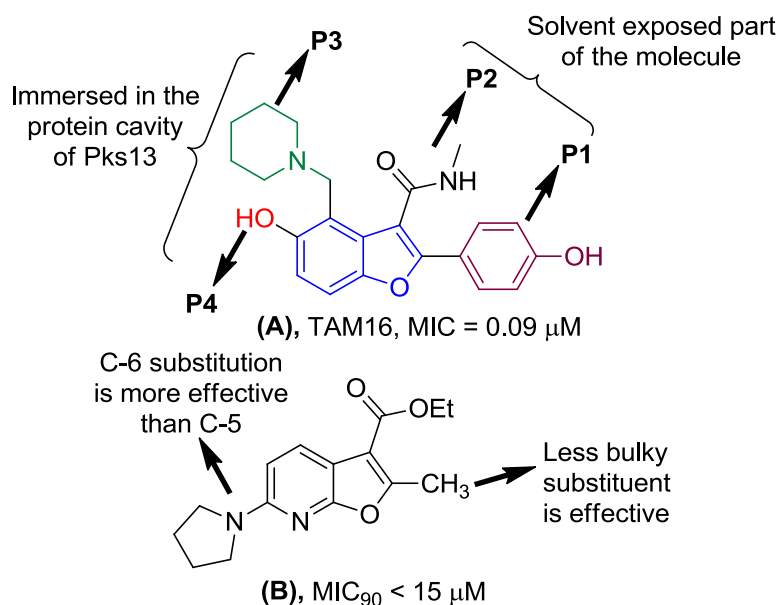


Figure 4.1 Potent anti-mycobacterial compounds targeting Pks13 (A) the structure of TAM16, (B) the furopyridine derivative active against MDR-TB

During our exploration of heterocyclic iminoesters as a valuable synthetic building block, we serendipitously discovered metal and solvent-free one-pot synthetic protocol for the synthesis of fused aza-heteroaromatics. Several new azaindoles [13] and carboline [14] derivatives have been synthesized and screened for their biological and photophysical properties. Further, we envisaged that we can synthesize novel furopyridine derivatives by this newly developed protocol for aza-heteroaromatics and explore the activity of new molecular scaffolds against recently emerged target protein Pks13 for the treatment of tuberculosis.

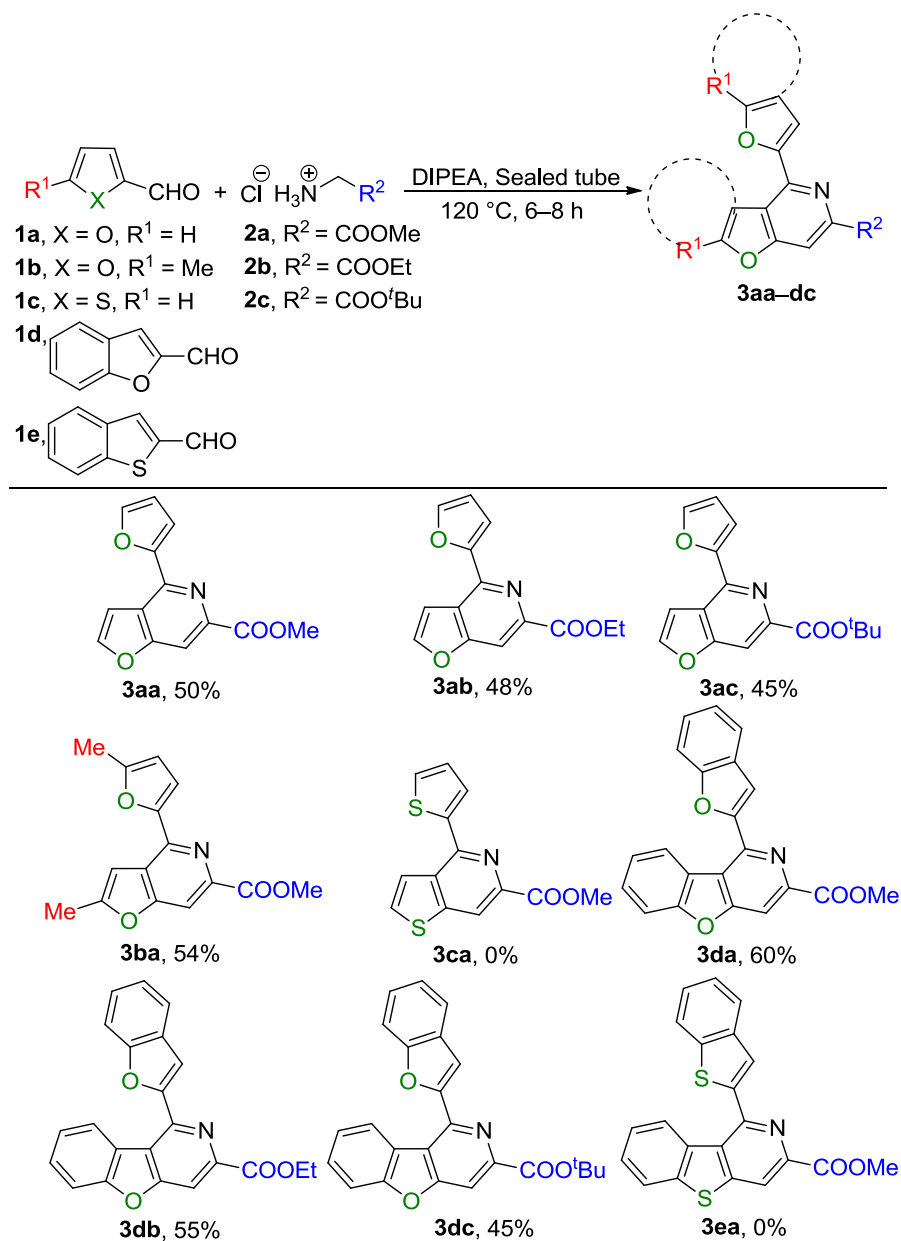
This chapter describes the synthesis of substituted furo[3,2-*c*]pyridines, benzofuro[3,2-*c*]pyridines, isatin molecular hybrids, and their applications in the treatment of tuberculosis. Initially, we explored the developed methodology for the preparation of methyl 4-(furan-2-yl)furo[3,2-*c*]pyridine-6-carboxylate **3aa** by a reaction between furan-2-carboxaldehyde **1a** and glycine methyl ester hydrochloride **2a** in the presence of the Hunig's base (DIPEA) in toluene at room temperature. In this attempt, a trace amount of corresponding imine product was observed, which could not be isolated or characterized. However, when we heated the reaction mixture to reflux, we were able to identify the desired furo[3,2-*c*]pyridine **3aa**, albeit in a poor yield of 25% (Entry 1, Table 4.1).

In order to improve the yield of **3aa**, we systematically scrutinized several reaction conditions. During optimization experiments, we examined the heterocyclization reaction using a strong inorganic base, sodium hydride (Entry 2, Table 4.1), to weak inorganic bases like K₂CO₃, Cs₂CO₃ (Entries 3-4, Table 4.1), and organic bases such as Et₃N, and

DBU (Entries 5-6, Table 4.1), in polar aprotic solvents such as THF, Et₂O, DMF to less polar solvents like toluene. In most of these reaction conditions, the substrate **1a** underwent decomposition into a tar-like substance that remained insoluble in organic solvents (Table 4.1). Finally, we were able to optimize the heterocyclization reaction under solvent-free one-pot protocol, wherein heating furan-2-carboxaldehyde (**1a**, 2.0 equiv.) and glycine methyl ester hydrochloride (**2a**, 1.0 equiv.) with DIPEA (3.5 equiv.) in a sealed tube at 120 °C resulted in formation of **3aa** in a moderate yield of 50% (Entry 7, Table 4.1).

Entry	Base (3.5 equiv.)	Solvent	Temp.	Yield of 3aa
1	DIPEA	Toluene ^a	RT to reflux	25%
2	NaH	THF ^a	RT to reflux	No product
3	K ₂ CO ₃	Et ₂ O ^a	RT to reflux	No product
4	Cs ₂ CO ₃	DMF ^a	RT to reflux	No product
5	Et ₃ N	Toluene ^a	RT to reflux	No product
6	DBU	Toluene ^a	RT to reflux	Trace
7	DIPEA ^b	---	120 °C	50%

Table 4.1 Optimization of reaction conditions: ^aReactions were monitored by TLC for 3 h at room temperature followed by reflux for 16 h in an appropriate solvent; ^bSolvent-free reaction was carried out in a 25 mL borosilicate sealed tube in a preheated oil bath at 120 °C under normal atmosphere



Scheme 4.1 Synthesis of furo[3,2-*c*]pyridine **3aa–ba** and benzofuro[3,2-*c*]pyridine derivatives **3da–dc**

The optimized reaction conditions were used to prepare other derivatives such as **3ab** and **3ac**, showing that the change of alkyl ester group on glycine ester hydrochloride salt does not affect the heterocyclization reaction. In general, glycine methyl ester HCl salt **2a** was more effective in terms of higher yields in a given transformation compared to an ethyl ester and *tert*-butyl esters of glycine.

The methodology was further extended to other 5-substituted furan-2-carboxaldehyde **1b** to examine the scope of the reaction for a general furo[3,2-*c*]pyridine synthesis, and the results are summarized in Scheme 4.1. In general, electron-rich 5-methyl furan-2-carboxaldehyde **1a** having higher nucleophilicity in the furan ring resulted in corresponding 2,4,6-substituted furo[3,2-*c*]pyridine **3ba** in 54% yield.

However, when thiophene-2-carboxaldehyde **1c** was utilized as the substrate to prepare the corresponding thieno[3,2-*c*]pyridine **3ca**, the reaction failed to yield without trace of formation of **3ca** due to possible decomposition of **1c** within the first 15-minutes of the reaction.

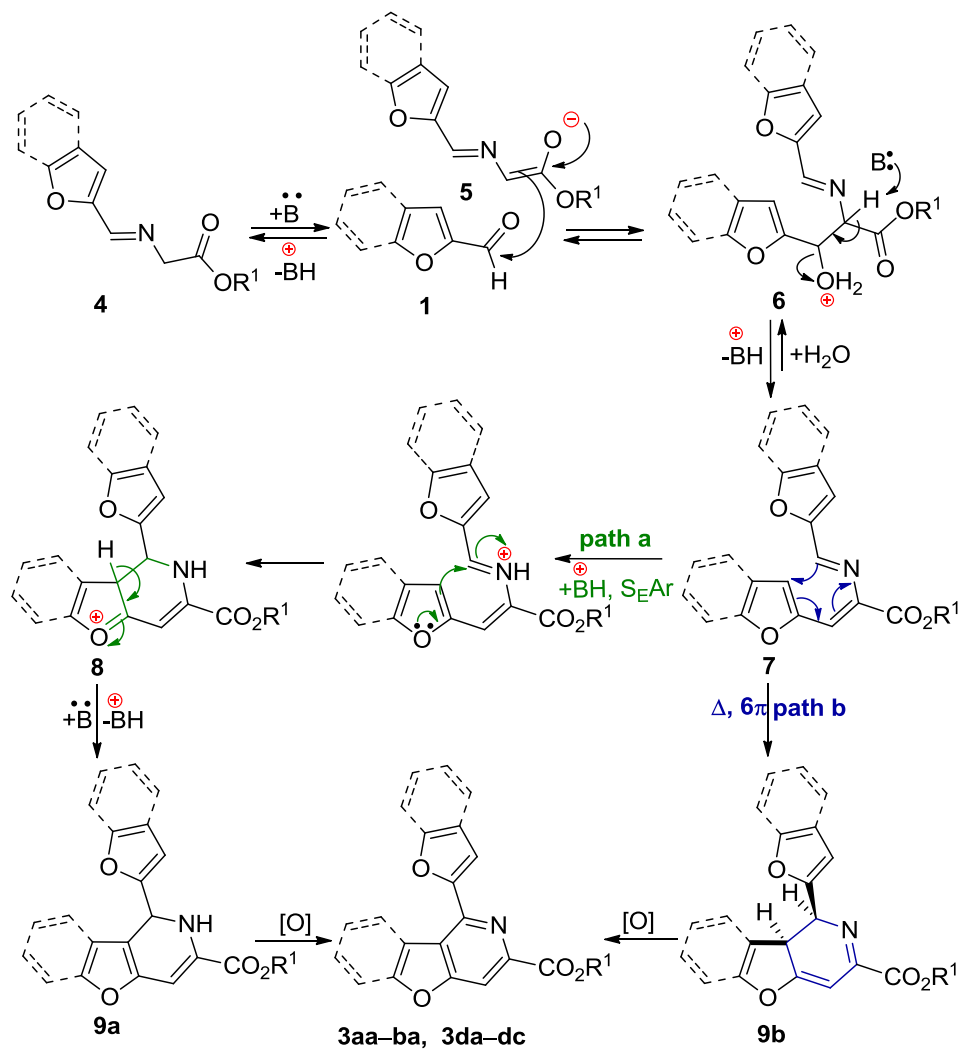
Interestingly when benzo-fused furan-2-carboxaldehyde derivative such as benzofuran-2-carboxaldehyde **1d** was reacted with glycine methyl ester hydrochloride **2a** in the presence of the Hunig's base (DIPEA) in a sealed tube under optimized reaction conditions, the corresponding methyl 1-(benzofuran-2-yl)benzofuro[3,2-*c*]pyridine-3-carboxylate **3da** was obtained in 60% yield. With the success of this reaction, additionally, the heterocyclization reaction was found to be general with glycine ethyl ester hydrochloride **2b** and glycine *tert*-butyl ester hydrochloride **2c** to form the corresponding ethyl 1-(benzofuran-2-yl)benzofuro[3,2-*c*]pyridine-3-carboxylate **3db** and *tert*-butyl 1-(benzofuran-2-yl)benzofuro[3,2-*c*]pyridine-3-carboxylate **3dc** in 55% and 45% yields, respectively.

Next, our attempts to convert benzo[*b*]thiophene-2-carboxaldehyde **1e** into the corresponding benzo[4,5]thieno[3,2-*c*]pyridine **3ea** by following a similar protocol does not result in the formation of **3ea** probably due to decomposition of the substrate **1e**.

The probable mechanistic explanation (Scheme 4.2) for the formation of furo[3,2-*c*]pyridine **3aa–ba** and benzofuro[3,2-*c*]pyridine derivatives **3da–dc** involves the initial formation of *trans* iminoester **4**

from furan-2-carboxaldehydes **1a–b** or benzofuran-2-carboxaldehyde **1d** and glycine alkyl esters **2a–c**. The Hunig's base, DIPEA, helps abstracts active methylene proton from iminoester **4** to generate enolate ion **5**, which undergoes nucleophilic addition with another molecule of aldehyde **1** to furnish iminoalcohol intermediate **6**. The iminoalcohol **6** undergoes dehydration under the reaction condition to give iminoenamine intermediate **7**, which plays a decisive role in determining ring closure *via* path a or path b.

In path a, protonation of imine nitrogen in **7** by conjugate acid (+BH) drives the reaction in the forward direction for electrophilic aromatic substitution at the 3-position of the furan unit to form a carbon-carbon bond in the intermediate **8**. Further, proton abstraction in **8** by base gives 2-substituted 4-(furan-2-yl)-4,5-dihydrofuro[3,2-*c*]pyridine-6-carboxylate or 1-(benzofuran-2-yl)-1,2-dihydrobenzofuro[3,2-*c*]pyridine-3-carboxylate intermediate **9a**. In path b, the intermediate **7** would undergo thermal 6 π -electrocyclic reaction of a conjugated triene system to form 2-substituted 4-(furan-2-yl)-4,8-dihydrofuro[3,2-*c*]pyridine-6-carboxylate or 1-(benzofuran-2-yl)-1,11-dihydrobenzofuro[3,2-*c*]pyridine-3-carboxylate intermediate **9b**. *In situ* oxidation of **9a** or **9b**, probably from the dissolved oxygen present in the reaction mixture, leads to the formation of the furo[2,3-*c*]pyridine **3aa–ba** and benzofuro[2,3-*c*]pyridine **3da–dc** derivatives described in this chapter.



Scheme 4.2 Plausible mechanism for the formation of 4-(furo-2-yl) furo[3,2-*c*]pyridine-6-carboxylate **3aa–ba** and 1-(benzofuro-2-yl) benzofuran[3,2-*c*]pyridine-3-carboxylate **3da–3dc** derivatives

During the formation of furo or benzofuro[3,2-*c*]pyridines, the substrates, **1a–c** and **1d** were exclusively transformed to 4,5-dihydrofuro[3,2-*c*]pyridines or 1,2-dihydrobenzofuro[3,2-*c*]pyridines **9a** and no traces of furo or benzofuro[3,2-*d*]pyridine regioisomers **9c** were observed, which proves that the heterocyclization reaction is highly regiospecific (Figure 4.2). The exclusive formation of furo or benzofuro[3,2-*c*]pyridine regioisomer is explained by proposing an intermediate **7** before the heterocyclization reaction takes place. Furan or

benzofuran ring A predominantly participates in electrophilic aromatic substitution on the intermediate **7** over Michael's addition of furan or benzofuran ring B.

Density functional theoretical calculations were carried out using the B3LYP/6-311++G** level of theory to understand the reaction pathways (path a or path b) and regioselectivity for the formation of furo or benzofuro[3,2-*c*]pyridines from **9a** or **9b** and furo or benzofuro[3,2-*d*]pyridine regioisomers **9c** from **7**.

First, we have calculated the total energies of the two intermediates, **9a** and **9b**, formed from **7** *via* two different pathways, as shown in scheme 4.2. The calculated total energies of the intermediates show that the intermediate **9a** generated *via* path a to be more stable (by 21.7 or 17.9 Kcal/mol respectively for furo[3,2-*c*]pyridine or benzofuro[3,2-*c*]pyridine derivatives) compared to the intermediate **9b** generated *via* path b. Therefore, we can conclude that path a is preferable over path b based on the total energies of the intermediates (Scheme 4.2).

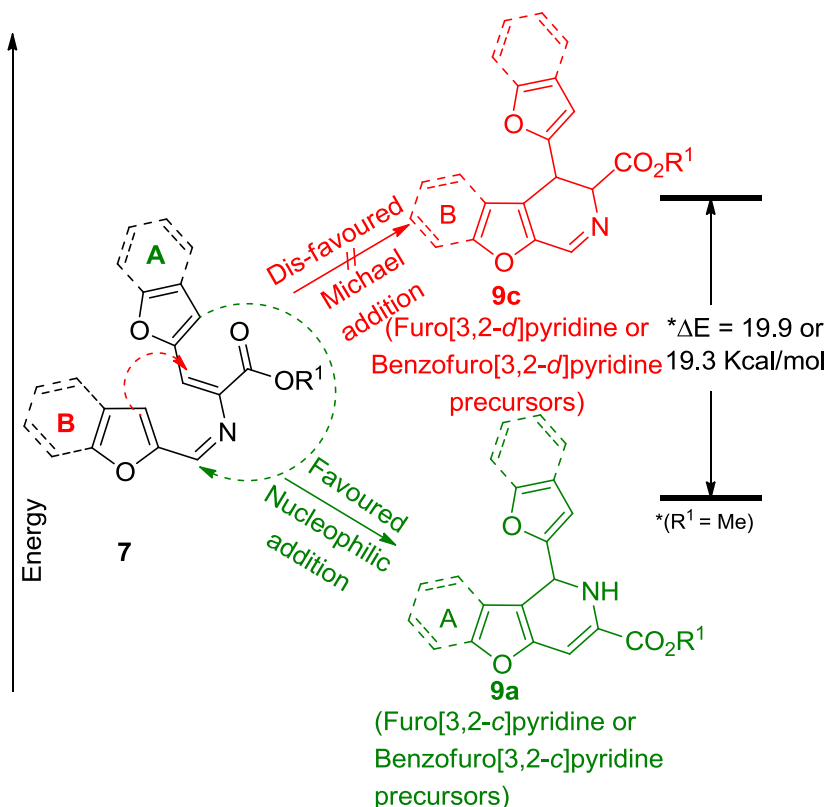


Figure 4.2 DFT relative energy calculation for the formation of furo or benzofuro[3,2-*c*]pyridines **9a** over furo or benzofuro[3,2-*d*]pyridines **9c** regioisomer using B3LYP/6-311++G** level of theory

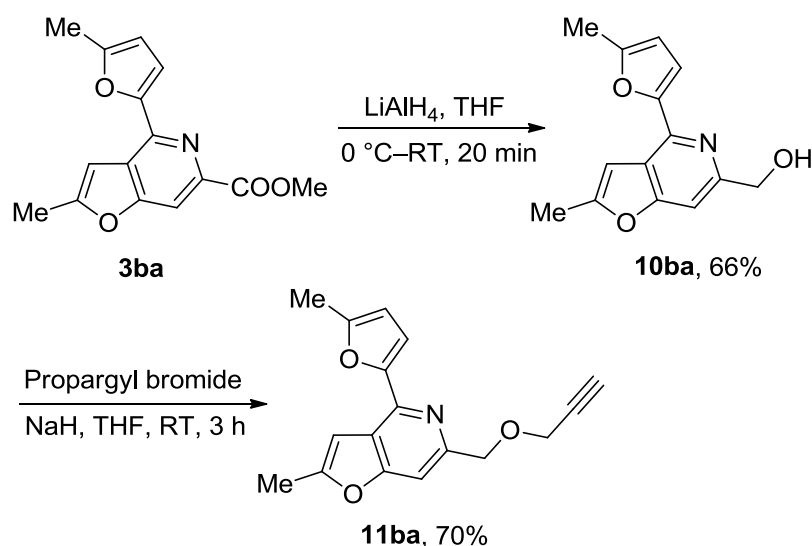
Next, we have calculated the zero-point corrected total energies of the intermediates **9a**, **9b**, and **9c** to understand the regioselectivity of the formation of furo or benzofuropyridines through electrophilic aromatic substitution (**9a**), thermal 6π -electrocyclization (**9b**) or Michael addition (**9c**) reactions (Scheme 4.2 and Figure 4.2). The calculated total energy values show that the precursor, 4,5-dihydrofuro[3,2-*c*]pyridine or 1,2-dihydrobenzofuro[3,2-*c*]pyridine, **9a** formed *via* electrophilic aromatic substitution is 19.9 or 19.3 Kcal/mol more stable, respectively, over the product, 4,5-dihydrofuro[3,2-*d*]pyridine or 1,2-dihydrobenzofuro[3,2-*d*]pyridine regioisomer, **9c** formed *via* Michael addition reaction. This indicates that the furo or benzofuro[3,2-*c*]pyridine regioisomer **9a** is thermodynamically stable over furo or benzofuro[3,2-*d*]pyridine regioisomer **9c** (Figure 4.2).

The use of molecular hybrids in drug discovery programs is a relatively new concept, in which two pharmacophores are chemically combined to a single molecular entity for synergistic effect [15]. Isatin or indoline-2,3-dione is a chemically and biologically very stable molecule. It has been extensively used in drug design because of its innate pharmacological activities as anti-TB, antibacterial, antiviral, antitumour, anticonvulsant, antihelmintic, antidepressant, anti-inflammatory and antioxidant agent. The anti-mycobacterial properties of isatin core have been exploited to the most in the form of quinolone-isatin, thiazole-isatin, tetrahydropyrimidine-isatin, thiolactone-isatin, isoniazid-isatin, and β -lactam-isatin hybrids [16].

Gao *et al.* have recently developed a benzofuran-isatin hybrid series against MTB H₃₇Rv and MDR-TB strains [17]. This study inspired

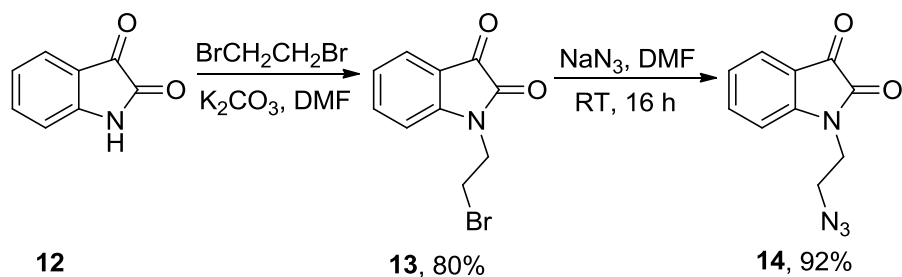
us to build novel furopyridine-isatin hybrids for anti-mycobacterial properties. According to our hypothesis, the furopyridine moiety will bind to the target Pks13 enzyme due to its structural similarity with the benzofuran core of the TAM16 molecule to arrest the mycolic acid synthesis, and the isatin unit will be able to kill the bacteria.

The furopyridine derivative **3ba** was reduced by lithium aluminum hydride in polar aprotic solvent to afford corresponding primary alcohol **10ba** in 66% yield to achieve this target. Alcohol **10ba** was propargylated by generating alkoxide ion using a strong base, sodium hydride, and subsequent nucleophilic substitution with propargyl bromide (80% in toluene) to provide the terminal alkyne **11ba** in 70% yield (Scheme 4.3).



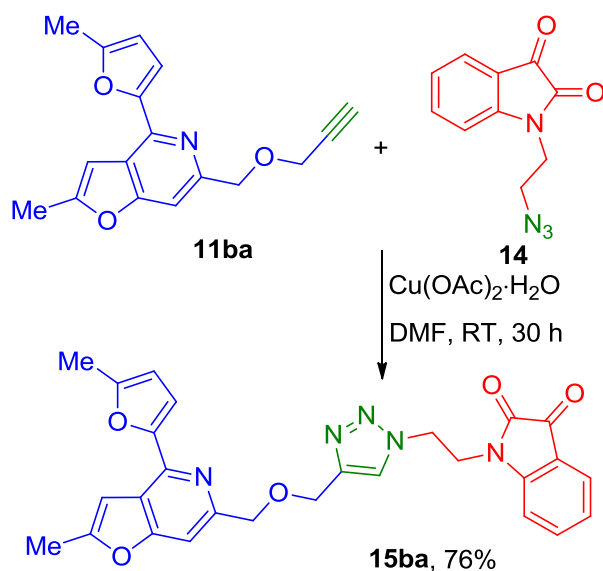
Scheme 4.3 Synthesis of terminal alkyne derivative **11ba**

Isatin **12** was treated with 1,2-dibromoethane in the presence of K_2CO_3 in DMF to obtain *N*-(2-bromoethyl)indoline-2,3-dione **13** in 80% yield. The bromine atom in **13** can be readily replaced with azido group by overnight reaction with sodium azide in dimethylformamide (DMF) at room temperature to afford **14** in 92% yield (Scheme 4.4).



Scheme 4.4 Synthesis of azido isatin derivative **14**

The final step of this multistep synthesis was crucial, wherein, terminal alkynes **11ba** and azide **14** were coupled by standard click chemistry reaction, using monohydrated copper acetate as a catalyst for 1,3-dipolar cycloaddition in dimethylformamide (DMF) solvent at room temperature to afford the final molecule fuopyridine-isatin hybrid **15ba** in 76% yield (Scheme 4.5).



Scheme 4.5 Synthesis of triazole-tethered fuopyridine-isatin hybrid **15ba**

Next, we were curious to examine the anti-mycobacterial activity of this newly developed fuopyridine-isatin hybrid **15ba**. We began our studies with a drug-susceptible, non-virulent strain of the Mtb. *Mycobacterium smegmatis* single colony was inoculated in 7H9

Middlebrook media containing Tween80 and incubated at 37 °C for 36 h for visible bacterial culture. OD₆₀₀ of the bacterial culture was measured and set to 0.1 optical density (OD). A mixture of bacterial culture and different concentrations of **15ba** was prepared in different microcentrifuge tubes, maintaining 200 µL as the final volume of the mixture for all the concentrations. The above mixtures were incubated at 37 °C for different time durations such as 0, 6, 12, and 24 h. The mixtures were serially diluted up to 10⁻⁵ M concentrations of **15ba**. 5 µL of each of the mixture was drawn-out for plating in Petri-dishes containing 7H9/LB agar media. The Petri-dishes were further incubated at 37 °C for 36 h or more for visible bacterial colonies to appear. Then, colony counting was performed using the colony counter. The results of this study are depicted in figure 4.3. To our delight, bacterial growth was inhibited to a great extent while using 50–100 µM concentration of fuopyridine-isatin hybrid **15ba**.

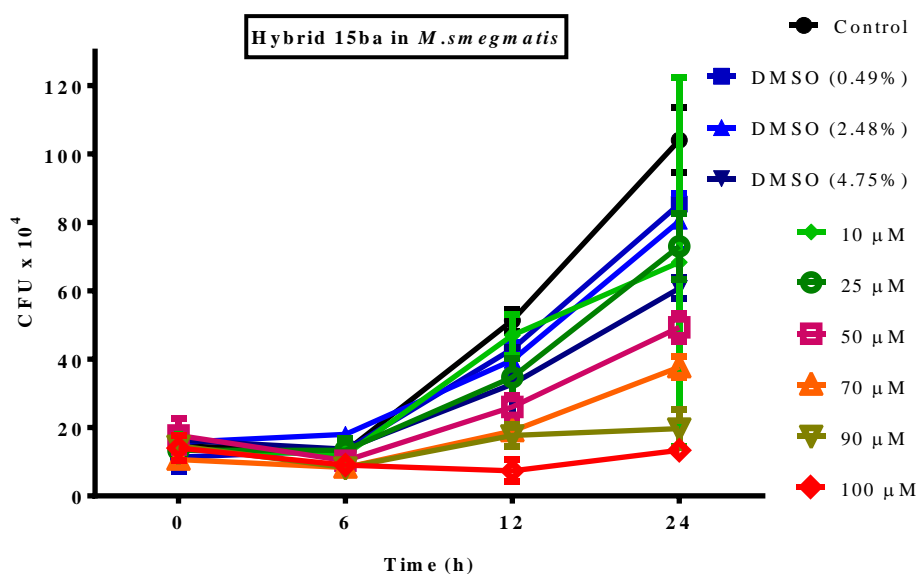


Figure 4.3 Anti-tuberculosis activity of fuopyridine-isatin hybrid **15ba** on non-virulent strain *Mycobacterium smegmatis*; IC₅₀ = 50–100 µM

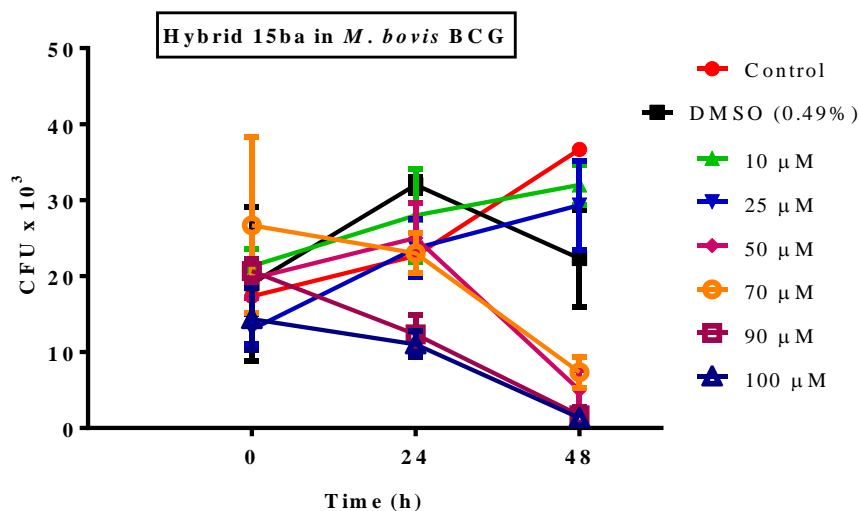


Figure 4.4 Anti-tuberculosis activity of furopyridine-isatin hybrid **15ba** on virulent strain *Mycobacterium bovis* BCG; $IC_{50} = 50\text{--}100\text{ }\mu\text{M}$

With the initial success, we decided to perform the anti-mycobacterial activity of **15ba** on the virulent strain of the mycobacterium. Following the protocol mentioned earlier, we performed the anti-mycobacterial activity, with a virulent strain of mycobacterium, *Mycobacterium bovis* BCG (7H9 Middlebrook media with Tween80 and a nutrient supplement OADC was used). The furopyridine-isatin hybrid **15ba** once again was found to kill *Mycobacterium bovis* BCG strain with a concentration of 50–100 μM (Figure 4.4).

4.3 Conclusion

We have developed in chapter an unprecedented one-pot protocol for the synthesis of substituted furo[3,2-*c*]pyridines and substituted benzofuro[3,2-*c*]pyridines. The representative furo[3,2-*c*]pyridine derivative **3ba** was transformed into a novel therapeutic tool for tuberculosis in the form of furopyridine-isatin hybrid **15ba**. The novel hybrid **15ba** possesses anti-mycobacterial activity and inhibits bacterial growth in micromolar concentrations.

Further, we are in the process of examining the anti-mycobacterial activity of **15ba** on multidrug-resistant strains of Mtb. Besides, at present, we are also improving the efficacy of the newly designed hybrid derivative. With SAR studies and molecular modeling, designing more potent anti-TB molecules of this series is currently underway in our research group.

4.4 Experimental section

4.4.1 General information

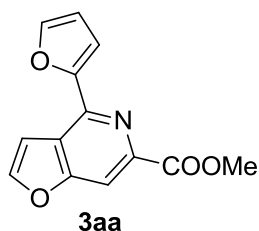
All reactions were carried out in oven-dried glasswares with magnetic stirring. Starting substrates and other reagents were obtained from a commercial supplier and used without further purification. NMR spectra were recorded on Avance III 400 Ascend Bruker. CDCl₃ and D₂O were used as NMR solvents. Chemical shifts (δ) reported as part per million (ppm), and TMS was used as an internal reference. High-resolution mass spectra were recorded through Bruker Daltonik High-Performance LC-MS (Electrospray Ionization Quadrupole time-of-flight) spectrometer. X-ray structure analysis was carried out at a Single crystal X-ray diffractometer Bruker KAPPA APEXII. Melting points (m.p.) are uncorrected and were measured on Veego melting point apparatus (Capillary method). Analytical thin-layer chromatography (TLC) was carried out on silica gel plates (silica gel 60 F254 aluminum supported plates) and the spots were visualized with an UV lamp (254 nm and 365 nm) and using chemical staining with Brady's reagent, KMnO₄, ninhydrin, iodine, and bromocresol. Column chromatography was performed using silica gel (100–200 mesh or 230–400 mesh) and neutral alumina (175 mesh). DMF, DCM, DMA, toluene, and acetonitrile were dried using CaH₂ and distilled over flame-dried 4Å molecular sieves. THF and Et₂O were dried over Na/benzophenone and stored over flame-dried 4Å molecular sieves under an inert atmosphere prior to use. Organic bases

including DIPEA, Et₃N, and DBU were stored over anhydrous KOH pellets.

4.4.2 Experimental section and characterization data

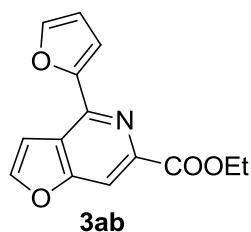
4.4.2.1 General procedure for the synthesis of furo[3,2-*c*]pyridines **3aa–ba** and benzofuro[3,2-*c*]pyridines **3da–dc**

A mixture of glycine alkyl ester hydrochloride **2a–c** (1.0 mmol), heterocyclic aldehyde **1a–e** (2.0 mmol) and *N,N*-Diisopropylethylamine (3.5 mmol) was heated at 120 °C for 6–8 h in a sealed tube (25 mL, Borosilicate) with constant stirring (monitored by TLC). The reaction mixture was cooled to room temperature, diluted with CH₂Cl₂ (1 × 10 mL), and washed with brine (1 × 10 mL). The reaction mixture was further extracted with CH₂Cl₂ (3 × 10 mL). The combined organic layer was dried over anhydrous Na₂SO₄, filtered, concentrated, and purified over neutral alumina (175 mesh) column chromatography using hexane-EtOAc solvent mixture as eluent.



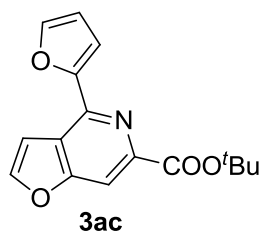
*Methyl 4-(furan-2-yl)furo[3,2-*c*]pyridine-6-carboxylate (3aa)*. According to the general procedure mentioned above, **1a** (200 mg, 2.08 mmol), **2a** (130 mg, 1.04 mmol) and DIPEA (0.670 mL, 3.72 mmol) were heated in a sealed tube at 120 °C for 6 h. After workup, the crude reaction mixture was purified through alumina (neutral, 175 mesh) column chromatography using hexane-EtOAc (98:2) as eluent; Yield 50% (126 mg); Off white solid; m.p. = 95–97 °C; *R_f* 0.65 (4:1 hexane-EtOAc); IR (KBr) 3032 (=C–H), 2957–2856 (C–H), 1731 (C=O), 1713–1560 (C=C), 1359 (C–H bend), 1112–993 (C–O), 722 (=C–H bend) cm^{–1}; ¹H NMR (400 MHz, CDCl₃) δ 8.19 (s, 1H), 7.85 (d, *J* = 3.0 Hz, 1H),

7.65 (dd, $J = 1.9, 0.9$ Hz, 1H), 7.45–7.40 (m, 1H), 7.36 (d, $J = 3.0$ Hz, 1H), 6.61 (dd, $J = 3.5$ Hz, 1.9 Hz, 1H), 4.03 (s, 3H); ^{13}C NMR (100 MHz, CDCl_3) δ 166.0, 160.6, 153.2, 148.1, 144.2, 143.5, 143.2, 122.7, 112.2, 111.4, 107.9, 106.9, 53.0; HRMS (ESI) calcd for $[\text{C}_{13}\text{H}_9\text{NO}_4 + \text{Na}^+]$ 266.0424, found 266.0417.



Ethyl 4-(furan-2-yl)furo[3,2-c]pyridine-6-carboxylate

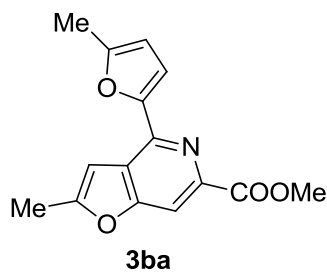
(**3ab**). According to the general procedure mentioned above, **1a** (200 mg, 2.08 mmol), **2b** (145 mg, 1.04 mmol) and DIPEA (0.670 mL, 3.72 mmol) were heated in a sealed tube at 120 °C for 6 h. After workup, the crude reaction mixture was purified through alumina (neutral, 175 mesh) column chromatography using hexane-EtOAc (99:1) as eluent; Yield 48% (128 mg); Yellow liquid; R_f 0.70 (4:1 hexane-EtOAc); IR (KBr) 3032 (=C–H), 2976–2855 (C–H), 1742 (C=O), 1730–1524 (C=C), 1371 (C–H bend), 1165–1005 (C–O), 741 (=C–H bend) cm^{-1} ; ^1H NMR (400 MHz, CDCl_3) δ 8.17 (s, 1H), 7.83 (d, $J = 2.0$ Hz, 1H), 7.64 (m, 1H), 7.42 (dd, $J = 2.0$ Hz, 0.8 Hz, 1H), 7.37 (d, $J = 3.2$ Hz, 1H), 6.60 (dd, $J = 3.3$ Hz, 1.8 Hz, 1H), 4.49 (q, $J = 7.3$ Hz, 2H), 1.47 (t, $J = 7.3$ Hz, 3H); ^{13}C NMR (400 MHz, CDCl_3) δ 165.4, 160.7, 153.4, 148.1, 144.1, 143.6, 143.5, 122.5, 112.3, 111.4, 107.8, 106.9, 62.0, 14.4; HRMS (ESI) calcd for $[\text{C}_{14}\text{H}_{11}\text{NO}_4 + \text{Na}^+]$ 280.0580, found 280.0571.



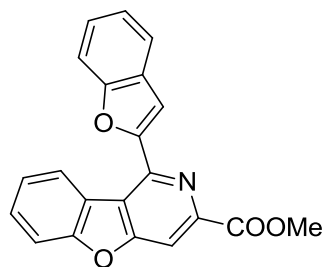
Tert-butyl 4-(furan-2-yl)furo[3,2-c]pyridine-6-

carboxylate (3ac). According to the general procedure mentioned above,

1a (200 mg, 2.08 mmol), **2c** (175 mg, 1.04 mmol) and DIPEA (0.670 mL, 3.72 mmol) were heated in a sealed tube at 120 °C for 8 h. After workup, the crude reaction mixture was purified through alumina (neutral, 175 mesh) column chromatography using hexane-EtOAc (99:1) as eluent; Yield 45% (133 mg); Off white solid; m.p. = 78–80 °C; R_f 0.70 (4:1 hexane-EtOAc); IR (KBr) 3032 (=C–H), 2976–2855 (C–H), 1742 (C=O), 1730–1524 (C=C), 1371 (C–H bend), 1165–1005 (C–O), 741 (=C–H bend) cm^{-1} ; ^1H NMR (400 MHz, CDCl_3) δ 8.08 (s, 1H), 7.82 (d, J = 3.0 Hz, 1H), 7.63 (dd, J = 1.5, 0.5 Hz, 1H), 7.43 (dd, J = 2.0 Hz, 0.8 Hz, 1H), 7.39 (d, J = 3.0 Hz, 1H), 6.60 (dd, J = 3.5 Hz, 1.8 Hz, 1H), 1.66 (s, 9H); ^{13}C NMR (400 MHz, CDCl_3) δ 164.0, 160.7, 153.7, 147.9, 144.6, 143.9, 143.4, 122.2, 112.2, 111.2, 107.4, 106.9, 82.0, 28.2*; HRMS (ESI) calcd for $[\text{C}_{16}\text{H}_{15}\text{NO}_4 + \text{Na}^+]$ 308.0893, found 308.0890. *(higher intensity carbon)

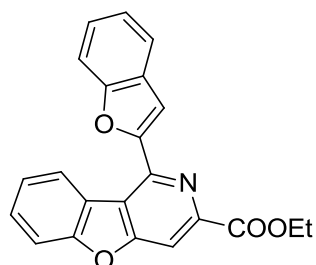


Methyl 2-methyl-4-(5-methylfuran-2-yl)furo[3,2-c]pyridine-6-carboxylate (**3ba**). According to the general procedure mentioned above, **1b** (200 mg, 1.82 mmol), **2a** (114 mg, 0.91 mmol) and DIPEA (0.555 mL, 3.18 mmol) were heated in a sealed tube at 120 °C for 6 h. After workup, the crude reaction mixture was purified through alumina (neutral, 175 mesh) column chromatography using hexane-EtOAc (99:1) as eluent; Yield 54% (133 mg); Off white solid; R_f 0.70 (4:1 hexane-EtOAc); ^1H NMR (400 MHz, CDCl_3) δ 8.04 (s, 1H), 7.17 (d, J = 3.0 Hz, 1H), 6.96 (s, 1H), 6.18 (d, J = 3.0 Hz, 1H), 4.00 (s, 3H), 2.55 (s, 3H), 2.45 (s, 3H); ^{13}C NMR (400 MHz, CDCl_3) δ 166.2, 160.3, 159.4, 154.2, 151.5, 142.3, 142.2, 124.0, 112.3, 108.5, 106.8, 102.9, 52.8, 14.2, 14.0; HRMS (ESI) calcd for $[\text{C}_{15}\text{H}_{13}\text{NO}_4 + \text{Na}^+]$ 294.0742, found 294.0749.

**3da**

Methyl 1-(benzofuran-2-yl)benzofuro[3,2-

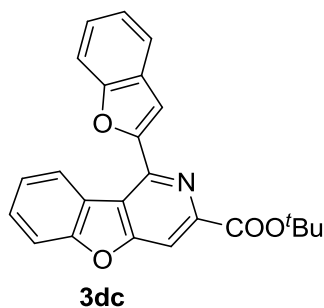
c]pyridine-3-carboxylate (3da). According to the general procedure mentioned above, **1d** (100 mg, 0.68 mmol), **2a** (43 mg, 0.34 mmol) and DIPEA (0.24 mL, 1.36 mmol) were heated in a sealed tube at 120 °C for 6 h. After workup, the crude reaction mixture was purified through alumina (neutral, 175 mesh) column chromatography using hexane-EtOAc (98:2) as eluent; Yield 60% (70 mg); Yellow-orange solid; m.p. = 163–165 °C; R_f 0.40 (8:2 hexane-EtOAc); IR (KBr) 3065 (=C–H), 2948–2850 (C–H), 1720 (C=O), 1612–1539 (C=C), 1350–1338 (C–H bend), 1256–1094 (C–O), 735 (=C–H bend) cm^{-1} ; ^1H NMR (400 MHz, CDCl_3) δ 8.85 (d, J = 7.8 Hz, 1H), 8.30 (s, 1H), 7.81 (s, 1H), 7.78–7.71 (m, 2H), 7.69 (d, J = 8.0 Hz, 1H), 7.63 (dd, J = 8.0, 7.3 Hz, 1H), 7.51 (dd, J = 7.6, 7.5 Hz, 1H), 7.44 (dd, J = 7.8, 7.5 Hz, 1H), 7.34 (dd, J = 7.6, 7.5 Hz, 1H), 4.08 (s, 3H); ^{13}C NMR (400 MHz, CDCl_3) δ 165.5, 162.7, 157.4, 155.4, 154.5, 145.4, 144.3, 129.6, 128.4, 125.7, 125.6, 124.3, 123.7, 122.1, 120.9, 120.8, 111.9, 111.5, 108.7, 108.4, 53.1; HRMS (ESI) calcd for $[\text{C}_{21}\text{H}_{13}\text{NO}_4 + \text{Na}^+]$ 366.0737, found 366.0693.

**3db**

Ethyl 1-(benzofuran-2-yl)benzofuro[3,2-

c]pyridine-3-carboxylate (3db). According to the general procedure mentioned above, **1d** (100 mg, 0.68 mmol), **2b** (48 mg, 0.34 mmol) and

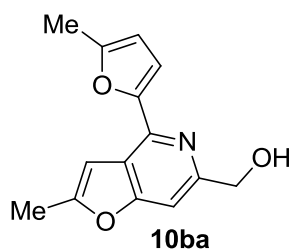
DIPEA (0.240 mL, 1.36 mmol) were heated in a sealed tube at 120 °C for 6 h. After workup, the crude reaction mixture was purified through alumina (neutral, 175 mesh) column chromatography using hexane-EtOAc (98:2) as eluent; Yield 55% (67 mg); Yellow solid; m.p. = 141–143 °C; R_f 0.40 (8:2 hexane-EtOAc); IR (KBr) 3065 (=C–H), 2987–2850 (C–H), 1714 (C=O), 1625–1540 (C=C), 1367–1340 (C–H bend), 1266–1097 (C–O), 750 (=C–H bend) cm^{-1} ; ^1H NMR (400 MHz, CDCl_3) δ 8.85 (d, J = 8.0 Hz, 1H), 8.26 (s, 1H), 7.81 (s, 1H), 7.75 (d, J = 8.0 Hz, 1H), 7.72 (d, J = 7.8 Hz, 1H), 7.67 (d, J = 8.3 Hz, 1H), 7.61 (dd, J = 8.0, 7.5 Hz, 1H), 7.49 (dd, J = 8.0, 8.3 Hz, 1H), 7.43 (dd, J = 7.8, 7.5 Hz, 1H), 7.34 (dd, J = 8.0, 8.3 Hz, 1H), 4.54 (q, 7.1 Hz, 2H), 1.51 (t, J = 7.1 Hz, 3H); ^{13}C NMR (100 MHz, CDCl_3) δ 164.9, 162.8, 157.4, 155.5, 154.7, 145.8, 144.3, 129.6, 128.5, 125.74, 125.73, 124.3, 123.7, 122.2, 121.0, 120.7, 111.9, 111.6, 108.7, 108.3, 62.2, 14.4; HRMS (ESI) calcd for $[\text{C}_{22}\text{H}_{15}\text{NO}_4 + \text{Na}^+]$ 380.0893, found 380.0844.



Tert-butyl 1-(benzofuran-2-yl)benzofuro[3,2-c]pyridine-3-carboxylate (3dc). According to the general procedure mentioned above, **1d** (100 mg, 0.68 mmol), **2c** (57 mg, 0.34 mmol) and DIPEA (0.240 mL, 1.36 mmol) were heated in a sealed tube at 120 °C for 7 h. After workup, the crude reaction mixture was purified through alumina (neutral, 175 mesh) column chromatography using hexane-EtOAc (98:2) as eluent; Yield 45% (64 mg); Yellow solid; m.p. = 100–102 °C; R_f 0.40 (8:2 hexane-EtOAc); IR (KBr) 3060 (=C–H), 2977–2851 (C–H), 1715 (C=O), 1626–1540 (C=C), 1365–1340 (C–H bend), 1273–1074 (C–O), 738 (=C–H bend) cm^{-1} ; ^1H NMR (400 MHz, CDCl_3) δ 8.88 (d, J = 8.0

Hz, 1H), 8.18 (s, 1H), 7.83 (s, 1H), 7.74 (d, $J = 7.8$ Hz, 1H), 7.71 (d, $J = 8.3$ Hz, 1H), 7.65 (d, $J = 8.0$ Hz, 1H), 7.59 (dd, $J = 8.0, 7.3$ Hz, 1H), 7.48 (dd, $J = 7.6, 7.5$ Hz, 1H), 7.42 (dd, $J = 8.3, 7.3$ Hz, 1H), 7.33 (dd, $J = 7.5, 7.3$ Hz, 1H), 1.71 (s, 9H); ^{13}C NMR (100 MHz, CDCl_3) δ 163.6, 162.8, 157.4, 155.4, 154.9, 146.8, 144.1, 129.3, 128.5, 125.7, 125.6, 124.2, 123.6, 122.1, 121.0, 120.2, 111.8, 111.5, 108.6, 107.9, 82.4, 28.2*; HRMS (ESI) calcd for $[\text{C}_{24}\text{H}_{19}\text{NO}_4 + \text{Na}^+]$ 408.1206, found 408.1153. *(higher intensity carbon)

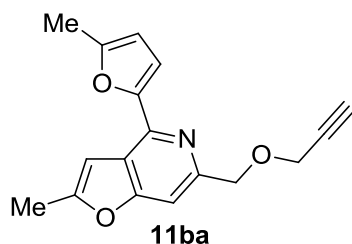
4.4.2.2 Synthesis of furo[3,2-*c*]pyridine-isatin hybrid **15ba**



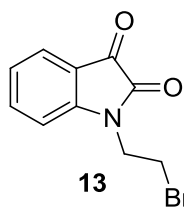
(2-Methyl-4-(5-methylfuran-2-yl)furo[3,2-

c]pyridin-6-yl)methanol (**10ba**). In a two-neck round-bottom flask (50 mL), methyl 2-methyl-4-(5-methylfuran-2-yl)furo[3,2-*c*]pyridine-6-carboxylate **3ba** (250 mg, 0.92 mmol) was dissolved in dry THF (5 mL) under an inert atmosphere. The reaction mixture was cooled to 0 °C before addition of solid LiAlH_4 (104 mg, 2.76 mmol) in a single portion. The reaction mixture was warmed to room temperature and stirred further for 20 min. After the consumption of ester **3ba**, as confirmed by TLC, the reaction mixture was cautiously quenched with saturated NH_4Cl (10 mL) solution and further diluted with EtOAc (10 mL). The aqueous layer was extracted using EtOAc (10×3 mL). The combined organic extracts were dried over anhydrous Na_2SO_4 , filtered, evaporated under reduced pressure, and the crude residue was purified through alumina (neutral, 175 mesh) column chromatography using hexane-EtOAc (80:20) as eluent; Yield 66% (148 mg); Yellow liquid; R_f 0.45 (1:1 hexane-EtOAc); IR (KBr) cm^{-1} ; ^1H NMR (400 MHz, CDCl_3) δ 7.15–7.05 (m, 2H), 6.90 (s, 1H), 6.17 (d, $J = 1.7$ Hz, 1H), 4.80 (s, 2H), 2.50 (s, 3H), 2.45 (s, 3H); ^{13}C NMR (400

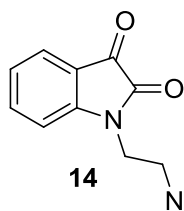
MHz, CDCl₃) δ 161.2, 156.7, 153.8, 153.2, 152.3, 140.9, 120.4, 111.1, 108.3, 102.3, 100.9, 64.3, 14.04, 14.01; HRMS (ESI) calcd for [C₁₄H₁₃NO₃+H⁺] 244.0968, found 244.0967.



2-Methyl-4-(5-methylfuran-2-yl)-6-((prop-2-yn-1-yloxy)methyl)furo[3,2-c]pyridine (11ba). In a two-neck round-bottom flask (50 mL), (2-methyl-4-(5-methylfuran-2-yl)furo[3,2-c]pyridin-6-yl)methanol **10ba** (70 mg, 0.29 mmol) was dissolved in dry DMF (2 mL) under an inert atmosphere. The reaction mixture was cooled to 0 °C before the addition of sodium hydride (55–60% suspension in mineral oil, 14 mg, 0.35 mmol) in a single portion, and the reaction mixture was stirred for 20 min at the same temperature. Propargyl bromide (80% in toluene, 33 μ L, 0.35 mmol) was added drop-wise through a micropipette, and the reaction mixture was allowed to warm to room temperature and further stirred for 3 h. After the complete consumption of alcohol **10ba**, as confirmed by TLC, the reaction mixture was quenched with brine (5 mL) solution and further diluted with EtOAc (10 mL). The aqueous layer was extracted using EtOAc (10 \times 3 mL). The combined organic extracts were dried over anhydrous Na₂SO₄, filtered, evaporated under reduced pressure, and the crude residue purified through alumina (neutral, 175 mesh) column chromatography using hexane-EtOAc (97:3) as eluent and used for further transformation without characterization; Yield 70% (57 mg); Yellow oily liquid; *R_f* 0.70 (7:3 hexane-EtOAc).

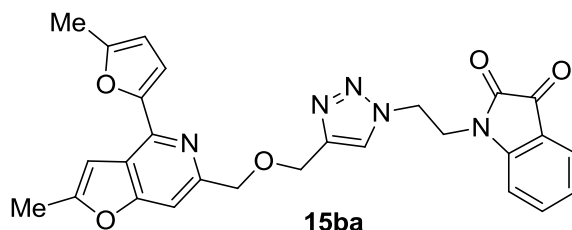


13 *1-(2-Bromoethyl)indoline-2,3-dione (13)*. In a two neck round bottom flask (50 mL), a suspension of sodium hydride (55–60% suspension in mineral oil, 60 mg, 1.50 mmol) was prepared in dry DMF (2 mL) at room temperature. Isatin **12** (147 mg, 1.00 mmol) was added to this suspension at room temperature, and the reaction mixture was stirred for 20 min at the same temperature. 1,2-Dibromoethane (90 μ L, 1.00 mmol) was added drop-wise, and the reaction mixture was heated at 70 $^{\circ}$ C for 1 h. After the completion of the reaction (as evident by TLC), EtOAc (10 mL) and cold brine (10 mL) was added to the reaction mixture. The aqueous layer was further extracted with EtOAc (3×10 mL), and the organic layers were pooled to dry over anhydrous Na_2SO_4 . The organic layer was filtered, concentrated, and purified through silica gel (230–400 mesh) column chromatography using hexane-EtOAc (67:33) as eluent; Yield 80% (203 mg); Yellow-orange solid; R_f 0.30 (2:1 hexane-EtOAc); ^1H NMR (400 MHz, CDCl_3) δ 7.67–7.57 (m, 2H), 7.14 (dd, $J = 7.5$, 7.5 Hz, 1H), 6.99 (d, $J = 7.8$ Hz, 1H), 4.14 (t, $J = 6.5$ Hz, 2H), 3.60 (t, $J = 6.5$ Hz, 2H); ^{13}C NMR (400 MHz, CDCl_3) δ 182.7, 158.2, 150.5, 138.4, 125.7, 124.1, 117.6, 110.2, 42.0, 27.1.



14 *1-(2-Azidoethyl)indoline-2,3-dione (14)*. In an oven-dried one neck round-bottom flask (50 mL), 1-(2-bromoethyl)indoline-2,3-dione **13**, (50 mg, 0.20 mmol) was dissolved in DMF (3 mL), and sodium azide (52 mg, 0.80 mmol) was added to the reaction mixture in one portion, under an inert atmosphere at room temperature. The reaction mixture was stirred at room temperature overnight. After the completion of the

reaction, CH₂Cl₂ (10 mL) was added to the reaction mixture, followed by MQ water (10 mL). The aqueous layer was extracted with CH₂Cl₂ (3 × 10 mL), and the organic layers were pooled to dry over anhydrous Na₂SO₄. The organic layer was filtered, concentrated, and purified through silica gel (230–400 mesh) column chromatography using hexane-EtOAc (67:33) as eluent; Yield 92% (40 mg); Orange solid; R_f 0.50 (2:1 hexane-EtOAc); ¹H NMR (400 MHz, CDCl₃) δ 7.67–7.55 (m, 2H), 7.14 (dd, *J* = 7.5, 7.3 Hz, 1H), 7.00 (d, *J* = 8.0 Hz, 1H), 3.88 (t, *J* = 5.8 Hz, 2H), 3.66 (t, *J* = 5.8 Hz, 2H); ¹³C NMR (400 MHz, CDCl₃) δ 182.7, 158.4, 150.7, 138.5, 125.6, 124.1, 117.6, 110.3, 49.1, 39.7.



1-(2-(4-(((2-methyl-4-(5-methylfuran-2-yl)furo[3,2-c]pyridin-6-yl)methoxy)methyl)-1H-1,2,3-triazol-1-yl)ethyl)indoline-2,3-dione (15ba).

In a round bottom flask (25 mL), 2-methyl-4-(5-methylfuran-2-yl)-6-((prop-2-yn-1-yloxy)methyl)furo[3,2-c]pyridine **11ba**, (30 mg, 0.11 mmol) and 1-(2-azidoethyl)indoline-2,3-dione **14**, (24 mg, 0.11 mmol) were dissolved in DMF (2 mL). Monohydrate copper acetate (12 mg, 0.06 mmol) was added in one portion to the above solution at room temperature under an inert atmosphere. The reaction mixture was stirred at the same temperature for 24 h. After the complete consumption of the starting materials, as confirmed by TLC, the reaction mixture was quenched with brine (5 mL) solution and further diluted with EtOAc (5 mL). The aqueous layer was extracted using EtOAc (5 × 3 mL). The combined organic extracts were dried over anhydrous Na₂SO₄, filtered, evaporated under reduced pressure, and the crude residue was purified through alumina (neutral, 175 mesh) column chromatography using CH₂Cl₂-MeOH (95:5)

as eluent; Yield 76% (41 mg); Yellow-orange amorphous solid; R_f 0.25 (1:3 hexane-EtOAc); ^1H NMR (400 MHz, CDCl_3) δ 7.61 (s, 1H), 7.50 (d, $J = 7.6$ Hz, 1H), 7.44 (dd, $J = 7.8, 7.6$ Hz, 1H), 7.24 (s, 1H), 7.03–6.93 (m, 2H), 6.86 (s, 1H), 6.51 (d, $J = 8.0$ Hz, 1H), 6.16 (d, $J = 2.8$ Hz, 1H), 4.73–4.67 (m, 4H), 4.66 (s, 2H), 4.24 (t, $J = 6.0$ Hz, 2H), 2.50 (s, 3H), 2.44 (s, 3H); HRMS (ESI) calcd for $[\text{C}_{27}\text{H}_{23}\text{N}_5\text{O}_5 + \text{Na}^+]$ 520.1591, found 520.1361.

4.4.2.3 Density Functional Theory Calculations

All the calculations have been carried out using the Becke's three-parameter hybrid exchange functional and Lee–Yang–Parr's correlation functional (B3LYP) and 6-311++G**(d,p) basis sets as implemented in the Gaussian 09 program. The calculated (B3LYP/6-311++G**) total energies of the intermediates **7**, **9a**, **9b**, and **9c** for furopyridine and benzofuropyridine derivatives are as follows:

Furopyridine derivatives	Electronic Energy + ZPE (hartrees)	Relative energies (kcal/mol)
Furyl iminoenamine (7)	−857.6055	5.39
4,5-Dihydrofuro[3,2- <i>c</i>]pyridines (9a)	−857.6141	0.00
4,8-Dihydrofuro[3,2- <i>c</i>]pyridine (9b)	−857.5795	21.71
4,5-Dihydrofuro[3,2- <i>d</i>]pyridine (9c)	−857.5855	19.95

Benzofuropyridine derivatives	Electronic Energy + ZPE (hartrees)	Relative Energies (kcal/mol)
Benzofuryliminoenamine (7)	−1164.8831	7.59

1,2-Dihydrobenzofuro[3,2- <i>c</i>]pyridines (9a)	-1164.8952	0.00
1,11-Dihydrobenzofuro[3,2- <i>c</i>]pyridine (9b)	-1164.8666	17.95
1,2-Dihydrobenzofuro[3,2- <i>d</i>]pyridine (9c)	-1164.8645	19.26

4.4.3 Copies of ^1H , ^{13}C NMR spectra for synthesized compounds

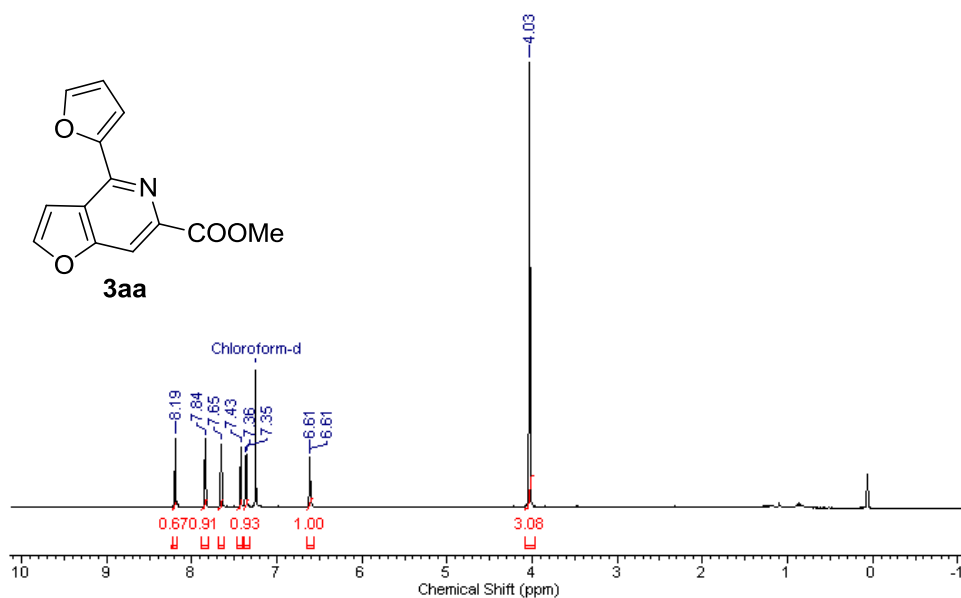


Figure 4.5 ^1H NMR spectrum of *methyl 4-(furan-2-yl)furo[3,2-*c*]pyridine-6-carboxylate (3aa)*

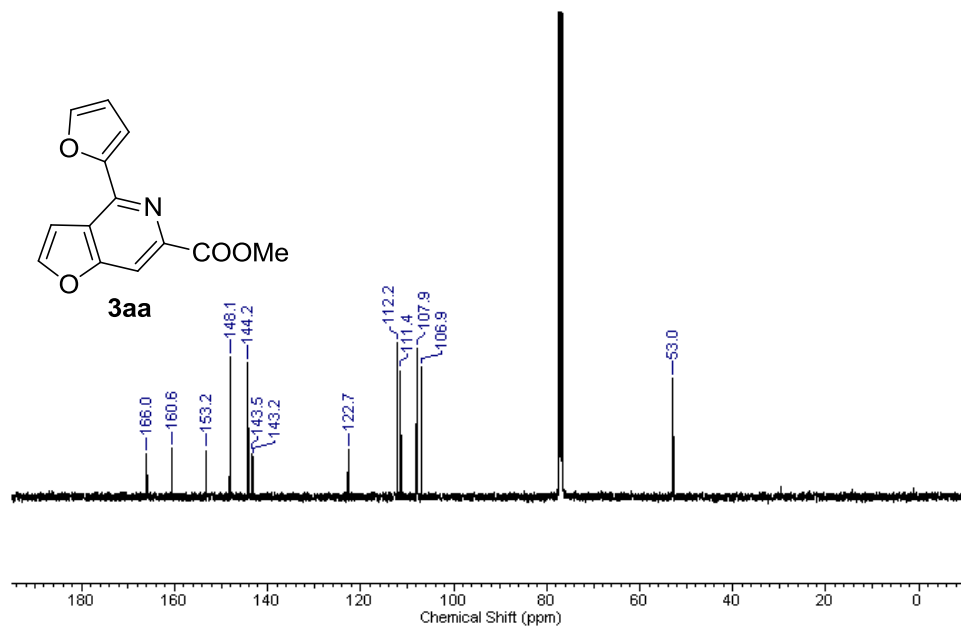


Figure 4.6 ¹³C NMR spectrum of *methyl 4-(furan-2-yl)furo[3,2-*c*]pyridine-6-carboxylate (3aa)*

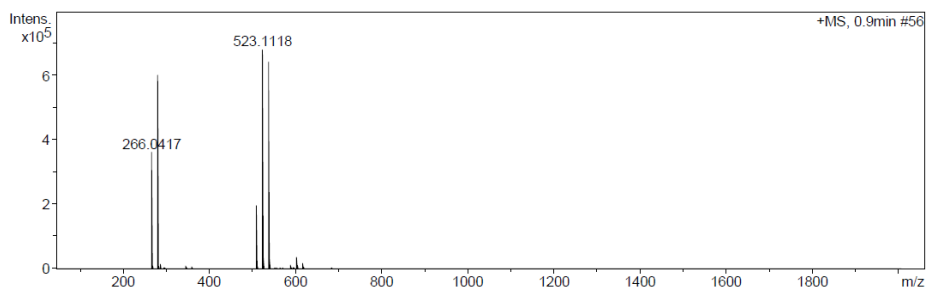


Figure 4.7 HRMS of *methyl 4-(furan-2-yl)furo[3,2-*c*]pyridine-6-carboxylate (3aa)*

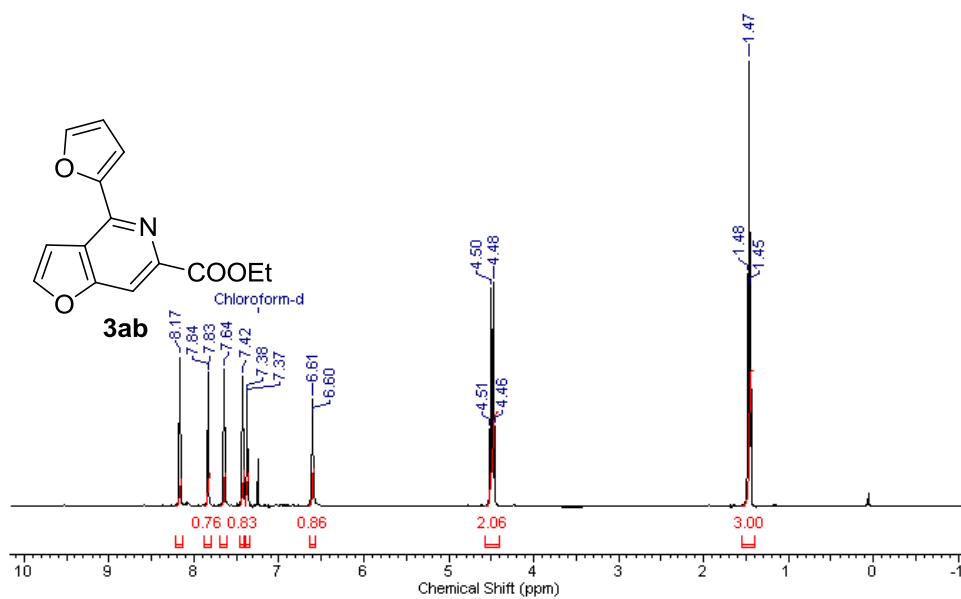


Figure 4.8 ^1H NMR spectrum of ethyl 4-(furan-2-yl)furo[3,2-c]pyridine-6-carboxylate (**3ab**)

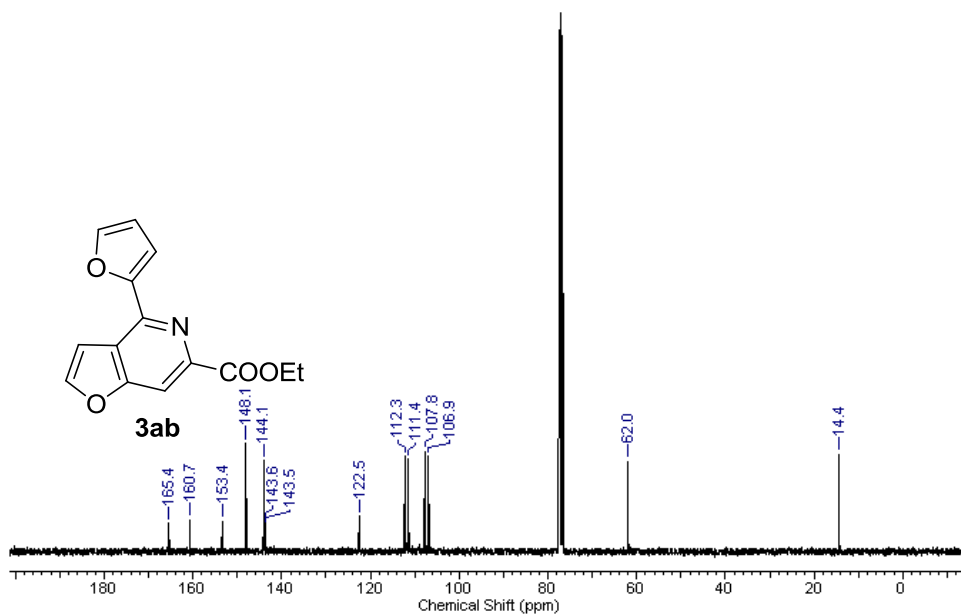


Figure 4.9 ^{13}C NMR spectrum of ethyl 4-(furan-2-yl)furo[3,2-c]pyridine-6-carboxylate (**3ab**)

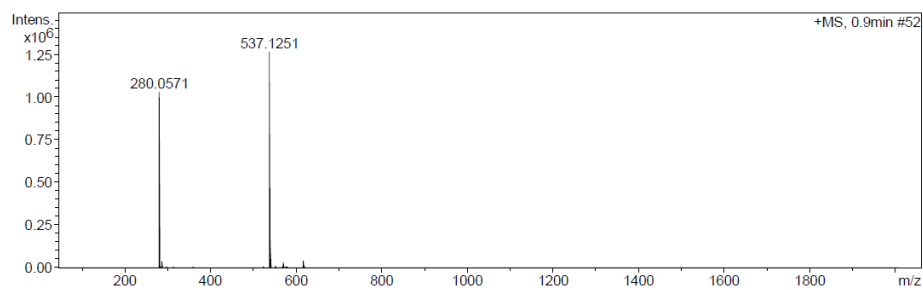


Figure 4.10 HRMS of *ethyl 4-(furan-2-yl)furo[3,2-c]pyridine-6-carboxylate (3ab)*

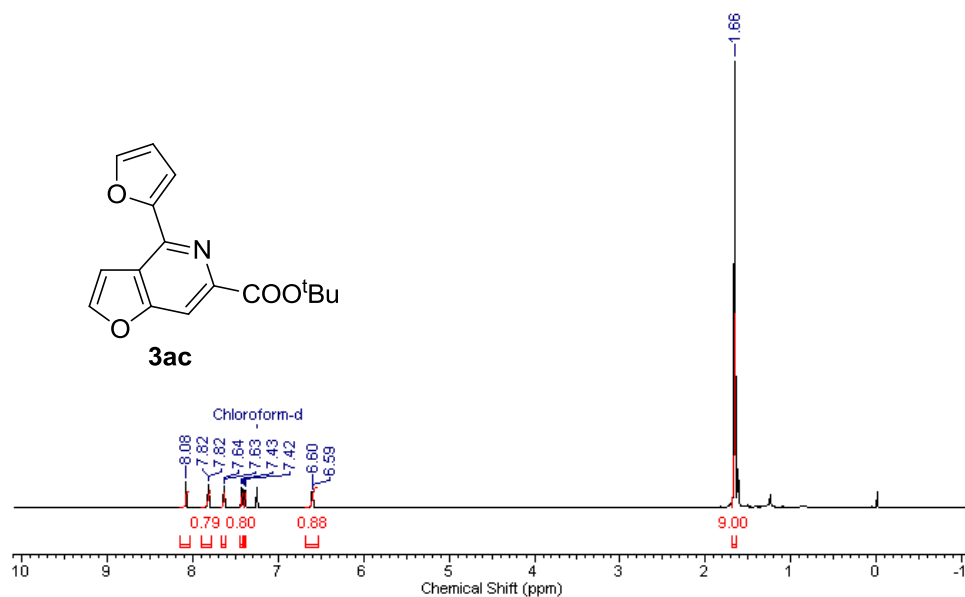


Figure 4.11 ¹H NMR spectrum of *tert-butyl 4-(furan-2-yl)furo[3,2-c]pyridine-6-carboxylate (3ac)*

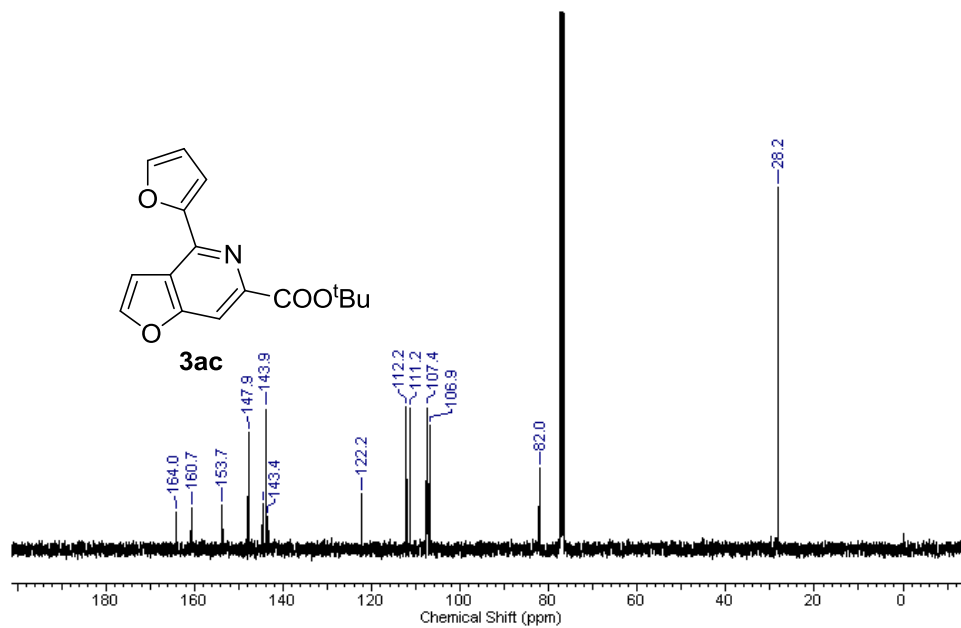


Figure 4.12 ¹³C NMR spectrum of *tert*-butyl 4-(furan-2-yl)furo[3,2-*c*]pyridine-6-carboxylate (**3ac**)

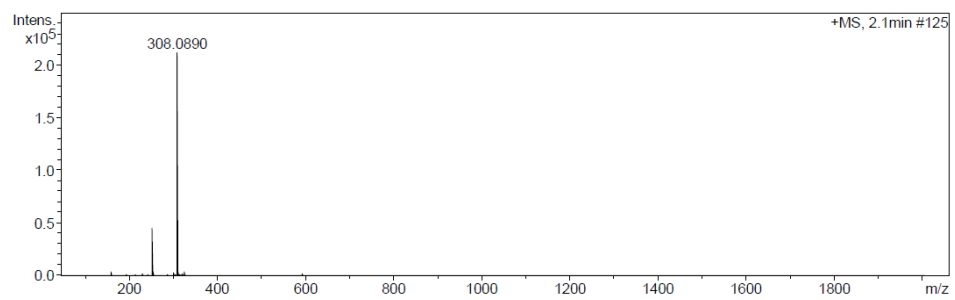


Figure 4.13 HRMS of *tert*-butyl 4-(furan-2-yl)furo[3,2-*c*]pyridine-6-carboxylate (**3ac**)

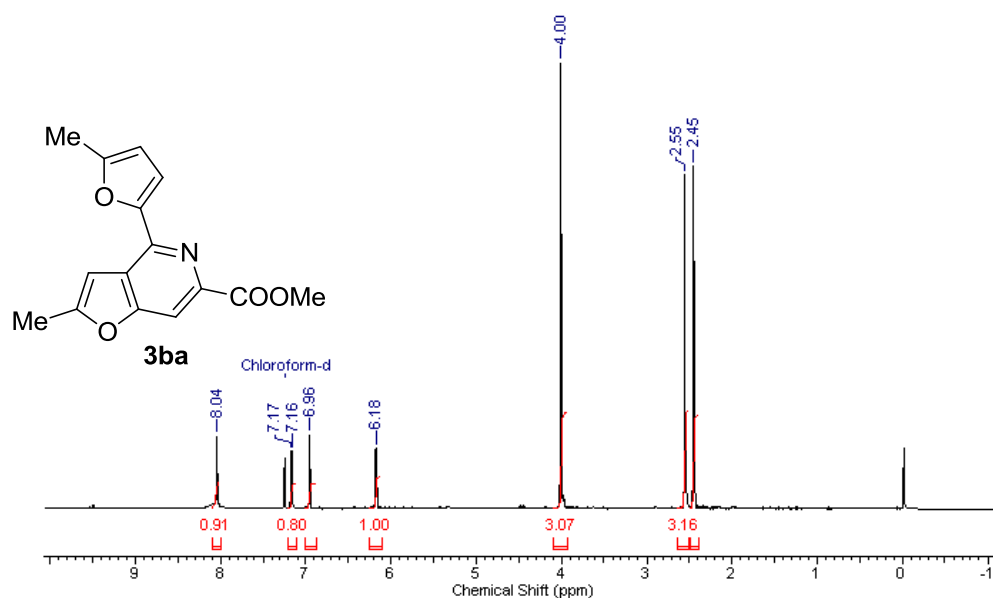


Figure 4.14 ¹H NMR spectrum of *methyl 2-methyl-4-(5-methylfuran-2-yl)furo[3,2-c]pyridine-6-carboxylate (3ba)*

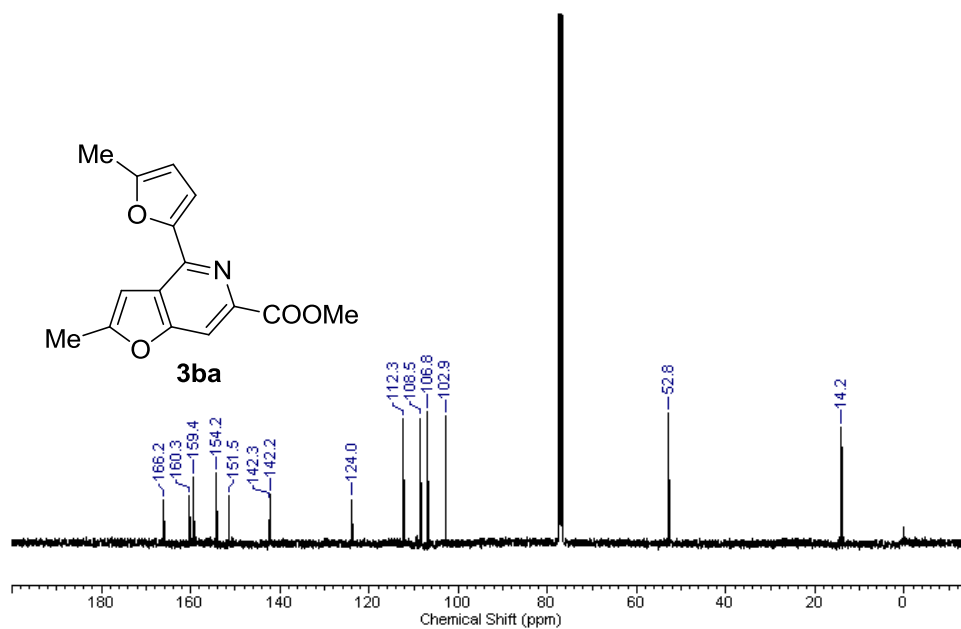


Figure 4.15 ¹³C NMR spectrum of *methyl 2-methyl-4-(5-methylfuran-2-yl)furo[3,2-c]pyridine-6-carboxylate (3ba)*

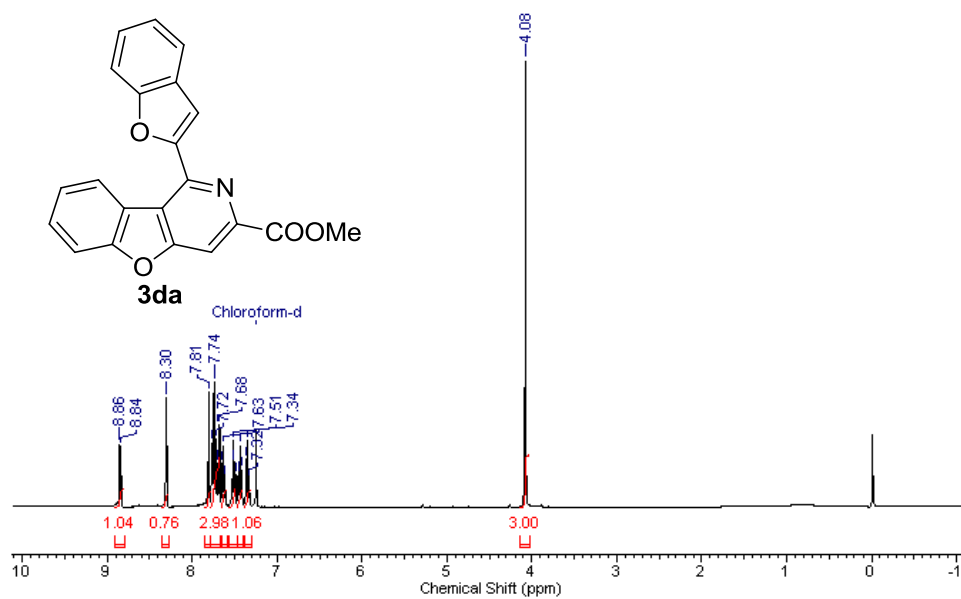


Figure 4.16 ^1H NMR spectrum of methyl 1-(benzofuran-2-yl)benzofuro[3,2-c]pyridine-3-carboxylate (**3da**)

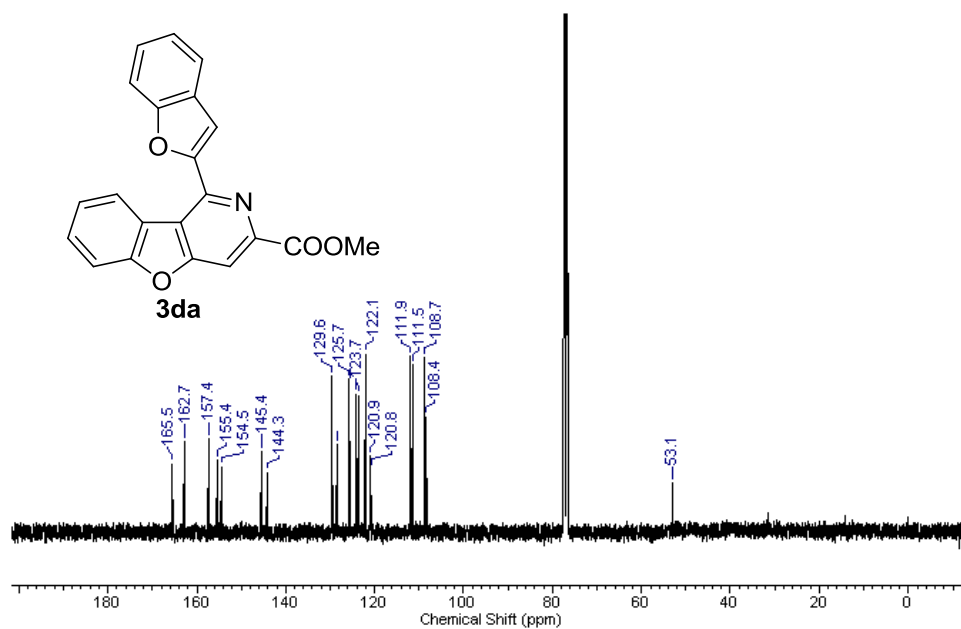


Figure 4.17 ^{13}C NMR spectrum of methyl 1-(benzofuran-2-yl)benzofuro[3,2-c]pyridine-3-carboxylate (**3da**)

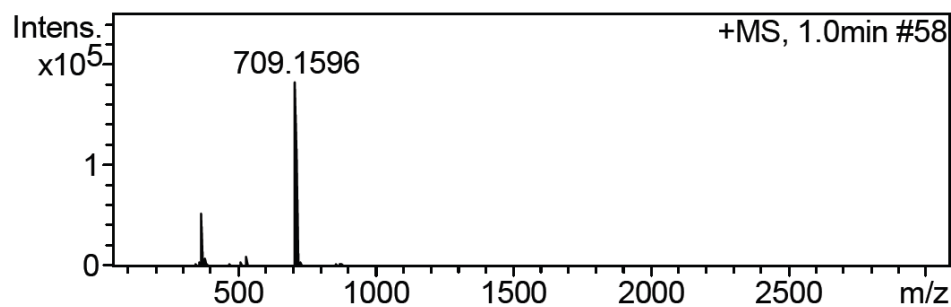


Figure 4.18 HRMS of *methyl 1-(benzofuran-2-yl)benzofuro[3,2-c]pyridine-3-carboxylate (3da)*

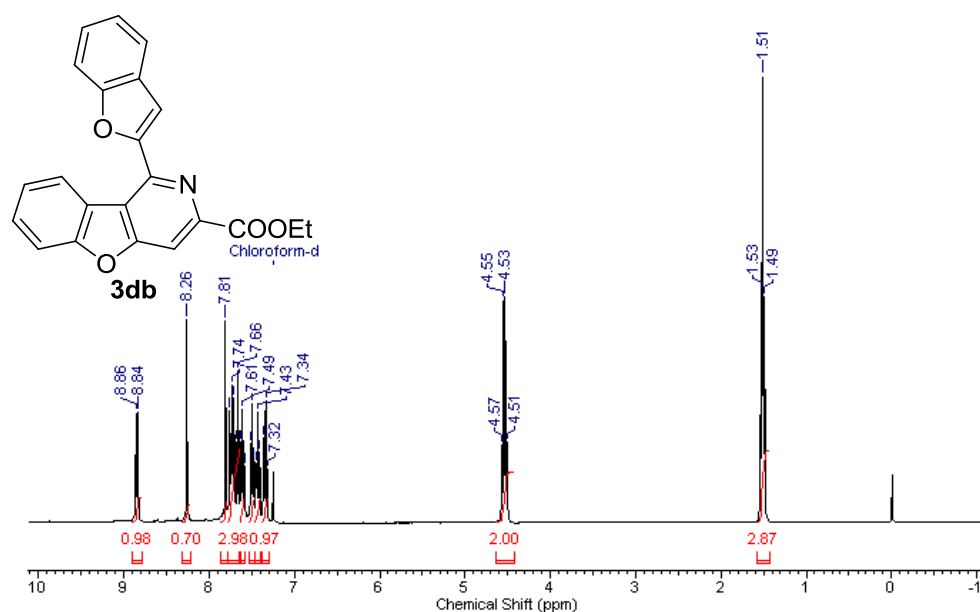


Figure 4.19 ^1H NMR spectrum of *ethyl 1-(benzofuran-2-yl)benzofuro[3,2-c]pyridine-3-carboxylate (3db)*

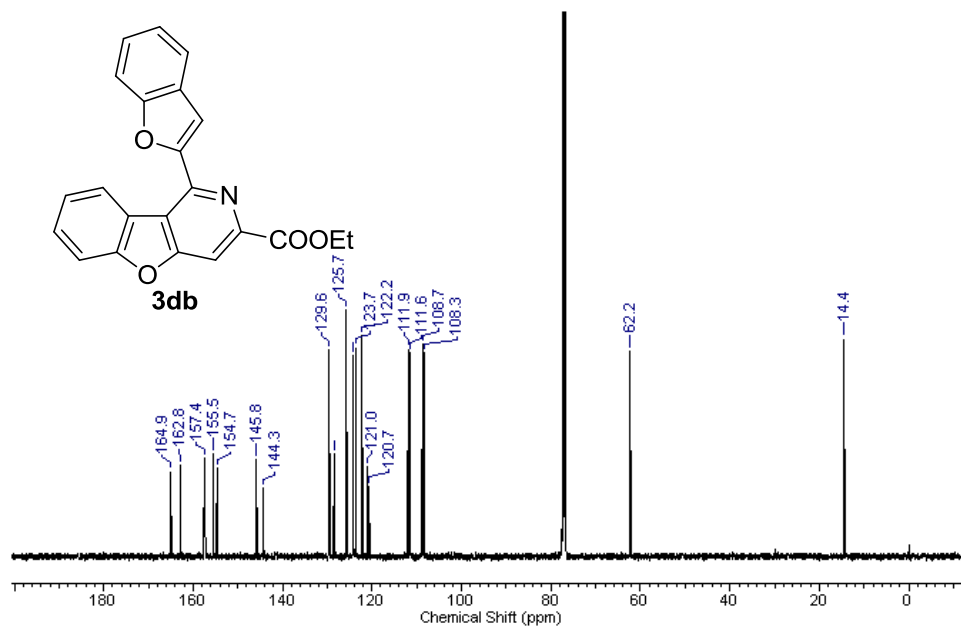


Figure 4.20 ¹³C NMR spectrum of *ethyl 1-(benzofuran-2-yl)benzofuro[3,2-c]pyridine-3-carboxylate (3db)*

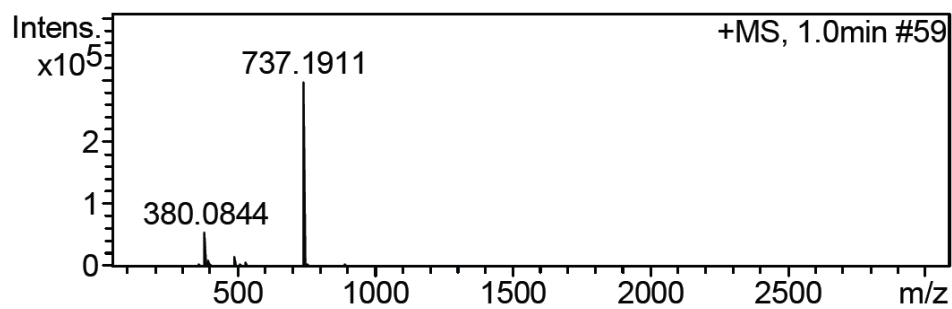


Figure 4.21 HRMS of *ethyl 1-(benzofuran-2-yl)benzofuro[3,2-c]pyridine-3-carboxylate (3db)*

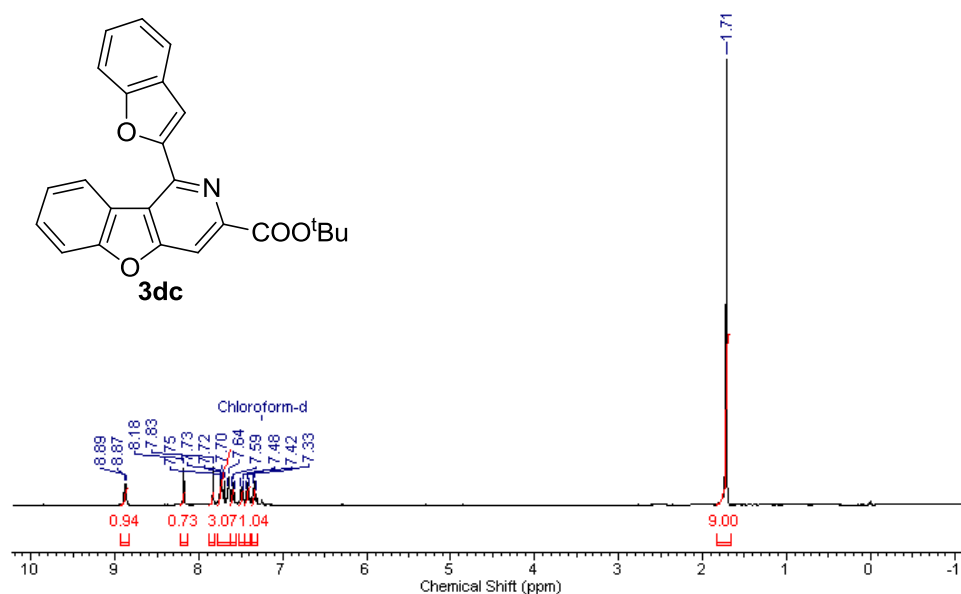


Figure 4.22 ¹H NMR spectrum of *tert*-butyl 1-(benzofuran-2-yl)benzofuro[3,2-*c*]pyridine-3-carboxylate (**3dc**)

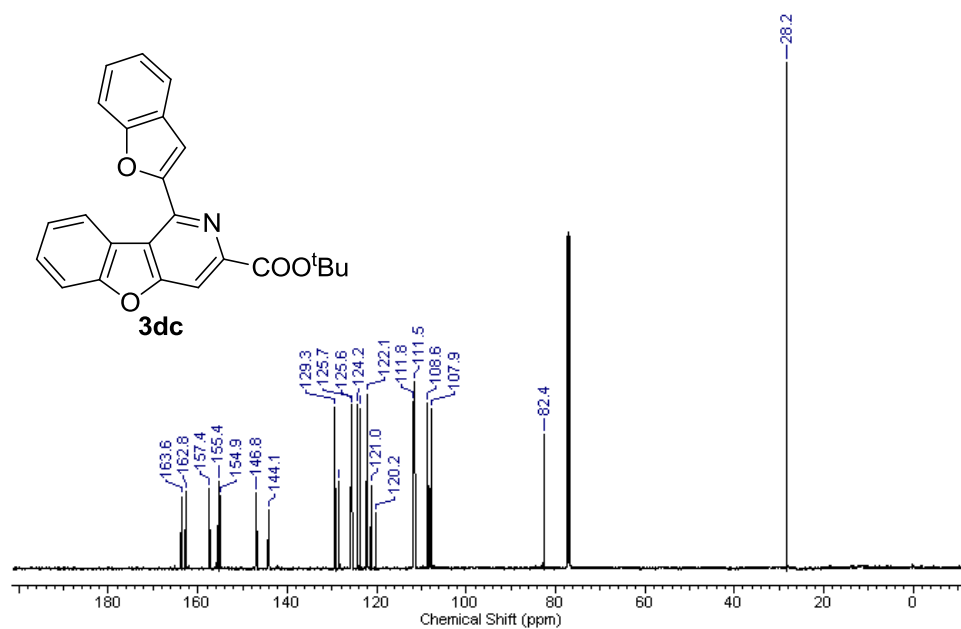


Figure 4.23 ¹³C NMR spectrum of *tert*-butyl 1-(benzofuran-2-yl)benzofuro[3,2-*c*]pyridine-3-carboxylate (**3dc**)

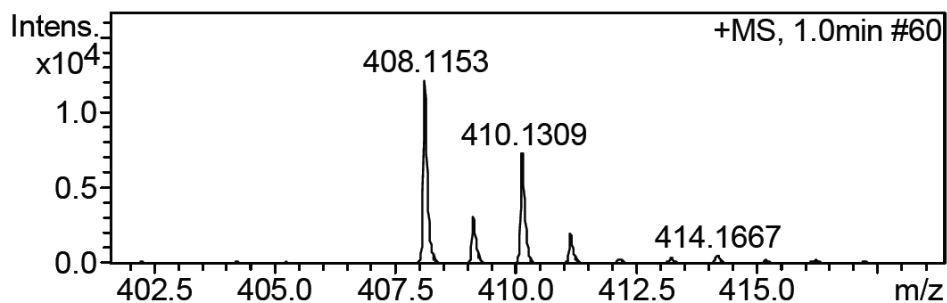


Figure 4.24 Mass data of *tert*-butyl 1-(benzofuran-2-yl)benzofuro[3,2-*c*]pyridine-3-carboxylate (**3dc**)

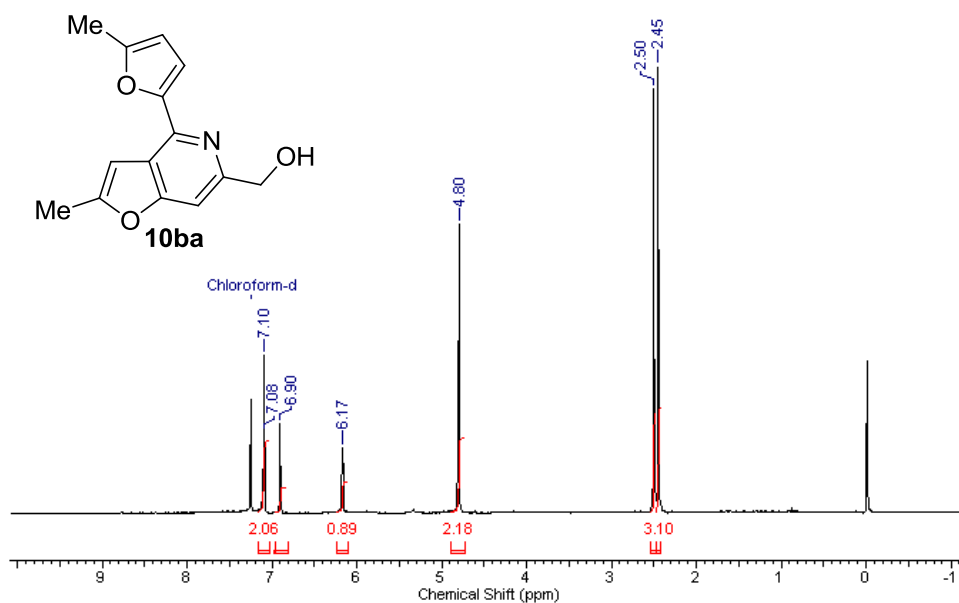


Figure 4.25 ¹H NMR spectrum of (2-methyl-4-(5-methylfuran-2-yl)furo[3,2-*c*]pyridin-6-yl)methanol (**10ba**)

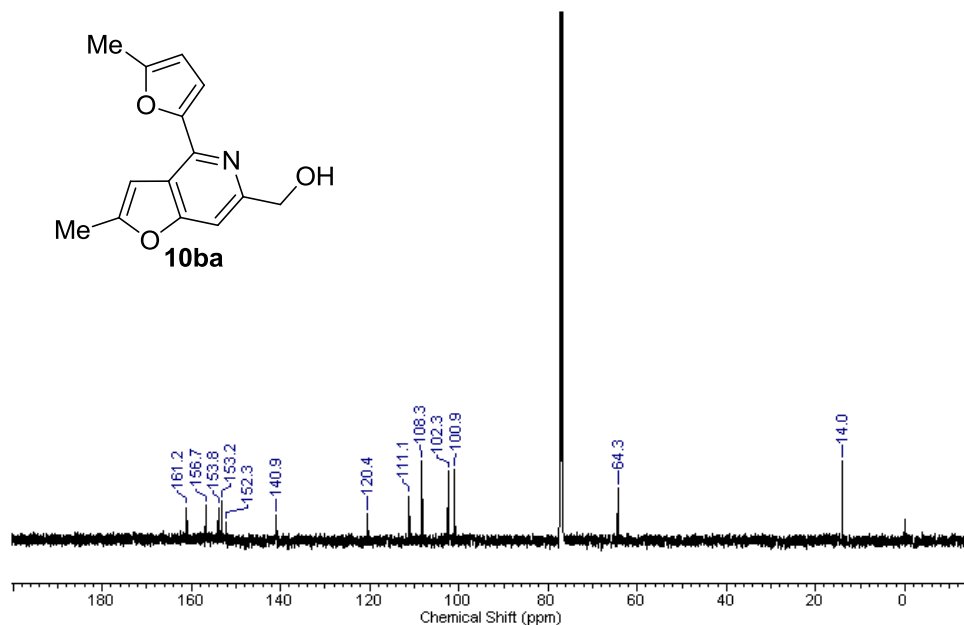


Figure 4.26 ^{13}C NMR spectrum of (2-methyl-4-(5-methylfuran-2-yl)furo[3,2-c]pyridin-6-yl)methanol (**10ba**)

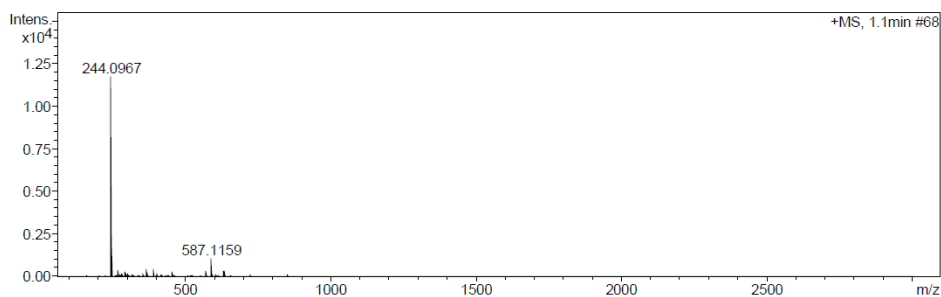


Figure 4.27 HRMS of (2-methyl-4-(5-methylfuran-2-yl)furo[3,2-c]pyridin-6-yl)methanol (**10ba**)

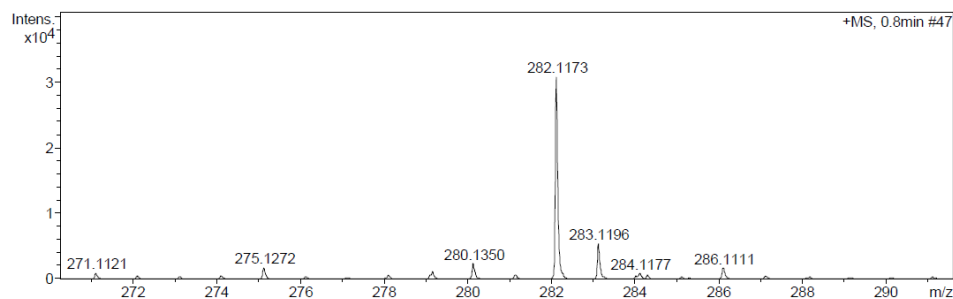


Figure 4.28 Mass data of 2-methyl-4-(5-methylfuran-2-yl)-6-((prop-2-yn-1-yloxy)methyl)furo[3,2-c]pyridine (**11ba**)

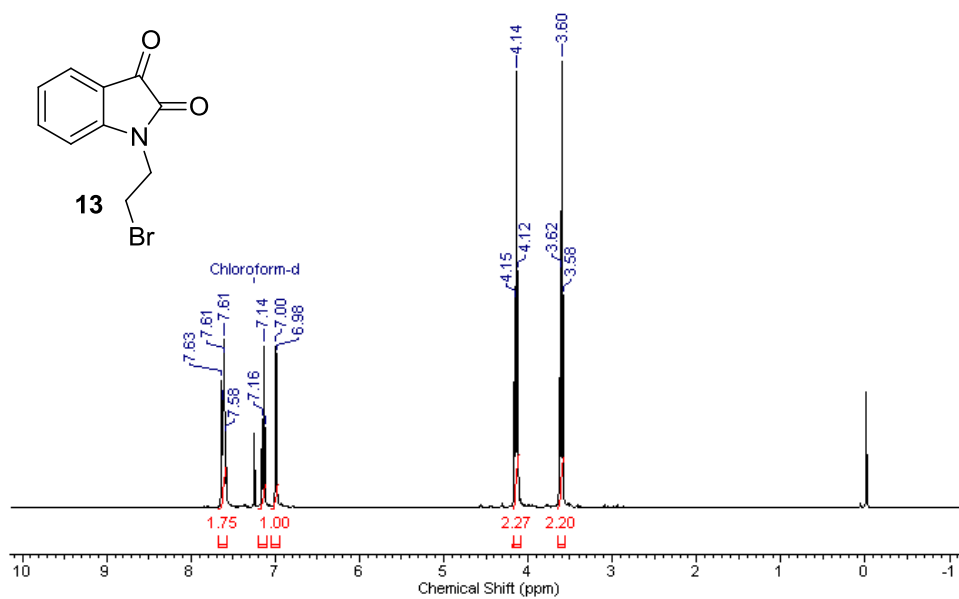


Figure 4.29 ¹H NMR spectrum of 1-(2-bromoethyl)indoline-2,3-dione (13)

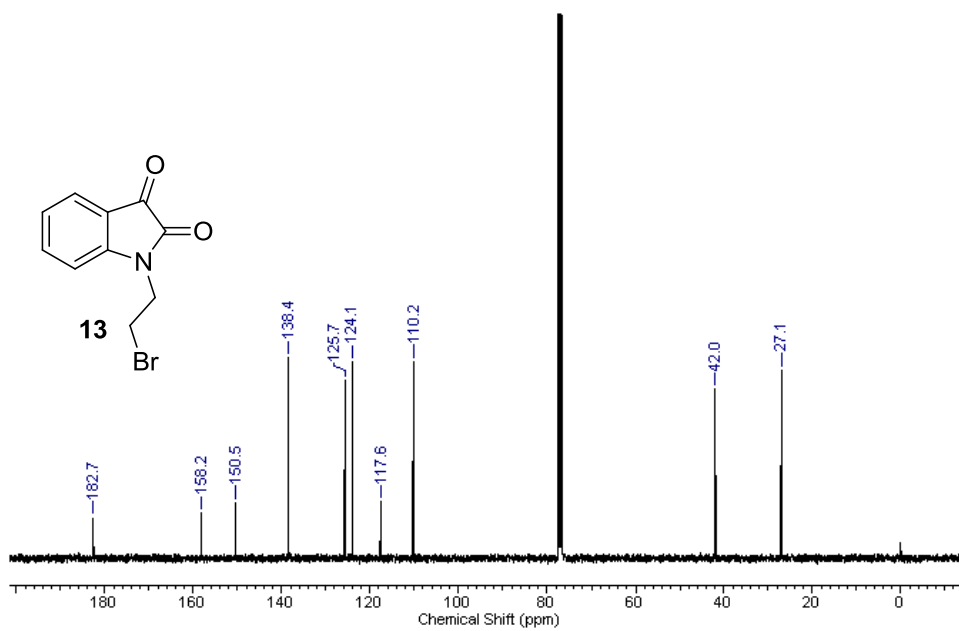


Figure 4.30 ¹³C NMR spectrum of 1-(2-bromoethyl)indoline-2,3-dione (13)

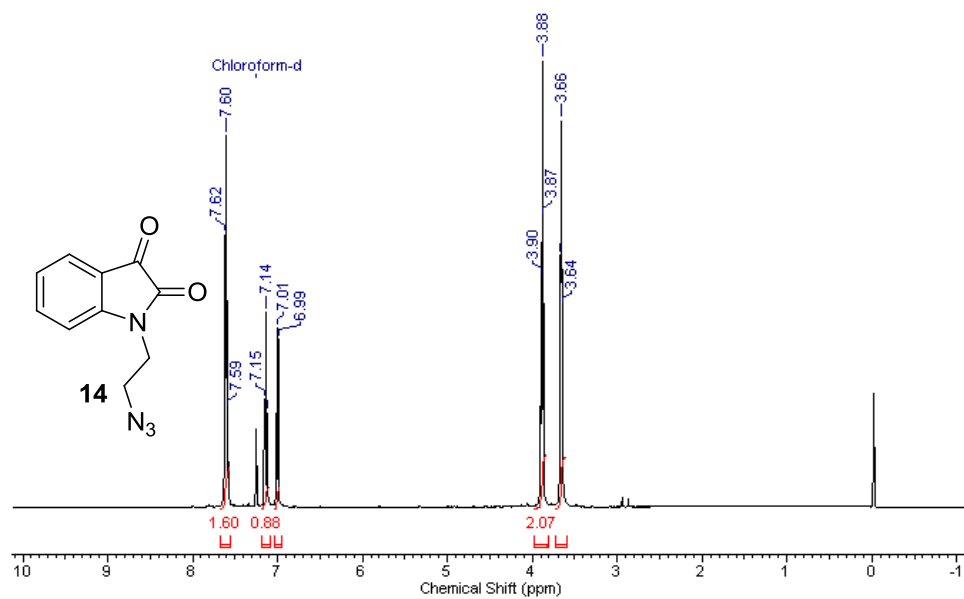


Figure 4.31 ¹H NMR spectrum of 1-(2-azidoethyl)indoline-2,3-dione (**14**)

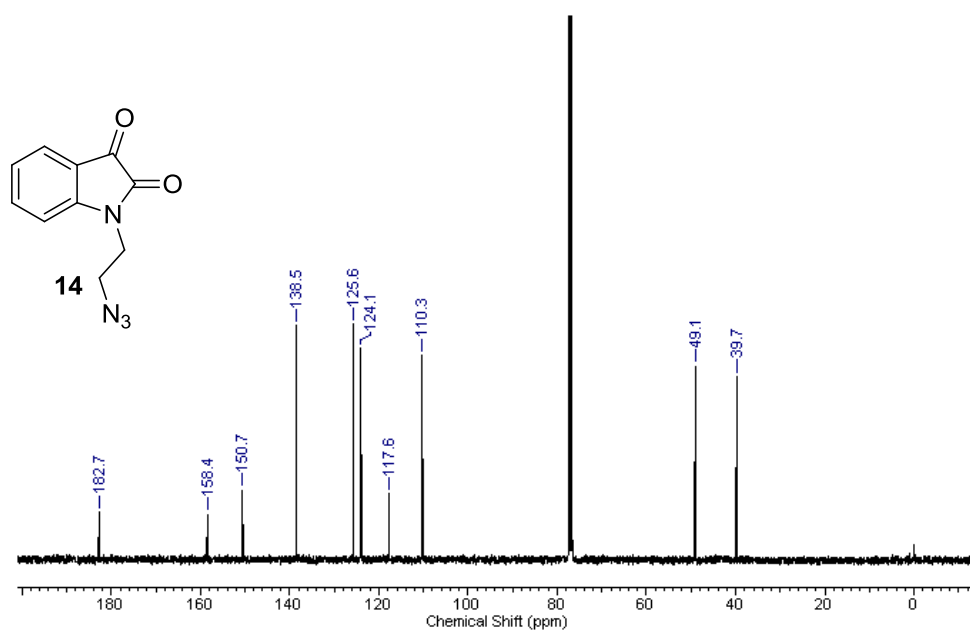


Figure 4.32 ¹³C NMR spectrum of 1-(2-azidoethyl)indoline-2,3-dione (**14**)

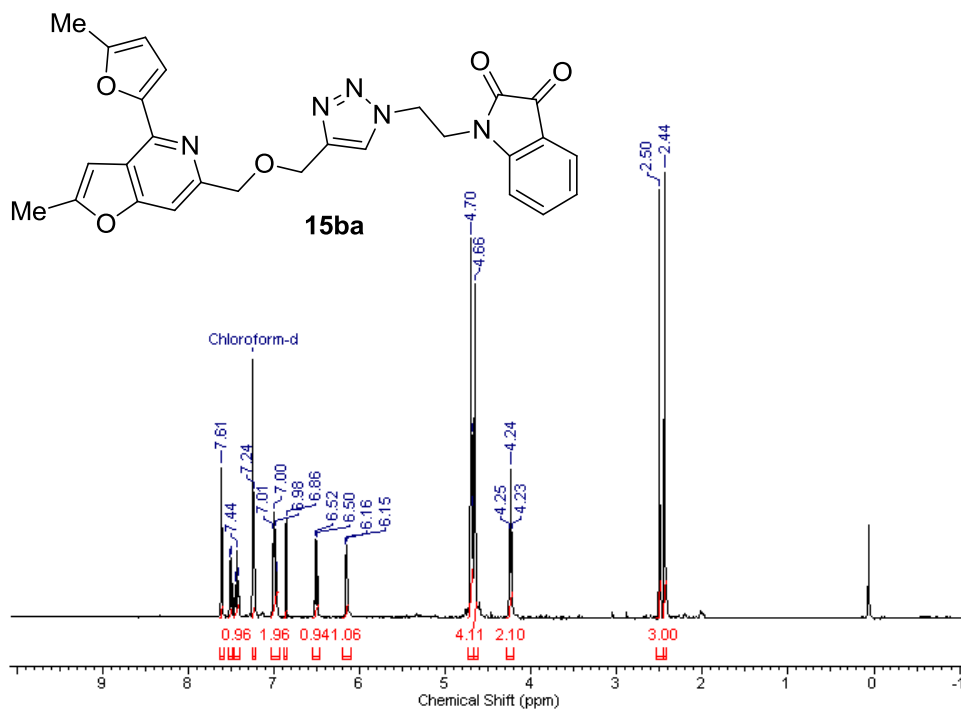


Figure 4.33 ^1H NMR spectrum of *1-(2-(4-(((2-methyl-4-(5-methylfuran-2-yl)furo[3,2-*c*]pyridin-6-yl)methoxy)methyl)-1*H*-1,2,3-triazol-1-yl)ethyl)indoline-2,3-dione (15ba)*

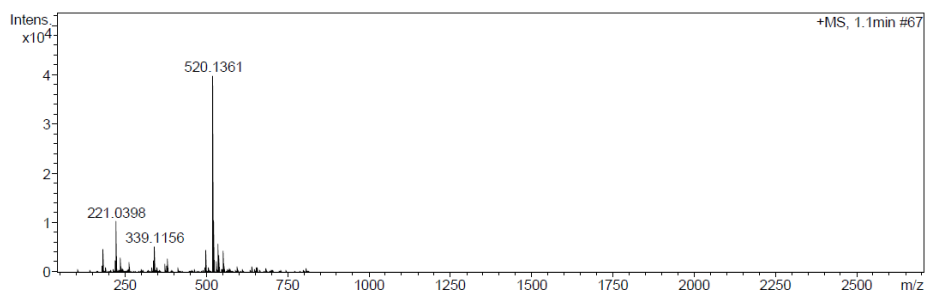


Figure 4.34 HRMS of *1-(2-(4-(((2-methyl-4-(5-methylfuran-2-yl)furo[3,2-*c*]pyridin-6-yl)methoxy)methyl)-1*H*-1,2,3-triazol-1-yl)ethyl)indoline-2,3-dione (15ba)*

4.5 References

- [1] Global tuberculosis report 2020, Geneva: World Health Organization, (2020), Licence: CC BY-NC-SA 3.0 IGO
- [2] Seung K.J., Keshavjee S., Rich M.L. (2015), Multidrug-resistant tuberculosis and extensively drug-resistant tuberculosis, *Cold Spring Harb Perspect Med*, 5, a017863 (DOI: 10.1101/cshperspect.a017863)
- [3] Vilchèze C., Jacobs Jr W.R. (2014), Resistance to isoniazid and ethionamide in *Mycobacterium tuberculosis*: Genes, mutations, and causalities, *Microbiol Spectr*, 2, 431–453 (DOI: 10.1128/microbiolspec.MGM2-0014-2013)
- [4] Jeffrey North E., Jackson M., Lee R.E. (2014), New approaches to target the mycolic acid biosynthesis pathway for the development of tuberculosis therapeutics, *Curr Pharm Des*, 20, 4357–4378
- [5] Jasselin-Hinschberger A., Comoy C., Chartoire A., Fort Y. (2015), Elaboration of Furopyridine Scaffolds, *Eur J Med Chem*, 11, 2321–2331 (DOI: 10.1002/ejoc.201403412)
- [6] Shiotani S., Morita H. (1982), Furopyridines synthesis of furo[2,3-*c*] pyridine, *J Heterocycl Chem*, 19, 1207–1209 (DOI: 10.1002/jhet.5570190544)
- [7] Denisenko A.V., Tverdokhlebov A.V., Tolmachev A.A., Volovenko Y.M., Shishkina S.V., Shishkin O.V. (2010), Synthesis of masked 2-amino-3-furancarboxaldehydes, *Synthesis*, 6, 1009–1013 (DOI: 10.1055/s-0029-1218641)
- [8] Volochnyuk D.M., Ryabukhin S.V., Plaskon A.S., Dmytriv Y.V., Grygorenko O.O., Mykhailiuk P.K., Krotko D.G., Pushechnikov A., Tolmachev A.A. (2010), Approach to the library of fused pyridine-4-carboxylic acids by Combes-type reaction of acyl pyruvates and electron-rich amino heterocycles, *J Comb Chem*, 12, 510–517 (DOI: 10.1021/cc100040q)
- [9] Fumagalli F., de Melo S.M.G., Ribeiro C.M., Solcia M.C., Pavan F.R., Silva Emery F. (2019), Exploiting the furo[2,3-*b*] pyridine core against

- multidrug-resistant *Mycobacterium tuberculosis*, *Bioorg Med Chem Lett*, 29, 974–977 (DOI: 10.1016/j.bmcl.2019.02.019)
- [10] Surman M.D., Freeman E.E., Grabowski J.F., Hadden M., Henderson A.J., Jiang G., Luche M., Khmel'nitsky Y., Vickers S., Viggers J., Cheetham S. (2010), 5-(Pyridinon-1-yl) indazoles and 5-(furopyridinon-5-yl) indazoles as MCH-1 antagonists, *Bioorg Med Chem Lett*, 20, 7015–7019 (DOI: 10.1016/j.bmcl.2010.09.039)
- [11] Hempel C., Najjar A., Totzke F., Schächtele C., Sippl W., Ritter C., Hilgeroth, A. (2016), Discovery of dually acting small-molecule inhibitors of cancer-resistance relevant receptor tyrosine kinases EGFR and IGF-1R, *Med Chem Comm*, 7, 2159–2166 (DOI: 10.1039/c6md00329j)
- [12] Aggarwal A., Parai M.K., Shetty N., Wallis D., Woolhiser L., Hastings C., Dutta N.K., Galaviz S., Dhakal R.C., Shrestha R., Wakabayashi S. (2017), Development of a novel lead that targets *M. tuberculosis* polyketide synthase 13, *Cell*, 170, 249–259 (DOI: 10.1016/j.cell.2017.06.025)
- [13] Dudhe P., Venkatasubbaiah K., Pathak B., Chelvam V. (2020), Serendipitous base-catalyzed condensation–heteroannulation of iminoesters: A regioselective route to the synthesis of 4,6-disubstituted 5-azaindoles, *Org Biomol Chem*, 18, 1582–1587 (DOI: 10.1039/C9OB02657F)
- [14] Dudhe P., Krishnan M.A., Yada K., Roy D., Venkatasubbaiah K., Pathak B., Chelvam V. (2021), Synthesis of 1-indolyl-3,5,8-substituted γ -carboline: One-pot solvent-free protocol and biological evaluation, *Beilstein J Org Chem*, 00, 000 (in press)
- [15] Bérubé G. (2016), An overview of molecular hybrids in drug discovery, *Expert Opin Drug Discov*, 11, 281–305 (DOI: 10.1517/17460441.2016.1135125)

- [16] Ding Z., Zhou M., Zeng C. (2020), Recent advances in isatin hybrids as potential anticancer agents, *Archiv der Pharmazie*, 353, e1900367 (DOI: 10.1002/ardp.201900367)
- [17] Gao F., Yang H., Lu T., Chen Z., Ma L., Xu Z., Schaffer P., Lu G., (2018), Design, synthesis and anti-mycobacterial activity evaluation of benzofuran-isatin hybrids, *Eur J Med Chem*, 159, 277–281 (DOI: 10.1016/j.ejmech.2018.09.049)

Chapter 5

Conclusions and scope for future work

5.1 Conclusion

Fused-pyrido heterocycles is a significant class of nitrogen heterocycles because of their wide range of drug design and development applications. Several drug candidates have emerged from this class in recent times. The present thesis elicits developing a new synthetic strategy for fused-pyrido heterocycles such as 5-azaindoles, γ -carboline, and furo[3,2-*c*]pyridines, and benzofuro[3,2-*c*]pyridines. Further, the newly synthesized molecules have been used in designing small molecule inhibitors to find alternative therapeutic solutions for diseases such as cancer and tuberculosis.

Chapter 1 of the thesis provides a general outline of the topic. The key structural feature of fused-pyrido heterocycles and their different isomeric forms are discussed. An account of recent publications on developing novel synthetic procedures for the title molecules is described. The mentioned heterocycles are also present in several drug-like molecules. A summary of biologically significant members of pyrido heterocycles is given in this chapter.

Chapter 2 describes a serendipitous discovery of a novel one-pot method to synthesize a 5-azaindole class of molecules. The synthetic protocol is further developed into a solvent-free one-pot cascade reaction for the above heterocycles. The optimized protocol is used to synthesize a range of compounds of this class. The effect of substituents at different positions of the pyrrole ring is examined for generalizing the scope of this heterocyclic transformation. A plausible mechanism for the given transformation is proposed, further verified by theoretical (DFT) calculations. With the help of standard functional group transformations,

several unique azaindole derivatives are prepared, which are difficult to prepare by conventional methods. A possible CB2 agonist analog is prepared and tested *in vitro*.

Chapters 3 delineates the design and development of a novel synthetic protocol for γ -carbolines. A series of *N*-substituted indole-2-carboxaldehyde derivatives is prepared, and the novel protocol for the synthesis of γ -carbolines is optimized. The developed one-pot solvent-free method is used to synthesize various derivatives, and the scope of the reaction is examined. The regioselective nature of the reaction is established via theoretical (DFT) calculations. The optical properties of these novel compounds are studied through excitation-emission studies. The representative members of the γ -carboline series are tested against a panel of cancer cell lines for their innate cytotoxicity. Representative γ -carboline compound is traced inside the cervical (HeLa) cancer cells through cell uptake (confocal microscopy) studies.

Chapter 4 describes a novel one-pot synthesis of furo[3,2-*c*]pyridines and benzofuro[3,2-*c*]pyridines in the presence of Hunig's base. A representative member of the furo[3,2-*c*]pyridine class is transformed into a corresponding isatin hybrid by using a standard click chemistry reaction. The newly developed furopyridine-isatin hybrid is tested for its anti-mycobacterial efficacy in non-virulent (*M. smegmatis*), and virulent (*M. bovis* BCG) strains of tuberculosis causing bacteria. The hybrid compound can control the bacterial population to a great extent while used in 50 to 100 μ M concentrations.

5.2 Scope for future work

This thesis work contains the discovery of a novel one-pot protocol to synthesize fused-pyrido heterocycles. A library of heterocycles has been synthesized using this protocol. This work has enormous possibilities for future work. Some of these are enlisted below-

A) A library of novel fused-pyrido heterocycles has been prepared by a newly developed synthetic methodology. Synthetic azaindoles are known for their applications as kinase inhibitors. Kinase inhibitors play a key role in cancer therapy. The newly synthesized 5-azaindole derivatives can be screened for their kinase inhibitor activities.

B) The molecular architecture of γ -carbolines has been exploited widely to develop DNA intercalators in the literature. The DNA intercalation properties of the synthesized γ -carbolines may be examined for further understanding of the mechanism of action. We are already working on understanding the exact mode of action of newly synthesized γ -carbolines in our laboratory. This may lead to the discovery of a new mechanism to kill cancer cells.

C) We have reported our initial success in developing a potent anti-mycobacterial compound in the form of a furopyridine-isatin hybrid. Further, we are analyzing the efficacy of this new molecular hybrid against the multidrug-resistant strain of Mtb. This may lead to the discovery of a potent drug against multidrug-resistant tuberculosis. Moreover, with the help of *in silico* studies, we can design more potent derivatives of the furo[3,2-*c*]pyridine family. This may bring a revolutionary change in the treatment of tuberculosis.

